Structural studies on receptor binding and antibody neutralization mechanisms of EV71

Daming Zhou

Linacre College
and
Division of Structural Biology
Nuffield Department of Medicine
University of Oxford

A thesis submitted for the degree of
Doctor of Philosophy

Trinity Term 2019

Contents

Contents..... I
Detailed contents..... II
List of figures V
List of tables..... VIII
Abstract..... IX
Abbreviations..... XI
Acknowledgements..... XIV
Declaration of work..... XV
Chapter 1 Introduction..... 1
Chapter 2 Material and methods..... 39
Chapter 3 Cryo-EM studies on the interaction of EV71 with SCARB2..... 61
Chapter 4 Anti-EV71 human monoclonal antibodies..... 84
Chapter 5 Cryo-EM studies on EV71-antibody interactions..... 105
Chapter 6 Final summary and future plan..... 172
Appendix..... 176
Reference..... 213

Detailed contents

Contents.....I
Detailed contents.....II
List of figures.....V
List of tables.....XIII
Abstract.....IX
Abbreviations.....XI
Acknowledgements.....XIV
Declaration of work.....XV
Chapter 1 Introduction.....1
1.1 Hand, foot and mouth disease.....2
1.2 Picornaviridae.....4
1.3 Enterovirus genus.....5
1.4 Enterovirus 71.....7
1.4.1 Epidemiology.....7
1.4.2 Virion morphology.....8
1.4.3 Genome and viral proteins.....12
1.4.4 Phylogenetic relationship.....14
1.4.5 Evolution and recombination.....15
1.4.6 Life cycle.....17
1.4.6.1 Attachment.....18
1.4.6.2 Internalization.....21
1.4.6.3 Uncoating.....26
1.4.6.4 Viral replication and assembly.....28
1.4.7 Anti-EV71 drugs and vaccine.....30
1.5 Anti-EV71 human mAbs from EV71-infected children.....32
1.6 Aims.....37
Chapter 2 Material and methods.....39
2.1 Production of SCARB2 and anti-EV71 Fabs.....40
2.1.1 Preparation of Fabs from IgGs.....40
2.1.2 DNA synthesis.....40
2.1.3 PCR.....41
2.1.4 Analysis of PCR products.....42
2.1.5 Purification of PCR products.....42
2.1.6 Restriction digestion of vectors.....43
2.1.7 Ligation independent cloning reactions.....44
2.1.8 E. coli cell transformation.....44
2.1.9 Colony picking and cell culture.....45
2.1.10 Plasmid mini-preps.....45
2.1.11 Construct verification.....45

2.1.12 Transient expression screen..... 46
2.1.13 DNA Mega-prep for large-scale transfection..... 47
2.1.14 Transfection and protein expression..... 47
2.1.15 Dialysis..... 48
2.1.16 Affinity purification.....48
2.1.17 Gel filtration..... 49
2.2 Fab crystallization and crystal structure determination.....49
2.2.1 Fab crystallization..... 49
2.2.2 X-ray data collection..... 50
2.2.3 Structure determination..... 50
2.3 Virus production and purification.....51
2.3.1 EV71 strains used in this study.....51
2.3.2 EV71 production..... 51
2.3.3 EV71 purification..... 52
2.4 Cryo-EM experiments.....53
2.4.1 Negative-stain electron microscopy..... 53
2.4.2 Cryo-EM sample preparation of EV71-SCARB2 complex..... 54
2.4.3 Cryo-EM sample preparation of EV71-Fab complexes.....54
2.4.4 Cryo-EM data collection..... 56
2.4.5. Cryo-EM data processing.....56
2.4.6 Model building.....57
2.5 Other experiments..... 58
2.5.1 Thermal stability assay..... 58
2.5.2 Octet experiments..... 59
Chapter 3 Cryo-EM studies on the interaction of EV71 with SCARB2.....61
3.1 Receptors of the HFMD-causing enteroviruses.....62
3.2 Production, purification and characterization of EV71..... 64
3.3 Cryo-EM data collection and structure determination..... 65
3.4 Cryo-EM structure of EV71-SCARB2 complex..... 68
3.5 Conservation of the SCARB2-binding residues..... 76
3.6 Proposed mechanism of SCARB2-induced uncoating of EV71..... 81
3.7 Summary..... 83
Chapter 4 Anti-EV71 human monoclonal antibodies..... 84
4.1 Crystal structures of anti-EV71 Fabs.....85
4.2 Somatic mutations of anti-EV71 antibodies..... 93
4.3 Antibodies 16-2-8C and 16-2-9D..... 100
4.4 Summary..... 103
Chapter 5 Cryo-EM studies on EV71-antibody interactions..... 105
5.1 Binding patterns of mAbs..... 110
5.2 Somatic mutations involved in EV71-antibody interactions.....120
5.3 Conformational changes of EV71 and Fabs in the process of binding..... 122

5.4 Empty particles caused by three Fabs....125
5.5 Escape mutants and binding residues....126
5.6 MAbs' inability to neutralize some strains of EV71....145
5.7 Comparison of binding areas of mAbs and SCARB2....148
5.8 Overlapped volume of Fabs and SCARB2 binding on EV71 capsid....162
5.9 Binding affinities of Fabs with full or empty particles of EV71....164
5.10 Fabs' effect on the stability of EV71 virions....168
5.11 Summary....170
Chapter 6 Final summary and future plan....172
6.1 Summary....173
6.2 Future Plan....174
Appendix....176
Reference....213

List of figures

Figure 1.1 Epidemics caused by enteroviruses since 1957, with countries and years marked..... 3
Figure 1.2 Virion and genome of EV71..... 9
Figure 1.3 Morphology of EV71. 11
Figure 1.4 Phylogenetic relationships among VP1 sequences of different EV71 strains..... 15
Figure 1.5 EV71 genotypes that caused epidemics in Asia-Pacific regions and Europe (EU)..... 16
Figure 1.6 Overview of EV71 life cycle.....19
Figure 1.7 Representation of SCARB2..... 21
Figure 1.8 Virus internalization by the host cell via clathrin-mediated endocytosis..... 23
Figure 1.9 Virus internalization by the host cell via caveolin-mediated endocytosis.....25
Figure 1.10 Cartoon of EV71 cell entry process mediated by SCARB2..... 27
Figure 1.11 Assembly and uncoating of human enterovirus.....29
Figure 1.12 The locations of substitutions of amino acids on the EV71 capsid causing escape mutants of EV71 strain 12-96015 and 11-96023 from anti-EV71 human mAbs.....34
Figure 3.1 Phylogenetic tree of the HFMD-causing enteroviruses..... 63
Figure 3.2 Purification and characterization of EV71 virions.....64
Figure 3.3 Cryo-EM image showing EV71-SCARB2 complexes..... 65
Figure 3.4 2D classification result of EV71-SCARB2 complex.....66
Figure 3.5 3D classification result of EV71-SCARB2 complex.....67
Figure 3.6 The final density map of EV71-SCARB2 complex.....68
Figure 3.7 The gold standard FSC curve of the final map of EV71-SCARB2 complex.....69
Figure 3.8 The quality of the EV71–SCARB2 EM structure.....69
Figure 3.9 EV71–SCARB2 complex viewed down the 2-fold icosahedral axis.....70
Figure 3.10 Complex formation of EV71 and SCARB2.....71
Figure 3.11 EV71 and SCARB2 interactions.....72
Figure 3.12 Overlay of receptor bound EV71 and the mature virus..... 73
Figure 3.13 Conformational differences of SCARB2 at different pH.....74
Figure 3.14 Surface representations of a EV71 protomer showing binding areas of SCARB2 with or without glycans.....75
Figure 3.15 Residues involved in EV71-SCARB2 interaction..... 77
Figure 3.16 EV71 and SCARB2 interface.....78
Figure 3.17 Comparison of residues in the receptor attachment area of EV71 with other type A enteroviruses that cause HFMD.....79
Figure 3.18 Epitopes of neutralizing antibodies compared to SCARB2 binding residues.....81
Figure 3.19 Proposed mechanism of uncoating.....83
Figure 4.1 Reducing SDS-PAGE of purified Fabs.....86
Figure 4.2 Crystals of 13 Fabs leading to high-resolution structures.....87
Figure 4.3 X-ray diffraction pattern from the crystal of Fab 16-2-9D..... 89

Figure 4.4 Crystal structures of Fabs....91
Figure 4.5 Structure-based unrooted phylogenetic tree for the 13 anti-EV71 Fabs....93
Figure 4.6 Somatic hypermutations causing amino acid alterations in framework regions and CDRs in heavy and light chains of anti-EV71 antibodies....100
Figure 4.7 Different somatic mutations in antibodies 16-2-8C and 16-2-9D....102
Figure 4.8 Overlay of crystal structures of Fabs 16-2-8C and 16-2-9D....103
Figure 4.9 Overlay of variable regions of Fabs 16-2-8C and 16-2-9D, showing different somatic mutations. 104
Figure 5.1 FSC curves of 13 EV71-Fab cryo-EM reconstructions....107
Figure 5.2 Cryo-EM reconstructions of EV71-Fab complexes....110
Figure 5.3 Surface and cartoon representations showing binding areas between EV71 and anti-EV71 Fabs.. 114
Figure 5.4 Roadmap showing footprints of anti-EV71 Fabs on the surface of EV71 capsid in an asymmetric unit....116
Figure 5.5 Lengths of HCDR3s of anti-EV71 antibodies....119
Figure 5.6 Different binding patterns of canyon binders of EV71....120
Figure 5.7 Examples of conformational changes on binding....125
Figure 5.8 Empty particles of EV71 induced by Fabs 16-2-12D, 16-3-3C and 16-2-2D....127
Figure 5.9 Substitution VP1 S283F causing escape mutants of EV71 from antibody 16-3-10B....128
Figure 5.10 Substitution VP3 E81G/K causing escape mutants of EV71 from antibodies 16-3-4D and 34-1-6D. 130
Figure 5.11 Substitution VP1 T232A causing escape mutants of EV71 from antibodies 16-2-8C, 16-2-9D and 16-2-12D in the same way....131
Figure 5.12 Roadmap of Fab 16-2-2D binding residues and escape mutant substitutions....133
Figure 5.13 Roadmap of Fab 16-2-8C binding residues and escape mutant substitutions....134
Figure 5.14 Roadmap of Fab 16-2-9D binding residues and escape mutant substitutions....135
Figure 5.15 Roadmap of Fab 16-2-11B binding residues and escape mutant substitutions....136
Figure 5.16 Roadmap of Fab 16-2-12D binding residues and escape mutant substitutions....137
Figure 5.17 Roadmap of Fab 16-3-3C binding residues and escape mutant substitutions....138
Figure 5.18 Roadmap of Fab 16-3-10B binding residues and escape mutant substitutions....139
Figure 5.19 Roadmap of Fab 17-2-2B binding residues and escape mutant substitutions....140
Figure 5.20 Roadmap of Fab 17-1-12A binding residues and escape mutant substitutions....141
Figure 5.21 Roadmap of Fab 17-2-12A binding residues and escape mutant substitutions....142
Figure 5.22 Roadmap of Fab 16-3-4D binding residues and escape mutant substitutions....143
Figure 5.23 Roadmap of Fab 34-1-6D binding residues and escape mutant substitutions....144
Figure 5.24 Roadmap of Fab 38-1-10A binding residues and escape mutant substitutions....145
Figure 5.25 Roadmap showing sites of escape mutations on the EV71 capsid....146
Figure 5.26 Sequence alignment of VP1 – VP3 showing variations between different EV71 strains....147
Figure 5.27 Roadmap showing variations between EV71 strains mentioned in Figure 5.26....148
Figure 5.28 Roadmap of Fab 16-2-2D binding residues and SCARB2 binding area....150
Figure 5.29 Roadmap of Fab 16-2-8C binding residues and SCARB2 binding area....151
Figure 5.30 Roadmap of Fab 16-2-9D binding residues and SCARB2 binding area....152
Figure 5.31 Roadmap of Fab 16-2-11B binding residues and SCARB2 binding area....153

Figure 5.32 Roadmap of Fab 16-2-12D binding residues and SCARB2 binding area..... 154
Figure 5.33 Roadmap of Fab 16-3-3C binding residues and SCARB2 binding area.....155
Figure 5.34 Roadmap of Fab 16-3-10B binding residues and SCARB2 binding area.....156
Figure 5.35 Roadmap of Fab 17-2-2B binding residues and SCARB2 binding area.....157
Figure 5.36 Roadmap of Fab 17-1-12A binding residues and SCARB2 binding area..... 158
Figure 5.37 Roadmap of Fab 17-2-12A binding residues and SCARB2 binding area..... 159
Figure 5.38 Roadmap of Fab 16-3-4D binding residues and SCARB2 binding area..... 160
Figure 5.39 Roadmap of Fab 34-1-6D binding residues and SCARB2 binding area..... 161
Figure 5.40 Roadmap of Fab 38-1-10A binding residues and SCARB2 binding area..... 162
Figure 5.41 Overlap of Fab 17-1-12A with SCARB2 as bound to the EV71 capsid 164
Figure 5.42 Binding K_Ds of 12 anti-EV71 Fabs with EV71 full and empty particles.....166
Figure 5.43 Scatter plot with log/log scale axes showing correlation between the binding K_Ds of Fabs with full and empty particles.....168
Figure 5.44 Scatter plot showing correlation between the binding K_Ds of Fabs and the EC_{50}s of corresponding IgGs..... 169
Figure 5.45 The effects of Fabs on the melting temperature of EV71 virions.....170
Appendix figure 1 Binding curves of Fabs with EV71 full particles measured on Octet.....187
Appendix figure 2 Binding curves of Fabs with EV71 empty particles measured on Octet.....200

List of tables

Table 1.1 Reported HFMD-related viruses..... 4
Table 1.2 Substitutions of amino acids on the EV71 capsid causing escape mutants of EV71 strain 12-96015 and 11-96023 from anti-EV71 human mAbs..... 33
Table 1.3 Neutralizing abilities of different antibodies against EV71 clinical strains in 1998-2016.....36
Table 1.4 Pre- and post-attachment neutralizing abilities of anti-EV71 antibodies.....37
Table 2.1 The reaction mix for PCR.....41
Table 2.2 Restriction digestion reactions of expression vectors..... 43
Table 2.3 The mix for fusion reactions.....44
Table 2.4 The reaction mix of PCR for construct verification..... 45
Table 2.5 Incubation conditions for preparation of EV71-Fab complexes..... 56
Table 4.1 Conditions used for crystallization of Fabs..... 88
Table 4.2 Data collection and refinement statistics of X-ray diffraction for Fab 16-2-9D..... 90
Table 4.3 Sequences and lengths of heavy-chain CDR3s of 13 anti-EV71 antibodies.....94
Table 4.4 Predicted heavy-chain V-D-J gene usage of 13 anti-EV71 antibodies..... 95
Table 4.5 Predicted light-chain V-J gene usage of 13 anti-EV71 antibodies.....96
Table 4.6 Somatic hypermutations causing amino acid alterations in framework regions and CDRs in heavy and light chains of anti-EV71 antibodies..... 98
Table 5.1 Summary of cryo-EM structures of EV71-Fab complexes..... 108
Table 5.2 Sequences and lengths of HCDR3s of anti-EV71 antibodies..... 118
Table 5.3 Somatic mutations directly involved in EV71-antibody interactions.....123
Table 5.4 Significant conformation changes of Fab and EV71 in the cryo-EM structures.....124
Table 5.5 Pre- and post-attachment Neutralizing abilities of anti-EV71 mAbs compared to overlapped volume of mAb's VHVL part with SCARB2..... 164
Table 5.6 Binding K_Ds of 12 anti-EV71 Fabs with EV71 full and empty particles and EC_{50}s of corresponding IgGs in the pre-attachment stage..... 167
Appendix table 1 Vectors, tags and primers used in the plasmid construction..... 178
Appendix table 2 Data collection and refinement statistics of X-ray diffraction..... 179
Appendix table 3 Data collection and refinement statistics of X-ray diffraction..... 180
Appendix table 4 Data collection and refinement statistics of X-ray diffraction..... 181
Appendix table 5 Data collection and refinement statistics of X-ray diffraction..... 182
Appendix table 6 Cryo-EM data collection and refinement statistics of EV71-Fab complexes..... 183
Appendix table 7 Cryo-EM data collection and refinement statistics of EV71-Fab complexes..... 184
Appendix table 8 Cryo-EM data collection and refinement statistics of EV71-Fab complexes..... 185
Appendix table 9 Cryo-EM data collection and refinement statistics of complexes EV71_Fab-38-1-10A and EV71-SCARB2..... 186
Appendix table 10 List of interactions between EV71 and SCARB2..... 187
Appendix table 11 Solvent accessible areas between chains of Fabs and viral proteins of EV71 in the EM structures of 13 EV71-Fab complexes.....188

Structural studies on receptor binding and antibody neutralization mechanisms of EV71

Daming Zhou

Linacre College and Division of Structural Biology

Nuffield Department of Medicine, University of Oxford

Trinity Term 2019

Abstract

Hand, foot and mouth disease (HFMD) is an infectious disease that mainly infects infants and children and has caused epidemics widely in the Asia-Pacific region in the last 20 years. Enterovirus 71 (EV71) is one of the most common causes of HFMD. HFMD caused by EV71 is sometimes quite harmful because EV71 can induce severe cardiac or central nervous system (CNS) complications.

Although EV71 vaccines have been approved in China, there are no other effective means to treat EV71 infection. Our collaborators have identified and characterized 13 human monoclonal antibodies (mAbs) that can neutralize EV71. Blocking EV71 entry with therapeutic antibodies could be a new useful strategy.

Human scavenger receptor class B, member 2 (SCARB2) is a cellular receptor for EV71 and can induce attachment and uncoating. SCARB2 is a key factor in the entry

process of EV71, however a structure of EV71-SCARB2 complex has not been available to clarify EV71-SCARB2 interaction.

We have determined the cryo-EM structure of the EV71-SCARB2 complex. SCARB2 was found to bind outside the canyon region, different from the binding patterns of many IgG-like picornavirus receptors. The VP1 GH and VP2 EF loops of the EV71 capsid, together with helices α5 and α7 of SCARB2, are involved in virus-receptor interactions.

With anti-EV71 antibodies from our collaborators, we also solved Fab structures as well as cryo-EM structures of EV71-Fab complexes. In these structures, the binding sites of antibodies can be classified into three groups: canyon, 2-fold-axis area and 3-fold-axis area. Antibodies that bind near the canyon region share some common binding residues or have overlapped volume with SCARB2 when binding with EV71, so may use a receptor-blocking neutralization mechanism. Antibodies binding near the 2-fold axis may block genome release of EV71, since it is thought EV71 releases its genome from the channel at the 2-fold axis. Antibodies binding near the 3-fold axis slightly increase the stability of EV71 virions, which may also contribute to the neutralization of EV71 by these antibodies.

Our studies on EV71-receptor interaction and neutralization mechanisms of antibodies may contribute to the development of structure-based anti-EV71 drugs and antibody-based therapy for HFMD.

Abbreviations

Å	Ångstrom (10^{-10} m)
ACBD3	acyl-coenzyme A binding domain containing 3 protein
AR2G	Amine Reactive 2nd Generation
BLI	bio-layer interferometry
CAR	coxsackievirus-adenovirus receptor
CDR	complementarity-determining region
CFDA	China Food and Drug Administration
CNS	central nervous system
CPE	cytopathic effect
CTF	contrast transfer function
CV	coxsackievirus
CypA	cyclophilin A
DAF	decay-accelerating factor
DC-SIGN	dendritic cell-specific ICAM-grabbing non-integrin
DMEM	Dulbecco's modified Eagle's medium
E-3	echovirus 3
EM	electron microscopy
EU	Europe
EV71	enterovirus A71
FcRn	human neonatal Fc receptor
FBS	fetal bovine serum

FMDV	Foot-and-mouth disease virus
FSC	fourier shell correlation
HCDR3	heavy-chain CDR3
HFMD	Hand, foot and mouth disease
HRV	human rhinovirus
ICAM-1	intercellular adhesion molecule 1
ICTV	International Committee on Taxonomy of Viruses
IFN	interferon
IFNR1	interferon receptor 1
IgG	immunoglobulin G
IRES	internal ribosome entry site
IRF7	interferon regulatory factor 7
KREMEN1	kringle-containing transmembrane protein 1
mAbs	monoclonal antibodies
MAVS	mitochondrial anti-viral signaling
MEM + NEAA	MEM with non-essential amino acids
ORF	open reading frame
PaSTRy	particle stability thermal release assay
PCR	polymerase chain reaction
PDB	Protein Data Bank
PEG	polyethylene glycol
PEI	polyethylenimine

PI4KB	phosphatidylinositol-4-kinase IIIβ
PSGL-1	P-selectin glycoprotein ligand-1
Pvr	poliovirus receptor
RD	rhabdomyosarcoma
RdRp	RNA-dependent RNA polymerase
Rmsd	root mean square deviation
SCARB2	scavenger receptor class B, member 2
SDS-PAGE	sodium dodecyl sulfate polyacrylamide gel electrophoresis
siRNA	short interfering RNA
TRIF	TIR-domain-containing adaptor-inducing interferon-β
UTR	untranslated region
VH	heavy chain variable domain
VL	light chain variable domain
VP	viral polypeptide
VPg	virus genome-linked protein
WHO	World Health Organization

Acknowledgements

I would like to express my deepest appreciation to my supervisor, David Stuart, for his guidance and support in the whole process of my PhD study. I am and will always be inspired and encouraged by his endless energy and enthusiasm for research. I am also grateful to Abhay Kotecha for his patience and comprehensive guidance for my research project. I learnt things about cryo-EM from him and I benefit a lot from his experience on all kinds of experiments. Many thanks to Jingshan Ren, for his contributions to crystal structures in my project and his valuable advices on research. Thanks should also go to Elizabeth Fry for her support on my study and to Yuguang Zhao, for his kind help with my experiments.

I also appreciate Ray Owens for his assistance with protein expression. I'd like to acknowledge the effort of Dimple Karia, Helen Duyvesteyn and Bilal Qureshi for EM data collection, Geoff Sutton for Octet experiments, Tom Walter for crystallization and Thermofluor assays, and Karl Harlos for mounting crystals. I'd like to recognize the assistance I have received in our lab from Margaret Jones, Weixian Lu, Oliver Hayward and Robin Parsons. I am also grateful to our collaborators, David Rowlands, James Kelly and Kuan Ying Arthur Huang, for their assistance and cooperation. I also feel appreciated to work with all the other guys from STRUBI.

Special thanks to Chinese government and University of Oxford, for their financial support. Thanks to all my teachers for their guidance and encouragement. Finally, love to my parents and other family members, for their endless caring and precious love.

Declaration of work

I certify that all the work described here is my own, except that detailed immediately below:

Signed Daming Zhou .....

Date Jan 21 2020

Daming Zhou

Chapter 3 (Cryo-EM studies on EV71-SCARB2 interaction)

This chapter is based on an article published in Nature Microbiology (Zhou *et al*. 2018). I am the co-first author of this article and performed the main part of experiments and also contributed to manuscript writing. Abhay Kotecha helped with cryo-EM data collection and Yuguang Zhao contributed to protein purification. David Stuart, Jingshan Ren and me analysed the results and, together with Elizabeth Fry and Yuguang Zhao, wrote the manuscript.

Publications:

Zhou, Daming#, Yuguang Zhao#, Abhay Kotecha, Elizabeth E. Fry, James T. Kelly, Xiangxi Wang, Zihe Rao, David J. Rowlands, Jingshan Ren, and David I. Stuart. "**Unexpected mode of engagement between enterovirus 71 and its receptor SCARB2**." *Nature microbiology* 4, no. 3 (2019): 414.

Machón, Cristina, Montserrat Fàbrega-Ferrer, **Daming Zhou**, Ana Cuervo, José L. Carrascosa, David I. Stuart, and Miquel Coll. "**Atomic structure of the Epstein-Barr virus portal**." *Nature communications* 10, no. 1 (2019): 1-7.

Yuguang Zhao#, **Daming Zhou**#, Tao Ni, Dimple Karia, Abhay Kotecha, Xiangxi Wang, Zihe Rao, E. Yvonne Jones, Elizabeth E. Fry, Jingshan Ren, David I. Stuart. "**Hand-foot-and-mouth disease virus receptor KREMEN1 binds the canyon of Coxsackie Virus A10**." *Nature communications* 11, no. 1 (2020): 1-8.

# These authors contributed equally to this work.

Chapter 1

Introduction

1.1 Hand, foot and mouth disease

The first reported case of hand, foot and mouth disease (HFMD) appeared in 1957[1]. HFMD is a contagious viral disease that affects mainly infants and children with a low mortality rate (around 0.03% - 0.05%)[2,3]. It can cause fever, cough, coryza, blisters or ulcers on the hands, feet and in the mouth. Symptoms usually appear 3 to 5 days after infection. Often there is a sore mouth for a few days before the blisters or ulcers appear[4-6]. The infection produces mild symptoms in most cases and HFMD usually resolves on its own after 7 to 10 days. However, in some cases, there can be severe neurological diseases, including aseptic meningitis, brainstem encephalitis and acute flaccid paralysis[7]. Brainstem encephalitis can further induce severe pulmonary edema and shock, which may lead to failure of circulatory and respiratory systems[8].

HFMD is usually transmitted through the fecal-oral route or by direct contact with contaminated objects[9]. The number of cases increases significantly with increased temperature and relative humidity, so HFMD appears throughout the year but epidemics usually peak in the summer and autumn[10]. HFMD is present in most countries, however many serious outbreaks (including all those with more than 10,000 cases) have been reported in the Asia-Pacific region since 1990s and HFMD has become a public health problem in this region (Figure 1.1)[11-16]. According to the online reports of World Health Organization (WHO), there have been about 2,000,000 cases of HFMD in Asian countries every year since 2010[17].

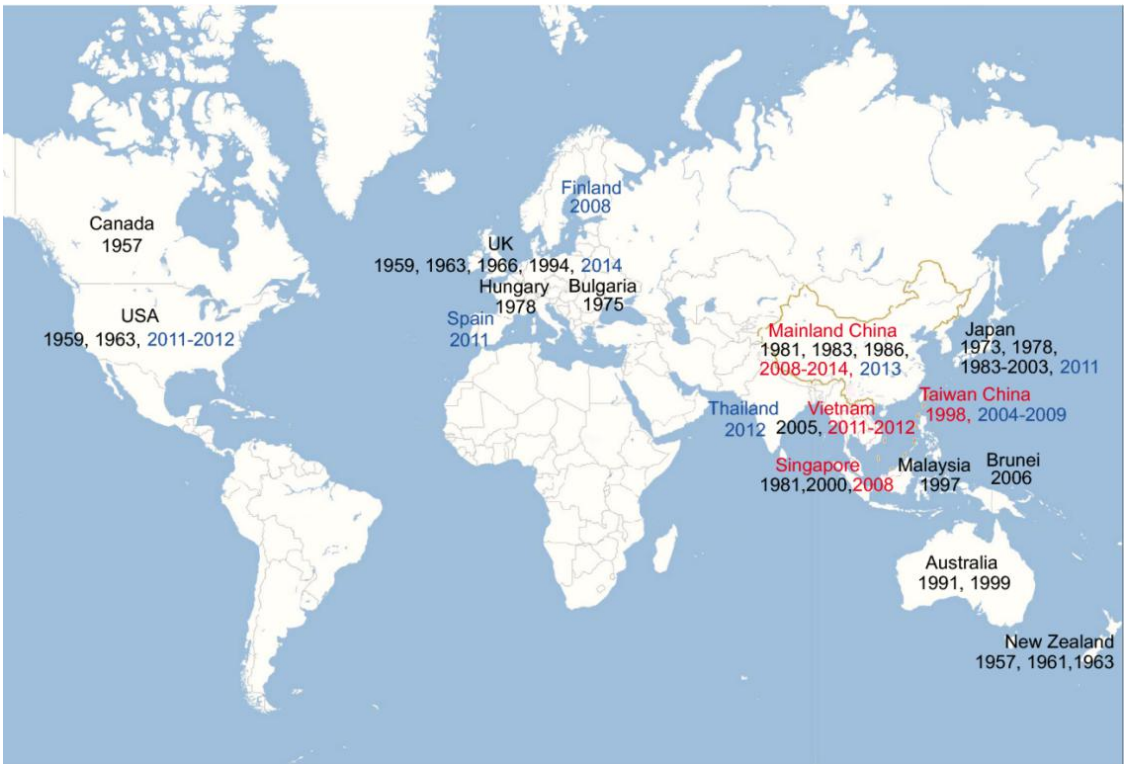

Figure 1.1 Epidemics caused by enteroviruses since 1957, with countries and years marked. Red indicates HFMD outbreaks with more than 10,000 cases and blue indicates CV-A6 infection involved, which is one of the common causes of HFMD in recent years (Adapted from Lei *et al*. 2015[18]).

HFMD can be diagnosed by the presenting symptoms, but laboratory tests are needed to determine what virus is causing the disease. Enterovirus 71 (EV71) and coxsackievirus A16 (CV-A16) have been the most common causes of HFMD[19,20]. A significant number of cases caused by coxsackievirus A6 (CV-A6) have also been reported recently (Figure 1.1)[21,22]. EV71 is genetically most closely related to CV-A16, however HFMD caused by EV71 can be more severe than that caused by CV-A16 or other enteroviruses because EV71 sometimes induces severe cardiac or CNS complications and can even cause death[23]. Based on the analysis of nearly 10,700,000 HFMD cases in China from 2008 to 2014, EV71 was responsible for about 70% of severe HFMD cases and 90% of HFMD-related deaths[20]. All the known viruses

causing HFMD belong to one of two different species (*Enterovirus A* and *B*) of the genus *Enterovirus*, in the *Picornaviridae* family (Table 1.1)[18,20,22,24-28].

Species	**HFMD-related viruses**
Enterovirus A	CV-A2~8, CV-A10, CV-A12, CV-A14, CV-A16, EV71
Enterovirus B	CV-B1~6, CV-A9, E-3~7, E-9, E-11, E-18, E-19, E-25, E-30, EV-B84

Table 1.1 Reported HFMD-related viruses. All the known viruses causing HFMD, including some coxsackievirus (CV), enterovirus (EV) and echoviruses (E), belong to one of two different species of the genus *Enterovirus*, in the *Picornaviridae* family[18,20,22,24-28].

1.2 *Picornaviridae*

The *Picornaviridae* is a family of viruses with small icosahedral capsids and positive single-stranded RNA genomes. The prefix "pico" in *Picornaviridae* indicates small size of the viruses and "rna" designates the type of viral genome. According to a report released by the International Committee on Taxonomy of Viruses (ICTV) in October 2017, this family is currently classified into 35 genera and 80 species, with some other viruses unclassified. The classification is based on morphology, antigenic structures, genomic sequence and mode of replication[29,30]. Characteristic features of picornaviruses include three capsid structural proteins with a β-barrel fold, polyprotein processing by proteinase(s) and replication by an RNA-dependent RNA polymerase.

Virions of picornaviruses have non-enveloped capsids, with a diameter of 30-32 nm and an RNA genome of 6.7-10.1 kb inside the capsid. The capsid is made of 60 identical protomers with icosahedral symmetry. Protomers of most picornaviruses are composed of four capsid proteins, with three surface proteins (1B, 1C and 1D) and one internal protein (1A). Other picornaviruses only have three capsid proteins (1AB, 1C and 1D), *i.e.* 1AB remains uncleaved. Proteins 1A, 1B, 1C, 1D and 1AB are also named VP4 (viral polypeptide 4), VP2, VP3, VP1 and VP0, respectively[29]. High-resolution structures[31-39] have revealed that proteins VP0, VP1, VP2 and VP3 all have a core β-barrel structure made of 8 β-strands, and often termed a viral 'jelly-roll' due to its topology. The external loops connecting the β-strands vary in length, composition and configuration among different genera of picornaviruses, causing either pronounced or relatively smooth surface relief and thickness of the capsid wall, which determine antigenicity and receptor usage of the viruses.

Vertebrates, including mammals and birds, are the natural hosts of picornaviruses, although closely related viruses infect insects[40-42]. Picornaviruses can cause a wide range of animal and human diseases, such as paralysis, hepatitis, meningitis, foot and mouth disease (FMD) and HFMD, however the pathogens cannot be characterized by any particular illness. Transmission of picornaviruses is mainly by fecal-oral, fomite (contaminated inanimate objects) or airborne routes[29].

1.3 *Enterovirus genus*

Enterovirus is a genus in the family *Picornaviridae* and viruses of this genus are

responsible for a range of human and mammalian diseases. Coxsackieviruses, echoviruses, enteroviruses, rhinoviruses and polioviruses all belong to this genus. The name *Enterovirus* describes the ability of many to replicate in the intestinal tract (*Entero* is from Greek *enteron*, which means intestine). This genus includes more than 200 enterovirus serotypes to date, which are divided into 15 species by the ICTV, including *Enterovirus A* to *L* and *Rhinovirus A* to *C*, based on phylogenetic analysis of VP1[29]. Poliovirus is the prototype virus for the *Enterovirus* genus and the *Picornaviridae* family.

Crystal structures of many *enteroviruses*[31,43-46] have revealed that viruses in this genus tend to have large VP1, VP2 and VP3, with long loops connecting β-strands. As a result, the capsid wall of *enteroviruses* is thicker than other viruses in the family. Virions of *enteroviruses* can be converted to expanded A-particles of 135S (S, sedimentation coefficient) by a variety of treatments in the absence of receptors (*e.g.* heating or the addition of certain neutralizing antibodies)[47]. The virions of most enterovirus species are stable in acid condition, while those of the rhinovirus species are unstable below pH 5-6[48,49]. Due to recombination and low-fidelity replication, enteroviruses have a high mutation rate, which helps them adapt to various environments[50,51]. Enteroviruses are usually transmitted through the fecal-oral route. The majority of enterovirus infections are asymptomatic, however more than 80 enteroviruses in this genus can cause disease in humans[52,53]. These can cause a wide range of human diseases, including the common cold, myelitis, myocarditis, mild meningitis, encephalitis and conjunctivitis[54,55]. Poliomyelitis caused by poliovirus was once the most significant enterovirus-related disease, but because poliovirus is nearly

eradicated[56], EV71 is thought to now be the most important neurotropic enterovirus.

1.4 Enterovirus 71

1.4.1 Epidemiology

EV71 belongs to species A of the *Enterovirus* genus. The first recorded case of EV71 was in California in 1969[57], however now EV71 has been implicated in outbreaks of HFMD throughout the world, especially in Asia-Pacific region (Figure 1.5)[20,58-61]. Indeed EV71 has been one of the most common causes of HFMD[19,20]. It can induce severe cardiac or CNS complications thus contributes to most severe HFMD cases and HFMD-related deaths. HFMD is the most common clinical manifestation of EV71 infection but not all patients infected by EV71 will develop HFMD.

EV71 can be transmitted by fecal-oral transmission, or by direct contact[62]. Humans are the only known hosts of EV71. EV71 mainly infects infants and children younger than five years old, but there have also been cases of adults infected by EV71[20,57]. EV71 infection usually causes mild complications and is self-limited, however sometimes it can induce serious life-threatening illness. Severe infection may involve the brain, causing encephalitis, or the meninges causing meningitis due to the ability of EV71 to replicate in cells of the CNS and induce inflammation. Severe infection of EV71 can also affect the heart, causing high blood pressure or irregular heart rate[60,63,64]. Children younger than 5 years old have a higher risk to develop a severe EV71 infection. EV71 and other enteroviruses are cytopathic so many of the acute diseases are a result of direct tissue destruction. Evidence of nonlytic viral spread of enteroviruses has also

been reported[65] and enterovirus infection may be associated with chronic diseases such as type 1 diabetes[66], myasthenia gravis[67] and post-polio syndrome[68].

1.4.2 Virion morphology

EV71 is a non-enveloped virus with an icosahedral capsid (~30 nm in diameter). Since it is non-enveloped, the EV71 capsid is resistant to alcohol, organic solvents and freezing. The capsid is composed of 60 copies of each of the four structural proteins: VP1 (33 kDa), VP2 (30 kDa), VP3 (26 kDa) and VP4 (7.5 kDa). One protomer of EV71 consists of one copy of each of these four proteins and 60 protomers form the capsid. VP1~3 share a common architecture and are arranged with pseudo T=3 icosahedral symmetry to form the outer surface of the capsid. they are also involved in immune response interactions. VP4 and the N-termini of VP1, VP2 and VP3 are located on the inner surface of the viral capsid and the single-stranded RNA genome lies inside the capsid (Figure 1.2.A). The narrow vertex of the VP1 is positioned near the 5-fold axis whilst the narrow vertices of VP2 and VP3 are arrayed near the 3-fold axis. The N-terminus of VP4 is located near the 5-fold axis and the C-terminus of VP4 near the 3-fold axis[31,32,69].

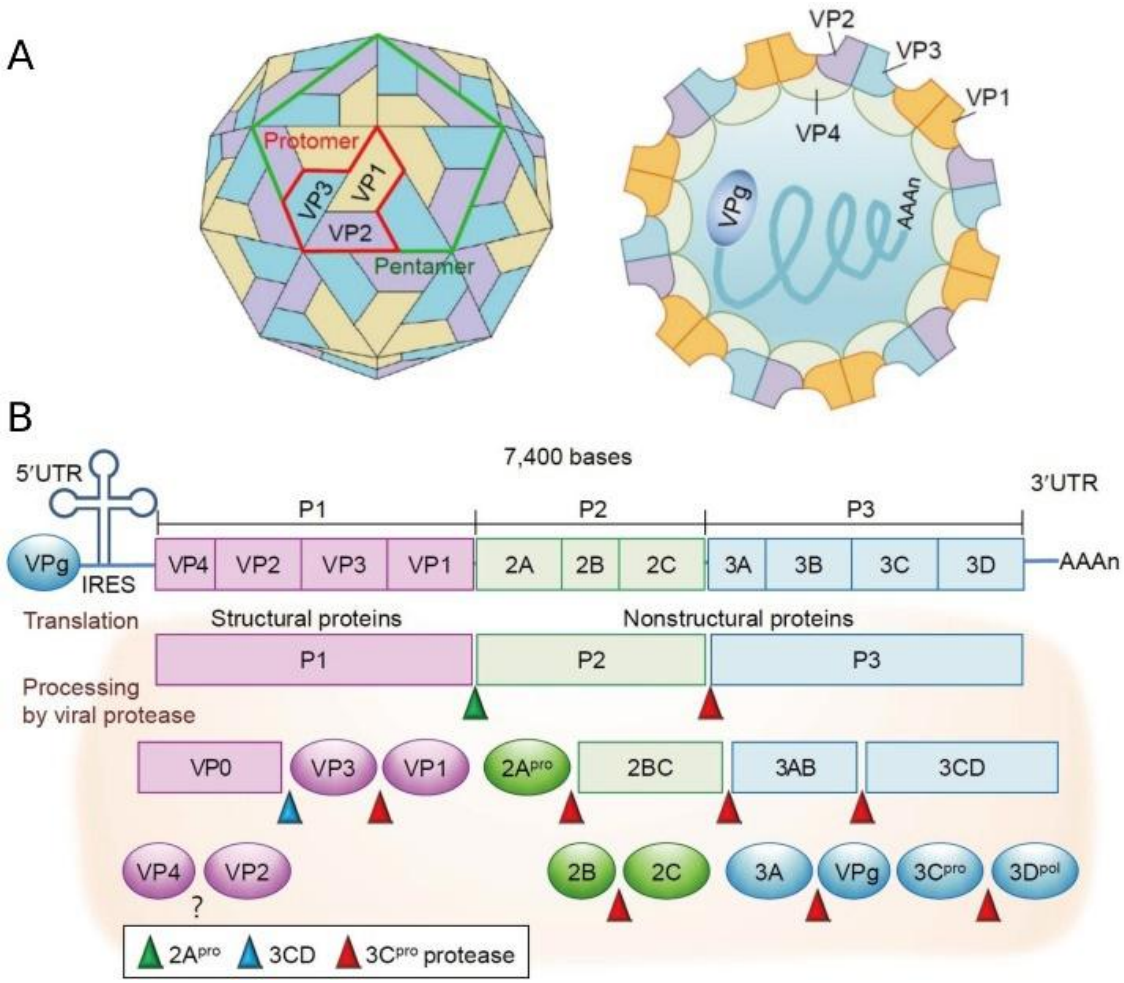

Figure 1.2 Virion and genome of EV71 (**A**) Structure of EV71 virion. One protomer of EV71 consists of one copy of VP1~4, 5 protomers form a pentamer and 60 protomers form the whole capsid in an icosahedral symmetry. VP1, VP2 and VP3 form the outer surface and VP4 is located on the inner surface of the capsid. The RNA genome, with virus genome-linked protein (VPg) and a poly-A tail, lies inside the virion. (**B**) Genome and polyprotein cleavage of EV71. EV71 RNA genome consists of VPg, a 5' untranslated region (UTR), a single open reading frame (ORF), a 3' UTR and a poly-A tail. The ORF is translated into a polyprotein, then cleaved into 11 viral proteins by proteases $2A^{pro}$, $3C^{pro}$ and $3CD^{pro}$ (Adapted from Yi *et al*, 2017[70]).

As noted above, VP1, VP2 and VP3 share an identical core structure called a jelly-roll. This is formed by two twisted β-sheets: one is made up of four β-strands B, D, G and I

(arranged in the order BIDG) while the other consists of strands C, E, F and H (arranged in the order CHEF). There are seven loops connecting these eight β-strands. Four short loops (BC, DE, FG and HI) connect these strands at the narrow vertex, while three long loops (CD, EF, GH) locate at the other end. These structural subunits are "wrapped" in this way to form a compact barrel shape (Figure 1.3.B).

VP4 is the smallest structural protein of EV71 and unlike VP1–3, has a more extended conformation. The N-terminus of VP4 is covalently attached to a myristic acid, which may function in capsid assembly or in the entry of virus into cells[71]. The N-terminal 20 amino acids of VP4 are highly conserved[72].

On the surface of the EV71 capsid, there is a circular deep depression called the "canyon" around each 5-fold axis of symmetry (Figure 1.3.A and C). The canyon region was initially proposed to be the binding site of IgG-like receptors of picornaviruses[73]. Receptors of a number of enteroviruses, including poliovirus receptor (Pvr) of poliovirus 1, intercellular adhesion molecule 1 (ICAM-1) of coxsackievirus A24 (CV-A24), human neonatal Fc receptor (FcRn) of echovirus 6, coxsackievirus- adenovirus receptor (CAR) of coxsackievirus B3 (CV-B3), do indeed bind at the canyon region of the viral capsid[74-77]. The “puff” region in VP2, which is the most prominent surface loop, forms the southern rim of the canyon. The “knob” is the largest surface protrusion in VP3 (Figure 1.3.C). Below the floor of the canyon, there is a hydrophobic pocket within the VP1 beta barrel. Hydrophobic compounds, called pocket factors can bind inside these pockets, which can enhance the stability of the capsid and inhibit uncoating (Figure 1.3.C).

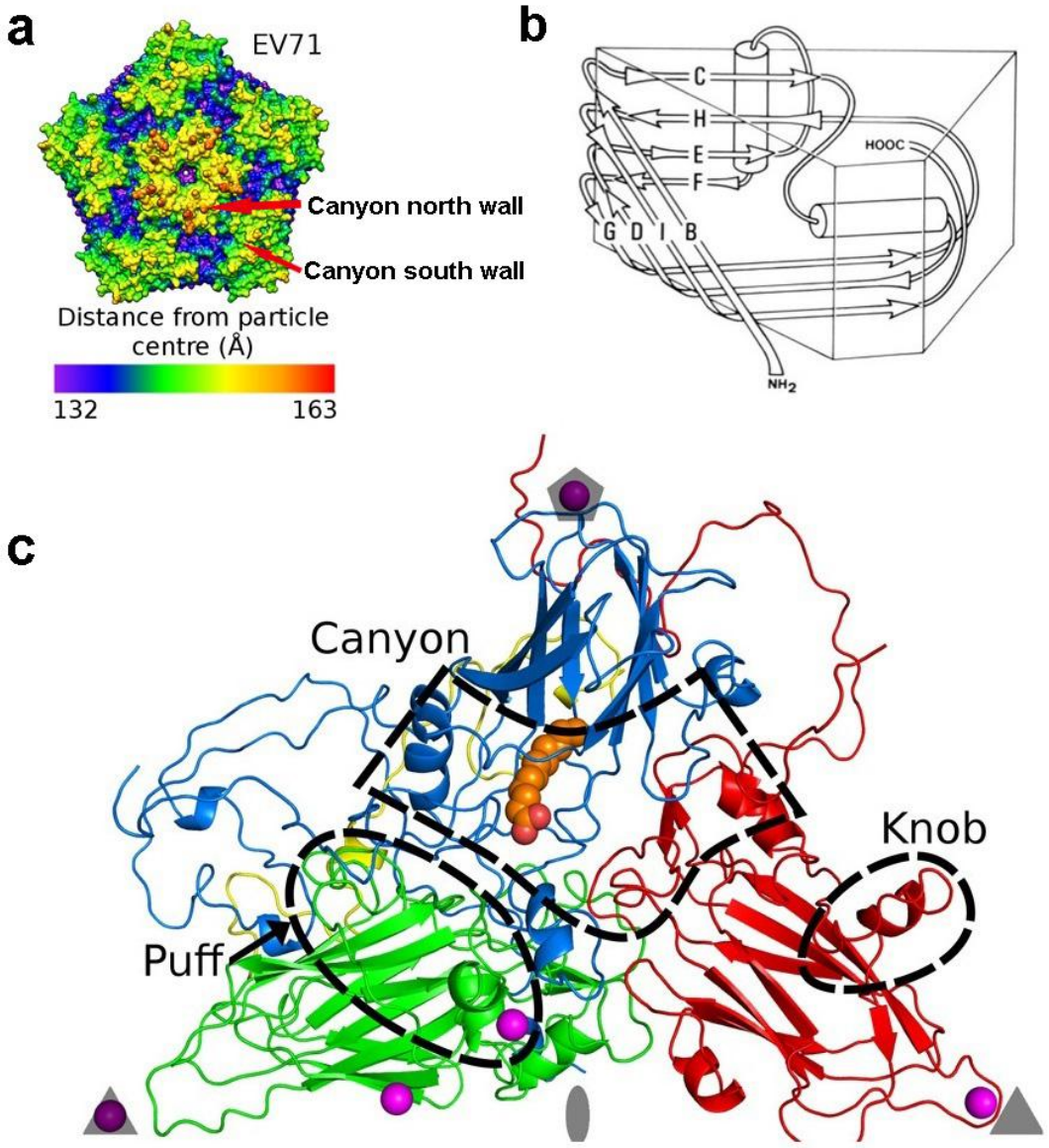

Figure 1.3 Morphology of EV71. (**a**) Surface representation of a pentamer of EV71. The surface is colored based on the distance from the particle center. The blue areas are canyon regions. The red arrows indicate the south and north wall of the canyon. (**b**) Geometric representation of the core structure of EV71 VP1, VP2 and VP3. (**c**) Cartoon diagram of an icosahedral asymmetric unit of EV71 showing VP1 (blue), VP2 (green), VP3 (red), VP4 (yellow), calcium ions (magenta) and the pocket factor (orange). The 2-fold, 3-fold and 5-fold axis are indicated with ellipse, triangle and pentagon, respectively. The canyon region, the puff region and the knob region are indicated by dashed lines (Adapted from Plevka *et al*, 2012[32] and Levy *et al*, 2010[78].

1.4.3 Genome and viral proteins

EV71 has a positive-sense single-stranded RNA genome. The genome has a length of about 7.4 kb. VPg, also known as EV71 3B protein, is covalently attached to the 5' end of the genome, followed by a 5' untranslated region (UTR), a single open reading frame (ORF), a 3' UTR and a poly-A tail[79]. VPg is involved in the RNA synthesis by acting as a primer for the RNA polymerase $3D^{pol}$. The 5' UTR of EV71 contains a cloverleaf structure which has six stem-loop structures (I–VI)[80,81]. Stem-loops I, II and IV are involved in viral RNA synthesis[82]. Stem-loops II–VI contain the internal ribosome entry site (IRES), which induces translation of viral protein in a cap-independent manner[83]. The 3' UTR is highly conserved and contains three putative stem-loop structures (X, Y, and Z)[84]. Together with the poly-A tail, the 3' UTR is implicated in both translation and replication of EV71[85-87].

The ORF encodes a large polyprotein. This polyprotein contains one structural (P1) and two nonstructural (P2 and P3) regions, which are eventually cleaved into 11 mature proteins (4 structural proteins VP1 to VP4 from the P1 region, and seven non-structural proteins: 2A to 2C from the P2 region, and 3A to 3D from the P3 region). This cleavage process is mediated by the virus-encoded proteases, $2A^{pro}$, $3C^{pro}$ and $3CD^{pro}$. $3C^{pro}$ is responsible for most of the cleavages[88]. The process of the cleavage is illustrated in Figure 1.2.B.

$2A^{pro}$ is a cysteine protease that catalyzes the first cleavage reaction in all enteroviral polyproteins. It is responsible for the cleavage between the P1 and P2 regions of the polyprotein (Figure 1.2.B). $2A^{pro}$ is also involved in viral RNA replication[89,90].

$3C^{pro}$ cleaves itself from the P3 region, and then cleaves P2 and P3 to produce viral proteins (Figure 1.2.B). $3C^{pro}$ is also involved in the initiation of viral RNA synthesis with its RNA-binding activity[91]. $3C^{pro}$ plays a major role in the switch from viral translation to RNA replication. Both $2A^{pro}$ and $3C^{pro}$ have been reported to cleave host translation initiation factors (eIFs) to inhibit host translation and thus favor IRES-dependent viral protein production[83,92]. $2A^{pro}$ and $3C^{pro}$ can also disrupt macromolecule trafficking through alterations to the nuclear pore complex that promote viral replication[93,94]. $3C^{pro}$ also inhibits host antiviral immune responses by cleaving a number of different cellular molecules including TIR-domain-containing adaptor-inducing interferon-β (TRIF) and interferon regulatory factor 7 (IRF7)[95,96] and $2A^{pro}$ inhibits the immune response by targeting the mitochondrial anti-viral signaling (MAVS) protein[97]. $2A^{pro}$ is also able to reduce interferon receptor 1 (IFNR1) level to inhibit the cellular type I IFN (interferon) response, although the host cells can sense EV71 infection and stimulate IFN-α/β production[98]. $2A^{pro}$ and $3C^{pro}$ also induce apoptosis of host cells through multiple pathways to cause cell death[99-101]. Induction of apoptosis in neural cells has been demonstrated to be an important cause of EV71-induced cell damage in the CNS of infected mice[102].

$3CD^{pro}$ is the precursor of $3C^{pro}$ and the RNA polymerase, $3D^{pol}$. $3CD^{pro}$ cleaves the polyprotein at the site between VP0 and VP3 (Figure 1.2.B). $3CD^{pro}$ is also a component of the viral replication complex for RNA synthesis[103,104].

Protein 2B of EV71 forms ion channels in the plasma membrane to increase the membrane permeability of cells[105]. 2B is also able to induces cell apoptosis[106]. $2C^{ATPase}$

functions as both an RNA helicase unwinding RNA helices and an ATP-independent RNA chaperone[107]. It can also inhibit the host antiviral response by inhibiting NF-κB activation[108]. Protein 3A facilitates viral RNA replication by interacting with acyl-coenzyme A-binding domain-containing 3 (ACBD3) of the host cell to recruit phosphatidylinositol-4-kinase IIIβ (PI4KB) to the genome replication sites[109]. 3A can also interact with the Golgi protein ACBD3 to facilitate EV71 replication[110]. 3B is also known as VPg, and as noted above acts as a primer for the RNA polymerase $3D^{pol}$ in the initiation of RNA synthesis[80]. $3D^{pol}$ is an RNA-dependent RNA polymerase (RdRp) and is also involved in VPg uridylation[111] and activation of host cell inflammatory response[112].

1.4.4 Phylogenetic relationship

As the most exposed capsid protein of EV71, VP1 is targeted by host neutralizing antibodies, placing it under constant immune selective pressure, and so the sequence of VP1 is usually used for determining evolutionary relationships between EV71 strains. EV71 has only one serotype which were initially classified into 3 genotypes (A, B and C), based on the VP1 gene sequence. Recently three additional genotypes including the Indian D genotype[113] and 2 African genotypes (E and F) have been identified[114,115]. The EV71 prototype strain, BrCr-CA-70, isolated in California in 1970, was for a long time the only member of genotype A[57]. Recently, several more strains of genotype A have been identified[116]. Genotype B and C each have 5 sub-genotypes ((B1–B5 and C1–C5), containing most of the EV71 strains identified. Phylogenetic relationships among VP1 sequences of different EV71 strains are shown in Figure 1.4, which reveal the significant diversity existing among EV71 isolates[117].

Note however that between different genotypes the amino acid sequence variation is only of the order of 5%[118].

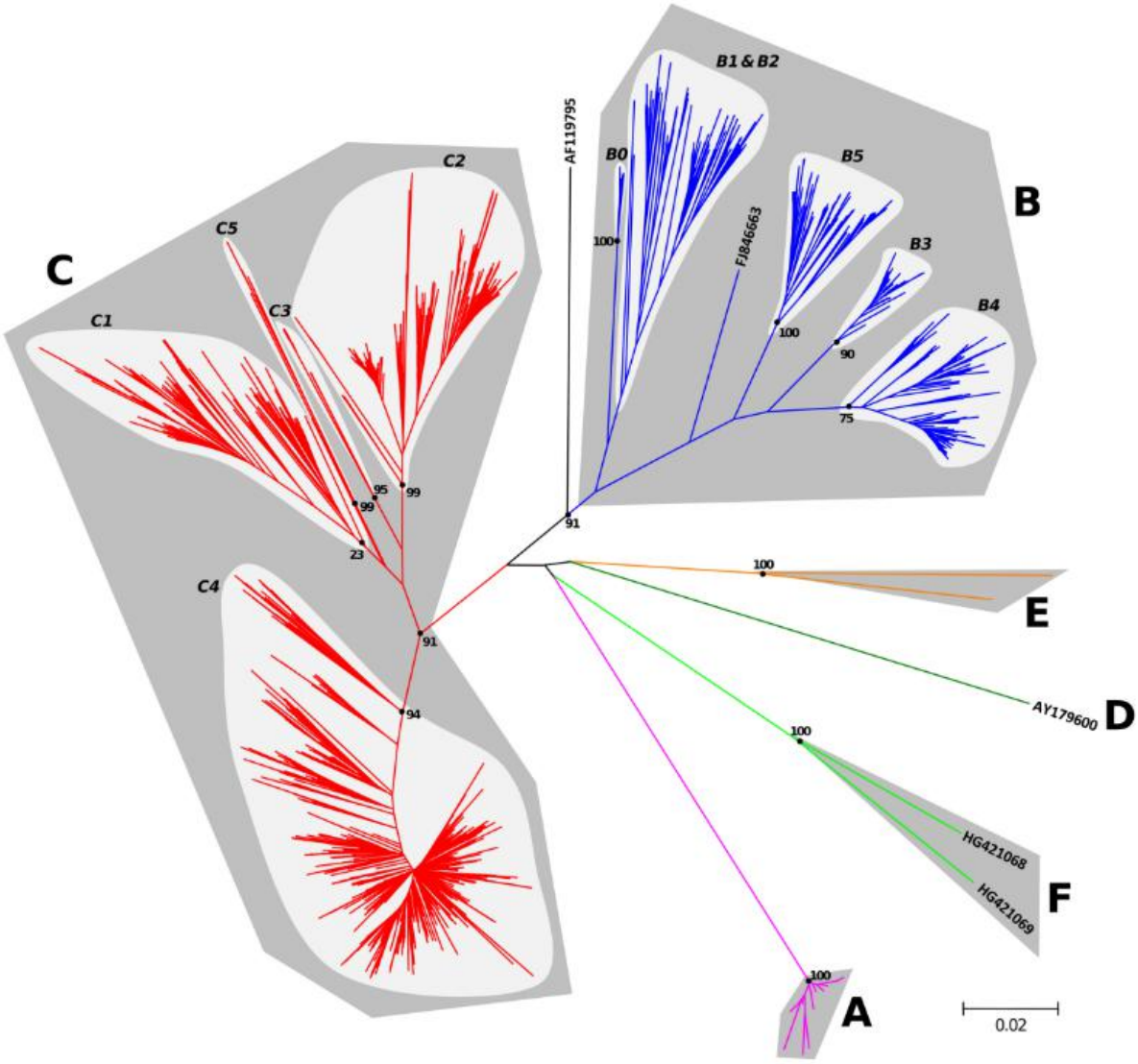

Figure 1.4 Phylogenetic relationships among VP1 sequences of different EV71 strains (Adapted from Bessaud *et al*. 2014[117]).

1.4.5 Evolution and recombination

RNA viruses, including EV71, generally have much higher mutation rates than DNA viruses[119], because RNA replication of these viruses is directed by RNA polymerases

which lack the proof-reading and error-correction abilities of DNA polymerases and so cannot get rid of misincorporation of nucleotides during chain elongation. The mutation rate of EV71 can be as high as one mutation per newly synthesized RNA molecule[120]. This high rate of mutation together with environmental selective pressures contribute to the rapid evolution of EV71. The high mutation rate of EV71 increases its ability to adapt to different environments and may underlie the diversity in its receptor usage (See chapter 1.4.6.1).

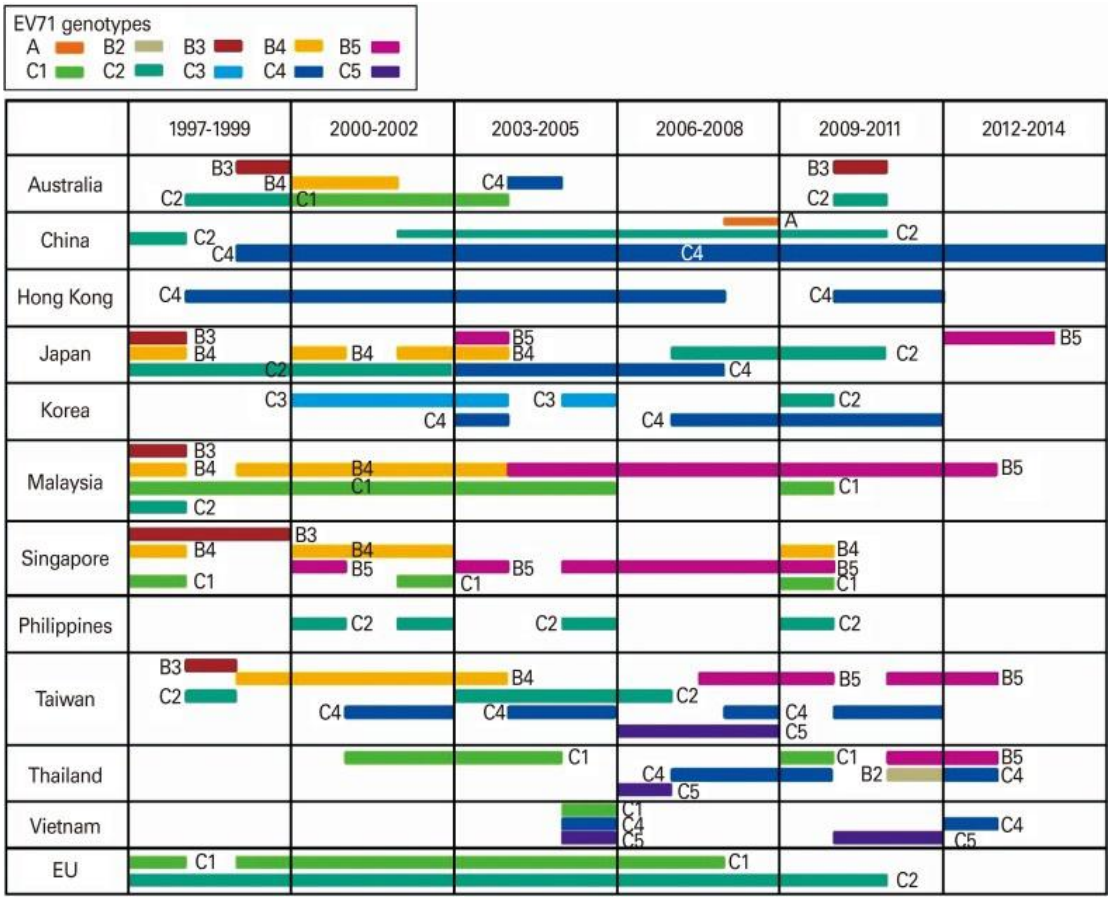

Figure 1.5 EV71 genotypes that caused epidemics in Asia-Pacific regions and Europe (EU) between 1997 and 2014. EU has data from Austria, Germany, the Netherlands, and the United Kingdom. Data in 2012-2014 may be incomplete due to unreleased information (Adapted from Yi *et al*.2017[70]).

In addition to the high rate of mutation, recombination between EV71 strains and with other enteroviruses also generates genetic variability in viral populations. Recombination is the process in which viral genomes exchange nucleotide sequences to produce a new genome molecule. Recombination happens when at least two viral genomes co-infect the same host cell. It is believed recombination occurs by a copy-choice mechanism, where the RNA polymerase switches from one template molecule to another in the process of negative strand RNA synthesis[121]. EV71 often circulates together with CVA-16 and other enteroviruses in epidemics. As a result, intratypic and intertypic recombination caused by their co-infection has been observed[122-126]. Due to recombination, a circulating EV71 strain can rapidly evolve into several different genotypes[127] or a major genotype of enterovirus 71 in outbreaks of HFMD in one area can be replaced by a new one in a short time[118].

1.4.6 Life cycle

The infection cycle of EV71 begins with viral capsid interaction with the host cell receptor(s), followed by internalization and the release of its genome into the cytoplasm. The presence of an internal ribosome entry site (IRES) substitutes for a cap structure and allows the genome to serve as mRNA and be translated into a single polyprotein by the viral polymerase. Structural and non-structural viral proteins are then generated from this polyprotein. The viral genome also serves as a template for viral replication, catalyzed by the viral polymerase. Thereafter, viral RNAs are packaged by capsid proteins to generate new infectious virions. Eventually the apoptotic pathway is initiated and the host cell lysed to release viral particles (Figure 1.6, 1.10)[128]. Since EV71 has a genome with a constrained size, which only encodes

11 proteins, it needs to exploit and manipulate the cellular machineries of the host cell, including cellular trafficking, metabolism and immunity-related functions, for most parts of its life cycle.

1.4.6.1 Attachment

Attachment to the cellular receptor is the first step in the life cycle of EV71. Identified receptors for EV71 include scavenger receptor class B member 2 (SCARB2 or LIMP-2)[129], P-selectin glycoprotein ligand-1 (PSGL-1 or CD162)[130], cyclophilin A (CypA)[131], sialylated glycans[132], vimentin[133], nucleolin[134], annexin II[135], heparan sulfate glycosaminoglycan[136] and dendritic cell-specific ICAM-grabbing non-integrin (DC-SIGN)[137]. EV71 uses different receptors to infect the host cell depending on the virus strain and cell line[132,137,138]. For example, some EV71 strains cannot use PSGL-1 as a receptor for infection[130], however, expression of human SCARB2 enables replication of all tested EV71 strains in unsusceptible cell lines[129]. SCARB2[139,140], CypA[141], vimentin[142], nucleolin[143], annexin II[144], and heparan sulfate[145] are widely expressed in many cell lines. PSGL-1 is expressed in cells of lymphoid, myeloid, and dendritic lineage and in some nonhematopoietic cells[140,146]. Sialylated glycans are abundant on gastrointestinal and respiratory epithelial cells[132]. DC-SIGN is found mainly on immature dendritic cells[147].

SCARB2 and CypA can bind EV71 and induce uncoating of EV71 virions at acid pH[131,148]. Nucleolin alone can mediate binding and infection of EV71 to host cells[134]. PSGL-1 is an attachment receptor of EV71 but cannot induce uncoating. That's why SCARB2 transgenic mice are susceptible to EV71 clinical strains, but PSGL-1 transgenic mice are not[149-151]. Uncoating of EV71 via all the other receptors mentioned

above has not been reported, so these receptors may only be attachment receptors of EV71. Attachment receptors that cannot initiate uncoating of EV71 may act as co-receptors to trigger endocytosis or tether the virus to the membrane and then deliver the virus to SCARB2 or other uncoating receptors for subsequent infection processes[152].

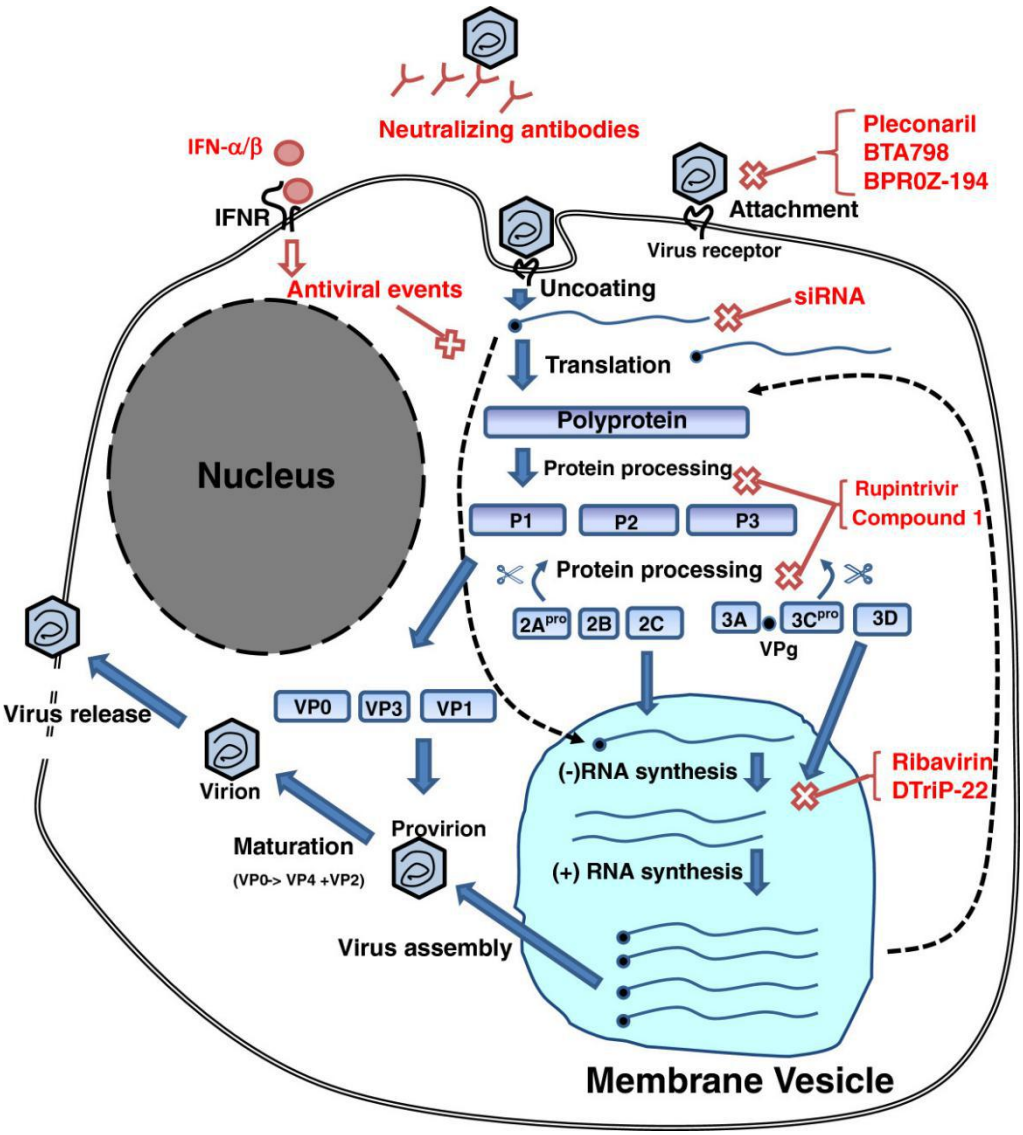

Figure 1.6 Overview of EV71 life cycle. The life cycle and antiviral drugs targeting different steps of EV71 life cycle are shown (Adapted from Yi *et al*. 2012[128]).

SCARB2 is thus the pivotal receptor for EV71 and it plays a key role in attachment, internalization and pH dependent uncoating of EV71[129,148,153]. SCARB2 is a type III membrane glycoprotein with N- and C-terminal transmembrane helices and two short intracellular tails[154]. It is widely expressed in many human organs and cell types, including the CNS and it acts as the mannose-6-phosphate-independent trafficking receptor for beta-glucocerebrosidase. Its 400-residue luminal domain is glycosylated with at least nine potential N-linked glycosylation sites (Figure 1.7). SCARB2 is mainly present in lysosomes and is transferred via vesicular transport to the plasma membrane through endosomes[139,155].

When SCARB2 is present at the plasma membrane, it is capable of capturing the EV71 virion. The binding of EV71 to cells expressing SCARB2 can be inhibited by an anti-SCARB2 antibody, however, binding to RD cells cannot be inhibited completely even at the highest concentration of anti-SCARB2 antibody, indicating SCARB2 is not the only uncoating receptor for EV71[129]. Unlike many other picornavirus receptors, SCARB2 does not have an immunoglobulin (Ig)-like motif. Thus, SCARB2 is different to most picornavirus receptors and may not use the canyon region as its binding site[156].

Some researchers have studied the nature of the EV71-SCARB2 interaction. Residues of SCARB2 involved in EV71-SCARB2 interaction were predicted to be located in residues 142 to 204 of SCARB2, where there are two helices α5 and α7[156,157]; while residues of EV71 implicated in interaction with SCARB2 are more distributed, mainly in areas near the canyon region[148,157,158]. However, there was no structure of the EV71-

SCARB2 complex reported to provide accurate and direct interaction information. SCARB2 is also a cellular receptor for coxsackievirus A7, A14 and A16[129,153].

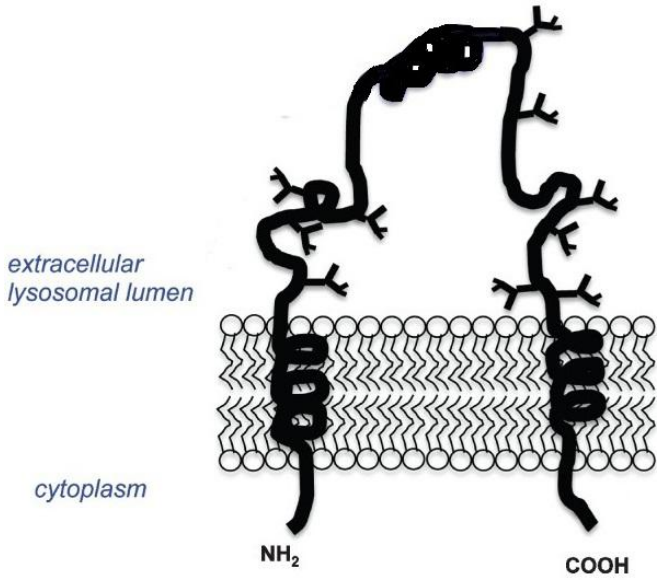

Figure 1.7 Representation of SCARB2. SACRB2 is a membrane glycoprotein with N- and C-terminal transmembrane helices and two short intracellular tails. Its luminal domain is heavily glycosylated (Adapted and modified from Schwake *et al*. 2013[159]).

1.4.6.2 Internalization

Virus releases its genome into the cytoplasm of the host cell after attachment to a cellular receptor. Many viruses utilize endocytosis for this entry process. Endocytosis is a form of active transport which generates small (60-120 nm) membrane vesicles that transport molecules from the plasma membrane into the cytoplasm of eukaryotic cells[160]. Viruses can utilize multiple endocytosis pathways for internalization based on the cell type and the receptors on the host cell surface. The internalization process of EV71 is via clathrin-dependent endocytosis with SCARB2 or caveolae-dependent endocytosis with PSGL-1[161,162].

In clathrin-mediated endocytosis, the binding of the EV71 virion to host receptor SCARB2 triggers the binding of an adaptor protein to the receptor cytoplasmic tail. Clathrin binds to adaptor proteins and clusters on the inner surface of the plasma membrane. Then the membrane is bent to form a clathrin-coated pit. EV71, bound to its receptor SCARB2, sinks into this pit and the clathrin-coated vesicle is separated from the plasma membrane with the help of dynamin and internalized into the cytoplasm. Finally, the coating proteins are released, the naked vesicle is formed and the vesicle containing the EV71-SCARB2 complex is transported to an early endosome for subsequent genome-release process of the virus[160,161] (Figure 1.8).

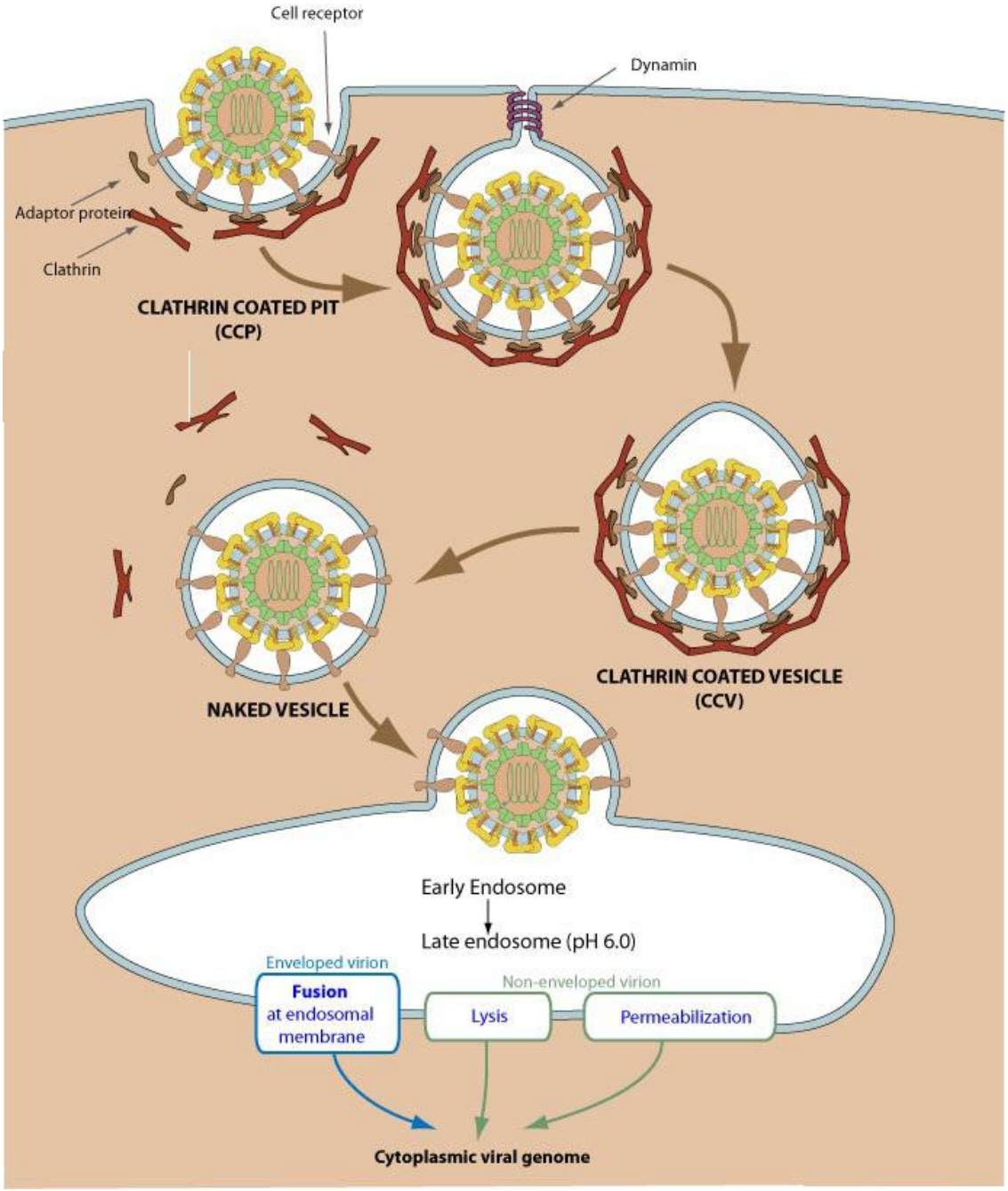

Figure 1.8 Virus internalization by the host cell via clathrin-mediated endocytosis. Once bound to the virus, the receptor interacts with an adaptor protein. The binding of the adaptor protein with clathrin induces the clustering of clathrin and the forming of a pit on the plasma membrane. Virus, bound to its receptor, is internalized into the cytoplasm. After the coating proteins are released, the vesicle is transported to an early endosome for subsequent genome-release process of the virus (Adapted from viralzone.expasy.org).

Caveolin-mediated endocytosis is a clathrin-independent endocytic process. This is not a constitutive process but only occurs when the cell is stimulated. The binding of the EV71 virion to PSGL-1 triggers the clustering of cholesterol enriched lipid rafts to form a 50-70 nm, bulb-shaped plasma membrane invaginations called caveolae. The structural backbone of caveolae is formed by caveolin and cavin. The caveolae is then internalized into the cytoplasm. Then EV71 may be delivered from PSGL-1 to SCARB2 or other uncoating receptors and transferred to the early endosome. The vesicle then fuses with the endosome for genome release of EV71 after caveolin and cavin are released[163-165](Figure 1.9).

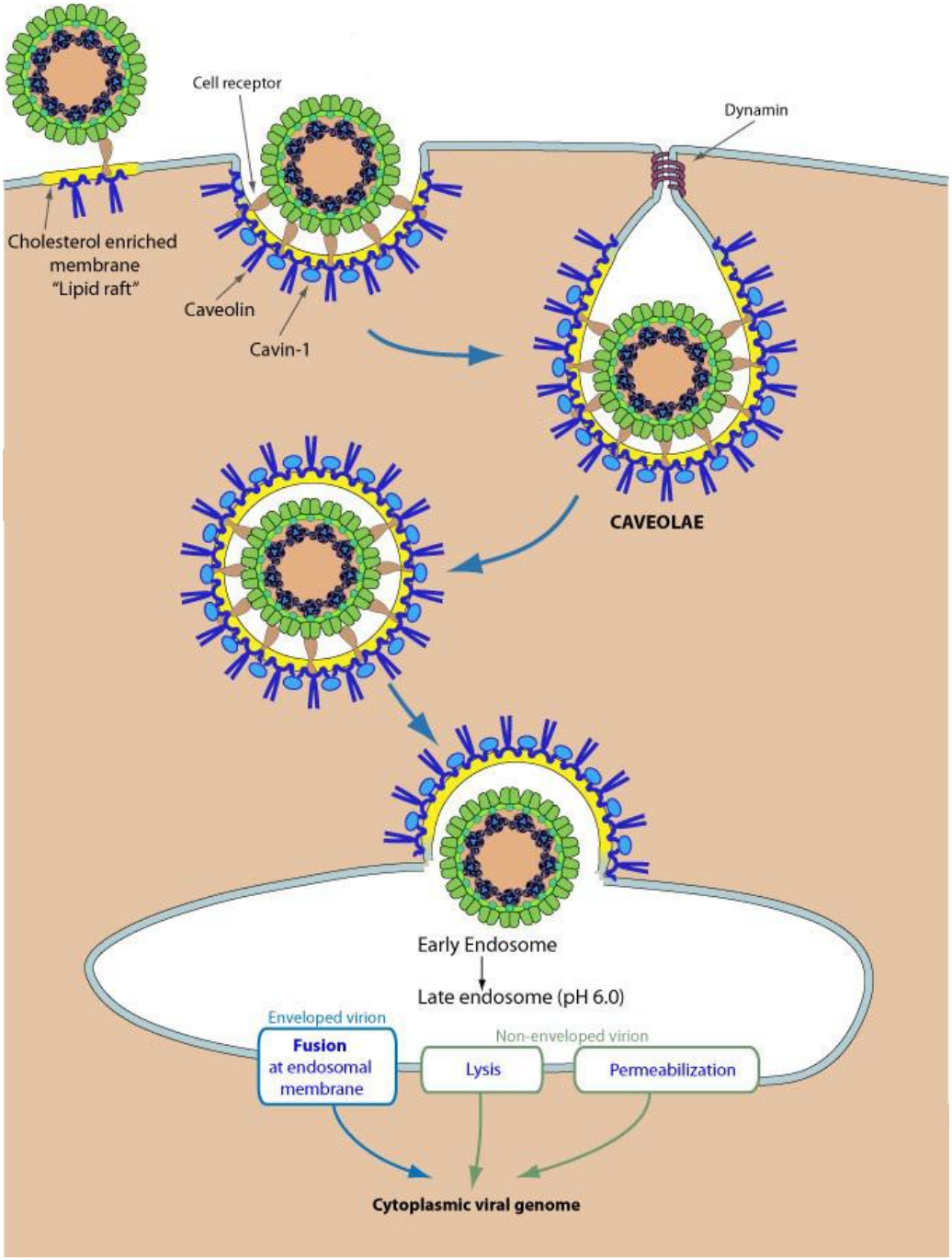

Figure 1.9 Virus internalization by the host cell via caveolin-mediated endocytosis. Virus binding with receptor triggers the clustering of lipid rafts to cause invagination of the plasma membrane and the caveolae is formed. Caveolin and cavin consist the backbone of the caveolae. The caveolae is internalized and delivered to the early and late endosomes and virus releases its genome into the cytoplasm (Adapted from viralzone.expasy.org).

1.4.6.3 Uncoating

There are two different proposed uncoating mechanisms of enterovirus. One is the receptor-induced uncoating process. After internalization and entering the late endosome, helices α4 and α5 of SCARB2 undergo conformational change due to the low pH in the endosome[148,161]. This induces a series of structural changes to EV71. The pocket factor bound in the VP1 pockets of the EV71 capsid is released, which induces conformational changes to the particle, resulting in the formation of an expanded intermediate particle (or A particle)[166], with externalization of VP4 and the N terminus of VP1 through either the channel at the base of the canyon or the channel at the 2-fold axis, which are thought to make a pore in the cell membrane or endosomes. Through the channel at the 2-fold axis and this pore, the viral genome is injected into the cytoplasm of the host cell (Figure 1.10)[31,148]. In this process, EV71 undergoes irreversible conformational changes, resulting in a shift in the sedimentation coefficient, from the mature virion (160S) to the A particle (135S) and eventually to the empty particle (80S).

Uncoating of EV71 therefore requires release of the pocket factor from the capsid, this is usually a natural lipid, thought to be predominantly sphingosine, bound in a hydrophobic pocket within the VP1 jelly-roll. Release of the pocket factor from the pocket makes the EV71 capsid less stable. A number of pocket factor-like compounds, for example, WIN 51711 and NLD, which bind tightly to the capsid, were developed to stabilize the capsid and prevent uncoating[167,168]. Soluble forms of SCARB2 can also induce uncoating of EV71[148,169].

Uncoating of EV71 also requires acidic pH conditions. It is proposed that Histidine 150 of SCARB2 acts as a pH sensor and at acidic pH, protonation of this residue induces the re-arrangement of helix α5[148]. Since helix α5 was reported to be involved in EV71-SCARB2 interaction[156,157], this conformational change of SCARB2 may trigger structural changes in the EV71 virion, dislodge the pocket factor and lead to uncoating.

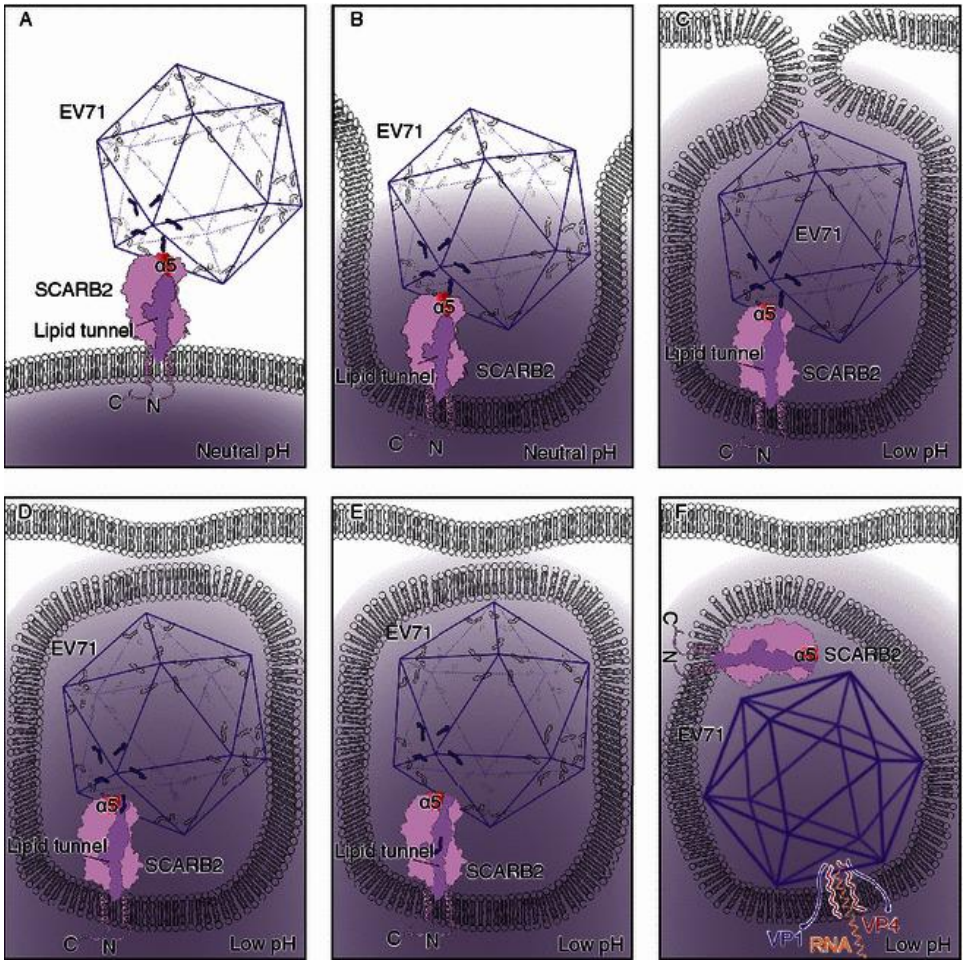

Figure 1.10 Cartoon of EV71 cell entry process mediated by SCARB2 (**A**) EV71 recognizes and interacts with SCARB2. (**B**) Internalization. (**C**) SCARB2 undergoes conformational change under acid pH. (**D**) Release of pocket factor from EV71 capsid. (**E**) EV71 undergoes conformational changes. (**F**) Release of genome (Adapted from

Dang *et al*. 2014[148]).

Another proposed uncoating model of enterovirus was based on the asymmetric single-particle reconstruction of echoviruses. Buchta *et al.* discovered that particles of echovirus exposed to pH 6.0 lost one, two, or three adjacent pentamers without the presence of an uncoating receptor. The large openings in the capsid of echovirus may enable the release of the genome[170].

1.4.6.4 Viral replication and assembly

The replication and assembly of EV71 occur within the cytoplasm of the host cell. During the initiation of viral RNA replication, $3D^{pol}$ performs the uridylylation of VPg to form VPg-pUpU[171,172]. Viral positive sense RNA is used as the template to synthesize negative sense RNA, which, in turn, is used as the template to produce positive sense RNA. In this process, the synthesis of both negative and positive RNA strands is primed by VPg-pUpU[111].

The translation of EV71 is initiated in a cap-independent manner from the internal ribosome entry site (IRES), which is located at the 5′-UTR of EV71 genome[83]. From the IRES, the ribosome moves along the RNA, translating it into a large polyprotein. In this process, EV71 and other picornaviruses recruit IRES trans-acting factors (ITAFs) from the host cell to mediate IRES-dependent translation. The P1 region of the polyprotein is cleaved to produce proteins VP0, VP1 and VP3. One copy of these three capsid proteins together form a protomer and five protomers combine to form a pentamer. There are two proposed models about how the pentamers form a virion. In model one, 12 pentamers first assemble into an empty procapsid, then the genome is

inserted to get a provirion. In the other model, which is currently more generally accepted, 12 pentamers condense around the viral genome to form a provirion. After cleavage of VP0 into VP2 and VP4, the provirion is changed into the native virus, with rearrangement of the capsid proteins and increased stability of the virion[173,174] (Figure 1.11). The last step in the life cycle of EV71 is to release the mature virus from the host cell.

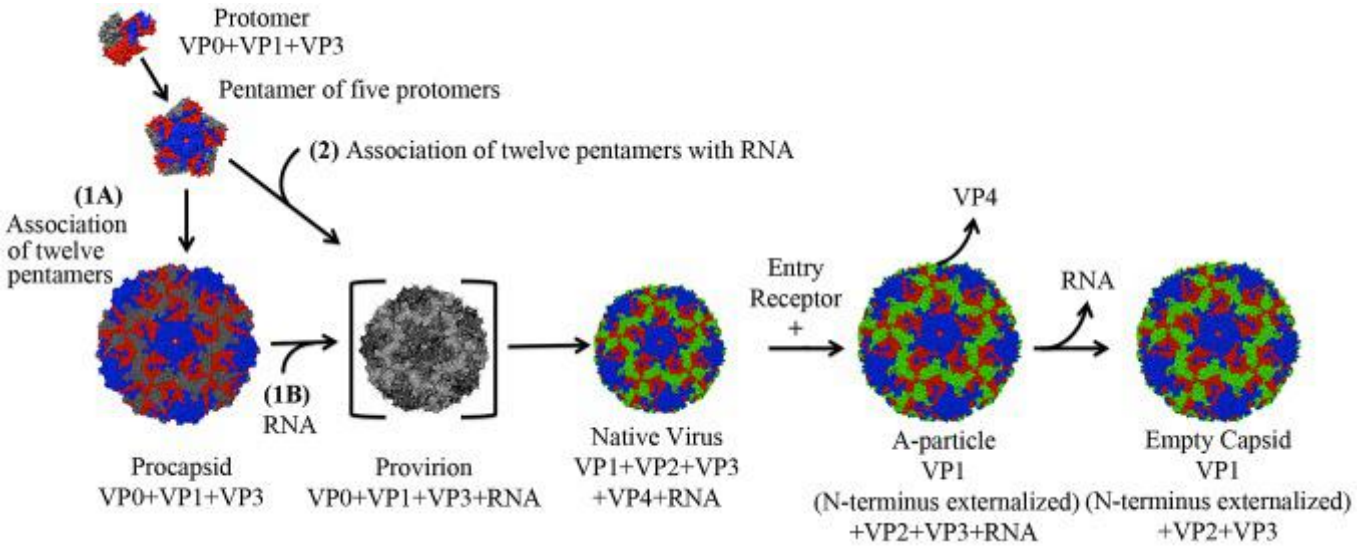

Figure 1.11 Assembly and uncoating of human enterovirus. VP0, VP1, and VP3 form a protomer. Five protomers form a pentamer. One possible pathway to form a provirion is first 12 pentamers form an empty procapsid (1A) then genome RNA is inserted to the procapsid to get a provirion (1B). Another pathway is 12 pentamers condense around the viral genome to form a provirion (2). After cleavage of VP0 into VP2 and VP4, provirion is changed into native virus. Once bound with its uncoating receptor and internalized, virus expels VP4 to produce the A-particle exposing the N-terminus of VP1 and leading to the release of genome leaving an empty capsid (Adapted from Shingler *et al*. 2013[174]).

The mechanism of virus release is still unclear. Some studies have reported that EV71 can manipulate host cell autophagy and the autophagy might contribute to viral

replication and release of infectious EV71 particles[175,176]. $2A^{pro}$ and $3C^{pro}$ of EV71 can also lead to apoptosis in a wide range of cells, result in apoptotic cell death and release of EV71 virions.[99,177-182].

1.4.7 Anti-EV71 drugs and vaccine

There is no specific treatment for EV71 infection so far. Target-based drug design and compound library screenings have been used to find potential anti-EV71 drugs. The targets for structure-based anti-EV71 drugs design include viral structural proteins, viral non-structural proteins, UTR of viral RNA and host proteins involved in virus infection (Figure 1.6).

WIN 51711[167] and NLD[168] are two compounds targeting VP1 of EV71, which can replace the natural pocket factor in the hydrophobic pocket of VP1, stabilize the EV71 virion and restrict the capsid dynamics necessary for genome release. Pleconaril, pirodavir, lactoferrin BPR0Z-194 and BTA798, also targeting VP1, show antiviral activity against enterovirus 71 infection[183-186]. However, since the structural proteins of enteroviruses are generally less conserved than the non-structural proteins, capsid-targeting compounds may quickly lead to the generation of drug-resistant virus.

Non-structural proteins $2A^{pro}$ and $3C^{pro}$ have highly conserved structures among different enterovirus serotypes, making them ideal targets for broad-spectrum antivirals. Rupintrivir and Compound 1, two human rhinovirus (HRV) inhibitors, which target the substrate-binding pocket of HRV 3C protein, was found to effectively inhibit EV71 replication in a similar way[187,188]. Another compound, peptidyl aldehyde

NK-1.8k, which also targets 3C, can inhibit EV71 and EV68 infections[189,190]. Another anti-EV71 compound, AN-12-H5, targets viral protein 3A and/or 3AB[191]. There are also inhibitors targeting the RNA-dependent RNA polymerase (3D protein) of EV71, these include aurintricarboxylic acid[192], the broad-spectrum anti- RNA virus drug, ribavirin[193] and the nucleoside analog, DTriP-22[194].

Host proteins involved in the EV71 life cycle are also potential targets for anti-EV71 drugs, although there is the risk of cellular toxicity. Kaempferol is able to inhibit enterovirus 71 replication and IRES activity through acting on FUBP and HNRP proteins[195]. GW5074, a Raf-1 inhibitor, was reported to influence EV-71 viral yield[196].

Other treatments, like short interfering RNA (siRNA) and type I interferons are also able to inhibit EV71 infection[197-199]. High mutation rates make it is difficult to produce long-term effective drugs and vaccines to prevent diseases caused by RNA viruses[200]. To deal with the drug resistance problems, combination treatments are likely to be effective. Ideally, drugs used for combination therapy should utilize different mechanisms to inhibit the virus.

Vaccination is the most efficient strategy to prevent EV71 infection. From 2015, the China Food and Drug Administration (CFDA) has approved two inactivated EV71 vaccines to control outbreaks of EV71[201]. However, since these whole-virus vaccines are made from EV71 genotype C4, there are still challenges for the worldwide use of the vaccine because of the diversity of EV71 strains in different regions and the change of the circulating strain in each region[79,202-205]. Monovalent EV71 vaccine also

cannot protect children from infection by other enteroviruses, including CVA16[206,207].

1.5 Anti-EV71 human mAbs from EV71-infected children

Our collaborator, Dr. Kuan-Ying Arthur Huang, has isolated a large number of monoclonal antibodies from recovered patients. Detailed analysis of these reveals 13 unique neutralizing anti-EV71 monoclonal antibodies from four EV71-infected children (donors C, Z, M, Y). Antibody 38-1-10A was from donor C and antibody 34-1-6D from donor Z. Antibodies from donor M were named 16-X-X and antibodies from Y were named 17-X-X. These children were infected by EV71 strain 12-96015 (genotype B5) and developed symptoms of hand-foot-and-mouth disease[208].

Escape mutants of two strains of EV71, 12-96015 (genotype B5) and 11-96023 (genotype C4), were selected by in vitro propagation with 13 antibodies. Amino acid substitutions at different residues of the EV71 capsid were identified. The locations of these substitutions were classified into five groups: canyon northern rim, canyon floor, canyon southern rim, 2-fold plateau and 3-fold plateau. These substitutions affect the interaction between antibodies and EV71 capsid and based on the locations of these substitutions, the binding areas of antibodies on EV71 capsid were roughly predicted as: antibody 16-2-2D, 16-2-11B and 16-3-3C bind around canyon northern rim, antibody 16-2-8C, 16-2-9D and 16-2-12D around canyon floor, 17-2-2B and 16-3-10B around canyon southern rim, 17-1-12A and 17-2-12A around the 2-fold axis, and 16-3-4D and 34-1-6D around the 3-fold axis (Table 1.2 and Figure 1.12)[208].

mAb	EV71 strain 12-96015	EV71 strain 11-96023
16-2-2D	VP1 Y106H	VP1 S241F
16-2-8C	VP1 T232A	VP1 T232A
	VP1 M229I	
16-2-9D	VP1 D110G	VP1 T232A
	VP1 T232A	VP1 K162E
	VP1 M229K	
16-2-11B	VP1 N104K	VP1 S241F
16-2-12D	VP3 F186L	VP1 D110G
	VP1 T232A	
16-3-3C	VP1 D164G	VP1 D164N
		VP1 D164V
16-3-10B	VP1 N282D	VP2 T139I
		VP2 T141M + VP1 S283F
17-2-2B	VP2 T141I	VP2 T141M
	VP1 S283F	
17-1-12A	VP2 K149E	VP2 E88V
	VP2 K149G	VP2 K149E
17-2-12A	VP3 K144E	Not done
	VP2 K149E	
	VP3 K144E + VP3 T148A	
16-3-4D	VP3 E81G	Not done
34-1-6D	VP3 E81G	VP3 E81K
	VP2 D225N	
38-1-10A	VP3 E81K	VP2 E72K
	VP3 S74F	

Table 1.2 Substitutions of amino acids on the EV71 capsid causing escape mutants of EV71 strain 12-96015 and 11-96023 from anti-EV71 human mAbs. For some mAbs,

there were more than one escape mutant caused by substitutions of amino acids for one EV71 strain[208]. Escape mutants of mAb 38-1-10A is from unpublished data.

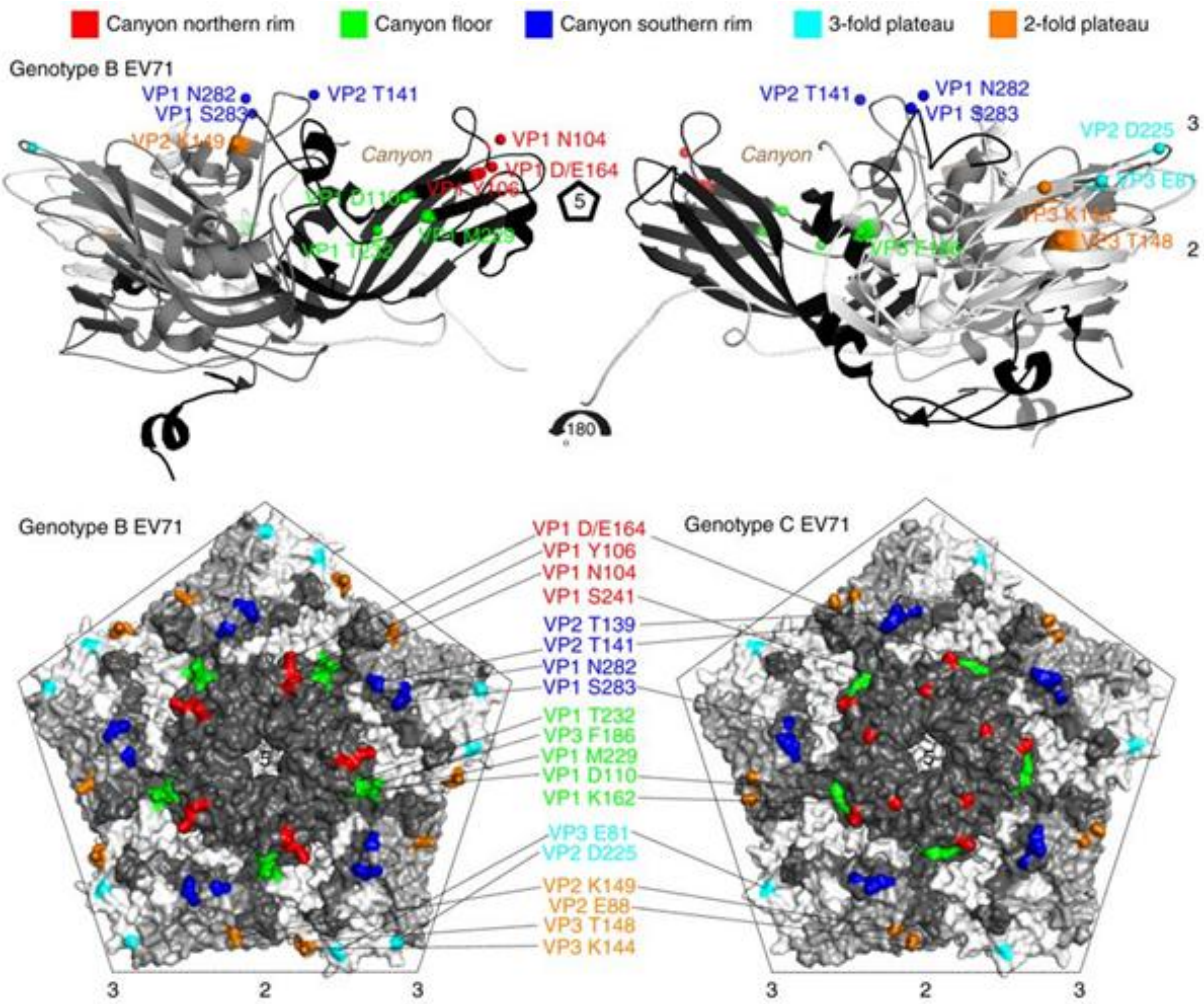

Figure 1.12 The locations of substitutions of amino acids on the EV71 capsid causing escape mutants of EV71 strain 12-96015 and 11-96023 from anti-EV71 human mAbs[208].

Antibodies targeting these different areas show different neutralizing potency and breadth against EV71. The canyon-floor and canyon-rim binders (except 16-3-3C) exhibit broad and potent neutralizing abilities against EV71 isolated in 1998–2016,

including genotype B4, B5, C4 and C5, while some 2-fold-plateau and 3-fold-plateau binders are weak and cannot neutralize EV71 genotype C strains (Table 1.3)[208].

Table 2 Neutralization of EV71 clinical strains in 1998–2016

Year	1998	1998	1999	1999	2000	2001	2002	2003	2004	2005	2007	2008	2010	2011	2012	2014	2015	2016	2016
Strain name	98-2086	98-4215	99-1691	99-3351	00-2278	01-1437	02-2792	03-70576	04-72232	05-1956	07-72043	08-96016	10-96018	11-96023	12-96015	14-51389	15-921	16-50444	16-50555
Genotype	C2	C1	C2	B4	B4	B4	B4	B4	C4	C4	C5	B5	C4	C4	B5	B5	B5	C4	C4
Representative mAbs[a]																			
16-3-10B	−	+	−	+++	++	++	++	+++	+++	++	++	++++	++++	++++	++++	+++	++++	+++	+++
16-2-8C	−	−	−	++	+++	++	+++	++	++	++	+++	++++	++++	++++	++++	+++	++++	+++	+++
16-2-11B	−	+	−	++	++	++	++	++	+++	++	++	+++	+++	+++	+++	++	++	++	++
17-2-2B	−	+	−	++	++	++	++	++	++	++	++	++	++	+++	+++	+++	+++	+++	+++
16-2-9D	−	−	−	++	++	++	++	++	+++	+++	++	++	++	+++	+++	++	++	++	+++
16-2-12D	−	−	−	++	++	+++	+++	++	+	++	++	++	+++	++	++	++	++	++	++
16-3-3C	−	+	−	−	−	−	−	−	++	++	++	++	++	++	++	++	++	++	++
16-2-2D	−	−	−	++	++	++	+++	++	+	++	+	++	++	++	+++	+++	++	++	++
17-1-12A	−	−	−	++	++	++	++	++	+	++	+	++	++	++	+++	+++	++	++	+++
34-1-6D	−	−	−	++	++	++	++	+	+	+	+	++	+	++	++	+	+	+	+
16-3-4D	−	−	−	+	+	+	+	+	−	−	−	+	−	−	++	++	+	−	−
17-2-12A	−	−	−	+	+	+	+	+	−	−	−	+	−	−	+	+	+	−	−
Controls[b]																			
17-1-10B	−	−	−	−	−	−	−	−	−	−	−	−	−	−	−	−	−	−	−
16-2-1A	−	−	−	−	−	−	−	−	−	−	−	−	−	−	−	−	−	−	−
D9 Serum	1:16	1:32	1:16	1:512	1:512	1:1024	1:512	1:512	1:256	1:512	1:512	1:2048	1:1024	1:4096	1:4096	1:2048	1:2048	1:1024	1:1024

Table 1.3 Neutralizing abilities of different antibodies against EV71 clinical strains in 1998-2016. Concentrations at which 100% neutralization was achieved: ++++, < 100 ng/ml; +++, 0.1 - 1 μg/ml; ++, 1- 10 μg/ml; +, 10 - 50 μg/ml; −, no neutralization. (Adapted from Huang *et al*. 2017[208]).

Antibodies binding at different sites do not compete with each other, while antibodies targeting the same site cross-inhibit each other in the binding assay, suggesting that the footprints of these antibodies overlap significantly. Pre- and post-attachment neutralization assays of these antibodies were also performed. Pre-attachment assays suggested that canyon-rim binders had stronger potency than other antibodies (Table 1.4)[208].

EC_{50} (μg ml^{-1})	16-2-11B	16-2-2D	16-3-3C	16-2-8C
Pre-	0.28	0.27	0.28	0.27
Post-	7.55	38.53	7.61	109.78
	16-2-9D	16-2-12D	17-2-2B	16-3-10B
Pre-	1.41	1.5	0.05	0.05
Post-	99.96	>400	1.39	1.41
	16-3-4D	34-1-6D	17-1-12A	17-2-12A
Pre-	4.37	1.43	1.42	234.24
Post-	>400	267.15	58.83	292.77

Table 1.4 Pre- and post-attachment neutralizing abilities of anti-EV71 antibodies. EC_{50}: 50% effective concentration[208].

1.6 Aims

One aim of this study is to determine the cryo-EM structure of the complex of EV71 with SCARB2, to show how EV71 interacts with its cellular receptor SCARB2 and possibly clarify the mechanism of SCARB2 induced uncoating process of EV71. Another aim is to solve cryo-EM structures of EV71-Fab complexes, and crystal structures of the Fabs, to help understand the neutralization mechanisms of different human monoclonal anti-EV71 antibodies and precisely map the epitopes onto the EV71 capsid. These findings can help us understand more about the attachment, entry

and antigenicity of EV71 and may contribute to future drug design and antibody therapy development for EV71.

Chapter 2

Material and methods

2.1 Production of SCARB2 and anti-EV71 Fabs

2.1.1 Preparation of Fabs from IgGs

Purified anti-EV71 IgGs were provided by our collaborator Dr. Arthur Huang[208] and Fab fragments of 16-2-9D and 17-2-2B were prepared from IgGs by papain digestion using the Pierce Fab Preparation Kit (Thermo Fisher Scientific), following the manufacturer's instructions. These Fab fragments were used for subsequent crystallization trials.

2.1.2 DNA synthesis

An expression plasmid for SCARB2 provided by Dr. Yuguang Zhao[209] was used directly for protein expression of SCARB2. This plasmid encodes the luminal domain of SCARB2 containing residues 28–431, with a C-terminal 6*His tag.

Sequences of all the 13 anti-EV71 human mAbs were provided by our collaborator Dr. Arthur Huang. These sequences were analyzed using online tool IMGT/V-QUEST (http://www.imgt.org) to identify the V-D-J-region of the heavy chains and the V-J-region of the light chains of all the antibodies. Based on the analysis, antibodies 17-1-12A, 34-1-6D and 38-1-10A have kappa light chains while all the other 10 antibodies have lambda light chains.

Different DNA tags were added to the 5' and 3' sequences of the V-D-J-region DNAs and V-J-region DNAs, based on the type of the chains (Appendix table 1). With these tags, these DNAs can be cloned into our expression vectors, using a method called Ligation Independent Cloning[210]. For each antibody, the V-D-J-region DNA encodes

the heavy chain variable domain (VH) and the V-J-region DNA encodes the light chain variable domain (VL). Once the VH or VL DNA is cloned to its corresponding vector, the VH or VL DNA and the constant domain DNA in the vector form an integrated gene, which encodes a fusion protein of the heavy or light chain of one Fab. When the heavy and light chains of one Fab are expressed together, they form a complex, which is the whole Fab protein.

These DNAs were then ordered online. Gene blocks of three Fabs (Fabs 16-2-9D, 17-2-2B and 38-1-10A) were ordered from Integrated DNA Technologies and DNAs of all the other 10 Fabs cloned in plasmids were ordered from Geneart. Gene blocks can be cloned directly into expression vectors, while all the other DNAs of Fabs inserted in commercial plasmids need to be amplified by PCR first and then cloned into expression vectors.

2.1.3 PCR

PCR was performed to amplify the DNAs ordered from Geneart. The sequences of primers for amplification of VH or VL DNAs are indicated in Appendix table 1. The reaction mix for the PCR was set up as below:

Template plasmid (~100 ng/μL)	1 μL
Forward primer (10 μM)	1 μL
Reverse primer (10 μM)	1 μL
2x Phusion Flash Master Mix (F-548L, Thermo Scientific)	25 μL
Sterile water	22 μL

Table 2.1 The reaction mix for PCR

The thermal cycling parameters were as follows:

Step 1: 98 °C, 10s

Step 2: 98 °C, 1s

Step 3: 60 °C, 5s

Step 4: 72 °C, 30s

Go to Step 2, run the cycle for 29 times

Step 5: 72 °C, 2 min

Step 6: 4 °C, hold

2.1.4 Analysis of PCR products

When the PCR completed, 5 μL of each PCR product was mixed with 2.0 μL 5x DNA Loading buffer (0.25% (w/v) Bromophenol Blue in 30% v/v glycerol). Then samples were loaded onto a 1.6% TBE agarose gel. The gel was run at 100 V for about 30 minutes and then imaged to check that the PCR was successful.

2.1.5 Purification of PCR products

AMPure magnetic beads (Agencourt/Beckman) were used to purify PCR products. 90 μL magnetic beads were mixed with the PCR reaction, after which a SPRIPlate 96R magnet (Beckman) was used to separate beads from solution. DNAs were bound to these beads and the solution was discarded and the beads were washed twice with 200 μL 70% ethanol. The ethanol was removed and the beads dried at room temperature. Then 30 μL of elution buffer (10 mM Tris, pH 8.0) was added and the eluent separated from the beads. A gel was run as before to check the purification had worked.

2.1.6 Restriction digestion of vectors

Vector pOPINhuVH was used for the expression of heavy chains of all the Fabs, pOPINhuVL_kappa for the kappa light chains of Fabs 17-1-12A, 34-1-6D and 38-1-10A, and pOPINhuVL_lambda for the lambda light chains of the other 10 Fabs. All three vectors were provided by Prof. Ray Owen[211]. In the expression vector pOPINhuVH, there are DNA sequences encoding a C-terminal 6*His tag, which was used for subsequent protein purification.

For linearization, ~5 μg of each vector was mixed with 10 μL of digestion buffer (10x stock) and 50 units of one restriction enzyme, with ultrapure water added to make the volume up to 100 μL. After the first digestion reaction ran for one hour, 10 μL of digestion buffer, 50 units of another restriction enzyme and water were added to the previous mixture to run the second digestion reaction (total volume 200 μL). The enzymes, temperatures and time duration used for each digestion steps for the three vectors are indicated in Table 2.2. All enzymes and buffers were from New England Biolabs (NEB). The digestion buffer used for digestion step 2 of vector pOPINhuVL_kappa was NEB Buffer 3.1, while the buffer used in all the other steps was NEB CutSmart Buffer.

Vector	Digestion (step1)	Digestion (step2)
pOPINhuVH	KpnI, at 37 °C, for 1h	SfoI, at 37 °C, for 1 h
pOPINhuVL_lambda		AvrIIg, at 37 °C, for 1 h
pOPINhuVL_kappa		BsiWI, at 55 °C, for 15 min

Table 2.2 Restriction digestion reactions of expression vectors

After restriction digestion, the linearized vectors were purified from the solution using DNA-binding spin columns from the Qiagen DNA Extraction Kit, following the manufacturer's instructions. Digested vectors were eluted in 50 µL elution buffer (10 mM Tris, pH 8.0, Qiagen) and the concentrations of digested vectors were measured using a Nanodrop spectrophotometer (Thermo Fisher Scientific). The vector stocks were normalized to 100 ng/µL before being stored in aliquots at –20 °C.

2.1.7 Ligation independent cloning reactions

The fusion reactions were performed using a Quick-fusion cloning kit (Bimake.com), following the manufacturer's instructions. Reactions were set up as Table 2.3. The molar ratio of tagged DNA: linearized vector was about 2:1. The fusion reactions were run at 42 °C for 30 min.

Linearized pOPIN vector (100 ng/µL)	1 µL
Tagged DNA (12 ng/µL)	1 µL
Fusion enzyme (Bimake.com)	0.5 µL
Buffer (5x stock, Bimake.com)	2 µL
Sterile water	5.5 µL

Table 2.3 The mix for fusion reactions

2.1.8 *E. coli* cell transformation

OmniMaxII competent *E. coli* cells (Invitogen) were thawed on ice (50 µL/tube). 3 µL of the In-Fusion reaction from the previous step was transferred to each tube containing competent cells. These tubes were then incubated on ice for 30 min before heating for 30 seconds at 42 °C. 300 µL of Power Broth (AthenaES) was added to

each tube and tubes were incubated at 37 °C for 1 h. 5 μL of cells were then transferred to LB agar plates (with 50 μg/mL Ampicillin, 0.02% X-Gal and 1 mM IPTG) for overnight incubation at 37 °C.

2.1.9 Colony picking and cell culture

1.2 mL of Power Broth supplemented with 50 μg/mL Ampicillin was added to each well in a 96-deep-well plate. Individual colonies with white color were picked into each well and the filled plates shaken in an incubator at 200 rpm at 37 °C overnight.

2.1.10 Plasmid mini-preps

The deep-well plate was centrifuged at 6,000 g for 15 minutes to harvest cells. Then a Qiagen Bio-Robot was used to perform plasmid mini-preps following the manufacturer's protocols.

2.1.11 Construct verification

PCR was performed to validate the recombinant plasmids prior to DNA sequencing. The reactions were set up as below:

2x Phusion Flash Master Mix (Thermo Scientific)	12.5 μL
Sterile water	9.35 μL
Forward primer (100 μM)	0.15 μL
Reverse primer at (10 μM)	1.5 μL
Recombinant plasmid (~100 ng/μL)	1.5 μL

Table 2.4 The reaction mix of PCR for construct verification

The thermal cycling parameters were as follows:

Step 1: 98 °C, 10s

Step 2: 98 °C, 1s

Step 3: 60 °C, 5s

Step 4: 72 °C, 30s

Go to Step 2, run the cycle for 29 times

Step 5: 72 °C, 2 min

Step 6: 4 °C, hold

Then 6.5 µL of each PCR product was loaded on a 1.6% agarose gel, in order to check if the fusion reactions had been successful. If verified by DNA gel, the recombinant plasmids were sent to SourceBioscience or GATC Biotech for sequencing for final validation.

2.1.12 Transient expression screen

First, between 150,000 and 200,000 HEK 293T cells were put into each well of a 24-well plate and incubated at 37 °C overnight in 1 mL Dulbecco's modified Eagle's medium (DMEM, Sigma-Aldrich) supplemented with 10% fetal bovine serum (FBS, Gibco), 1% 100x L-glutamin (Gibco) and 1% 100x MEM with non-essential amino acids (MEM + NEAA, Gibco). Then the medium was removed and 1 mL of DMEM with 2% FBS, 1% 100x L-glutamin and 1% 100x MEM + NEAA was added. In another plate, 1 µg of plasmid DNA was mixed thoroughly with 60 µL serum-free DMEM and 2 µL of 1.33 mg/mL GeneJuice. Reactions were incubated for 10 min at room temperature and then the DNA/GeneJuice cocktail was added to the cells in each

well. Then cells were incubated at 37 °C for 3 days.

Three days later, the supernatant was separated from the cells by centrifugation at 2,000 g for 20 min. Then 20 μL of supernatant were mixed with 20 μL of SDS-PAGE sample buffer and anti-His monoclonal antibody was used to run a Western Blot, comparing the expression yield with known positive and negative controls, to validate the expression of anti-EV71 Fabs.

2.1.13 DNA Mega-prep for large-scale transfection

Constructed plasmids were transformed into *E. coli* DH5α competent cells (Invitogen) as above. Then single colonies were picked, cultured in 10 mL LB medium supplemented with 50 μg/mL Ampicillin. Cells for each plasmid were added to 2.5 L of LB medium (with 50 μg/mL Ampicillin) to grow at 37 °C for 16 to 18 hours in an incubator shaking at 180 rpm. Cells were harvested by centrifugation at 6,000 g for 15 min. The DNA was purified from the cells following the protocol of HiSpeed Plasmid Giga EF Kits (Qiagen).

2.1.14 Transfection and protein expression

First, HEK293T cells were cultured in T175 flasks (Greiner Bio-One) with 30 mL DMEM supplemented with 10% FBS, 1% 100x L-glutamin and 1% 100x MEM + NEAA. When confluent, cells in each flask were transferred into one CellMaster cell culture roller bottle (Greiner Bio-One) and cultured at 37 °C for 3 days, in 200 mL DMEM supplemented with 10% FBS, 1% 100x L-glutamin and 1% 100x MEM + NEAA. Then the old medium was discarded and new medium (200mL DMEM

supplemented with 2% FBS, 1% 100x L-glutamin and 1% 100x MEM + NEAA) was added to each roller bottle. At the same time, for each Fab, 1mg of the heavy chain plasmid, 1 mg of the light chain plasmid, 200 mL DMEM and 4mL 1 mg/mL polyethylenimine (PEI) were mixed and incubated at room temperature for 10 minutes to prepare the transfection cocktail. Then 50 mL of transfection cocktail was transferred to each of four roller bottles and the cells were cultured at 37 °C for 4 days before harvest.

For the expression of SCARB2, the same procedure was followed, except that 0.5 mg of SCARB2 plasmid was added in each roller bottle for transfection.

2.1.15 Dialysis

Cells were harvested by centrifugation at 1,500 g for 20 min. Then the supernatant was filtered using a 0.45 μm filter to remove cell debris. The supernatant of each Fab (about 1 L) was put into a dialysis tube (Medicell Membranes Ltd) to perform dialysis in 15 L of buffer (23.2 mM Na_2HPO_4, 1.7 mM NaH_2PO_4, 250 mM NaCl, pH 8.0). The buffer was stirred gently at 4 °C. After one day, the old buffer was removed and new buffer was added and dialysis continued for a further day. The supernatant was then filtered again.

2.1.16 Affinity purification

5 mL nickel columns (GE) were used for affinity purification of SCARB2 and Fabs. Filtered supernatant was pumped through the nickel column for protein binding. Then 50 mL of washing buffer (20 mM Tris, pH8.0, 200 mM NaCl, 30 mM imidazole) was

used to wash the column followed by 5 mL of elution buffer (20 mM Tris, pH8.0, 200 mM NaCl, 500 mM imidazole) to elute the target protein. All the proteins purified in this step were examined by SDS-PAGE.

2.1.17 Gel filtration

Gel filtration chromatography was performed on an AKTA purifier system (GE Healthcare) with a Hiload 16/60 Superdex 75 column (GE Healthcare). The buffer used for gel filtration was 20 mM Tris, pH 8.0, 200 mM NaCl. UV (280nm) absorbance was used to detect the presence of protein. The flow rate was set at 1 mL/min and fractions of 0.5 mL were collected in tubes. Fractions showing high 280nm absorbance were harvested and 15 μL of these samples were mixed with 5 μL 4x protein loading buffer respectively to run SDS-PAGE, in order to assess the homogeneity of protein. Then all fractions containing pure Fab or SCARB2 were mixed and concentrated to about 200 μL using a 10 kD centrifugal filter (Sigma-Aldrich). Concentrated Fabs were stored at 4 °C. All purified proteins were examined by SDS-PAGE (see Figure 4.1).

2.2 Fab crystallization and crystal structure determination

2.2.1 Fab crystallization

The concentrations of Fabs used for crystallization ranged from ~10 to 50 mg/mL (Table 4.1). Crystals were grown in CrystalQuick X plates (Greiner Bio-One) at room temperature using the sitting-drop vapour-diffusion method with 100 nL Fab plus 100 nL precipitant dispensed with a Cartesian robot[212,213]. Buffers for crystallization screening were supplied by Hampton Research. Images were taken using a Rock

Imager 1000 (Formulatrix, Bedford, USA). Crystals appeared after a few days to a few months. Different conditions, including a range of pH, concentrations of precipitant, of protein and of salts were tried to optimize crystals. Micro-seeding was also applied to improve crystal quality of Fabs 17-1-12A and 16-2-12D[214]. Affinity and gel-filtration purified Fab 16-3-3C were further purified by ion exchange chromatography and then crystallized to get good crystals.

2.2.2 X-ray data collection

Good crystals were soaked in reservoir solutions containing 25% (v/v) glycerol or ethylene glycol, and then frozen in liquid nitrogen and taken to Diamond Light Source (Didcot, Oxford) for X-ray diffraction data collection. Diffraction images were collected at I03, I04 or I24 beamlines[215] using a Pilatus 6M detector (Dectris, Baden-Daettwil), with 0.01-0.1 s exposure time, 100% beam transmission and different wavelengths (For more information regarding data collection, see Appendix tables 2 to 5).

2.2.3 Structure determination

X-ray diffraction data were indexed and integrated with Xia2[216,217] and data of the same Fab with the same space group and similar unit cell parameters were merged together to get high multiplicity. Data were further processed with the STARANISO server[218] for anisotropicity corrections. Molrep[219] or Phaser-MR[220] were used to do molecular replacement. The reference models used for molecular replacement were structures of Fabs in the Protein Data Bank (PDB) having the highest sequence identity with our Fabs. ARP/wARP[221] was used to do automated model building for

high resolution structures Fab 16-2-8C and 16-2-9D. Rigid body refinement and restrained refinement of the structures were performed in REFMAC[222] and Phenix[223], with translation–libration–screw-rotation (TLS) parameters and individual B-factors refined. Model building was performed manually in COOT[224]. Refinement statistics are shown in Appendix tables 2 to 5. Figures of crystal structures were prepared using PyMOL[225].

2.3 Virus production and purification

2.3.1 EV71 strains used in this study

The EV71 strains used in this study were EV71 genotype B2 (strain MS742387), EV71 B2 mutant strain (EV71_B2_pH), C4 and B5 (strain 12-96015). Live viruses of EV71 B2 and EV71_B2_pH were provided by Prof. David Rowlands (Leeds University, UK) and Dr. James Kelly (The Pirbright Institute, UK). EV71_B2_pH was made by repeated exposure of EV71 B2 (strain MS742387) in acidic conditions, resulting in a substitution in residue 104 of VP1 (N104S) (James T. Kelly, personal communication). Live viruses of EV71 C4, isolated from Fuyang, Anhui Province, China, were provided by Prof. Xiangxi Wang (Chinese Academy of Sciences, China). Purified RNA of EV71 B5, was provided by Dr. Arthur Huang. As mentioned in Chapter 1, this virus was responsible for the infections of children from whom our 13 anti-EV71 monoclonal antibodies were isolated[208].

2.3.2 EV71 production

RNA of EV71 B5 was used to produce live viruses. First, rhabdomyosarcoma (RD) and Vero cells were grown separately at 37 °C in 4 wells of a 6-well plate (Greiner

Bio-One) in 2 mL of DMEM supplemented with 10% FBS, 1% 100x L-glutamine and 1% 100x MEM + NEAA. When cells were ~80% confluent, the old medium was removed and 1mL of new medium (20 mL DMEM with 2% FBS, 1% 100x L-glutamine and 1% 100x MEM + NEAA) added to each well. EV71 RNA to a final concentration 200 ng/μl was prepared in serum-free DMEM. Lipofectamine 2000 (Thermo Fisher Scientific) was mixed with an equal volume of serum-free DMEM, incubated at room temperature for 5 min and an appropriate volume mixed with 200 ng/μl RNA, such that 1 μg of RNA was mixed with 5 μL of 50% Lipofectamine, in order to make samples containing 100 ng, 500 ng and 1000 ng of RNA. Then transfection was performed by adding the samples containing different amount of RNA directly to the cells in each well, with the plate tilted and cells uncovered by the medium. After 2 hours, the medium was removed and 2 mL of new medium (20 mL DMEM with 2% FBS, 1% 100x L-glutamine and 1% 100x MEM + NEAA) added to each well. Cytopathic effect (CPE) appeared two days post transfection and EV71 B5 virus was harvested and stored at -80 °C.

Vero and RD cells were cultured in T175 flasks at 37 °C in 30 mL DMEM supplemented with 10% FBS, 1% 100x L-glutamine and 1% 100x MEM + NEAA, respectively. Once the cells in the flasks were confluent, the medium was removed and new medium (20 mL DMEM supplemented with 2% FBS, 1% 100x L-glutamine and 1% 100x MEM + NEAA) was added to the flasks. Cells were infected by EV71 B2, EV71_B2_pH, EV71 C4 and EV71 B5 respectively. Cells were left in the incubator for one more day after they were all killed to ensure the full release of virus from the dead cells.

2.3.3 EV71 purification

The samples containing viruses were harvested and mixed with 1% PBS (with 50% NP40). They were then frozen and thawed 3 times, DNase was added to a final concentration of 50 units/mL, samples centrifuged at 3,200 g for 0.5 h to remove cell debris and 8% (w/v) PEG 6000 (Sigma) dissolved in the supernatant. After storage overnight at 4 °C, the samples were centrifuged at 3,200 g for 1 h. The pellet was dissolved in 30 mL buffer A (50 mM HEPES, pH 7.8, 200 mM NaCl) and centrifuged at 3,200 g for 30 min. The supernatant was harvested and the viruses in the supernatant were spun through a 30% sucrose cushion at 29,000 rpm for 3 h with a Beckman SW 32 Ti rotor. The buffer used for the sucrose cushion was 50 mM HEPES, pH 7.8, 200 mM NaCl and 30% (w/v) sucrose. 0.5 mL of buffer A was added to the pellet which was then stored at 4 °C overnight. The softened pellet was dissolved and centrifuged twice for 30 min at 12,000 g to remove undissolved debris. Then samples were purified on a 15% - 45% continuous sucrose density gradient by centrifuging at 29,000 rpm for 3 h with a Beckman SW 32 Ti rotor. The buffers used were 50 mM HEPES, pH 7.8, 200 mM NaCl at 15% sucrose and 50 mM HEPES, pH 7.8, 20 0mM NaCl at 45% sucrose. Full and empty particles of EV71 were harvested using a pipette and then treated separately with a desalting column (Thermo Fisher Scientific) to remove sucrose, using buffer A as the exchange buffer. Then samples were concentrated using 100 kD centrifugal filters (Sigma-Aldrich). Concentrations of EV71 samples were measured by a Nanodrop and calculated using the equation: concentration (mg/mL) = $(1.55*A_{280}-0.76*A_{260})$ * dilution factor[226].

2.4 Cryo-EM experiments

2.4.1 Negative-stain electron microscopy

Negative-stain EM was used to assess virus samples before cryo-EM was performed. Formvar/carbon-coated 300 mesh copper grids (Agar Scientific) were glow-discharged using a plasma cleaner (Harrick Plasma) to make them hydrophilic, allowing solutions to spread easily on the surface of the grids. Samples of EV71 (4μL, ~0.1mg/mL) were first loaded on glow-discharged grids. Excess sample was blotted away with filter paper after incubation for 1 min. Grids were then washed three times with deionized water and stained with 1% uranyl acetate for 1 min. Excess stain was blotted away with filter paper and grids were examined on a FEI T12 electron microscope operated at 120 kV.

2.4.2 Cryo-EM sample preparation of EV71-SCARB2 complex

In order to replace the natural pocket factor in EV71 capsids, EV71 virions were incubated with a potent expansion inhibitor NLD[168] at 4 °C for 24 h, with a molar ratio of EV71 particle: NLD = 1:300 (i.e. 5x molar excess of NLD over available binding pockets). Then 0.5 μL of SCARB2 (6.5 mg/mL, in 20 mM Tris pH 8.0 and 200 mM NaCl) was mixed with 4.5 μL of EV71 (0.65 mg/mL, in 100 mM Na-acetate pH 5.0 and 200 mM NaCl), with a molar ratio of EV71 particles: SCARB2 = 1:100 (*i.e.* a slight excess assuming 60 receptors can bind per particle). The pH of the mixture was 5.1. Immediately after this, 4 μL of the mixture was applied to a glow-discharged ultrathin carbon grid (AG01824, Agar Scientific), blotted by filter paper from both sides (3.5 s blotting time) in 95% relative humidity and vitrified by plunging into

liquid ethane using a Vitrobot mark IV (FEI). Grids were stored in liquid nitrogen for subsequent data collection.

2.4.3 Cryo-EM sample preparation of EV71-Fab complexes

Purified EV71 virions of different genotypes and Fabs were separately mixed and incubated for 1 to 10 min on ice, at room temperature or at 37 °C, at a capsid/Fab molar ratio of 1:300. Based on Dr. Arthur Huang's paper[208], antibodies 16-3-4D and 17-2-12A can neutralize EV71 genotype B5 but not C4, so we used EV71 B5 to prepare EV71-Fab complexes for Fabs 16-3-4D and 17-2-12A. Since Fabs 16-2-12D and 16-3-3C can induce a significant number of empty particles of EV71 at a high concentration, these two Fabs were incubated with EV71 on ice for just a few seconds, with a capsid/Fab molar ratio of 1:90 (Chapter 5.3). Full information regarding usage of EV71 strains and incubation conditions is given in Table 2.5. After incubation, 4 μL of each sample was loaded on glow-discharged holey carbon-coated copper grids (CF-2/1-2C, Protochips) or ultrathin carbon grids (AG01824, Agar Scientific) and further incubated at room temperature for at least 10 seconds. Grids were blotted from both sides for 3 to 4 s in 95% relative humidity and vitrified in liquid ethane using a Vitrobot mark IV (FEI). Grids were then stored in liquid nitrogen for future use.

EV71 genotype	Fab	Incubation condition
B2	16-2-12D	on ice, for only a few seconds
B5	16-3-3C	
B2	38-1-10A	on ice, for 5 min
C4	16-3-10B	
B5	17-1-12A	
B5	17-2-2B	on ice, for 10 min
B2	34-1-6D	
B5	16-2-2D	37 °C, for 5 min
	17-2-12A	
	16-3-4D	
B5	16-2-8C	37 °C, for 10 min
B2	16-2-9D	
C4	16-2-11B	

Table 2.5 Incubation conditions for preparation of EV71-Fab complexes

2.4.4 Cryo-EM data collection

EM data were collected using a Tecnai F30 Polara microscope (FEI) operated at 300 kV, equipped with a Gatan GIF Quantum energy filter (20 or 30 eV energy selecting slit width) and a Gatan K2 Summit direct electron detector. Data was recorded as movies (30 to 40 frames, each of 0.2 to 0.25 s) in super-resolution mode using SerialEM[227] with a defocus range 0.5 to 2.5 μm. The calibrated magnification was 37037x, corresponding to pixel size of 1.35 Å. The dose rate was about 3 to 4 e-/Å^2/ s, resulting in a total electron dose of ~30 to 40 e-/Å^2. See Appendix tables 6 to 9 for more information about EM data collection.

2.4.5. Cryo-EM data processing

Frames of each movie set were aligned and averaged using MotionCor2[228]. In this

step, the first 2 frames of each movie set (with a relatively big drift) and the last 3 frames with serious radiation damage were discarded. The contrast transfer function parameters were determined with CTFFIND3[229]. Micrographs with astigmatism or significant drift were discarded. Particles were automatically picked using ETHAN[230] and then manually screened in EMAN2[231]. Relion 1.3 and 2[232,233] were used to calculate the EM maps following the gold-standard refinement procedure[232] with icosahedral symmetry constraints. Particles were extracted using Relion and Reference-free 2D-class averaging was performed, with particles being classified into 20 classes. Based on 2D classification results, good particles were selected and used for reference-based 3D classification, with particles being classified into 4 classes. The initial reference model used for 3D classification was generated by filtering the crystal structure of EV71 (PDB: 3VBS[31]) to 50 Å resolution. Good particles from 3D classification were selected for 3D refinement. The best map calculated from 3D classification was used as the initial reference model for 3D refinement. After 3D refinement all complexes were further processed using the post-processing function in Relion to sharpen the maps, by applying a negative B-factor to each map. The "gold" standard Fourier shell correlation (threshold = 0.143 criterion) between two independent 'half maps' was used to evaluate the overall resolutions[234]. The local resolutions of the maps were also calculated with Relion. Maps with the wrong handedness were flipped using the tool Z-flip in Chimera[235]. Refinement statistics are listed in Appendix tables 6 to 9.

2.4.6 Model building

The crystal structure of EV71 (PDB: 3VBS[31]), SCARB2 (PDB: 4Q4B[209]) or Fabs were

fitted into the electron potential maps using Chimera or COOT, initially as rigid bodies. As required, amino acids in the structure of EV71 were changed in COOT to get the correct sequences. The models were then further improved using iterations of Phenix.real_space_refine[236] to automatically optimize the fit model to the map and manual rebuilding in COOT (see Appendix tables 6 to 9 for more information about model refinement). The residues forming the EV71-SCARB2 interface or EV71-Fab interface were identified with PISA[237]. "Roadmaps" mapping interactions to a projection of the virus surface were calculated using Rivem[238]. Figures were prepared with PYMOL[225] and Chimera.

2.5 Other experiments

2.5.1 Thermal stability assay

Semi skirted 96-well PCR plates (4 Titude) were used for the PaSTRY thermal stability assay[239]. In each well, 0.3 ug of EV71 B5 live virus and SYTO9 stain (Thermo Fisher Scientific) with a final concentration of 5 μM were added. Different molar ratios of each Fab: EV71 particle (6:1, 20:1, 60:1, 200:1, 600:1) were analysed, by adding different amounts of each Fab, in order to see how Fabs affect the thermal stability of EV71 virions in the face of increasing Fab concentration. Both virus and Fabs were in 20 mM Tris, 200 mM NaCl, pH 7.4 buffer. Buffer was added to each well to make the final volume up to 50 μL. Wells with only virus and SYTO9 stain but no Fab were used as reference. Experiments were performed in triplicate. The PCR plates were sealed and spun at 500 g for 2 min, then placed into an Mx3005p qPCR machine (Stratagene, Agilent Technologies) and heated from 25 to 99 °C, at a rate of

1 °C per minute. Fluorescence changes were monitored with excitation and emission wavelengths at 492 and 585 nm respectively. The output data were analyzed using the online tool JTSA (http://paulsbond.co.uk).

2.5.2 Octet experiments

Binding kinetics assays were performed at 30 °C (recommended temperature by ForteBio) on a bio-layer interferometry (BLI) Octet RED96e (ForteBio) to measure the binding K_{DS} of Fabs with full and empty particles of EV71 genotype B5, by attaching purified particles to the Amine Reactive 2nd Generation (AR2G) biosensors using the protocol specified for the standard reagent Kit (ForteBio). First, the biosensors were equilibrated in deionized water for at least 10 min. Then biosensors were activated in the reagent containing 20 mM 1-Ethyl-3-[3-dimethylaminopropyl] carbodiimide hydrochloride and 10 mM N-hydroxysulfosuccinimide for 300 s. Biosensors were then soaked in purified EV71 full or empty particles (dissolved in 10 mM sodium acetate buffer, pH 6.0) for immobilization for 10 min. The final concentration of EV71 particles used for immobilization is ~200 μg/ml. Then biosensors were transferred to buffer (1M ethanolamine, pH 8.5) for quench for 300 s. Biosensors were washed with buffer (20 mM Tris, 200 mM NaCl, pH 7.4) for 60 s to get the baseline. Then purified anti-EV71 Fab was used as the analyte. Each Fab was first associated (duration: 150 s) and then dissociated (duration: 300 s) from the EV71 immobilized on the biosensors. Serial dilutions (2x) of the Fabs were used to enable dissociation constants to be calculated. The dilution range bracketed the expected dissociation constant to provide an accurate estimate. A change in the number of Fab molecules bound to the virus can cause a shift in the interference pattern of white light

reflected from the end of the tip and this shift can be detected by the Octet machine. All experiments were performed following the manufacturer's instructions. Data were analyzed and K_Ds of binding calculated using Octet Data Analysis HT 11.1 software (ForteBio), with a 1:1 binding model applied (since an Fab has a single binding site and no cooperativity was expected).

Chapter 3

Cryo-EM studies on the interaction of EV71 with SCARB2

3.1 Receptors of the HFMD-causing enteroviruses

Recently, receptors have been identified for many of the aetiological agents of HFMD. Notable receptors include SCARB2 (a receptor for EV71, CV-A16 and a subgroup of type A enteroviruses)[129,156], kringle-containing transmembrane protein 1 (KREMEN1) for another group of type A enteroviruses including CV-A10[240], and coxsackievirus and adenovirus receptor (CAR) and decay-accelerating factor (DAF) for group B enteroviruses[241]. Receptor usage correlates with the capsid structure, indicating that receptor switching drives evolution (Figure 3.1). Correct engagement with a specific receptor is critical to infectivity and can control virus tropism at both the species and tissue level[242-245]. This makes receptor–virus interactions attractive targets for antiviral therapeutics, since it may be more difficult for a virus to acquire resistance to such a compound than to a classic enzyme inhibitor.

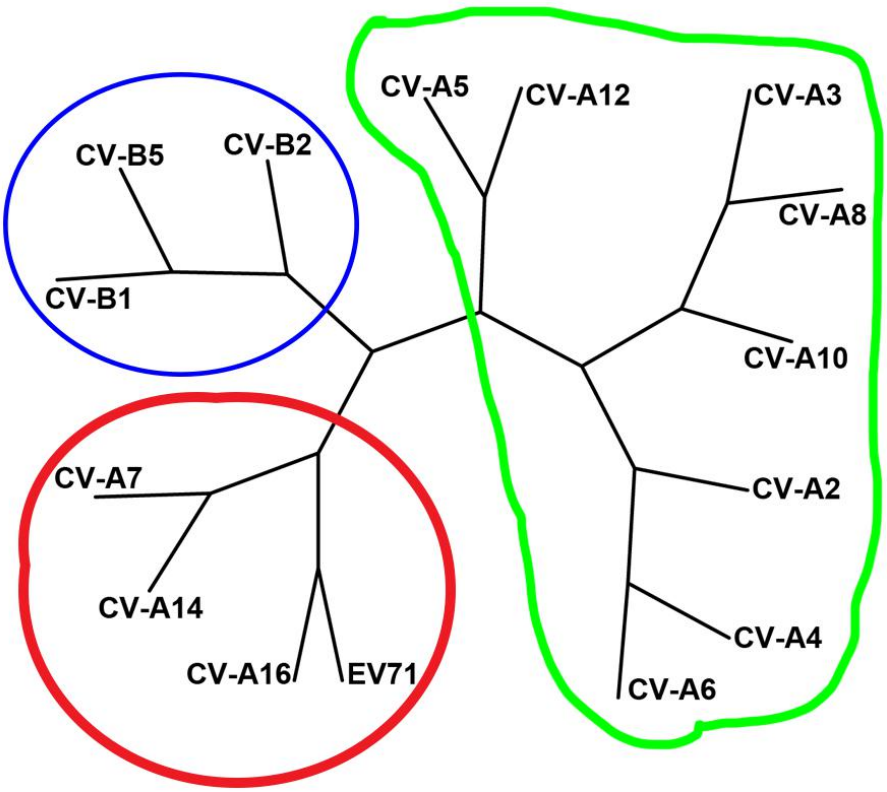

Figure 3.1 Phylogenetic tree of the HFMD-causing enteroviruses derived by comparing the capsid sequences using the Structure Homology Program (SHP)[246]. Viruses using SCARB2, CAR and KREMEN1 as receptors are circled in red, blue and green, respectively.

SCARB2 is the major receptor for EV71 and there is good evidence that SCARB2 attachment mediates EV71 internalization and uncoating at low pH[130,247]. The isolated structures of EV71 and SCARB2 had been determined[31,148,209,248], but how they interacted to initiate infection was not known when I started work on this problem.

3.2 Production, purification and characterization of EV71

EV71 was grown in Vero and RD cells and purified by centrifugation, sucrose cushion ultracentrifugation and sucrose density gradient ultracentrifugation (See Chapter 2.3). After gradient centrifugation, two clear layers could be observed, containing empty and full particles of EV71 separately (Figure 3.2.a). The layer containing EV71 full particles was harvested and concentrated. The A_{260}/A_{280} absorbance ratio of 1.66 and micrograph from negative-stain EM (Figure 3.2.b) also verified this sample was mature virus of EV71. The purified EV71 virions were used to make cryo-EM grids of EV71-SCARB2 complex with a molar ratio of EV71 virions: SCARB2 = 1:100.

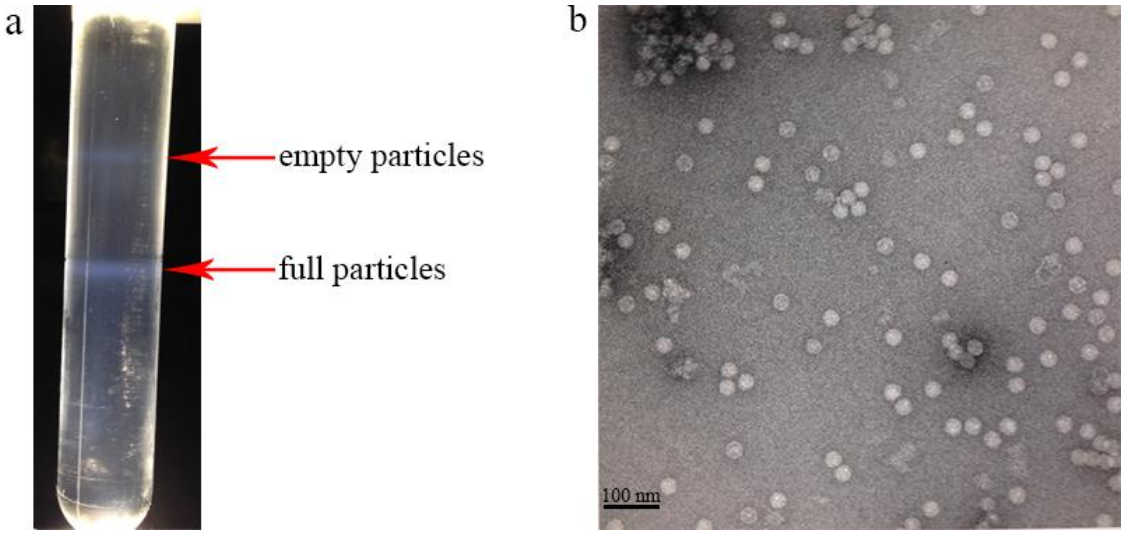

Figure 3.2 Purification and characterization of EV71 virions. (**a**). 15% to 45% sucrose density gradient centrifugation of EV71. Two layers containing empty and full particles of EV71 separately can be observed. (**b**). Negative-stain EM image of EV71 particles.

3.3 Cryo-EM data collection and structure determination

We collected cryo-EM micrographs of EV71-SCARB2 complex using a Polara microscope (FEI), equipped with a Gatan GIF Quantum energy filter and Gatan K2 Summit detector. Data were recorded with a dose rate of ~4 e-/Å^2/s, at a calibrated magnification of 37037x, with a pixel size of 1.35 Å. Frames of each movie set were aligned using MotionCor2[228] (see one of the aligned image stacks in Figure 3.3). Particles picked from aligned image stacks were used to do 2D alignment and 3D reconstruction using Relion [232,233] (see results in Figure 3.4 and 3.5). A total of 10443 particles from 757 micrographs were used to calculate the final EM map. Details for cryo-EM data collection and processing are included in Chapter 2.4. See Appendix table 9 for cryo-EM data collection and refinement statistics.

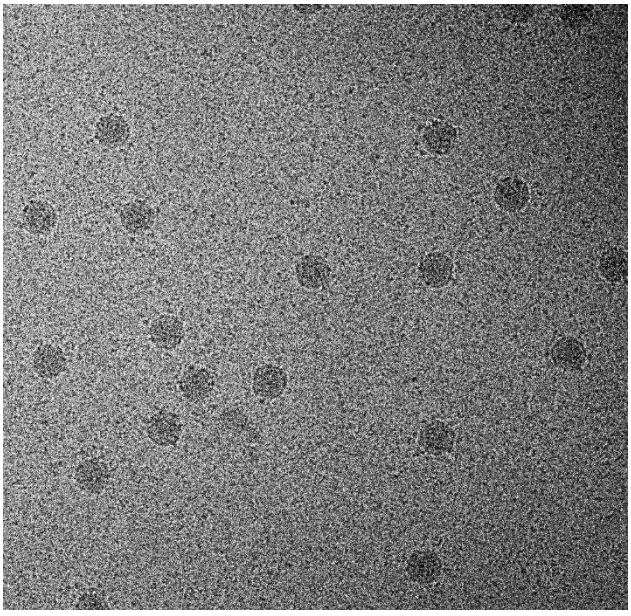

Figure 3.3 Cryo-EM image showing EV71-SCARB2 complexes.

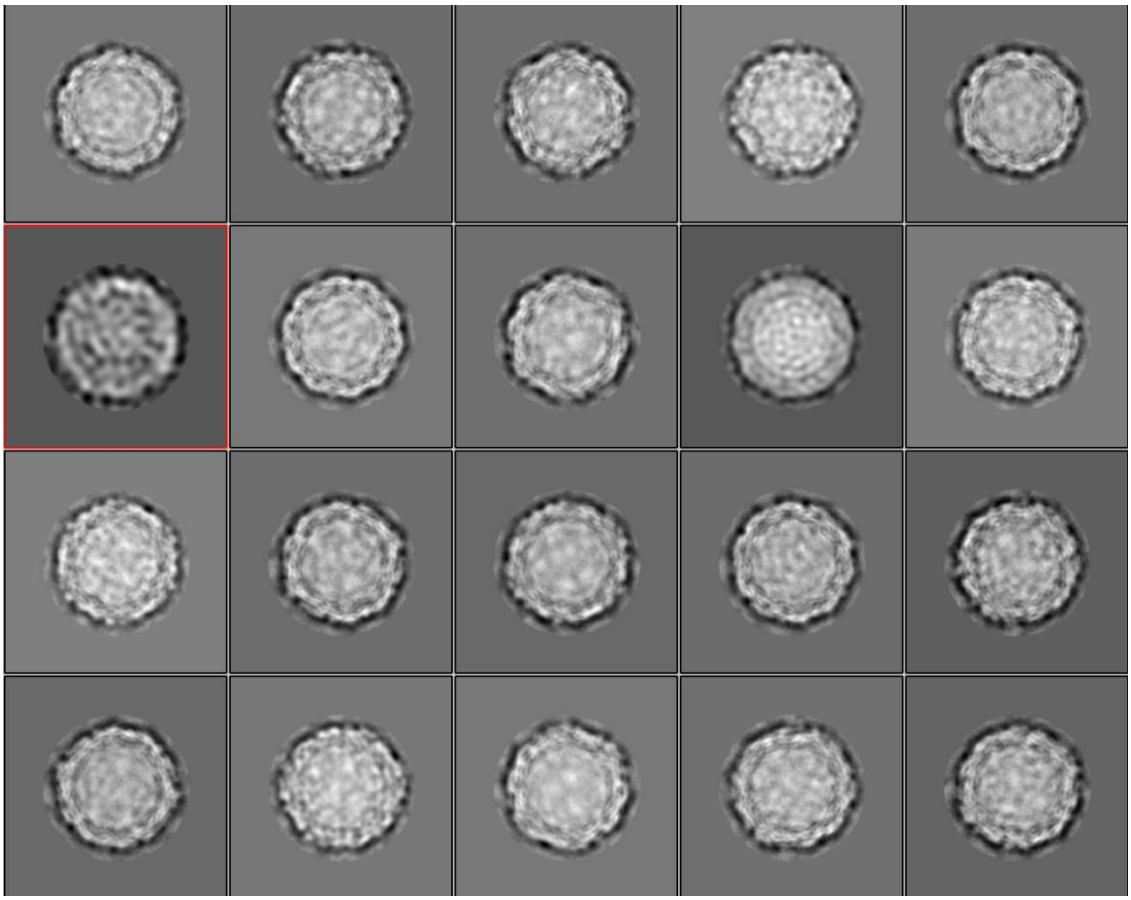

Figure 3.4 2D classification result of EV71-SCARB2 complex. Particles were classified into 20 classes in this step. Only one class of bad particles (marked in a red box, comprising less than 0.2% of total particles) were discarded and all the other 19 classes of particles (10443 particles in total) were used for subsequent 3D classification.

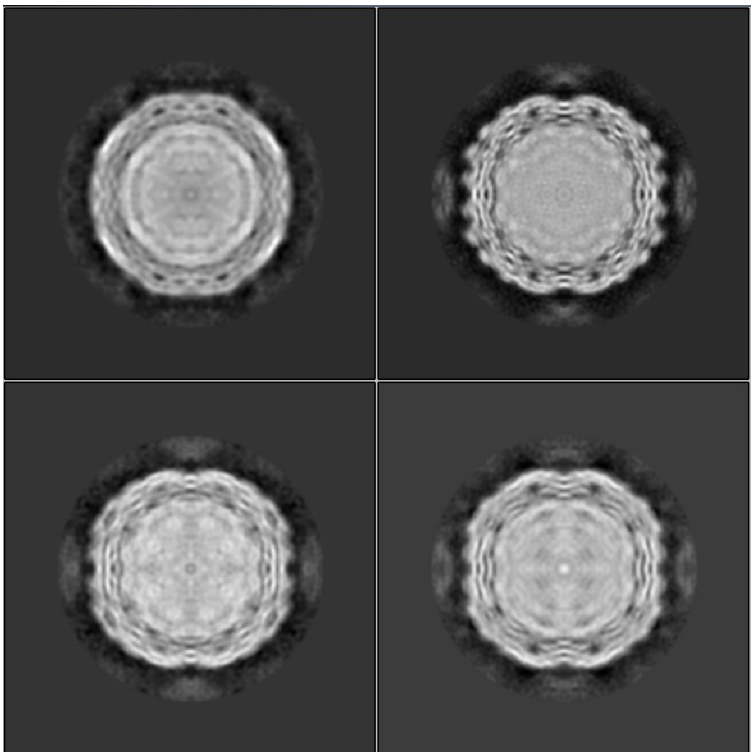

Figure 3.5 3D classification result of EV71-SCARB2 complex. Particles were classified into four classes in this step. All the four classes were good and selected for subsequent 3D refinement.

These results of cryo-EM image, 2D and 3D classification are representative of many of the structures I have determined and so for concision, unless there is something unusual, I will not present this level of detail for further structures.

3.4 Cryo-EM structure of EV71-SCARB2 complex

Using the data we collected, we determined the density map for an EV71–SCARB2 complex at a pH of 5.1. The cryo-EM map was determined at 3.4 Å resolution (see Chapter 2.4 and Figure 3.6 and 3.7). The map was at sufficient resolution to build and refine an atomic structure of the complex (Figure 3.8.a, b and 3.9, Chapter 2.4 and Appendix table 9).

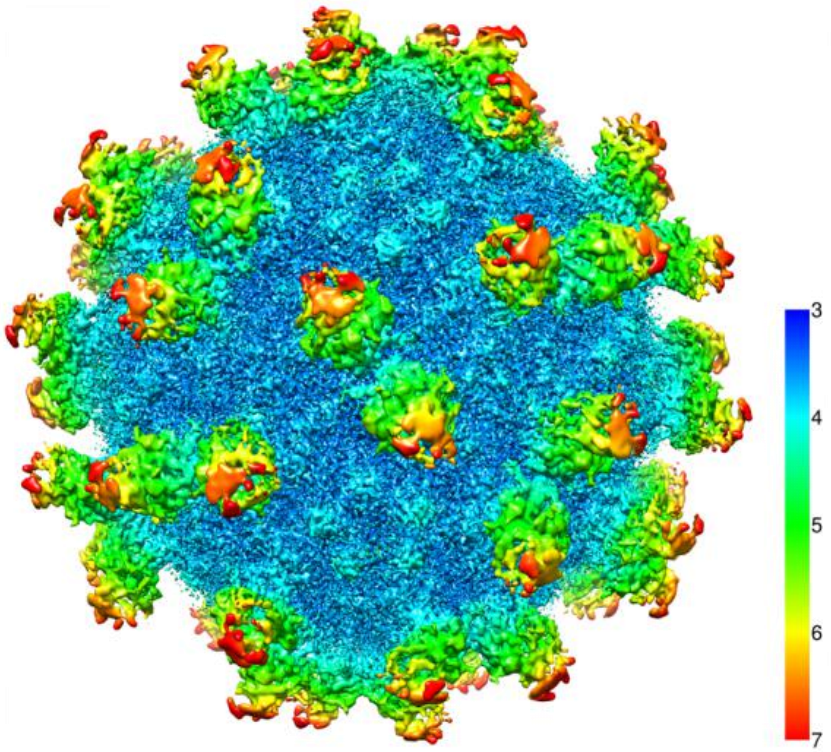

Figure 3.6 The final density map of EV71-SCARB2 complex colored by local resolution (the key shows the resolution in Å).

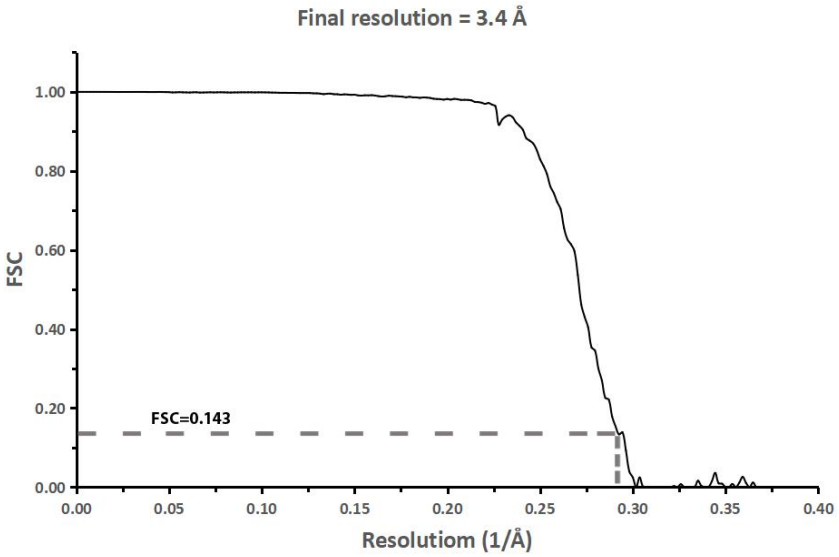

Figure 3.7 The gold standard FSC curve of the final map with a resolution of 3.4 Å at FSC = 0.143.

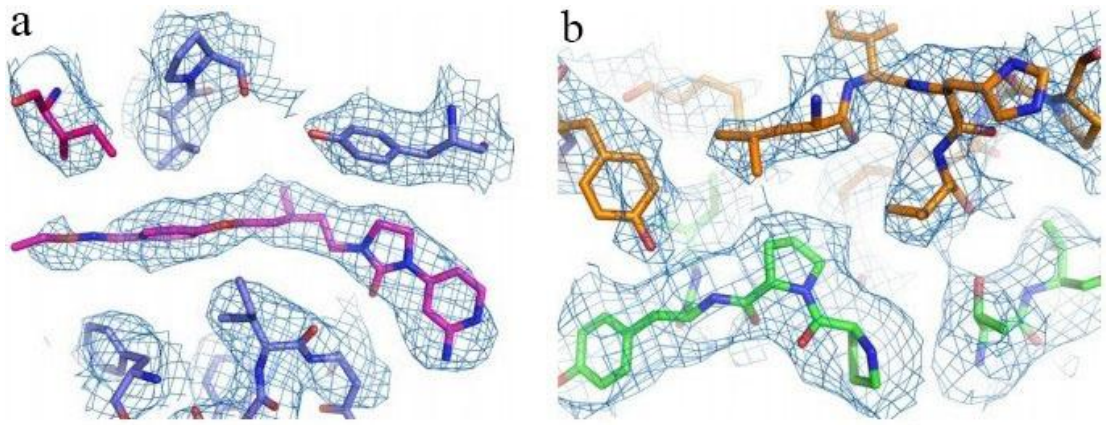

Figure 3.8 The quality of the EV71–SCARB2 EM structure. Electron potential maps for the bound pocket-binding inhibitor NLD (magenta) and surrounding residues (**a**), and for residues at the EV71 (green sticks)–SCARB2 (orange sticks) interface (**b**).

The cryo-EM structure of the EV71-SCARB2 complex reveals that SCARB2 binds EV71 on the southern rim of the canyon, rather than across the canyon, as predicted[148,157,249] (Figure 3.9). Helices 152–163 (α5) and 183–193 (α7) of SCARB2 and the VP1 GH and VP2 EF loops of EV71 dominate the interaction (Figure 3.10, Figure 3.11).

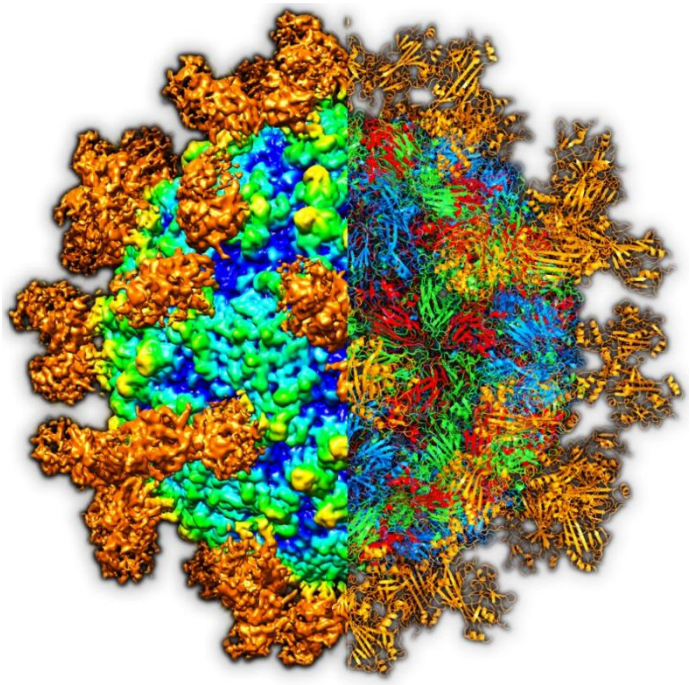

Figure 3.9 EV71–SCARB2 complex viewed down the 2-fold icosahedral axis, with the left half of the particle shown as a three-dimensional reconstruction colored by radius from blue, through cyan, green and yellow, to orange from lowest to highest radius, and the right half of the complex shown as ribbons colored in blue, green, red and orange for VP1, VP2, VP3 and SCARB2, respectively.

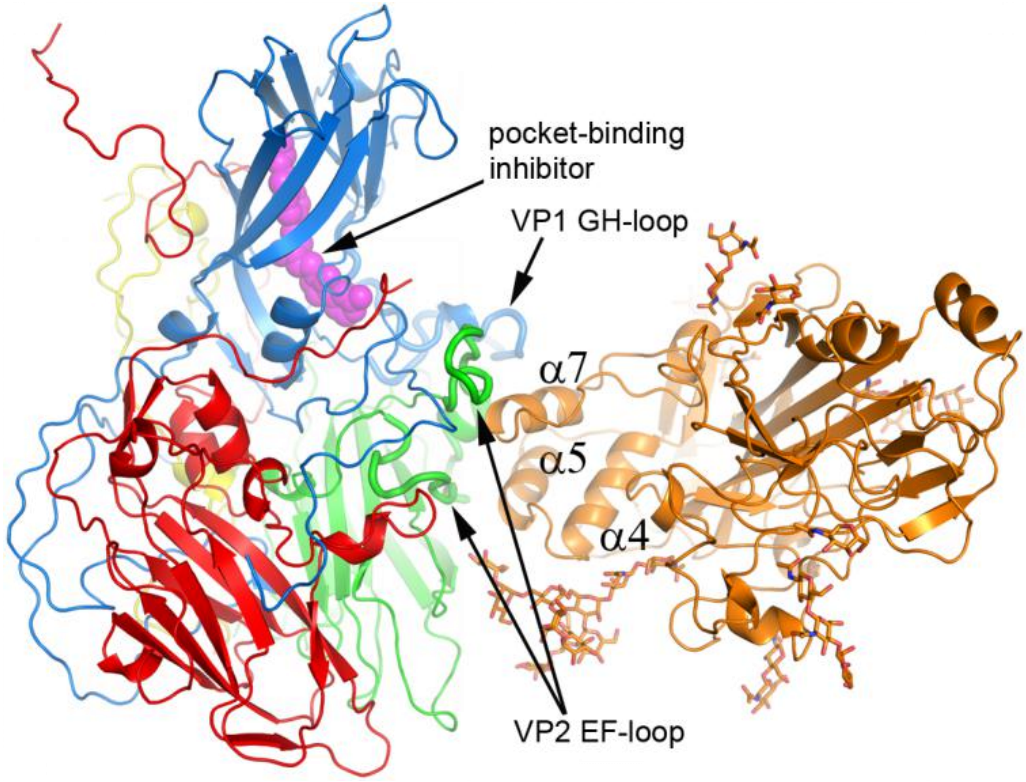

Figure 3.10 Complex formation of EV71 and SCARB2. Position and orientation of the bound SCARB2 on an EV71 protomer. EV71 VP1–VP4 are colored in blue, green, red and yellow, respectively. The pocket-binding inhibitor NLD is shown as magenta spheres. The VP1 GH and VP2 EF loops that interact directly with the receptor (orange ribbons) are drawn as thick coils.

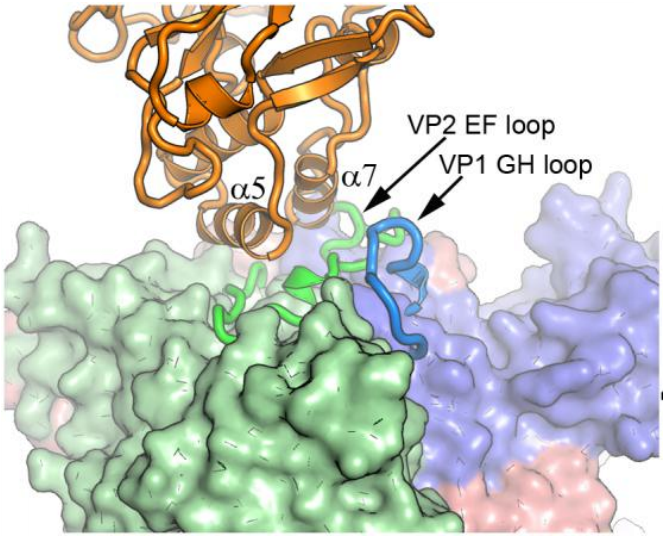

Figure 3.11 EV71 and SCARB2 interactions. VP1 GH and VP2 EF loops form a platform for SCARB2 binding. The two loops and receptor are shown in cartoon representation, and the rest of the viral protomer as surface representation. The color scheme is as in Figure 3.9.

In the structure of the complex, the virion is unexpanded, with NLD remaining bound in the VP1 pocket (Figure 3.6 and Figure 3.8.a), and is essentially indistinguishable from the native mature virus (root mean square deviation: 0.4 Å for 774 Cα atoms matched out of 784; Figure 3.12.a, b). The receptor interacts with the virus through helices α5 and α7, which—together with α4—form a bundle lying distal from the domain termini, and therefore from the membrane (Figure 3.10). Although this is consistent with the previous inference that the C-terminal end of α4 is involved in attachment, and the observation that α5 forms part of the epitope recognized by an antigen-binding fragment, which binds SCARB2 to prevent virus attachment, the binding areas on both the receptor and the virus are quite different from those predicted[148,157,249]. It has been noted that this helical bundle undergoes pH-dependent

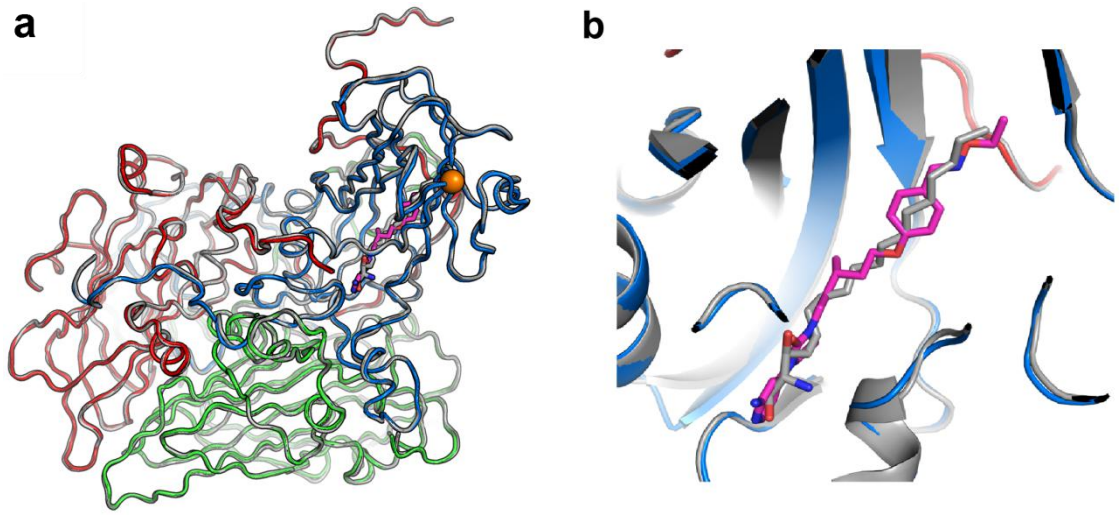

Figure 3.12 Overlay of receptor bound EV71 and the mature virus. **a**. SCARB2 bound EV71 (PDB: 6I2K[250]) is colored in blue, green, red and yellow for VP1-4, respectively and the pocket inhibitor, NLD, is shown as magenta sticks. The mature virus (PDB: 3VBS[31]) is colored in grey and its pocket factor, modelled as sphingosine, is shown as grey sticks. The blue sphere indicates the position of the acid resistant mutation N104S (see Chapter 2.3.1). **b**, close-up of VP1 pocket factor binding region of (**a**).

conformational changes, and it has been proposed that these are involved in the pH-dependent triggering of viral uncoating[148,209]. Interestingly, although our structural analysis was performed at relatively low pH (5.1), the structure of the helical bundle is essentially indistinguishable from that observed for the isolated protein at neutral pH[148,209,248] (Figure 3.13.b, c). One explanation for this may be because SCARB2 was first purified at pH 8.0, then mixed with EV71 (pH 5.0) and immediately after this the mixed sample was applied to the EM grid and frozen quickly.

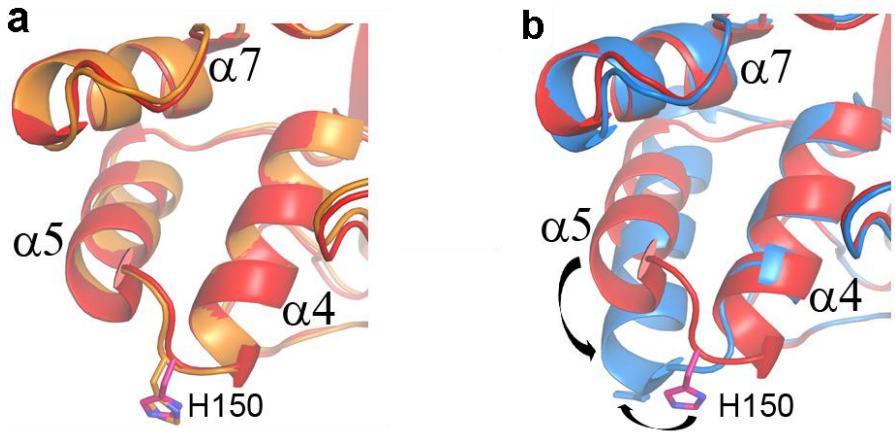

Figure 3.13 Conformational differences of SCARB2 at different pH**.** **a**, The α4, α5 and α7 helix bundle of the EV71-bound SCARB2 (orange, PDB: 6I2K[250]) has a similar conformation to that of the crystal structure at pH 6.5 (red, PDB: 4Q4B[209]). **b**, Conformational differences in the helix bundle of SCARB2 at pH 6.5 (red) and pH 4.8 (blue, PDB: 4TW0[148]). The side chain of the putative pH sensor H150 that caps the C terminus of α4 at pH 6.5 (red sticks) becomes the first residue of α5 at pH 4.8 (blue sticks).

The time from mixing (and reducing the pH) to freezing was only ~10 seconds, so the SCARB2 molecules may not have had time to undergo pH-induced conformational changes. But also the virus had the tight binding NLD pocket factor attached[168], overall the effect of these factors would be to stabilize the virus particle in the native form and hence presumably tend to maintain bound SCARB2 in the high-pH conformation.

While much of the SCARB2 surface is shielded by nine complex glycans, the EV71-binding site is largely unhindered, although a long well-ordered phosphorylated sugar has been seen to approach this region of the surface[209] (Figure 3.10 and 3.14). Considering that it is highly exposed in the apo structure, the binding site is

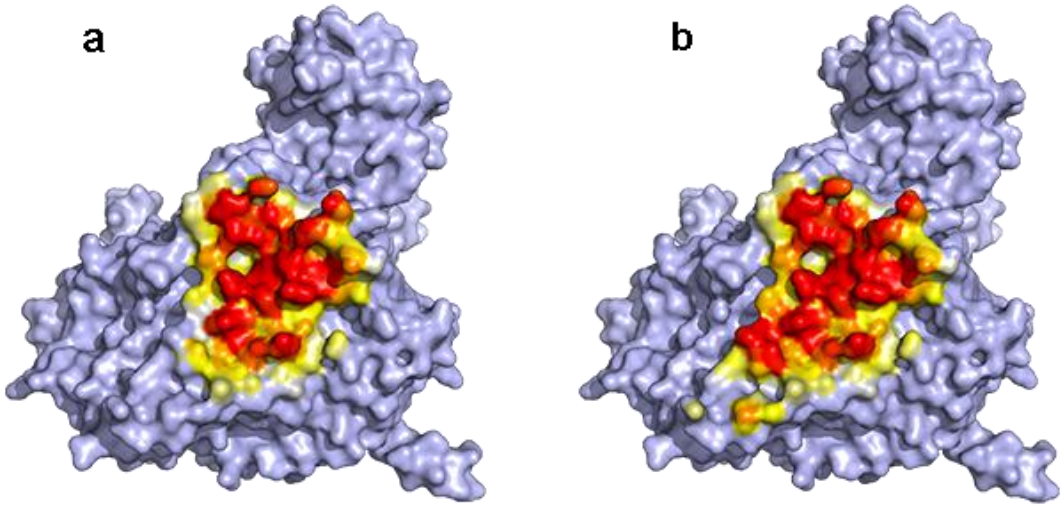

Figure 3.14 Surface representations of an EV71 protomer showing binding areas of SCARB2 with (**b**) or without glycans (**a**). Contact areas between the virus and SCARB2 with distances ≤ 4.0 Å are shown in bright red, > 4.0 Å and ≤ 9.0 Å in yellow. Different binding areas in **a** and **b** indicates glycans in SCARB2 interact with EV71 capsid.

surprisingly hydrophobic, suggesting that this region is involved in protein–protein interactions as part of its function in the host. Indeed, it has been proposed that its partner β-glucosidase uses this region as part of its attachment site[209], and the areas of α5 and α7 directly involved in viral interactions make face-to-face contacts with the same region of another SCARB2 molecule in a SCARB2–antigen-binding fragment crystal structure[249]. In addition to hydrophobic interactions, there are limited hydrogen bond and charge interactions, which are described below from the perspective of the virus. Overall, the footprint of the receptor on the virus is ~700 $Å^2$, which is similar to that observed for tightly binding antibodies[74].

The SCARB2-binding site on EV71 comprises residues from the VP2 EF and the VP1 GH loops, which form part of the south wall of the canyon and bear antigenic residues.

This contrasts with the notion inferred from peptide-scanning assays that receptor binding is mainly contributed by the GH loop and C terminus of VP1 and the GH loop of VP3[148]. The VP2 EF loop is shorter in EV71 than in most enteroviruses (for example, 15 residues shorter than in poliovirus type 1), and residues 134 to 162 from this loop, together with residues 214 to 216 in the VP1 GH loop form a platform on which the receptor sits (Figure 3.11). The first hypothesis for receptor binding to enteroviruses (the canyon hypothesis, proposed in 1985) was that slender receptors would insert into the canyon, thereby allowing the necessarily conserved attachment residues to be concealed from immune surveillance, since the rather blunt antibody would be unable to reach into the canyon[34]. Indeed in-canyon attachment is common among enteroviruses (exemplified by poliovirus22) and it had been assumed that SCARB2 binding would follow this pattern[157], so it is surprising that the binding site is actually a platform that lies outside the canyon, extending to the 'south' (Figure 3.11 and 3.18). This site is roughly similar to that observed for DAF binding to echovirus 7[251], and for integrin binding to FMDV[252].

3.5 Conservation of the SCARB2-binding residues

The binding residues on the viral capsid involved in virus-SCARB2 interaction are unremarkable and largely non-conserved among different SCARB2-dependent viruses (Figure 3.17), and there is no strong surface charge characterizing the region (Figure 3.15, 3.16 and Appendix table 10). In summary, there are 14 viral and 19 receptor residues involved in hydrophobic interactions (distance $\leq$ 4.0 Å), in addition to 4 potential hydrogen bonds and 2 potential charged interactions. Of these, two of the key interactions are with the VP2 main chain (Gly 137 and Pro 147). Of the 14 residues at

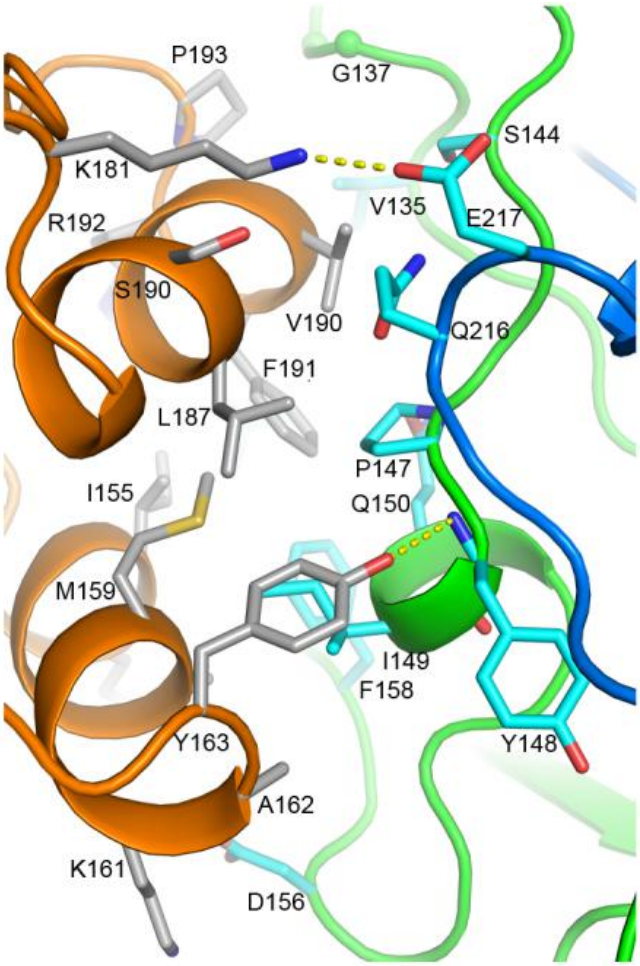

Figure 3.15 Residues involved in the EV71-SCARB2 interaction. VP1 GH and VP2 EF loops form a platform for SCARB2 binding. The two loops and receptor are shown in cartoon representation. The color scheme is as in Figure 3.10.

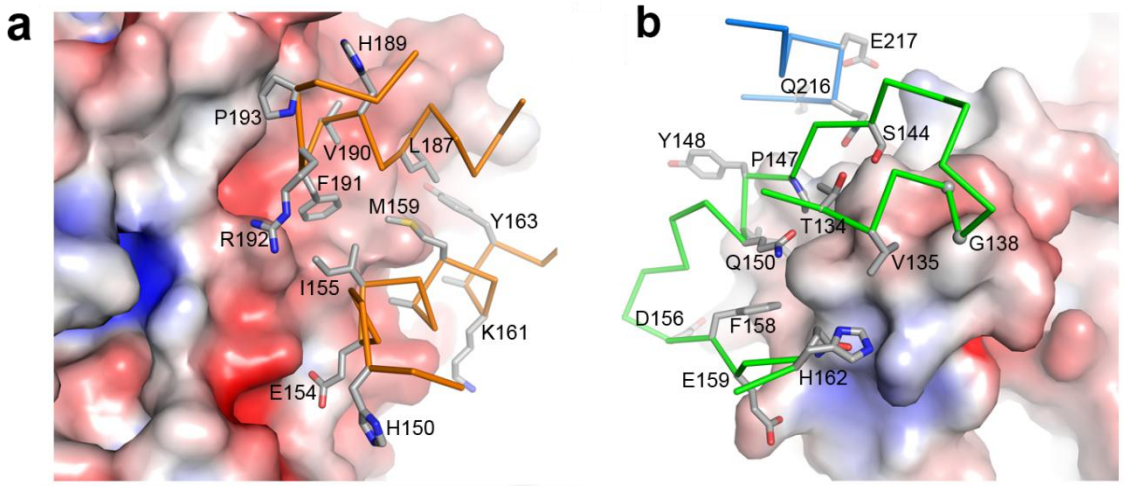

Figure 3.16 EV71 and SCARB2 interface, with EV71 shown as an electrostatic surface (color range from -5 to +5) and SCARB2 as sticks (**a**), and *vice versa* (**b**). The color scheme is as in Fig. 3.10.

the viral–receptor interface, 12 are conserved in EV71 genotypes (Figure 3.17). A significant subset of the agents of HFMD use SCARB2 as a receptor[153] (Figure 3.1); however, a surprisingly large number of residues in the binding site are not conserved across these viruses (10 out of 14 residues; Figure 3.17). We assume that this variability arises from antigenic variation, which has presumably led to the differentiation of the SCARB2-binding subset of enteroviruses. Indeed, EV71 vaccine does not provide protection against another SCARB2-binding virus, CV-A16. How then do these viruses maintain specificity for SCARB2 in the face of sequence variation? Of the SCARB2-binding residues, VP2 Gly 137, Pro 147 and Tyr 148 are conserved. From the antigenic perspective, only the tyrosine presents a signature side-chain recognition signal, but the other two have structural properties that can control local protein folding, thus glycine has greater regions of torsional space accessible and proline less accessible than other residues. All three residues are involved in tight interactions with SCARB2 (Figure 3.15 and 3.16.b). It appears that the recognition

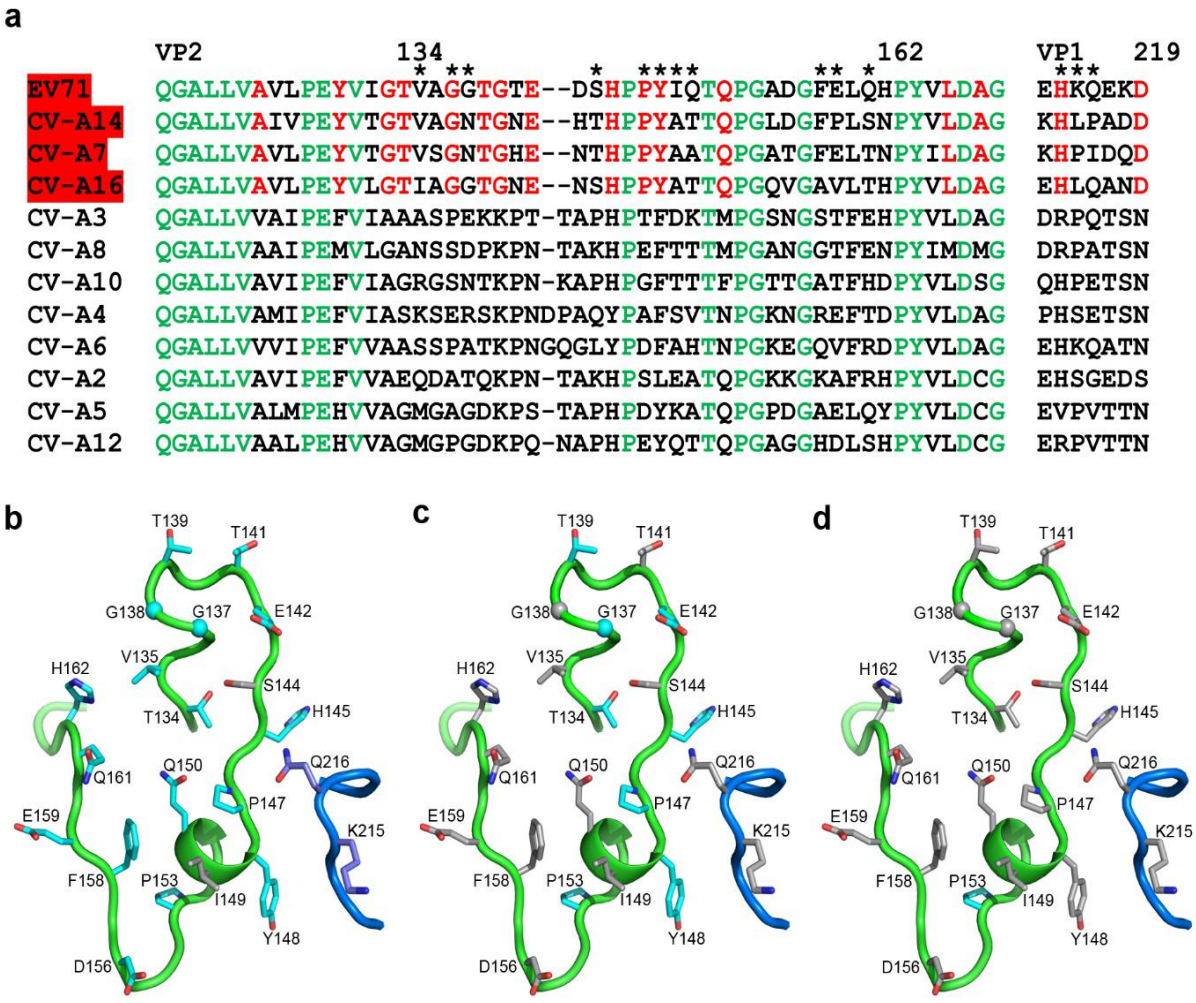

Figure 3.17 Comparison of residues in the receptor attachment area of EV71 with other type A enteroviruses that cause HFMD. **a**, Sequence alignment of the receptor binding region of EV71 with the HFMD causing type A enteroviruses. Virus names with red background are SCARB2 dependent, and the others SCARB2 independent. Conserved residues are in green, residues conserved in SCARB2 dependent viruses in red. Residue numbers of EV71 are indicated, and those having direct contacts with SCARB2 are marked with an asterisk. **b**-**d**, The structure of VP1 GH and VP2 EF loops that form the receptor-binding platform of EV71. The backbone of VP1 GH loop is colored in blue, and VP2 EF loop in green. Side chains which contact the receptor directly or fold towards the receptor are shown as sticks and colored in cyan (EF loop) or blue (GH loop), but in grey if not conserved. Residues among 11 EV71 genotypes (A, B1-B5, C1-C5) are highly conserved (**b**), less conserved among the 4 SCARB2 dependent viruses (**c**), and only VP2 P153 is conserved among the HFMD type A enteroviruses (**d**).

involves a significant proportion of side-chain independent interactions, which may mitigate the constraint imposed on antigenic variation. A snapshot of the generation of variation can be seen in an analysis of the immune response of recovered patients[208], where the epitopes of the key neutralizing antibodies were mapped by identifying mutations in EV71 that abrogated neutralization. The results are shown in Figure 3.18. It is striking that all except one of the escape mutations are outside the SCARB2 footprint, scattered widely on the capsid, suggesting that neutralizing responses are directed at epitopes that, at most, overlap the receptor-binding site only partially. It appears that, rather akin to the exposed receptor-binding site of FMDV[252], SCARB2-binding enteroviruses manage to hide their receptor-binding site in full view of the immune response.

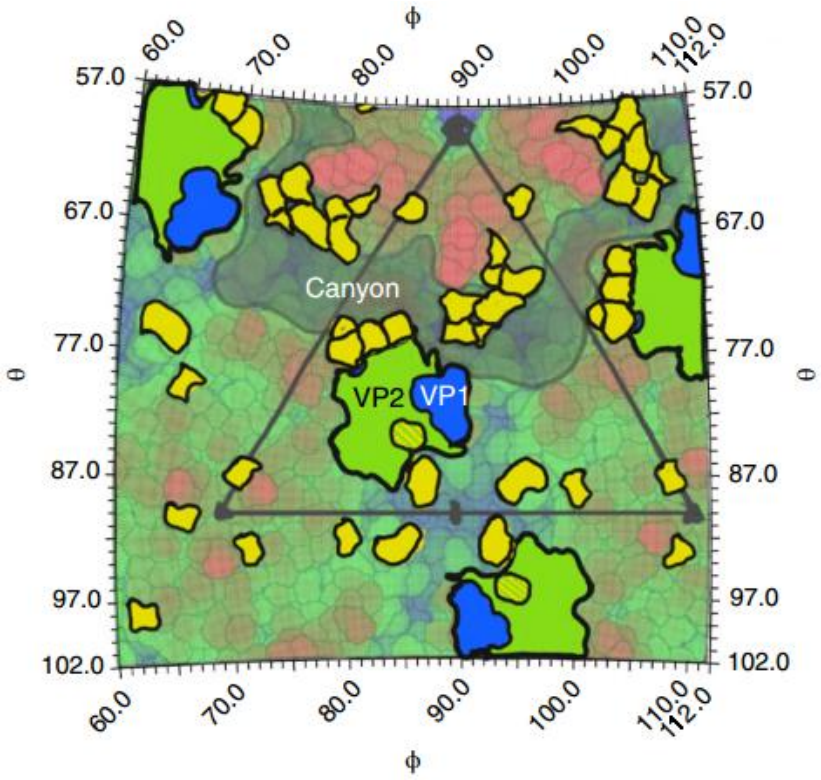

Figure 3.18 Epitopes of neutralizing antibodies compared to SCARB2 binding residues. Roadmap showing the relative positions of the receptor footprint (bright blue and green) and escape mutations of neutralizing antibodies (yellow).

3.6 Proposed mechanism of SCARB2-induced uncoating of EV71

In the absence of canyon binding, how might SCARB2 binding and low pH trigger uncoating of EV71? For the canyon-binding receptors, binding to the floor of the canyon could directly induce changes, leading to release of the pocket factor lying directly below, whereas SCARB2 must displace the pocket factor by an allosteric effect. Figure 3.19 shows the relative position of the SCARB2 attachment site, the pocket-factor-binding site and the conformational changes that occur on transition to the expanded form of the virus and low-pH form for SCARB2[148,248]. It seems plausible that in the wildtype virus, without additional stabilization of the pocket, structural changes in the SCARB2 helical bundle (Figure 3.13.b) induced as the pH drops (in the late endosome/lysosome) would exert mechanical strain on the virus capsid. Specifically, we find that SCARB2 attaches such that the pH-induced conformational change observed previously would act as a lever on the VP1 GH loop through movement of α7 away from α5, which is strongly anchored to the VP2 EF loop. This agrees with a previous proposal that the VP1 GH loop, which undergoes conformational changes on particle expansion, acts as the sensor in a sensor–adaptor uncoating mechanism[31,44,253], initiating a cascade of changes, which include the loss or expulsion of the pocket factor and expansion of the particle to facilitate the release of the N terminus of VP1, VP4 and, ultimately, the viral genome. In agreement with this, we note that mutation of one of the VP1 GH loop residues (K215A) increases thermostability, but produces a slow growth phenotype[254]. This mechanism, although attractive, remains speculative pending experimental evidence. Indeed, some experimental results remain hard to explain. For instance, the mutation Q172A in VP1,

which is about 30 Å from the binding site, abolished binding to SCARB2 in pull-downs. Also, the VP1 mutations K98E, E145A and L169F enable EV71 to interact with murine SCARB2[157,255]. Perhaps these residues, distant from the SCARB2-binding site, act through subtle allosteric affects, which agrees with recent data whereby point mutation of one of these residues, VP1 145, affects sensitivity to neutralizing antibodies recognizing a conserved epitope in the EF loop of VP2[256].

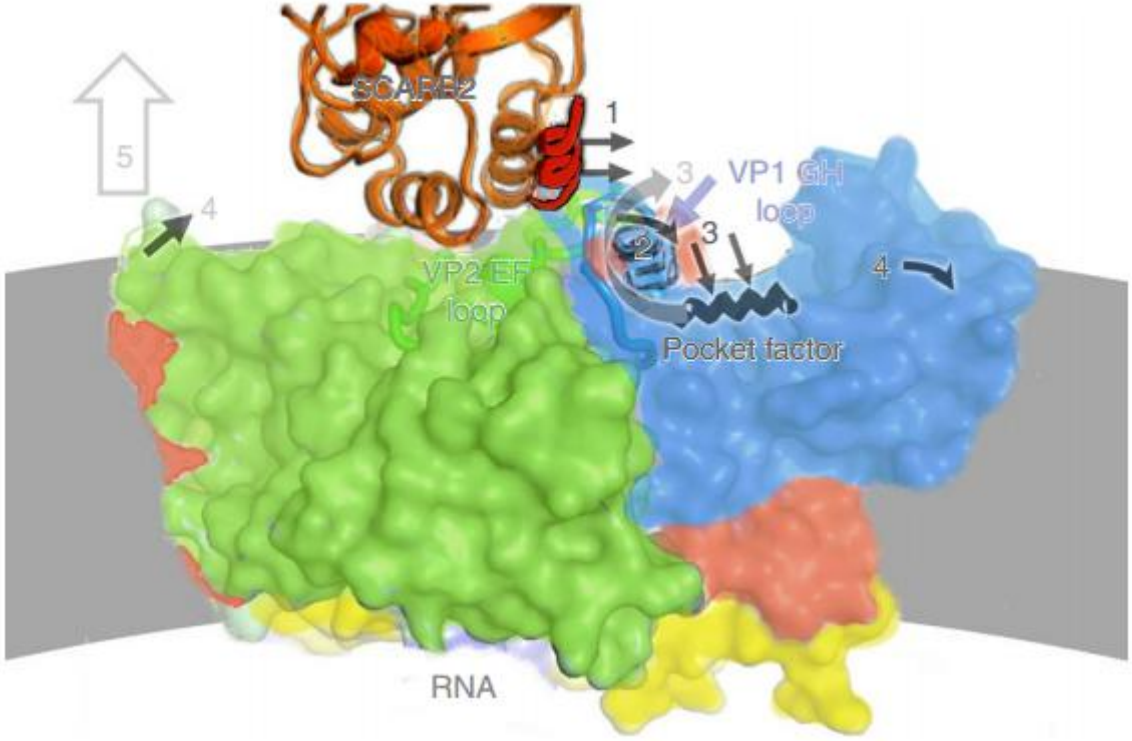

Figure 3.19 Proposed mechanism of uncoating. Schematic showing the mechanism of receptor-triggered uncoating of EV71. α5 of the bound SCARB2 (molecule drawn in orange with this helix being the one lying on top of VP2) anchors the receptor on the binding platform consisting of the VP1 GH (blue) and VP2 EF (green) loops. As the pH drops in the late endosome, the pH sensor H150 triggers conformational changes of the helix bundle of α4, α5 and α7 of the receptor. α7 moves towards (shown in red (1)) and distorts the conformation of the VP1 GH loop (2), which in turn triggers release of the VP1 pocket factor and collapse of the pocket (3), viral particle expansion (4) and VP1 N terminus, VP4 and RNA release (5).

3.7 Summary

The EV71–SCARB2 complex structure reveals that SCARB2 binds EV71 on the southern rim of the canyon, rather than across the canyon, as had been predicted. Helices 152-163 (α5) and 183-193 (α7) of SCARB2 and the VP1 GH and VP2 EF loops of EV71 dominate the interaction. This binding pattern suggests an allosteric mechanism by which receptor binding might facilitate the low-pH uncoating of the virus in the endosome/lysosome.

Many residues within the binding footprint are not conserved across SCARB2-dependent enteroviruses. However, a conserved proline and glycine seem to be key residues. Thus, although the virus maintains antigenic variability even within the receptor-binding footprint, knowledge of the specific 'hot spots' of this interaction may help in the design of small molecules, or more likely biologics that block viral entry. For instance, nanobodies, being smaller than antibodies, might be able to target residues that cannot be altered without compromising virus viability. Indeed, an unwitting proof of principle of this appears to have been made by Xu *et al*.[257], who grafted parts of the VP1 GH and VP2 EF loops into a recombinant vaccine that protected mice from a lethal EV71 challenge.

Chapter 4

Anti-EV71 human monoclonal antibodies

4.1 Crystal structures of anti-EV71 Fabs

All the 13 anti-EV71 Fabs were digested from IgG or expressed in mammalian cells and purified (Chapter 2.1). SDS-PAGE result showed that all the purified Fabs have high purity (Figure 4.1). The purified Fabs were used for crystallization and crystals of Fabs were obtained and optimized for the X-ray diffraction data collection (Figure 4.2). The crystallization conditions used to get high-quality crystals are listed in Table 4.1. X-ray diffraction data were collected (see Figure 4.3 and Table 4.2 for information regarding Fab 16-2-9D) and high-resolution crystal structures of Fabs with resolution ranging from 1.14-3.06 Å were solved (Figure 4.4, see Appendix tables 2-5 for more information).

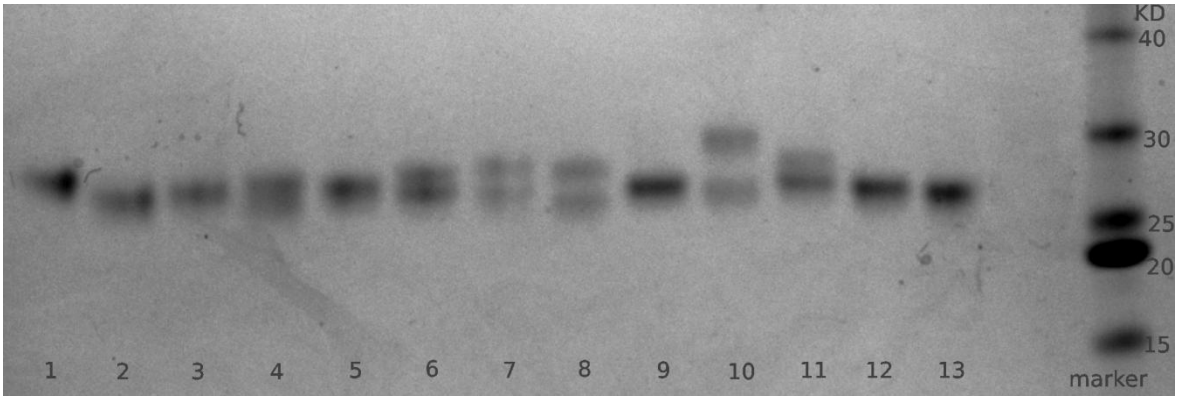

Figure 4.1 Reducing SDS-PAGE of purified Fabs. Lane 1 to 13: Fab 16-2-2D, 16-2-8C, 16-2-9D, 16-2-11B, 16-2-12D, 16-3-3C, 16-3-4D, 16-3-10B, 17-1-12A, 17-2-2B, 17-2-12A, 34-1-6D, 38-1-10A. There are two bands in lane 4, 6, 7, 8, 10, 11 because of differing light and heavy chains of these Fabs have distinct molecular weights.

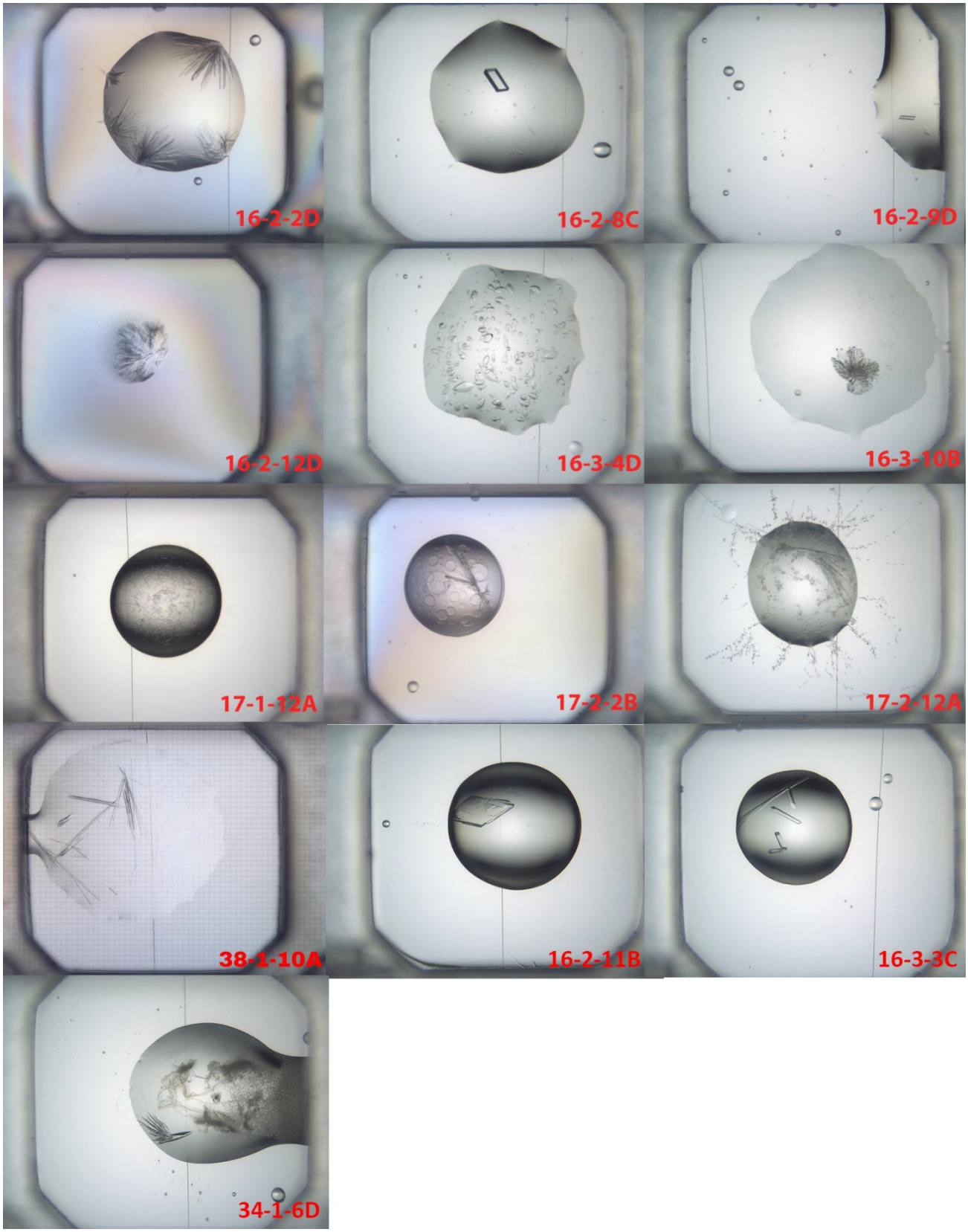

Figure 4.2 Crystals of 13 Fabs leading to high-resolution structures.

Fab	**condition**	**Fab Conc. (g/L)**
16-2-2D	30% (v/v) pentaerythritol ethoxylate (15/4 EO/OH), 0.05 M ammonium sulphate, 0.1 M bis-Tris, pH 6.5	51.7
16-2-8C	25% (w/v) PEG 3350, 0.1 M Bis-Tris, pH 6.5	26.4
16-2-9D	25% (w/v) PEG 3350, 0.1 M citrate, pH 3.5	12.6
16-2-12D	20% (w/v) PEG 3350, 0.2 M sodium di-hydrogen phosphate	49.9
16-3-4D	2% (v/v) PEG 400, 2 M ammonium sulphate,0.1 M HEPES-Na, pH 7.5	50.0
16-3-10B	30% (w/v) PEG 6000, 0.1 M HEPES, pH 7.0	35.3
17-1-12A	1.5 M lithium sulphate mon, 0.1 M HEPES-Na, pH 7.5	19.8
17-2-2B	2 M ammonium sulphate, 0.1 M citrate, pH 3.5	14.4
	30% (w/v) polyethylene glycol monomethyl ether 2000, 0.1 M sodium acetate, pH 4.6, 0.2 M ammonium sulphate	
17-2-12A	20% (w/v) PEG 3350, 0.2 M di-ammonium hydrogen citrate	30.2
	25% (w/v) PEG 3350, 0.1 M citrate, pH 3.5	
38-1-10A	20% (v/v) PEG 6000, 0.1 M citrate, pH 4.0, 1 M lithium chloride	45.0
16-2-11B	20% (w/v) PEG 3350, 0.2 M sodium formate	45.9
16-3-3C	25% (w/v) PEG 3350, 0.1 M bis-Tris, pH 5.5	32.1
34-1-6D	30% (w/v) PEG 3000, 0.1 M CHES, pH 9.6	44.7

Table 4.1 Conditions used for crystallization of Fabs.

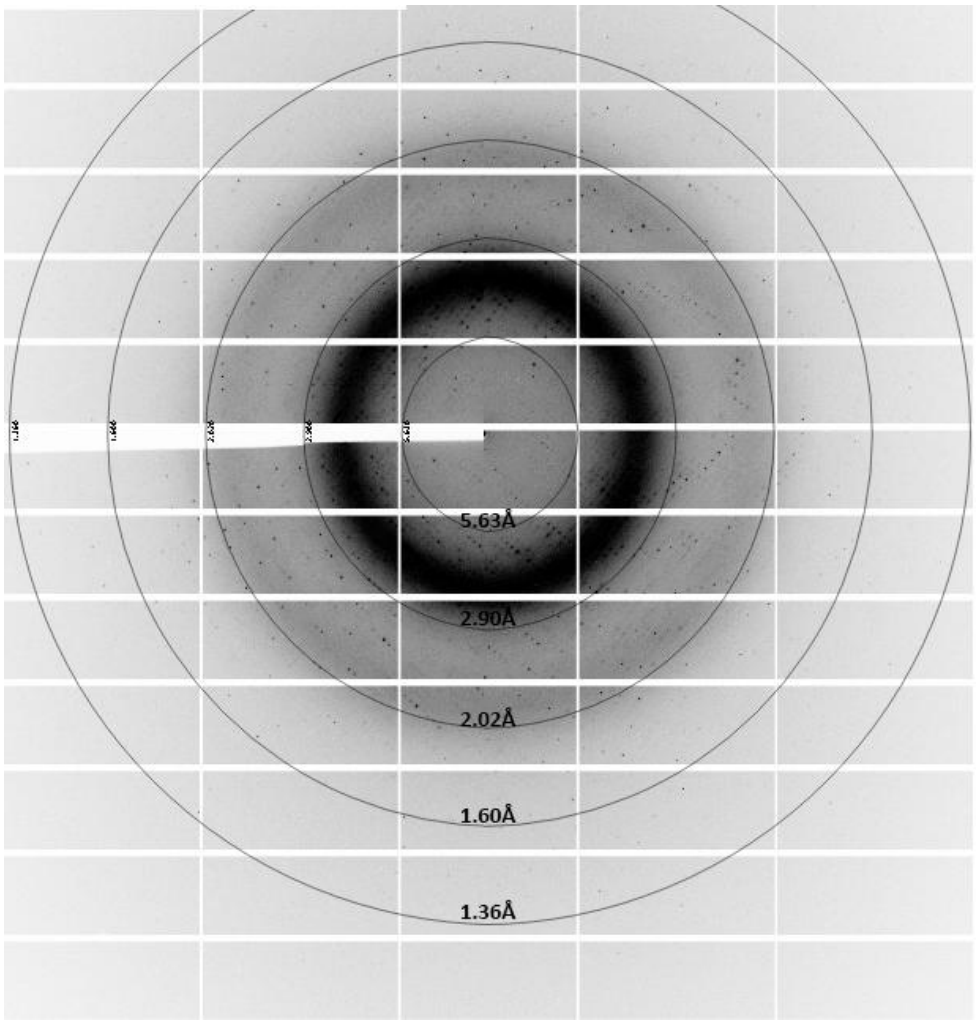

Figure 4.3 X-ray diffraction pattern from the crystal of Fab 16-2-9D

	Fab 16-2-9D
Data collection	
wavelength (Å)	0.9282
Space group	$P\ 1\ 2_1\ 1$
Cell dimensions	
a, b, c (Å)	47.7, 80.3, 57.5
α, β, γ (°)	90, 94.9, 90
Resolution (Å)	1.18
No. reflections	141520 (7009)
CC 1/2	1.0 (0.7)
I/σI	10.6 (2.0)
Rmerge	0.07 (-)
Completeness (%)	100 (99.6)
Redundancy	6.3 (4.9)
Refinement	
No. reflections	141486 (7068)
Number of molecules in each asymmetric unit	1
Rwork / Rfree	0.152/0.177
No. atoms	
Protein	3439
Ligand/ion	12
Water	618
B-factor	
Protein	18
Ligand/ion	37
Water	35
R.m.s. deviations	
Bond lengths (Å)	0.007
Bond angles (°)	1.12
Ramachandran plot	
Favored (%)	95.19
Allowed (%)	4.57
Outliers (%)	0.24

Table 4.2 Data collection and refinement statistics of X-ray diffraction for Fab 16-2-9D (Outer shell in parenthesis).

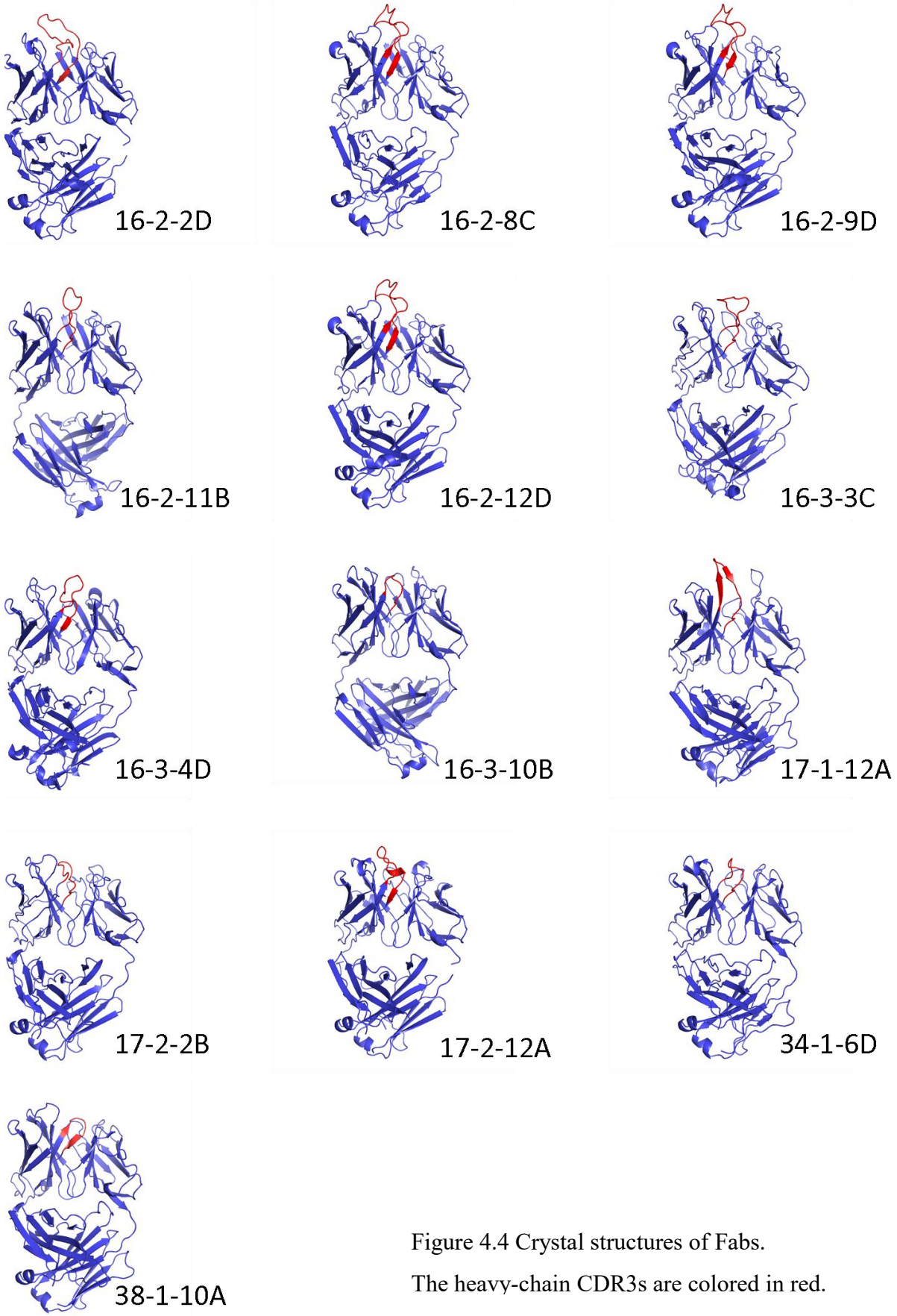

Figure 4.4 Crystal structures of Fabs.

The heavy-chain CDR3s are colored in red.

From the high-resolution crystal structures of these Fabs, we can easily see these antibodies have variable lengths of CDRs, especially heavy-chain HCDR3 (HCDR3). Across the set there is a significant variation in the length of the HCDR3s (between 9 and 24 aa, Table 4.3), consistent with them recognizing different epitopes (See Chapter 5). The CDR3s are determined by the Abnum numbering scheme[258] and crystal structures of Fabs. Overall the range of loop lengths is consistent with that expected for human IgGs and significantly longer, for instance, than that for murine antibodies, where this loop has an average length of 11.5 ± 1.9 AA residues[259]. There are two cysteine residues forming a disulphide bond in each of the HCDR3 regions of mAbs 16-2-8C, 16-2-9D, 16-2-11B and 16-2-12D (Table 4.3). These disulphide bonds stabilize the HCDR3 regions and affect the antigenicity of these antibodies.

Although glycosylation sites are predicted from the sequences of most of these antibodies, we cannot find any significant electron density for sugar in any of these crystal structures of Fabs, despite them being expressed in mammalian cells routinely used for the expression of glycoproteins. Based on the structures of the variable regions, we can draw an unrooted phylogenetic tree for the 13 anti-EV71 Fabs, showing the structural relationship among them (Figure 4.5).

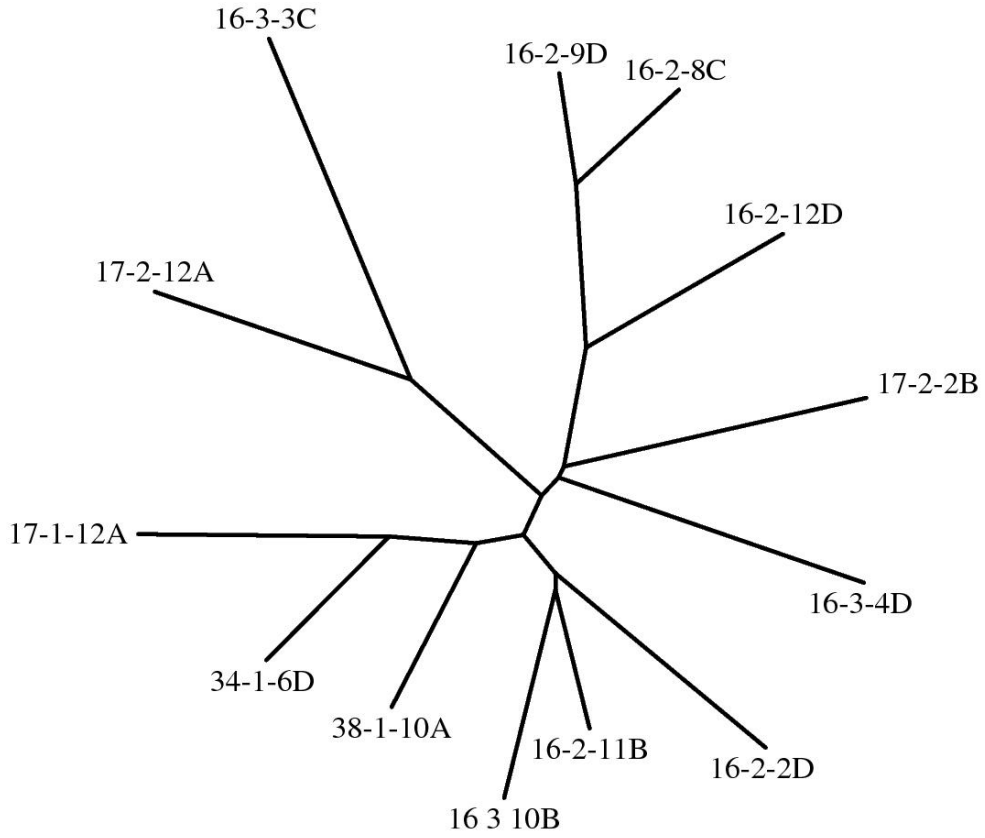

Figure 4.5 Structure-based unrooted phylogenetic tree for the 13 anti-EV71 Fabs. This tree is calculated in the Structure Homology Program (SHP)[246] using the crystal structures of the variable regions.

Antibody	Sequence of HCDR3	Length of HCDR3 (aa)
16-2-2D	GPGPGGKYYYDSSDAYYYYGMDV	23
16-2-8C	HSSPQCSPTSCYEGPYTRDWYVDY	24
16-2-9D	SSPQCSPTSCYEGPYTRDWYVDY	24
16-2-11B	NYNGYCAGDCYSPDF	15
16-2-12D	HASPHCSSTSCYDGPYNKNWYVDL	24
16-3-3C	DGPSSGWSYQNYYNAMDV	18
16-3-10B	DPLGNWFDP	9
17-2-2B	TYGSGSYWGYFEY	13
17-1-12A	EKWEKLGKLYYYGLDV	16
17-2-12A	SVAARRFYFYYGMDA	15
16-3-4D	HVPVAGFGYYYYGMDV	16
34-1-6D	AKALLYYGMDV	11
38-1-10A	EITMIAWFDP	10

Table 4.3 Sequences and lengths of heavy-chain CDR3s of 13 anti-EV71 antibodies. Cysteines in the heavy-chain CDR3s are colored in orange.

4.2 Somatic mutations of anti-EV71 antibodies

Even with a relatively limited number of antibody genes, a human can probably generate more than 10 billion different antibodies to recognize and eradicate various types of microbes[260]. V-(D)-J recombination and somatic hypermutation are two factors leading to immunoglobulin diversity.

The variable regions of antibodies are encoded by V (variable), D (diversity), and J (joining) gene segments. For each antibody, one copy of V, D and J gene segments are randomly selected from multiple copies and combined together to encode the variable region of the heavy chain (For light chain, only V and J segments are combined).

Tables 4.2 and 4.3 indicate the predicted V-(D)-J gene usage of heavy and light chains of these 13 anti-EV71 antibodies. Antibodies 17-1-12A, 34-1-6D and 38-1-10A have kappa light chains, while the other 10 anti-EV71 antibodies have lambda light chains. A wide range of V, D and J genes were used to generate these antibodies, indicating one strategy used by the EV71-infected patient to eradicate virus. A previous study showed that the somatic hypermutation of anti-rotavirus antibodies requires both hotspot-directed and randomly-directed processes[261], these anti-EV71 antibodies may be generated in a similar way.

Antibody-HC	**Top V gene match**	**Top D gene match**	**Top J gene match**
16-2-2D	IGHV1-46*01 / IGHV1-46*02	IGHD3-22*01	IGHD3-22*01
16-2-8C	IGHV4-39*01	IGHD2-2*01 / IGHD2-2*03	IGHJ4*02
16-2-9D	IGHV4-39*01	IGHD2-2*01 / IGHD2-2*03	IGHJ4*02
16-2-11B	IGHV1-46*01	IGHD2-21*02	IGHJ4*02
16-2-12D	IGHV4-39*01	IGHD2-2*01 / IGHD2-2*03	IGHJ5*02
16-3-3C	IGHV3-9*01	IGHD6-19*01	IGHJ6*02
16-3-10B	IGHV7-4-1*02	IGHD3-16*01 / IGHD3-16*02 / IGHD3-22*01	IGHJ5*02
17-2-2B	IGHV4-39*01	IGHD3-10*01	IGHJ4*02
17-1-12A	IGHV3-11*05	IGHD7-27*01	IGHJ6*02
17-2-12A	IGHV3-23*04	IGHD6-6*01	IGHJ6*02
16-3-4D	IGHV4-39*01	IGHD6-19*01	IGHJ6*02
34-1-6D	IGHV7-4-1*02	IGHD1-26*01 / IGHD1-26*01 / IGHD1-7*01	IGHJ6*02
38-1-10A	IGHV5-51*01	IGHD6-13*01	IGHJ6*02

Table 4.4 Predicted heavy-chain V-D-J gene usage of 13 anti-EV71 antibodies, predicted by IgBlast[262].

Antibody-LC	Top V gene match	Top J gene match
16-2-2D	IGLV1-44*01	IGLJ1*01
16-2-8C	IGLV1-44*01	IGLJ3*02
16-2-9D	IGLV1-44*01	IGLJ3*02
16-2-11B	IGLV2-14*01	IGLJ2*01 / IGLJ3*01 / IGLJ3*02
16-2-12D	IGLV1-47*02	IGLJ2*01 / IGLJ3*01
16-3-3C	IGLV2-11*01	IGLJ2*01 / IGLJ3*01 / IGLJ3*02
16-3-10B	IGLV2-23*01 / IGLV2-23*03	IGLJ1*01
17-2-2B	IGLV2-8*01	IGLV2-8*01
17-1-12A	IGKV2-28*01 / IGKV2D-28*01	IGKJ2*01 / IGKJ2*02
17-2-12A	IGLV7-43*01	IGLJ3*02
16-3-4D	IGLV1-44*01	IGLJ3*02
34-1-6D	IGKV1-39*01 / IGKV1D-39*01	IGKJ4*01
38-1-10A	IGKV1-39*01 / IGKV1D-39*01	IGKJ3*01

Table 4.5 Predicted light-chain V-J gene usage of 13 anti-EV71 antibodies, predicted by IgBlast[262].

Somatic hypermutation also happened in the generation process of nearly all these antibodies. Table 4.4 shows the somatic hypermutations causing amino acid alterations of these 13 antibodies, compared to their germline genes. Generally, each antibody has more mutations in the heavy chain than its light chain. Most of these mutations are located at the framework regions, rather than CDRs, which is quite interesting, since CDRs are the main regions bind to antigens and determine the specificities of most antibodies. However, a study has also indicated somatic mutations in the framework regions are required for broad and potent neutralization abilities of some anti-HIV human antibodies[263]. More experiments need to be done to check if and how the somatic mutations in the framework regions of these anti-EV71

antibodies contribute to the neutralization against EV71. Moreover, most of the sites where most somatic mutations happened are not involved in EV71-antibody interaction, we will talk about this in detail in Chapter 5.

Chain of antibody	**Somatic hypermutation**	**No. of mutations in framework regions / CDRs**
16-2-2D_HC	K12R, K13E, T28N, T30I, S31Y, M34I, I50M, I51V, N52R, S57R, S59I, Q62R, S75F, S77N, V79L, Y80F, S88P	**12/5**
16-2-2D_LC	I20S, S31R, N35D, Q39K, Y50H, S71T, S95R, T103S	**5/3**
16-2-8C_HC	T23S, G27V, S32R, S33T, S52M, S58I, Y60H, N62S, R68P, T75K, K83V, S85T, V94M, A98V, T128V	**11/4**
16-2-8C_LC	G30R, S31G, Q39K, T43A, K46T, S51T, Y88F, D94G	**4/4**
16-2-9D_HC	L2V, T23S, G27V, S32R, S33T, S52T, S58I, Y60H, N62S, R68P, T75K, K83E, S85T, V94M, T128V	**11/4**
16-2-9D_LC	V3A, G30R, Q39K, T43A, K46T, S51T, Y88F, D94G	**5/3**
16-2-11B_HC	A24T, S31N, Y32F, I50V, I51M, N52D, S54R, S57G, S59V, K63R, V68L, M70V, E82D, R87K, G105A, Y113F	**9/7**
16-2-11B_LC	A3V, T23I, V29I, G30D, G31A, L48V, M49I, E52D, S54R, S92A, Y93F, S95T, T108A	**7/6**
16-2-12D_HC	K13R, S31T, S32R, S33T, E48D, S52I, I53V, S58I, Y60H, T70S, K77R, K83S, S85R, A93T, P123L, Q126P	**11/5**
16-2-12D_LC	V3A, Y35F, Q38R, S51T	**2/2**
16-3-3C_HC	R16G, A33V, G50S, N54H, S55G, G59A, D62G, K76R, Y80F, A88T, Y95F, Y112N, G113A	**8/5**
16-3-3C_LC	S21T, T25S, S27I, M49I, S54G, D62A, A86T, Y97D	**3/5**
16-3-10B_HC	A24V, G26R, Y27S, T30V, S31N, M34V, Q82L, S85G, E89D, T91S	**6/4**
16-3-10B_LC	D28I, V29F, N33Y, H41Y, M49I, I50V, D87A, S96T, S97R	**3/6**
17-2-2B_HC	L2V, I29V, D111E	**2/1**
17-2-2B_LC	none	**0/0**
17-1-12A_HC	A23E, G26E, F29S, S30N, V48I, Y50D, S52R, S54R,	**10/8**

	S55G, Y57H, I70M, N74I, A75G, K76E, L79V, Q82H, A88V, M112L	
17-1-12A_LC	H31N, D65G, V90I, Y91F, L109V	**4/1**
17-2-12A_HC	S30N, S35N, K43R, A50V, G53D, S54T, S57T, A61T, D62K, I70V, Q82D, M83L, V93I, Y107F, V113A	**10/5**
17-2-12A_LC	T2A, G32D, A48S, K56T, G79N, E83K, Y89F, A97S	**5/3**
16-3-4D_HC	T23S, S31I, Q41L, I53V, S58P, Y61H, V73L, S76A, K77N, S85T, A89G, T92A	**8/4**
16-3-4D_LC	G12E, S26R, S31R, N32K, Q39R, N52D, N53T	**3/4**
34-1-6D_HC	Q6E	**1/0**
34-1-6D_LC	none	**0/0**
38-1-10A_HC	none	**0/0**
38-1-10A_LC	none	**0/0**

Table 4.6 Somatic hypermutations causing amino acid alterations in framework regions (black) and CDRs (blue) in heavy (HC) and light chains (LC) of anti-EV71 antibodies. Numbers of amino acid alterations in framework regions and CDRs of each chain are listed. If there are more than one germline genes predicted for one antibody in Table 4.4 and 4.5, the first predicted one is used for the amino acid alteration in this table.

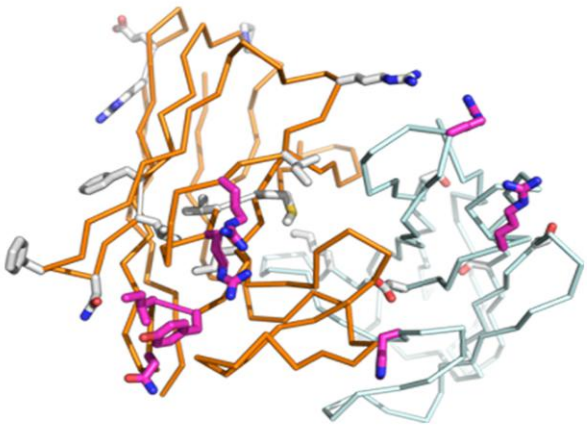

16-2-2D

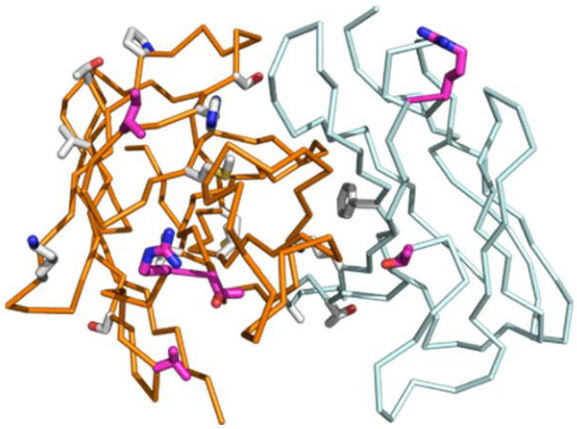

16-2-8C

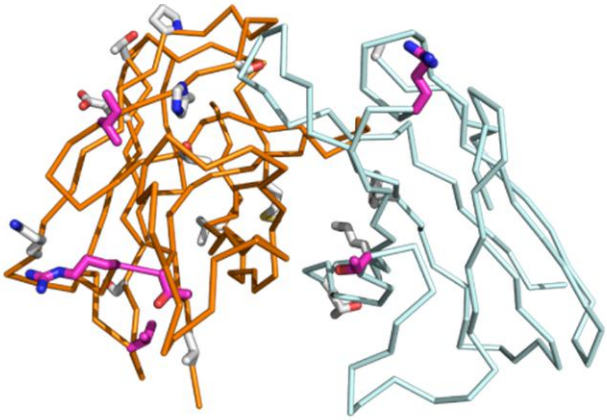

16-2-9D

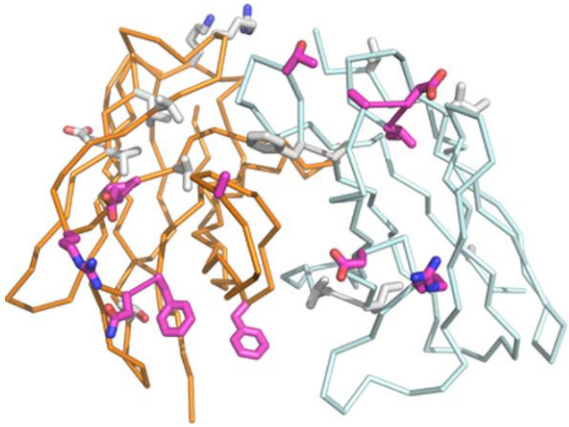

16-2-11B

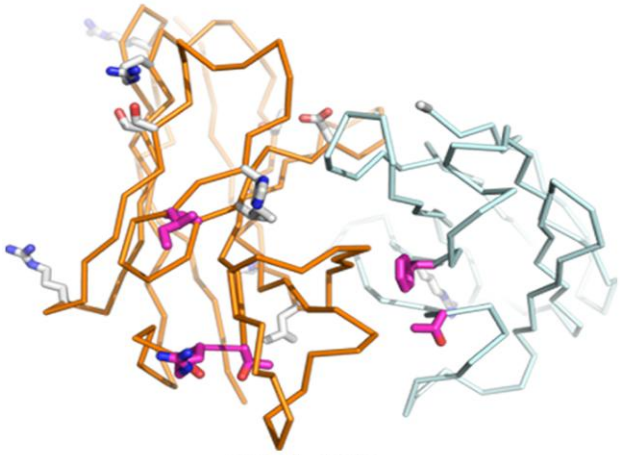

16-2-12D

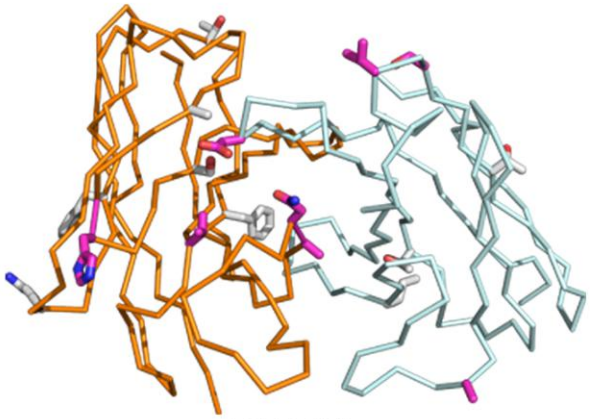

16-3-3C

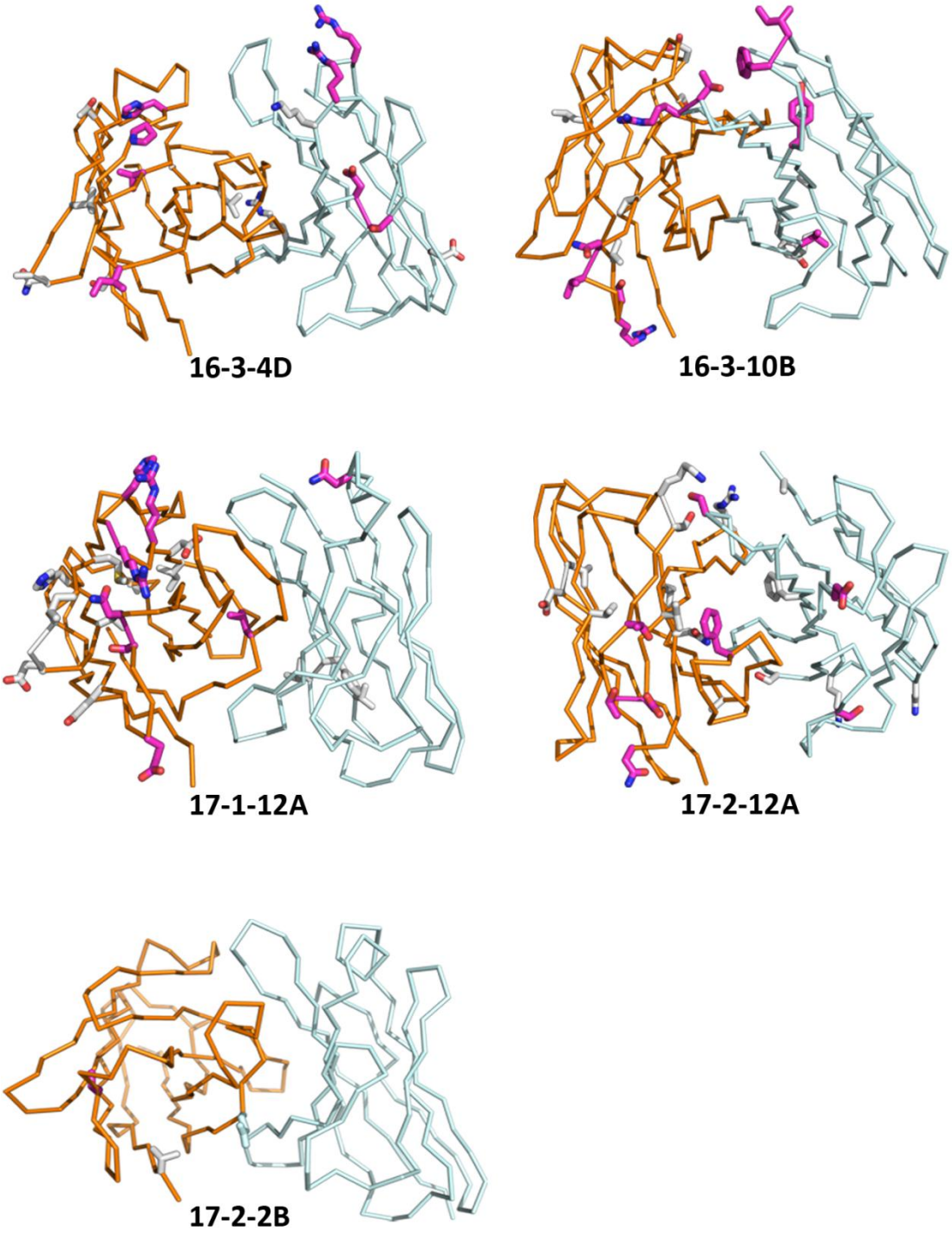

Figure 4.6 Somatic hypermutations causing amino acid alterations in framework regions (grey sticks) and CDRs (pink sticks) in heavy (orange ribbon) and light chains (cyan ribbon) of anti-EV71 antibodies.

4.3 Antibodies 16-2-8C and 16-2-9D

Anti-EV71 antibodies 16-2-8C and 16-2-9D were both generated by the same EV71-infected patient (donors M)[208] and they are quite similar to each other. The sequence similarity between Fab regions of these two antibodies is as high as 98.7%, with only four and two amino acid variations in the variable regions of the heavy and light chains, separately (Figure 4.6.b), while the sequence similarity between other antibodies ranges from ~40% - 80%. As expected, the structure-based phylogenetic tree also indicates antibodies 16-2-8C and 16-2-9D are close to each other (Figure 4.5). Cα RMSD between variable region structures of these two antibodies is only 0.39 Å and the crystal structures of Fab 16-2-8C and 16-2-9D are essentially indistinguishable from each other (Figure 4.7). Tables 4.2 and 4.3 also show they use the same germline genes. Although most of the somatic mutations that happened to these two antibodies were exactly the same, there were different somatic mutations in six sites (Table 4.4 and Figure 4.6.a). Thus different somatic mutations are responsible for the different sequences of these two antibodies, although they were generated from the same germline genes (Figure 4.4 and 4.5).

a

Mutation site	mAb 16-2-8C	mAb 16-2-9D
HC 2	No mutation	L2V
HC 52	S52M	S52T
HC 83	No mutation	K83E
HC 98	A98V	No mutation
LC 3	No mutation	V3A
LC 31	S31G	No mutation

b

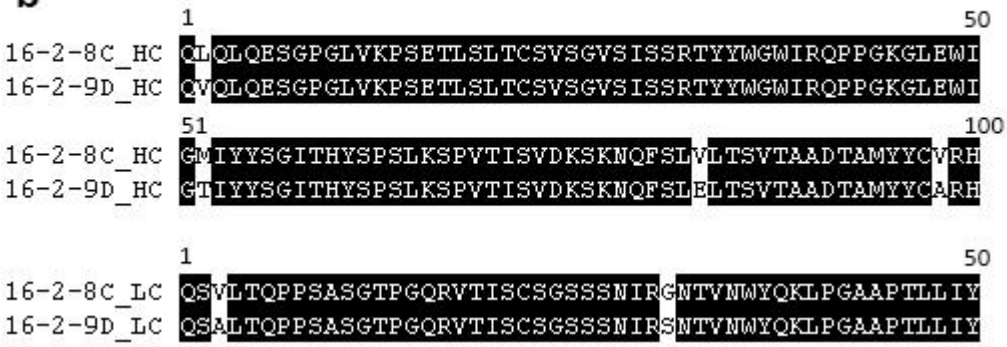

Figure 4.7 Different somatic mutations in antibodies 16-2-8C and 16-2-9D (**a**) amino acid sequence alignment of variable regions of these two antibodies (**b**). In **b**, same amino acids are with black background while different ones are with white. Different mutations in **a** lead to different sequences in **b**, although these two antibodies were generated from the same germline genes.

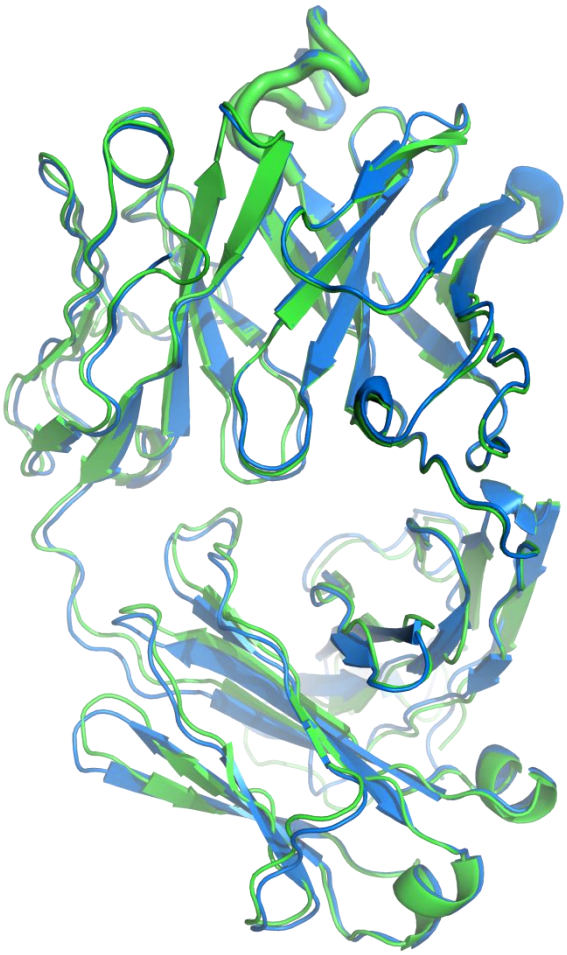

Figure 4.8 Overlay of crystal structures of Fabs 16-2-8C (green) and 16-2-9D (blue). CDRs of these two Fabs are drawn as thick loops.

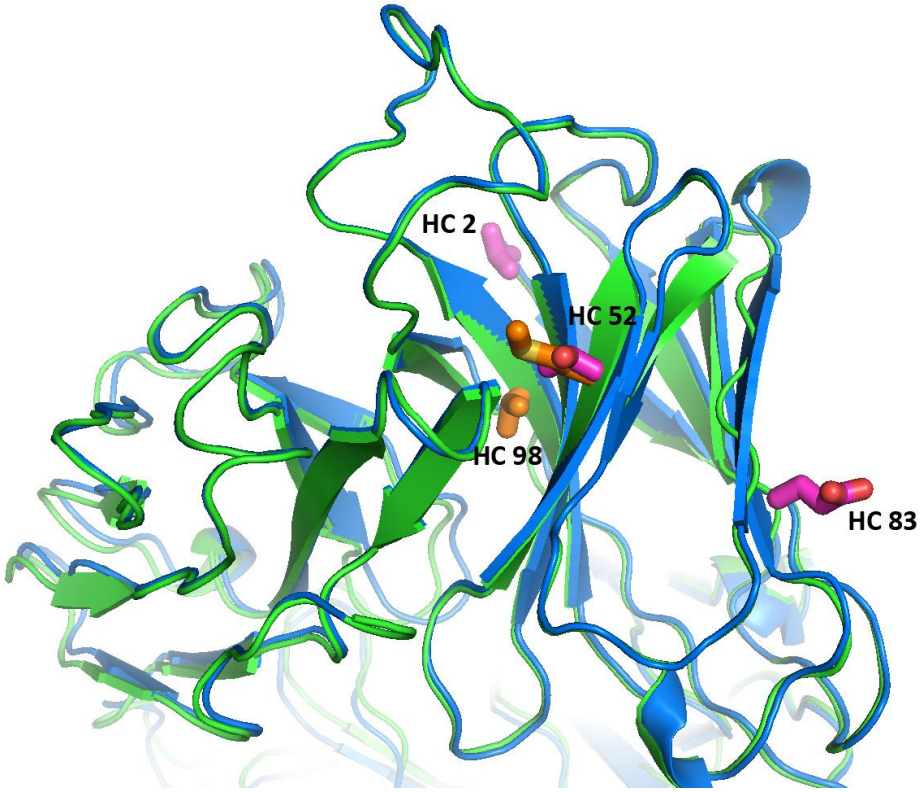

Figure 4.9 Overlay of variable regions of Fabs 16-2-8C (green) and 16-2-9D (blue), showing different somatic mutations (orange sticks for 16-2-8C and pink sticks for 16-2-9D). The site HC 2 is not shown here because it is absent from the crystal structure of 16-2-9D.

The extreme similarity of antibodies 16-2-8C and 16-2-9D leads to nearly identical binding patterns for these two antibodies with EV71 virion (Chapter 5). However, the neutralizing abilities of these two antibodies against EV71 are different, especially with different EC_{50} in the pre-attachment stage, which is related to the amino acid variation and different somatic mutations of these two antibodies[208].

4.4 Summary

The high-resolution structures of anti-EV71 Fabs indicate these antibodies have

variable lengths of HCDR3, recognizing different epitopes on the surface of the EV71 capsid. There are two cysteine residues forming a disulphide bond in each of the HCDR3 regions of mAbs 16-2-8C, 16-2-9D, 16-2-11B and 16-2-12D. These disulphide bonds stabilize the HCDR3 regions and affect the antigenicity of these antibodies. Fabs 16-2-8C and 16-2-9D were generated from the same germline genes, with high-identity sequences and indistinguishable crystal structures. There are only six amino acid variations between these two Fabs and five of these variations locate at the framework region. These variations cause different flexibility of the antibodies and are responsible for the different EC_{50}s of these two antibodies in the pre-attachment stage of EV71 infection.

A wide range of germline genes were used to generate these antibodies, indicating one strategy used by the EV71-infected patient to eradicate virus with various antibodies. Nearly all these antibodies have somatic hypermutations compared to their germline genes. Most of these mutations are located at the framework regions, rather than CDRs. Mutations at the framework regions may not be directly involved in interaction with EV71, but may affect the flexibility of the antibodies, which is required for broad and potent neutralization.

Chapter 5

Cryo-EM studies on EV71-antibody interactions

We have solved the crystal structures of 13 anti-EV71 Fabs (resolutions between 1.14 and 3.06 Å, see Chapter 2, 4 and Appendix tables 2 - 5). Cryo-EM structures of all 13 EV71-Fab complexes were also solved at high resolution (between 3.0 and 4.1 Å, Figure 5.1, and 5.2). Crystal structures of EV71 (PDB: 3VBS[31]) and the appropriate Fabs were fitted into these cryo-EM maps and then refined to obtain atomic models of EV71-Fab complexes. Details of the methods and statistics are given in Chapter 2 and Appendix tables 6 – 9, and a summary is provided in Table 5.1.

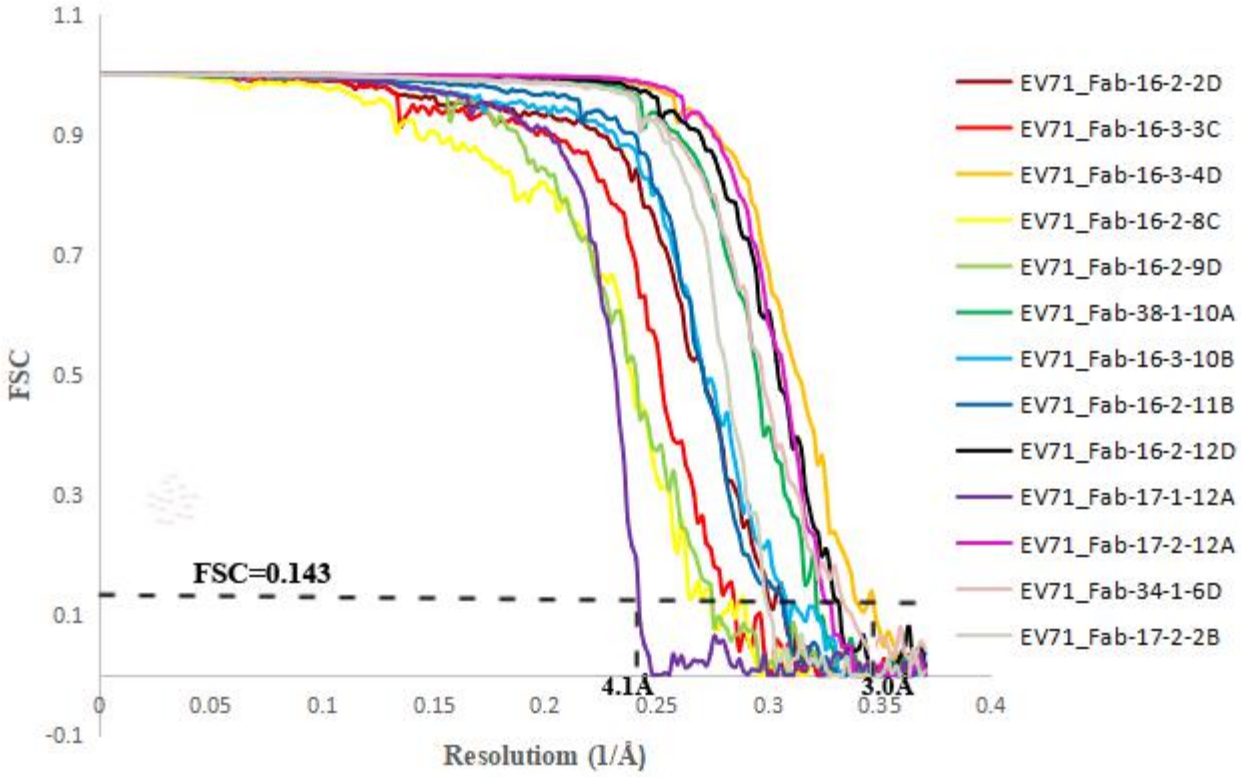

Figure 5.1 Fourier shell correlation (FSC) curves of 13 EV71-Fab cryo-EM reconstructions

EV71-Fab structure	**Resolution (Å)**	Ramachandran plot (Favored, %)	R.m.s.d., bonds (Å)	R.m.s.d., angles (°)	Map sharpening B-factor (Å^2)
16-2-2D	3.4	93.8	0.01	0.85	-103.1
16-2-8C	3.8	93.1	0.009	0.880	-123.7
16-2-9D	3.7	95.3	0.009	0.862	-145.4
16-2-11B	3.3	92.7	0.01	0.96	-140.0
16-2-12D	3.1	93.7	0.013	1.067	-132.8
16-3-3C	3.6	93.6	0.01	0.953	-124.6
16-3-10B	3.3	93.6	0.01	1.07	-110.5
17-2-2B	3.4	94.0	0.006	0.809	-156.5
17-1-12A	4.1	90.7	0.01	0.85	-175.3
17-2-12A	3.1	94.8	0.007	0.865	-150.5
16-3-4D	3.0	95.0	0.007	0.863	-127.6
34-1-6D	3.0	93.8	0.01	0.99	-113.0
38-1-10A	3.1	94.2	0.007	0.875	-131.2

Table 5.1 Summary of cryo-EM structures of EV71-Fab complexes

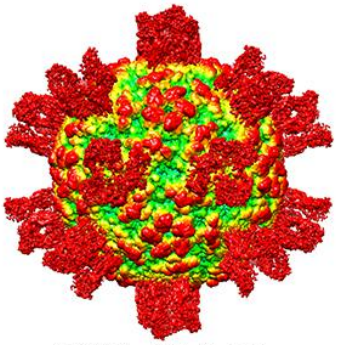

EV71_16-3-4D

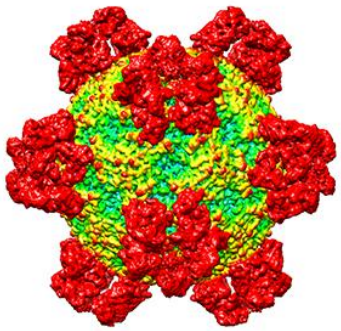

EV71_16-3-10B

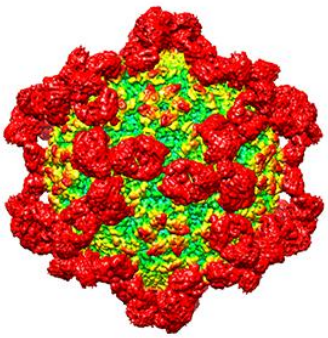

EV71_17-1-12A

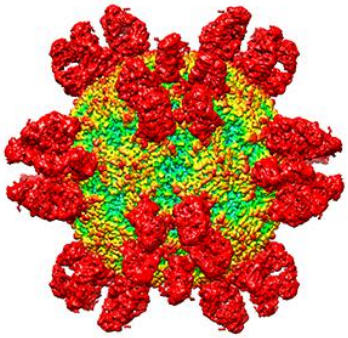

EV71_17-2-2B

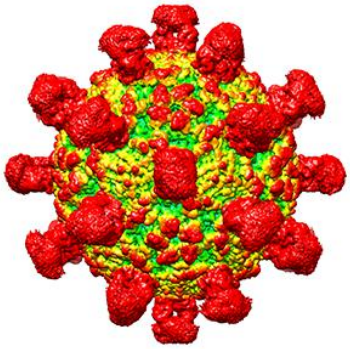

EV71_17-2-12A

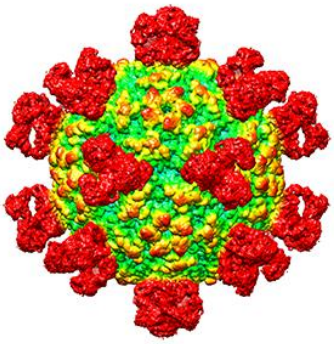

EV71_34-1-6D

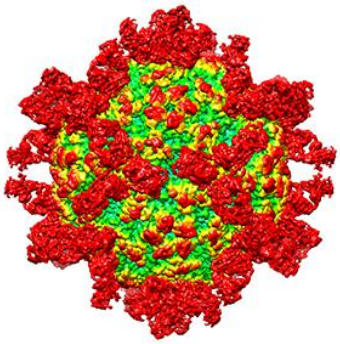

EV71_38-1-10A

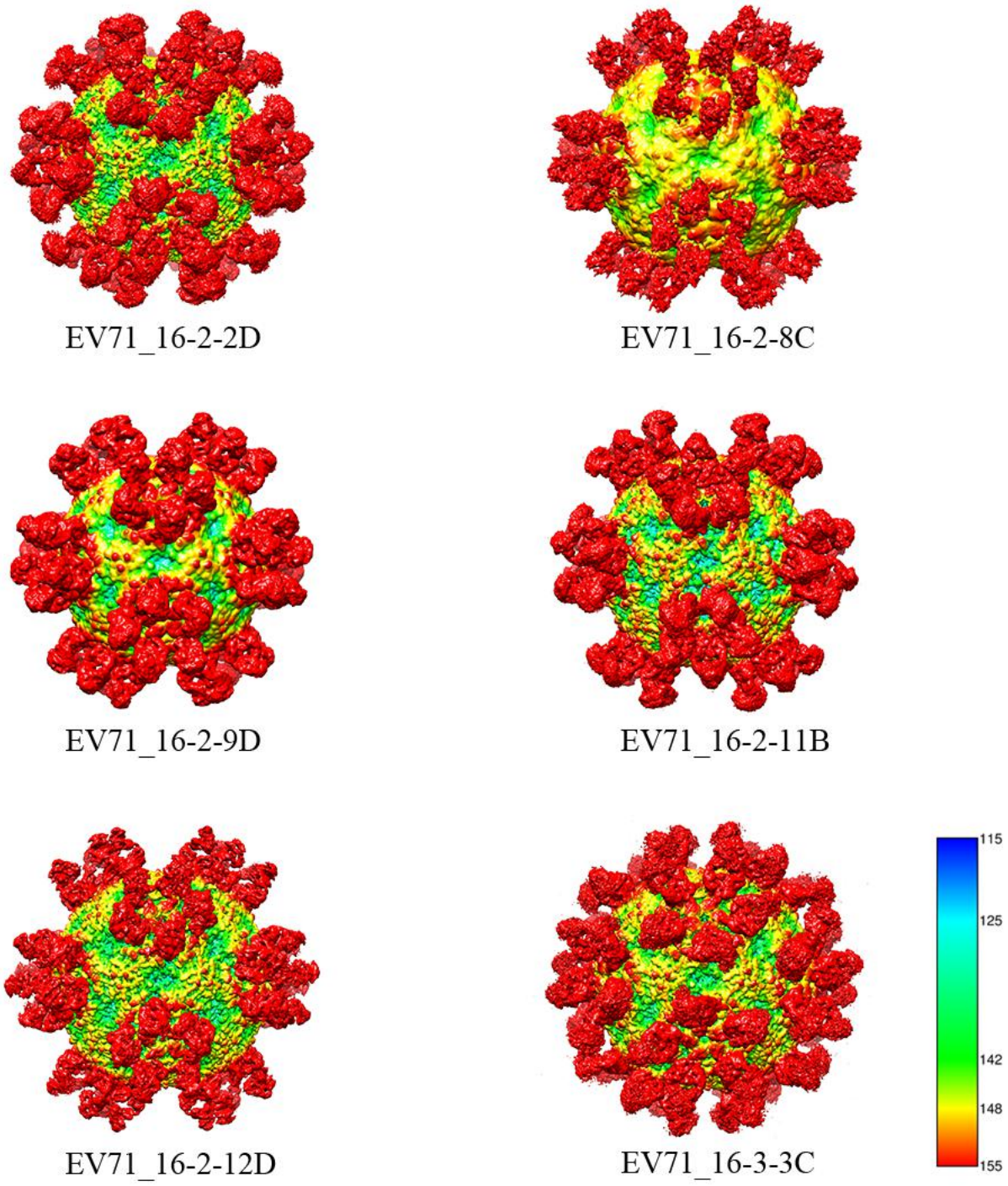

Figure 5.2 Cryo-EM reconstructions of EV71-Fab complexes. The reconstructions are rainbow colored based on the distance (Å) of the surface from the center of the particle.

5.1 Binding patterns of mAbs

The high-resolution structures allow us to precisely map the interactions between EV71 and different mAbs. In these EV71-Fab complexes, one molecule of Fab 17-2-2B interacts with only one protomer of the EV71 capsid, while all the other Fabs interact with two protomers. Fab 17-2-12A and Fab 34-1-6D can bind at most 30 and 20 molecules respectively to a single capsid whilst for all the other Fabs, 60 molecules can attach to one capsid. All Fabs have a significant footprint on the viral surface (area of interaction of each Fab with the EV71 capsid is between ~ 900 and ~1700 $Å^2$, see Appendix table 11). Figure 5.3 shows the binding areas between EV71 and each Fab. We also drew the binding residues of EV71 on 2D roadmaps of the EV71 capsid surface (Figure 5.12 – 24). From these roadmaps, it is easy to see the different binding patterns of the 13 Fabs.

Prior to structural analysis these Fabs had been classified into five distinct groups, three of these were canyon associated and were termed canyon-floor, canyon-northern-rim and canyon-southern-rim binders[208]. The structures indicate that these all interact with residues in the canyon region and there are not distinct regions of interaction. The two remaining binding sites were defined as regions close to the 2-fold-axes and 3-fold-axes respectively. Based on the binding areas of Fabs, these last two categories are appropriate and we therefore re-classified the epitopes into three groups: canyon binders (Fabs 16-2-2D, 16-2-8C 16-2-9D, 16-2-11B, 16-2-12D, 16-3-3C, 16-3-10B, 17-2-2B), 2-fold-axis binders (Fabs 17-1-12A and 17-2-12A) and 3-fold-axis binders (Fabs 16-3-4D, 34-1-6D and 38-1-10A).

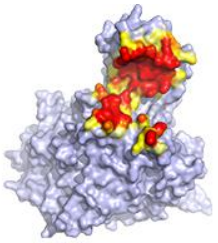
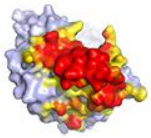


16-2-2D

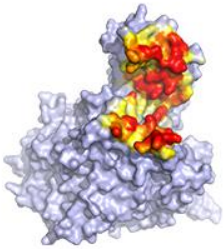

16-2-8C

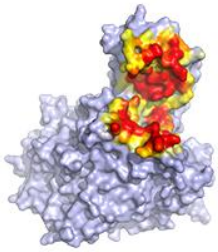
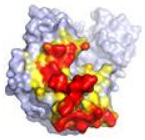
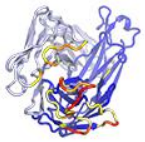

16-2-9D

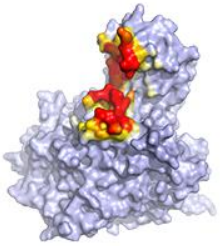

16-2-11B

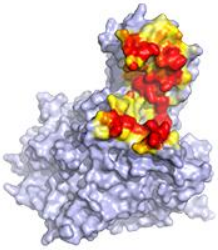

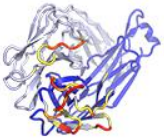

16-2-12D

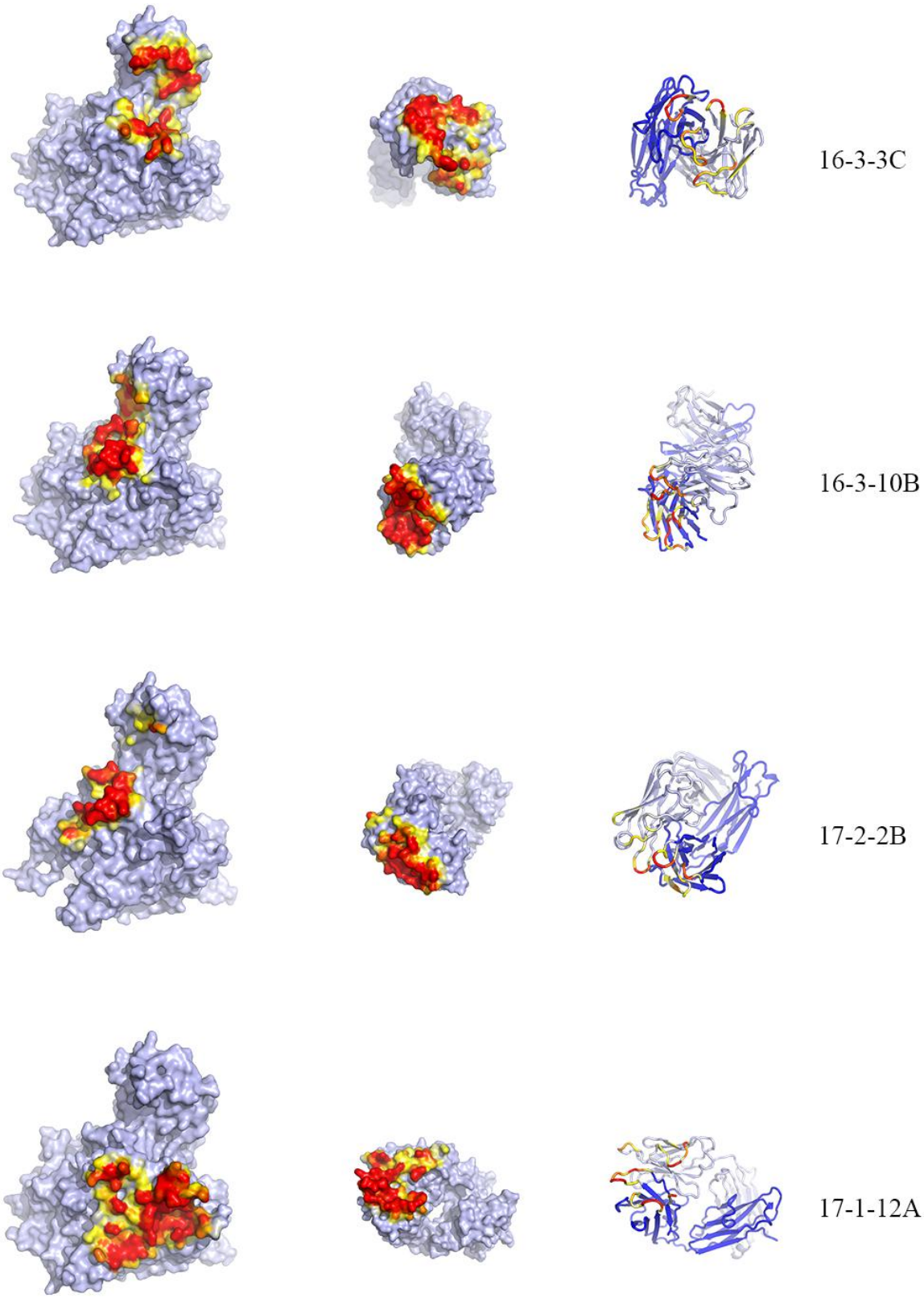
16-3-3C
16-3-10B
17-2-2B
17-1-12A

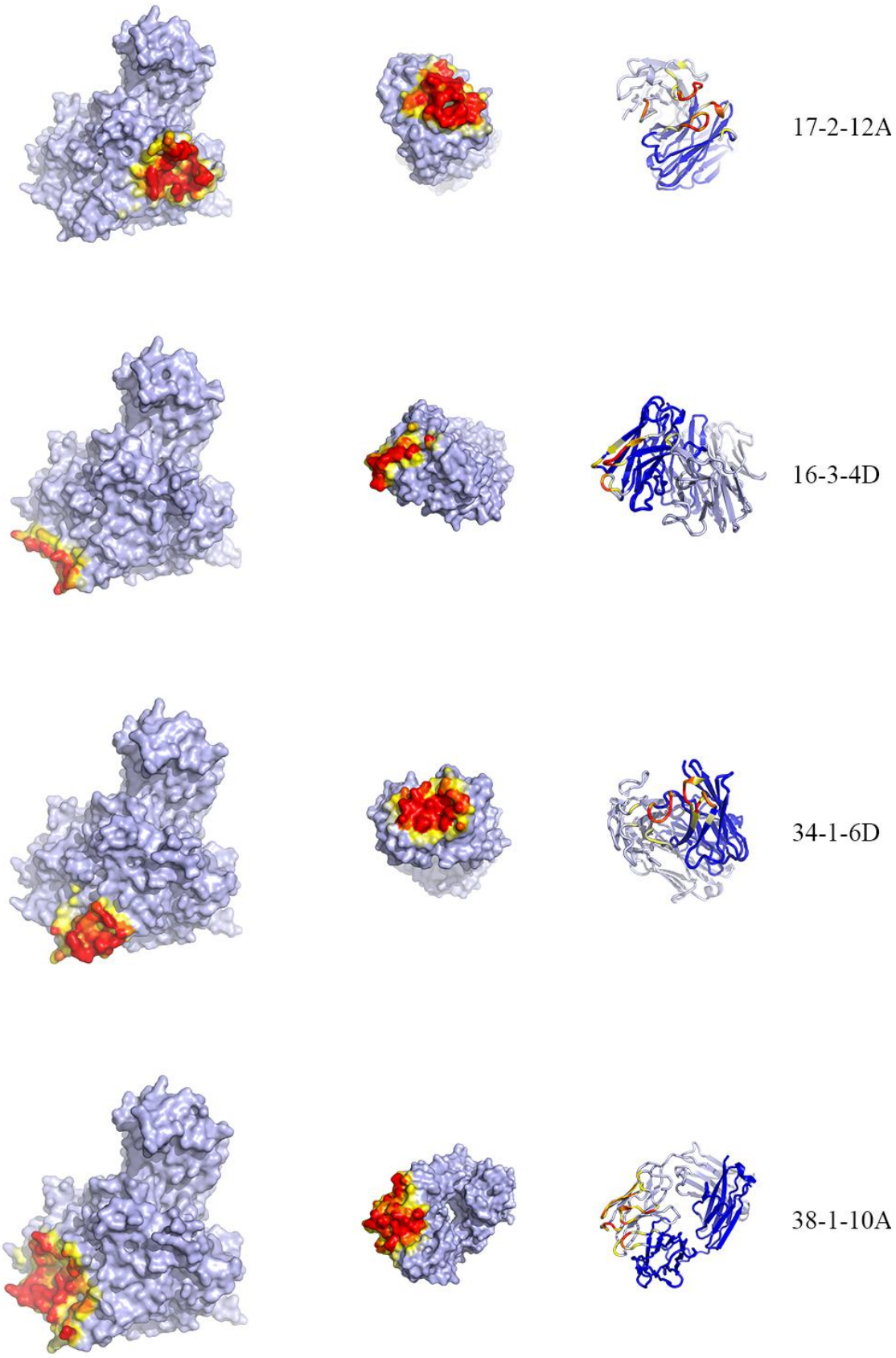

Figure 5.3 Surface and cartoon representations showing binding areas between EV71

and anti-EV71 Fabs. Contact areas between the virus and Fab with distances ≤ 4.0 Å are shown in bright red, > 4.0 Å and ≤ 9.0 Å in yellow. Heavy and light chains of Fabs in the cartoon representations are colored in blue and grey, respectively.

Antibodies targeting each of these three areas (canyon, 2-fold-axis area or 3-fold-axis area) have partially overlapped footprints, which explains our collaborator's results that antibodies of the same group can cross-inhibit each other in the binding assay. However, antibodies targeting different areas share no or few common binding residues, so they can hardly compete with each other[208] (Figure 5.4). Nevertheless, overall the observed epitopes include ~90% of the residues exposed on the virus surface, a remarkably high coverage.

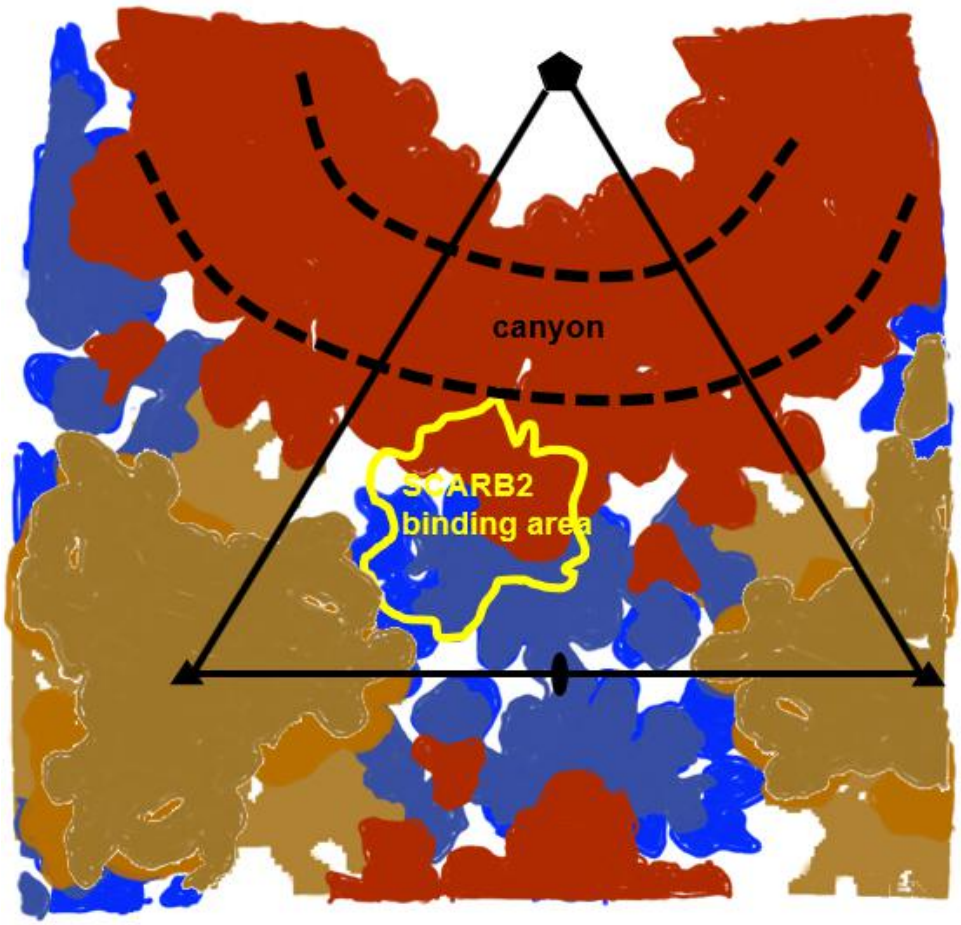

Figure 5.4 Roadmap showing footprints of anti-EV71 Fabs on the surface of EV71 capsid in an asymmetric unit. Footprints of canyon binders are colored in red whilst 2- and 3-fold-axis binders are colored blue and brown respectively. The binding area of the EV71 receptor, SCARB2, is marked with yellow line and the canyon region with a dashed line. In this roadmap, and all subsequent ones, the positions of the 5-, 3-, and 2-fold icosahedral symmetry axes are marked as pentagons, triangles, and ovals, respectively.

Canyon binders Fabs 17-2-2B and 16-3-10B show no significant preference to bind any one viral protein, while all the other canyon binders mainly interact with VP1. 2-fold-axis binders mainly bind VP2 and 3-fold-axis binders mainly interact with VP2 and VP3 (See Figure 5.12 - 24 and Appendix table 11).

The heavy chains of most of the Fabs have a much larger area of interaction with the capsid than the light chains, indicating that the heavy chains of these Fabs play the major role in Fab-EV71 interactions. The two exceptions are Fab 17-2-2B and 16-3-10B. The heavy and light chains of Fab 17-2-2B have nearly equal areas of interaction, while interestingly, the heavy chain of Fab 16-3-10B has much less area of interaction than its light chain (505 vs 900 $Å^2$ respectively) (for full details see Appendix table 11).

Heavy-chain CDR3 (HCDR3) is an important region involved in EV71-Fab interaction in these complexes. Canyon binders (except antibodies 16-3-10B and 17-2-2B) tend to have long HCDR3s ($\geq$ 23 aa for each of 4 Fabs, 18 aa for one Fab and 15 aa for another one), with which they can go deep into the canyon and interact with the residues at the base of the canyon (HCDR3 information is summarized in Table 5.2 and Figure 5.5). However, canyon binders Fabs 16-3-10B and 17-2-2B have shorter HCDR3s (9 aa for Fab 16-3-10B and 13 aa for Fab 17-2-2B). Instead of HCDR3, the light-chain CDR1 of mAb 16-3-10B stretches deep into the canyon whilst no part of mAb 17-2-2B penetrates deep into the canyon. Instead of the canyon region, the HCDR3 and LCDR3 of mAb 17-2-2B mainly interact with the south wall of the canyon (Figure 5.6). This may explain why the binding patterns of these two Fabs are totally different from other canyon binders, as mentioned previously. In contrast to most canyon binders, 2- and 3-fold-axis binders have relatively shorter HCDR3s (16aa at most) (Table 5.2).

	Sequence of HCDR3	Length of HCDR3 (aa)
	Canyon binders	
16-2-2D	GPGPGGKYYYDSSDAYYYYGMDV	23
16-2-8C	HSSPQCSPTSCYEGPYTRDWYVDY	24
16-2-9D	HSSPQCSPTSCYEGPYTRDWYVDY	24
16-2-11B	NYNGYCAGDCYSPDF	15
16-2-12D	HASPHCSSTSCYDGPYNKNWYVDL	24
16-3-3C	DGPSSGWSYQNYYNAMDV	18
16-3-10B	DPLGNWFDP	9
17-2-2B	TYGSGSYWGYFEY	13
	2-fold-axis binders	
17-1-12A	EKWEKLGKLYYYGLDV	16
17-2-12A	SVAARRFYFYYGMDA	15
	3-fold-axis binders	
16-3-4D	HVPVAGFGYYYYGMDV	16
34-1-6D	AKALLYYGMDV	11
38-1-10A	EITMIAWFDP	10

Table 5.2 Sequences and lengths of HCDR3s of anti-EV71 antibodies. Canyon binders (except antibodies 16-3-10B and 17-2-2B) tend to have longer HCDR3s than 2- and 3-fold-axis binders.

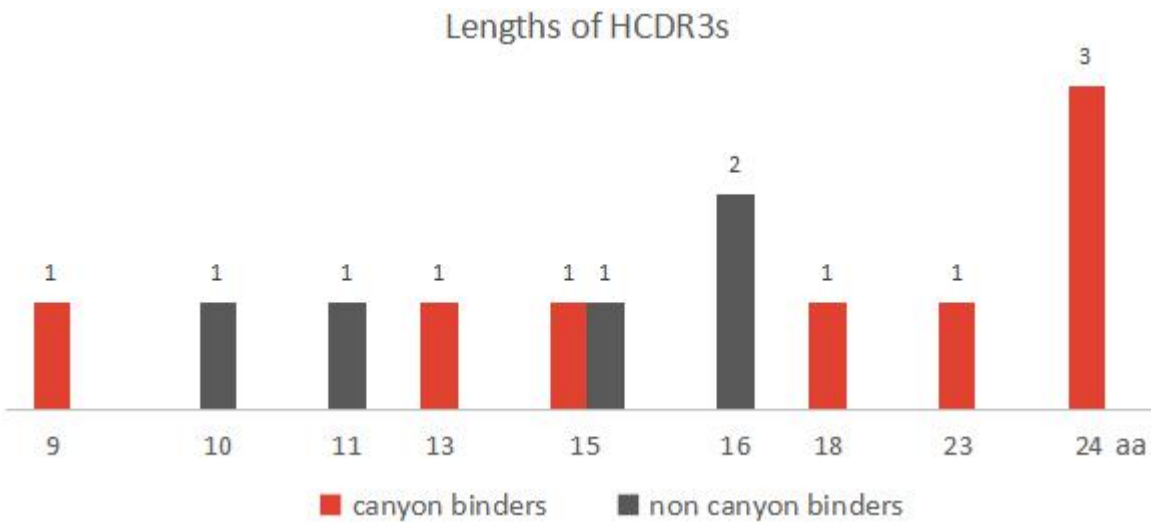

Figure 5.5 Lengths of HCDR3s of anti-EV71 antibodies. X axis represents length of HCDR3 (aa) and Y axis represents the number of antibodies having a certain length of HCDR3. Canyon binders are colored in red and non-canyon binders in black. This figure indicates that canyon binders tend to have longer HCDR3s.

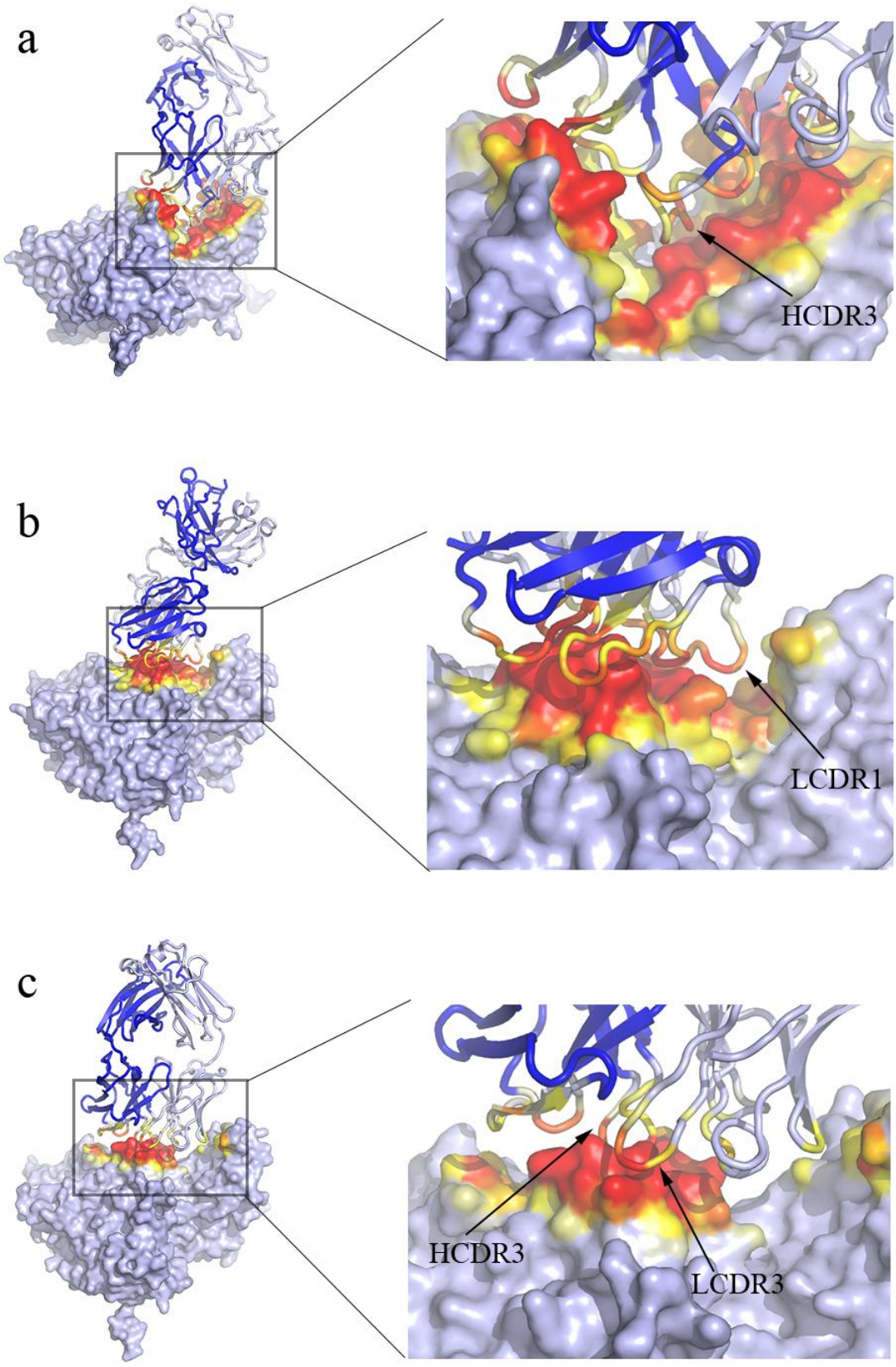

Figure 5.6 Different binding patterns of canyon binders of EV71. **a**. Antibody 16-2-12D, representing most of the canyon binders, of which the HCDR3s go deep into the

bottom of the canyon region. **b**. the light-chain CDR1 of Fab 16-3-10B stretches deep into the canyon. **c**. no part of Fab 17-2-2B goes deep into the canyon at all. The HCDR3 and LCDR3 of this Fab interact with the south wall of the canyon. The protomer of EV71 is shown in surface representation and Fabs shown in cartoon representation. Contact areas between the virus and Fab with distances ≤ 4.0 Å are shown in bright red, > 4.0 Å and ≤ 9.0 Å in yellow. Heavy and light chains of Fabs are colored in blue and grey, respectively.

The two 2-fold-axis binders are also distinct from each other. Fab 17-1-12A binds near while Fab 17-2-12A binds right at the 2-fold axis. The two arms of the IgG 17-1-12A molecule may span the 2-fold axis to bind adjacent pentamers in a bivalent binding pattern, which may strengthen this antibody's ability to block genome release. However, the IgG 17-2-12A Fab binds overlapping 2-fold axis that bivalent binding is prevented. 3-fold-axis binders are also distinguished in this way. Fab 34-1-6D occupies the 3-fold axis while Fabs 16-3-4D and 38-1-10A does not. Since the axes of symmetry are occupied, Fab 17-2-12A and Fab 34-1-6D can bind at most 30 and 20 molecules respectively to a single capsid.

5.2 Somatic mutations involved in EV71-antibody interactions

In Chapter 4.2 we talked about somatic mutations occurred in these anti-EV71 antibodies and the distribution of these mutations in the CDRs and framework regions. Here Table 5.3 shows most of these mutations are not directly involved in interaction with EV71. For those do interact with EV71, most of them locate at the CDRs, with only 6 out of 36 in the framework region (Table 5.3 and 4.6).

Chain of antibody	Somatic hypermutation	No. of mutations as binding/non-binding residues
16-2-2D_HC	K12R, K13E, T28N, T30I, S31Y, M34I, I50M, I51V, N52R, S57R, S59I, Q62R, S75F, S77N, V79L, Y80F, S88P	**2/15**
16-2-2D_LC	I20S, S31R, N35D, Q39K, Y50H, S71T, S95R, T103S	**0/8**
16-2-8C_HC	T23S, G27V, S32R, S33T, S52M, S58I, Y60H, N62S, R68P, (T75K), K83V, S85T, V94M, A98V, T128V	**2/13**
16-2-8C_LC	G30R, S31G, Q39K, T43A, K46T, S51T, Y88F, D94G	**2/6**
16-2-9D_HC	L2V, T23S, G27V, S32R, S33T, S52T, S58I, Y60H, N62S, R68P, T75K, K83E, S85T, V94M, T128V	**1/14**
16-2-9D_LC	V3A, G30R, Q39K, T43A, K46T, S51T, Y88F, D94G	**2/6**
16-2-11B_HC	A24T, S31N, Y32F, I50V, I51M, N52D, S54R, (S57G), (S59V), K63R, V68L, M70V, E82D, R87K, G105A, Y113F	**6/10**
16-2-11B_LC	A3V, T23I, V29I, G30D, G31A, L48V, M49I, E52D, S54R, S92A, Y93F, S95T, T108A	**3/10**
16-2-12D_HC	K13R, S31T, S32R, S33T, E48D, S52I, I53V, S58I, Y60H, T70S, K77R, K83S, S85R, A93T, P123L, Q126P	**1/15**
16-2-12D_LC	V3A, Y35F, Q38R, S51T	**0/4**
16-3-3C_HC	R16G, A33V, G50S, N54H, S55G, G59A, D62G, K76R, Y80F, A88T, Y95F, Y112N, G113A	**2/11**
16-3-3C_LC	S21T, T25S, S27I, M49I, S54G, D62A, A86T, Y97D	**0/8**
16-3-10B_HC	A24V, G26R, Y27S, T30V, S31N, M34V, Q82L, S85G, E89D, T91S	**1/9**
16-3-10B_LC	D28I, V29F, N33Y, H41Y, M49I, I50V, D87A, S96T, S97R	**3/6**
17-2-2B_HC	L2V, I29V, D111E	**0/3**
17-2-2B_LC	none	**0/0**
17-1-12A_HC	(A23E), G26E, F29S, S30N, V48I, Y50D, S52R, S54R, S55G, Y57H, I70M, (N74I), (A75G), K76E, L79V, Q82H, A88V, M112L	**5/13**
17-1-12A_LC	H31N, D65G, V90I, Y91F, L109V	**0/5**
17-2-12A_HC	S30N, S35N, K43R, A50V, G53D, S54T, S57T, A61T, D62K, I70V, Q82D, M83L, V93I, Y107F, V113A	**3/12**

17-2-12A_LC	T2A, G32D, A48S, K56T, G79N, E83K, Y89F, A97S	**1/7**
16-3-4D_HC	T23S, S31I, Q41L, I53V, S58P, Y61H, V73L, S76A, K77N, S85T, A89G, T92A	**2/10**
16-3-4D_LC	G12E, S26R, S31R, N32K, Q39R, N52D, N53T	**0/7**
34-1-6D_HC	Q6E	**0/1**
34-1-6D_LC	none	**0/0**
38-1-10A_HC	none	**0/0**
38-1-10A_LC	none	**0/0**

Table 5.3 Somatic mutations directly involved in EV71-antibody interactions (colored in red). Most of these mutations binding with EV71 locate at the CDRs, with just a few at the framework regions (marked with brackets).

5.3 Conformational changes of EV71 and Fabs in the process of binding

Conformational changes frequently occur during the process of protein-protein interaction. The same occurs on EV71-Fab binding. Whilst the cryo-EM structures of EV71 and Fabs closely resemble their crystal structures, significant conformational changes can be observed in the binding interfaces between EV71 and Fabs in most of the 13 EV71-Fab complexes. Seven out of these complexes show changes in the HCDR3s and in six out of 13 the EV71 capsid shows changes, mainly in the VP1 B-C and G-H loop (Table 5.4).

The conformational changes in the virus parts of four complexes (EV71_Fab-16-2-2D, EV71_Fab-17-1-12A, EV71_Fab-17-2-2B, EV71_Fab-17-2-12A) provide extra space, allowing the Fabs to fit into the binding sites. In the EV71_Fab-16-2-11B complex, conformational changes in the VP1 B-C loop increases complementarity with the virus capsid, increasing the binding affinity. None of these conformational changes in the

virus can be observed in related crystal structures or other EV71-Fab complexes mentioned here, so the binding of these Fabs fits the induced-fit model, which was proposed by Daniel Koshland in 1958[264].

Conformational changes are also observed in the C terminus of VP3 of EV71 in many of these EV71-Fab complexes, compared to crystal structure of EV71, however, these conformational changes were not caused by Fab binding. Instead, these represent different conformations of the C terminus of VP3 between EV71 genotype C4 and EV71 genotype B2 or B5.

	Significant conformation changes	
Complex	**Fab part**	**Virus part**
EV71_16-2-2D	HCDR3, HCDR2	VP1 B-C loop
EV71_16-2-8C	none	none
EV71_16-2-9D	none	none
EV71_16-2-11B	HCDR3	VP1 B-C loop
EV71_16-2-12D	HCDR2, HCDR3	none
EV71_16-3-3C	LCDR2, HCDR3	none
EV71_16-3-10B	LCDR2	none
EV71_17-2-2B	none	VP1 B-C loop
EV71_17-1-12A	none	VP1 GH loop, C terminus of VP2
EV71_17-2-12A	HCDR3	VP1 GH loop
EV71_16-3-4D	HCDR2	none
EV71_34-1-6D	HCDR3	none
EV71_38-1-10A	HCDR3	VP3 B-C loop

Table 5.4 Significant conformation changes of Fab and EV71 in the cryo-EM structures compared to their crystal structures

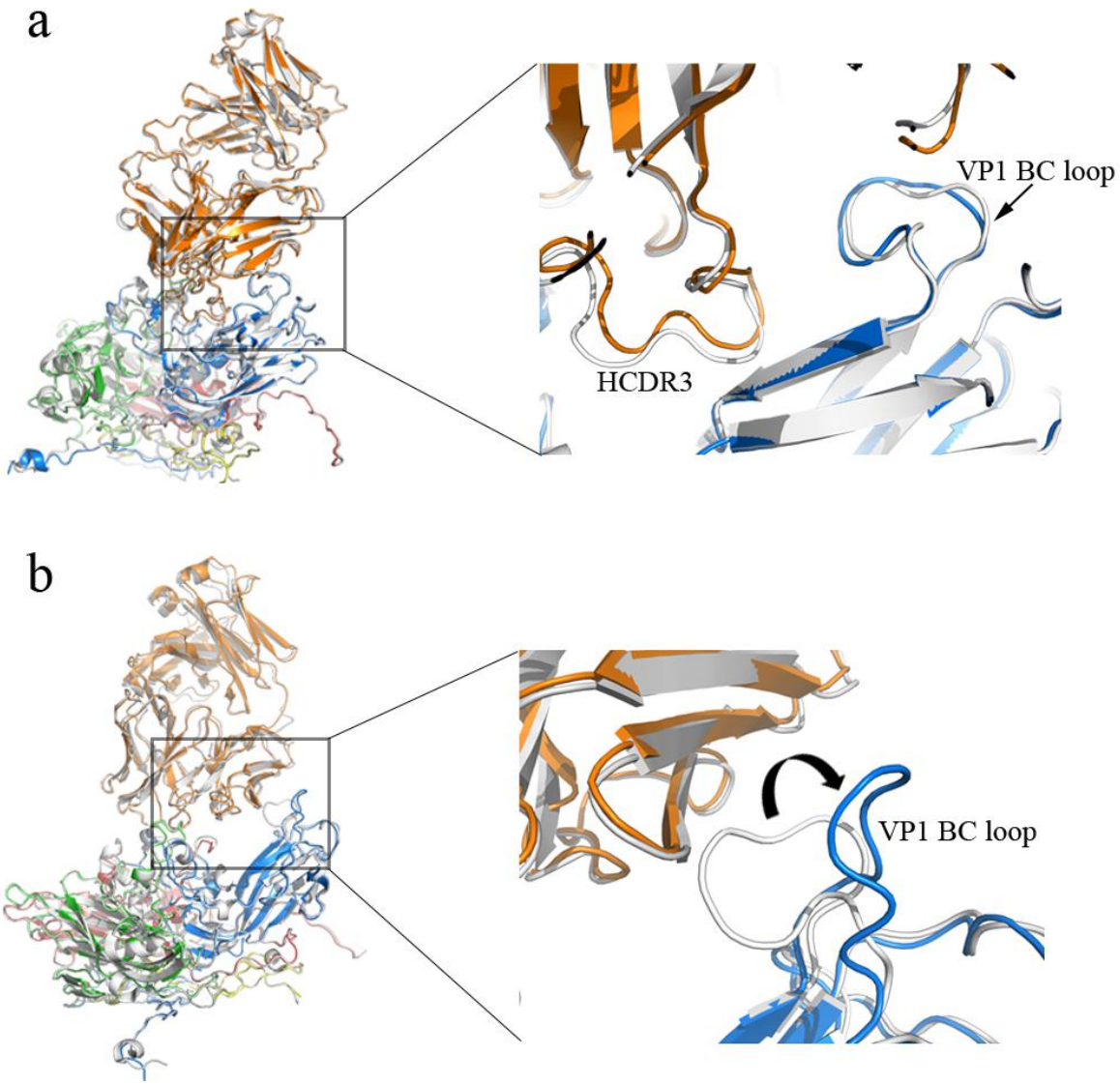

Figure 5.7 Examples of conformational changes on binding. These occur in the binding interfaces between EV71 and Fabs 16-2-12D (**a**) and 17-2-2B (**b**). VP1 – VP4 of EV71 are colored in blue, green, red and yellow, respectively. Fabs bound to EV71 are colored in orange. Native crystal structures of EV71 (PDB: 3VBS[31]) and Fabs are colored in grey.

5.4 Empty particles caused by three Fabs

It was reported a neutralizing antibody E18, can transform infectious virions of EV71 into empty particles[265]. A significant number of empty particles of EV71 were also observed on cryo-EM grids prepared after incubation with both Fabs 16-2-12D and 16-3-3C (at molar ratio EV71 particle: Fab = 1:200), despite the incubation process lasting for very short time (<10s) at low temperature (on ice) (Figure 5.8.a, b and d). Fab 16-2-2D also induced empty particles after being incubated with EV71 virions at 37 °C for 5 min (Figure 5.8.f). Thus Fabs 16-2-2D, 16-2-12D and 16-3-3C induce genome release and even destroy EV71 virions although the mechanism is not clear. All these antibodies are canyon binders and the changes they induce may be similar to those induced by binding of the uncoating receptors of EV71. We found that Fab 16-2-12D can induce genome release for EV71 genotypes B2 (Figure 5.8.a) and C4 (Figure 5.8.b), while Fab 16-3-3C and 16-2-2D can do this for EV71 genotype B5 (Figure 5.8.d, e and f). We have not investigated if they generate empty particles for other genotypes of EV71. Interestingly, when we changed the molar ratio of EV71: Fab to about 1:90 while keeping the other incubation conditions constant, Fab 16-3-3C can (Figure 5.8.e) but 16-2-12D cannot (Figure 5.8.c) cause empty particles.

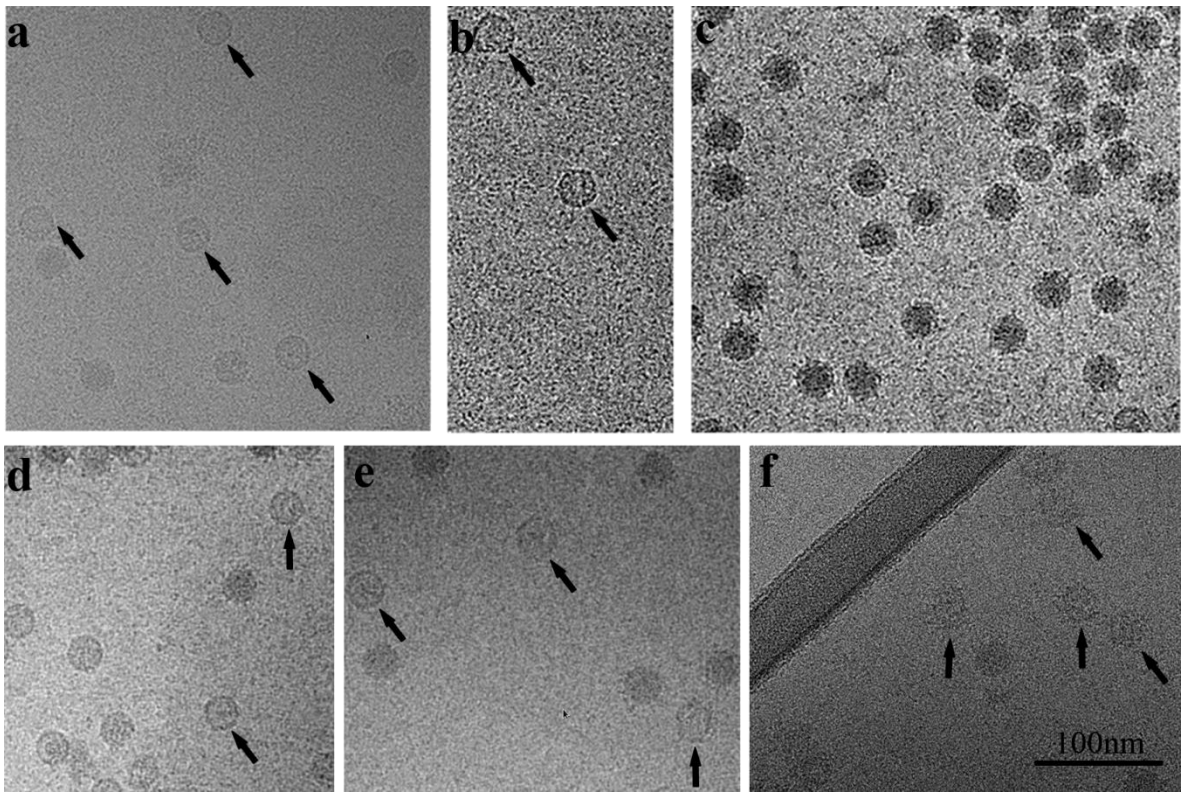

Figure 5.8 Empty particles of EV71 induced by Fabs 16-2-12D, 16-3-3C and 16-2-2D. **a**, **c**: EV71 genotype B2 complexed with Fab 16-2-12D. **b**: EV71-C4_Fab-16-2-12D complexes. **d** and **e**: EV71-B5_Fab-16-3-3C complexes. **f**: EV71-B5_Fab-16-2-2D complexes. Molar ratio of EV71 particle: Fab in **a**, **b**, **d, f** is ~1:200 and in **c** and **e** is ~1:90. Empty particles can be observed in all of these micrographs except **c**.

5.5 Escape mutants and binding residues

Our collaborator Arthur Huang identified some EV71 mutations that can effectively abolish binding and neutralization of anti-EV71 antibodies (Table 1.2 and Figure 1.12)[208]. We mapped these substitutions onto the cryo-EM structures of the EV71-Fab complexes and found that most substitutions (22 out of 28) occurred at residues directly involved in EV71-antibody interaction. These substitutions will therefore likely directly impair the interaction between EV71 and mAbs leading to escape from binding (Figure 5.12 – 24).

Approximately half of the mutations involve a change, loss or gain in charge, and the majority of the remaining mutations involve a significant change in the bulk of the sidechain. An example of this is the mutation of VP1 283S, a binding residue for antibody 16-3-10B, to Phe. The large phenylalanine side chain takes up space occupied by the bound mAb 16-3-10B, precluding attachment of the antibody (Figure 5.9).

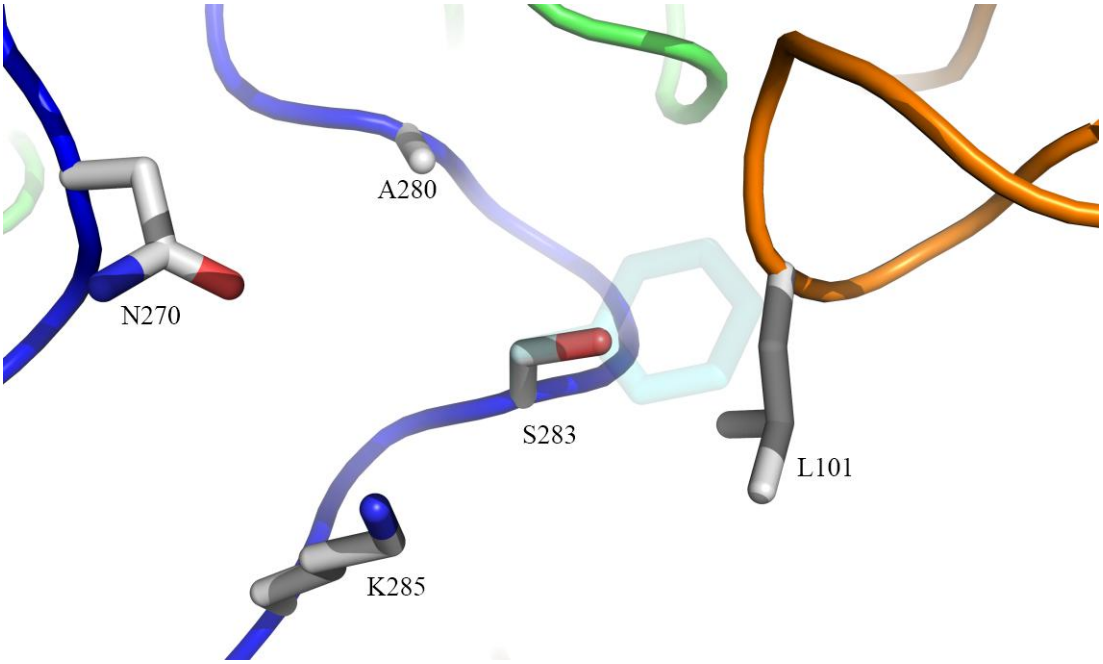

Figure 5.9 Substitution VP1 S283F causing escape mutants of EV71 from antibody 16-3-10B. The large side chain of Phenylalanine (shown as cyan semi-transparent sticks) induced by this substitution can take up the space, which should be occupied by mAb 16-3-10B, in this way there is no space for the antibody to fit into. In this figure and Figure 5.8 and 5.9, VP1, 2 and 3 of EV71 are colored in blue, green and red, separately, and Fabs are colored in orange. The structures are shown in cartoon and side chains of related residues are shown in sticks.

Some substitutions do not directly affect the EV71-antibody interaction, but are likely

to affect the presentation of residues that are directly involved in the binding, and in this way probably change the EV71-Fab interaction indirectly. EV71 VP3 E81G/K mutations abrogate binding of antibody 16-3-4D and 34-1-6D. Residue VP3 81 is not a binding residue, but through a number of interactions it stabilizes a nearby loop, which is bound by antibodies 16-3-4D and 34-1-6D. Both of the observed mutations, to glycine and lysine, will destabilize this loop, thus interfering with antibody binding (Figure 5.10).

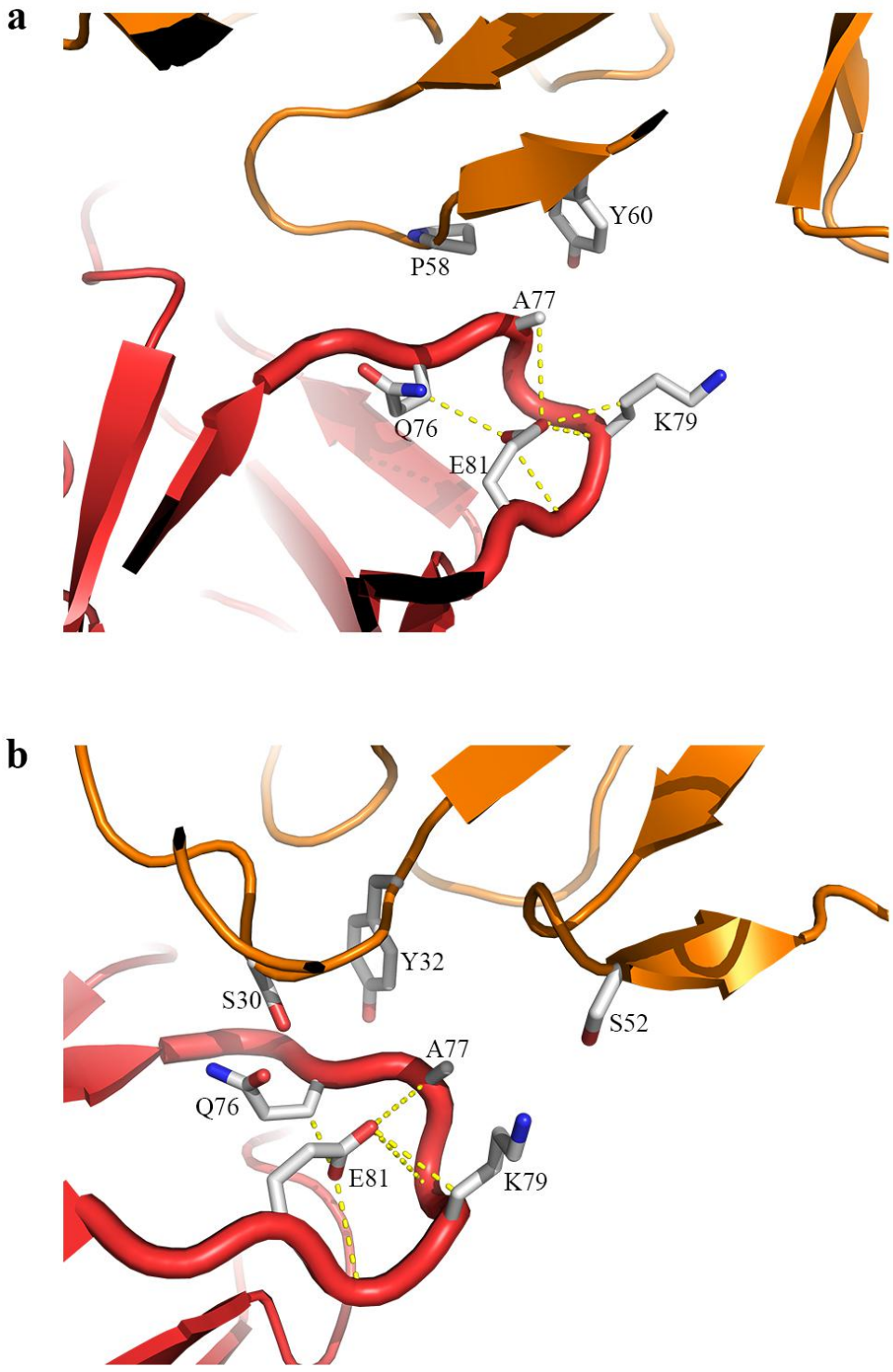

Figure 5.10 Substitution VP3 E81G/K causing escape mutants of EV71 from antibodies 16-3-4D (**a**) and 34-1-6D (**b**). Residue VP3 81E is not a binding residue, but it stabilizes a nearby loop (shown in thick loops), which is targeted by antibody 16-3-4D and 34-1-6D. The observed escape mutations VP3 E81G/K will destabilize this loop, interfering with antibody binding.

The interaction between VP1 232T and VP1 110D organises the side chain of VP1 110D into a special conformation, which allows VP1 110D to optimize key interactions for mAbs 16-2-8C, 16-2-9D and 16-2-12D. The observed mutation VP1 T232A impairs the interaction between VP1 232T and VP1 110D and makes the side chain of VP1 110D more flexible, thus leading to escape (Figure 5.11).

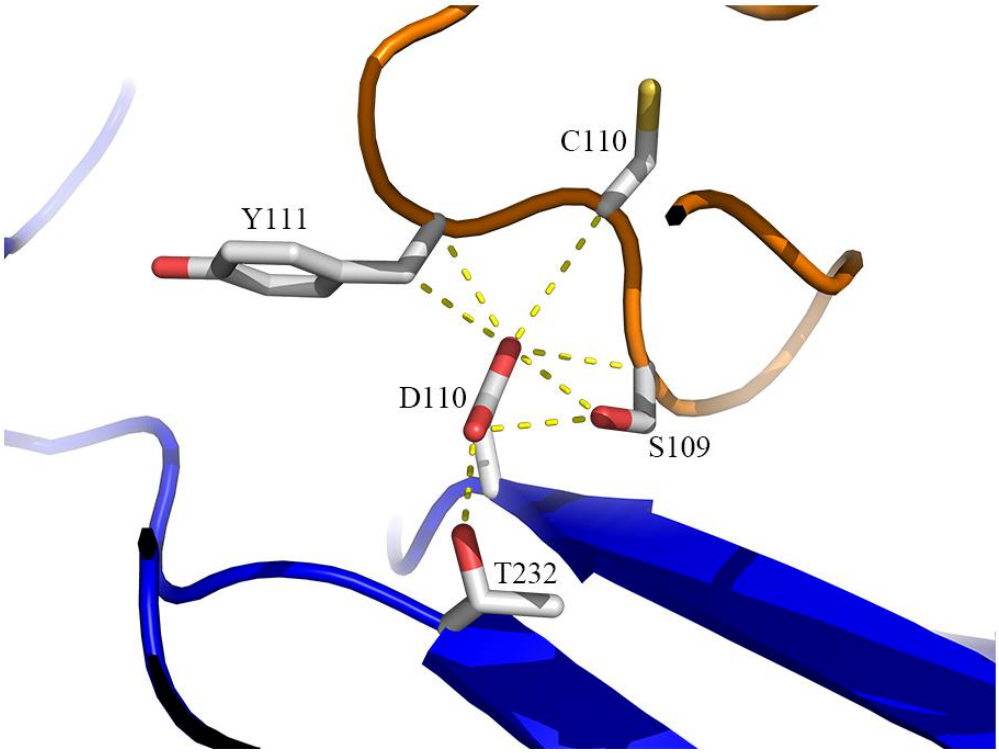

Figure 5.11 Substitution VP1 T232A causing escape mutants of EV71 from antibodies 16-2-8C, 16-2-9D and 16-2-12D. VP1 232T interacts with VP1 110D, making the side chain of VP1 110D interact with maximum numbers of atoms of mAbs 16-2-8C, 16-2-9D or 16-2-12D. The mutation VP1 T232A impairs the interaction between VP1 232T and VP1 110D and makes the side chain of VP1 110D more flexible, thus caused escape from antibodies.

The VP1 S241F substitution can cause escape from mAb 16-2-2D. However, based on our structure, this site has no direct contact with binding Fab 16-2-2D or either cannot affect nearby binding residues of EV71. The mechanism by which the VP1 S241F substitution causes escape remains unclear. This, and all other escape mutations, are shown in the context of the binding residues in Figures 5.12 to 5.24. Figure 5.25 aggregates all the escape mutations and shows that they are relatively evenly distributed across the capsid surface, with some canyon associated hotspots.

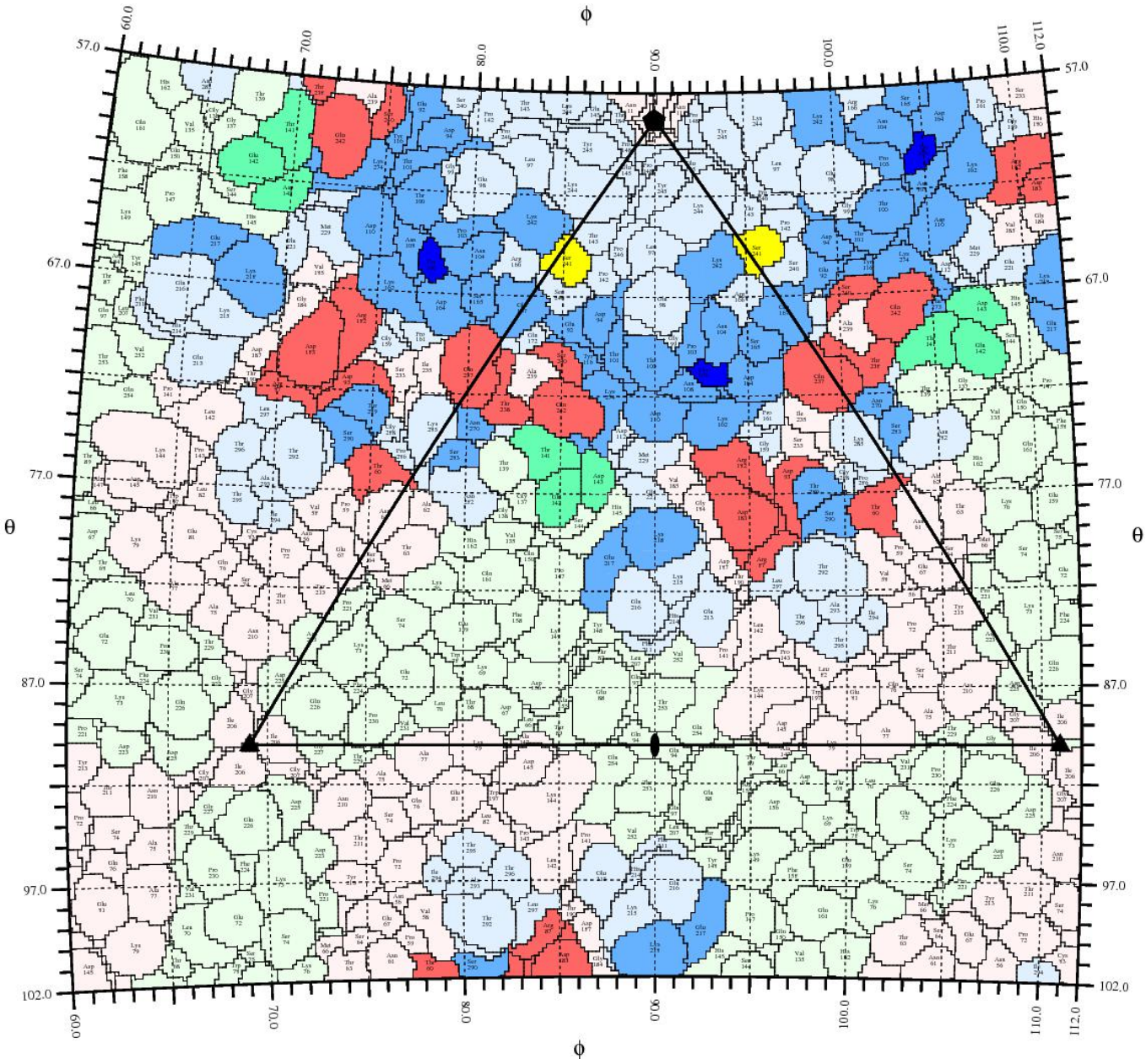

Figure 5.12 Roadmap of Fab 16-2-2D binding residues and escape mutant substitutions. In this roadmap, and all subsequent ones, residues of EV71 are colored in light blue (VP1), light green (VP2) and light red (VP3) respectively. Binding residues are colored in darker blue (VP1), green (VP2) and red (VP3) respectively. Binding residues that are identified as escape mutants are colored in pure bright blue (VP1), green (VP2) and red (VP3) respectively. Residues causing escape from this antibody, but not directly involved in binding are colored yellow (here for mAb 16-2-2D, it is Ser241 of VP1).

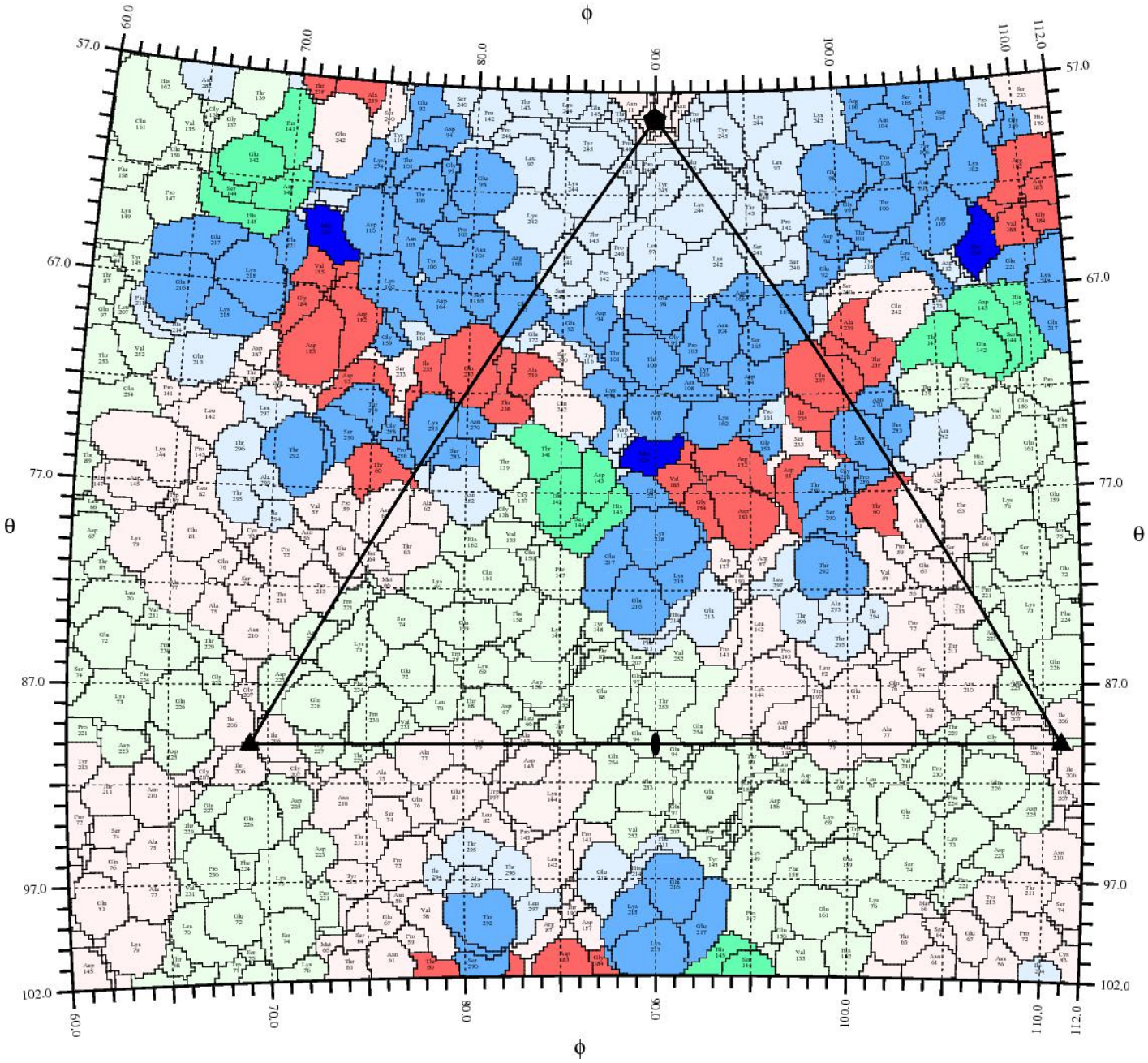

Figure 5.13 Roadmap of Fab 16-2-8C binding residues and escape mutant substitutions, colored as in Figure 5.12. VP1 232 is not a binding site for antibody 16-2-8C, 16-2-9D and 16-2-12D, but the substitution VP1 T232A can cause escape mutant of EV71 from these antibodies. VP1 232 would be colored in yellow but is not shown in this roadmap and Figure 5.14 (and can be hardly seen in Figure 5.16) because it is not on the virus surface.

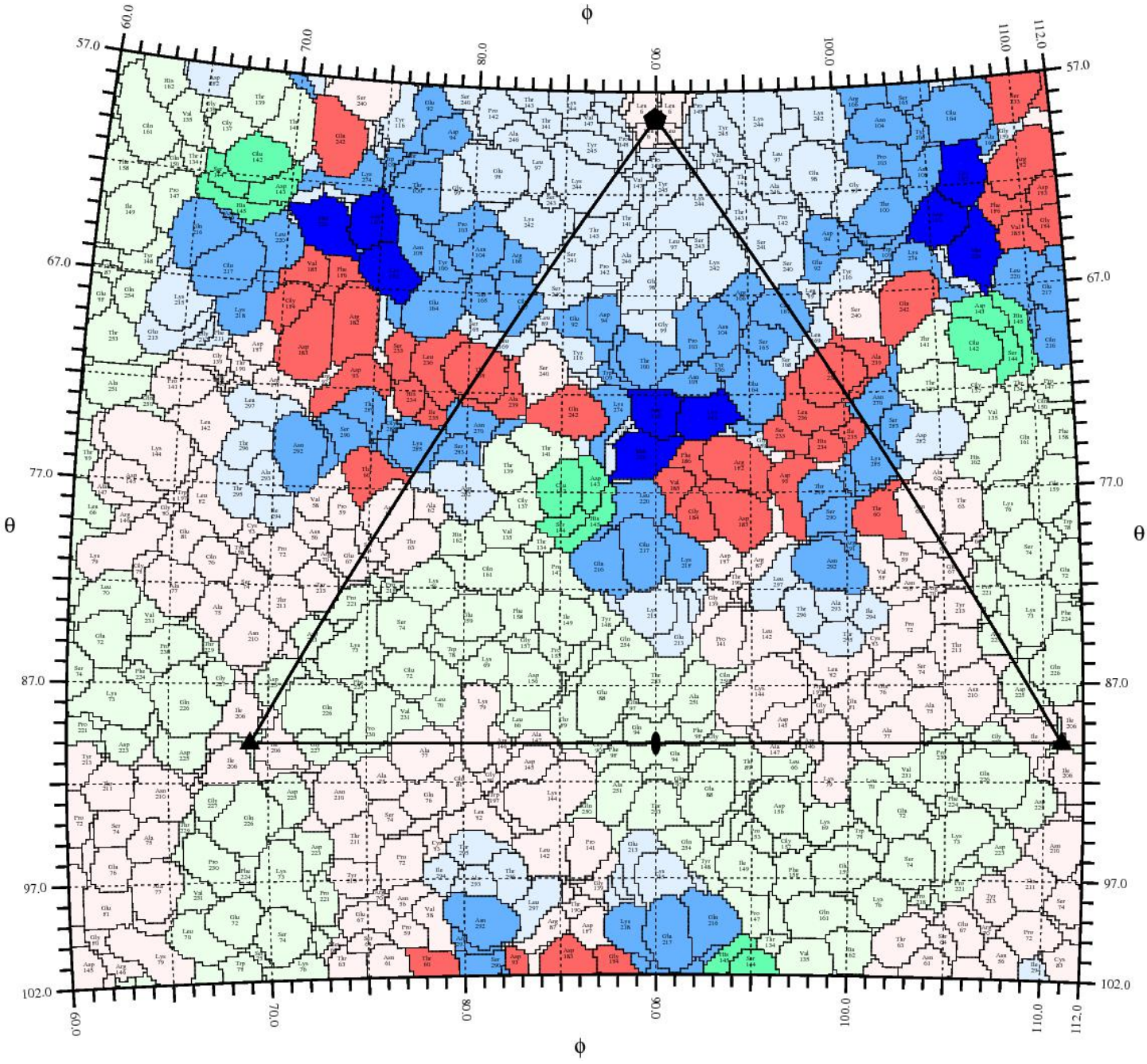

Figure 5.14 Roadmap of Fab 16-2-9D binding residues and escape mutant substitutions, colored as in Figure 5.10. VP1 232 would be colored in yellow but is not shown in this roadmap.

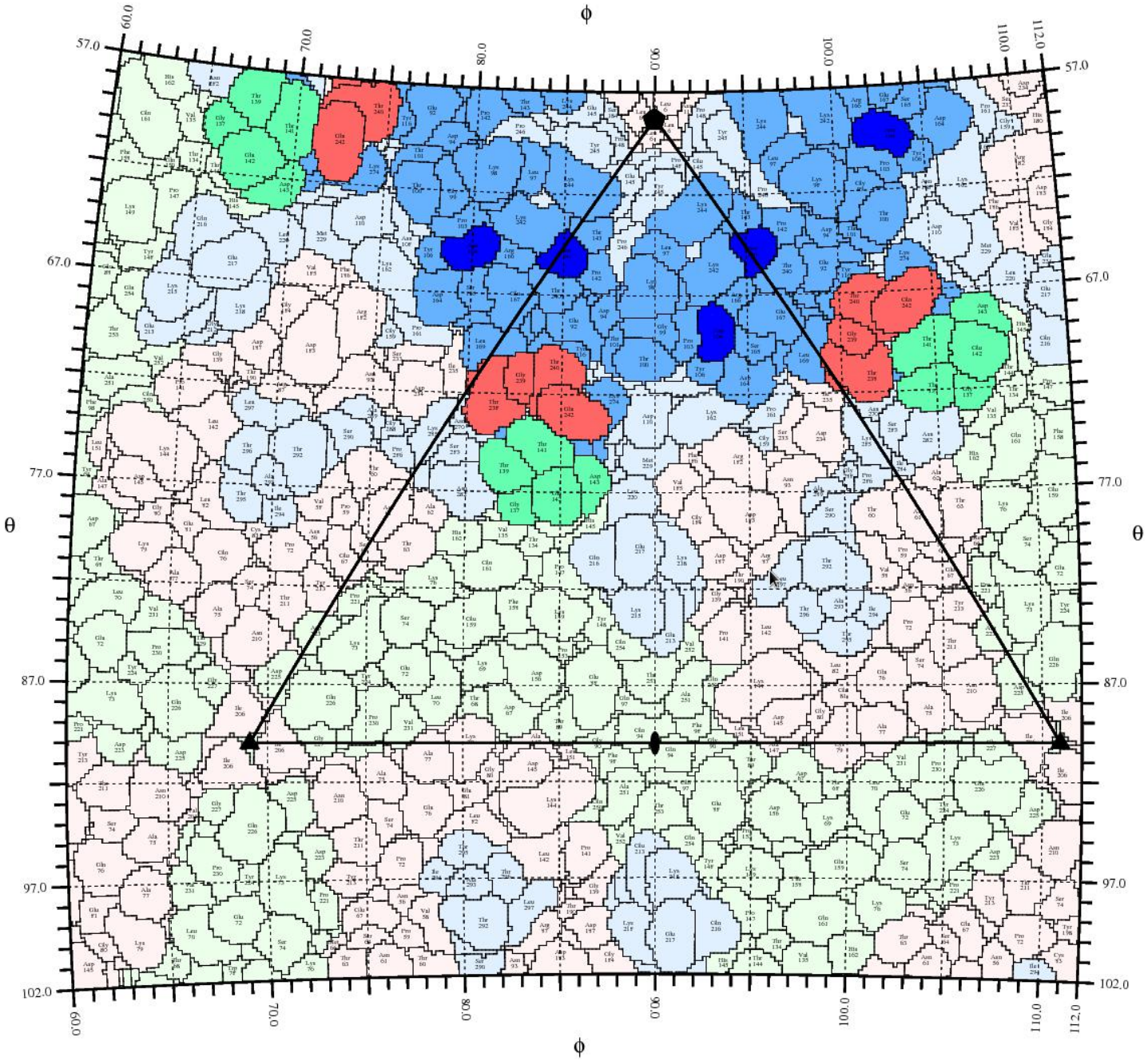

Figure 5.15 Roadmap of Fab 16-2-11B binding residues and escape mutant substitutions, colored as in Figure 5.10.

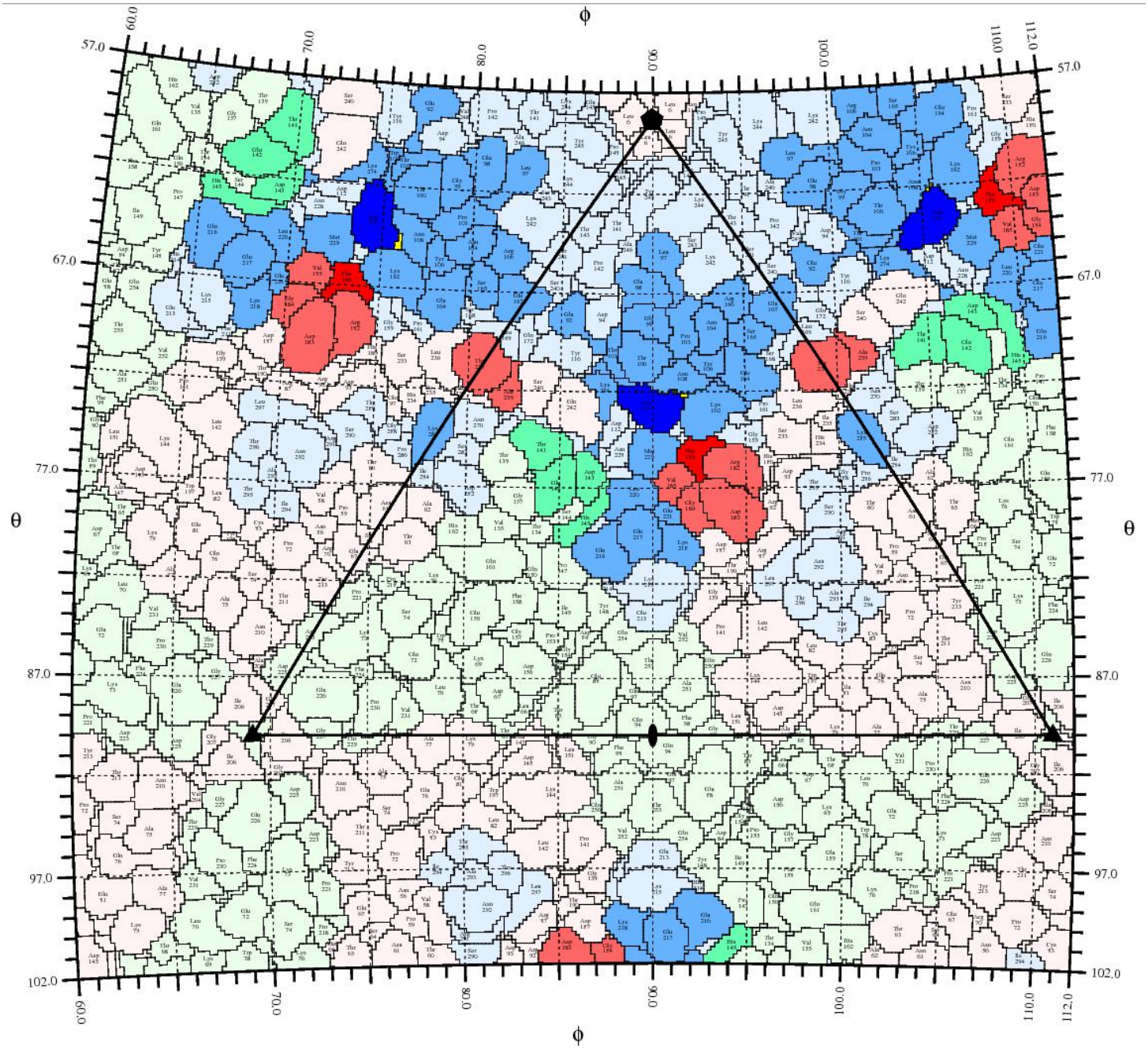

Figure 5.16 Roadmap of Fab 16-2-12D binding residues and escape mutant substitutions, colored as in Figure 5.10. The tiny yellow areas (adjacent to the mutations shown in bright blue (VP1 D110G)) in this roadmap represent the site of VP1 232. Substitution VP1 T232A can induce escape from this antibody.

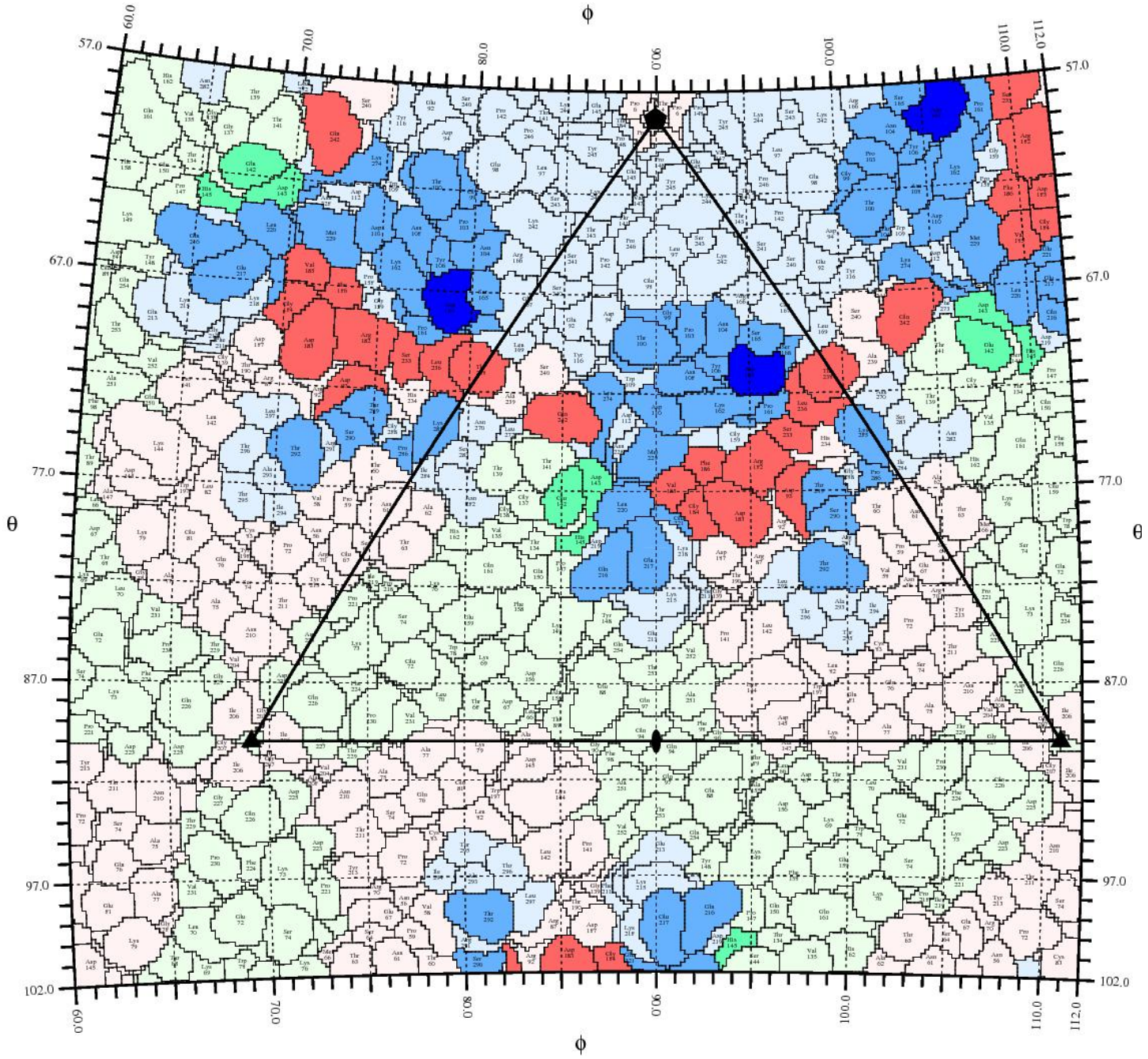

Figure 5.17 Roadmap of Fab 16-3-3C binding residues and escape mutant substitutions, colored as in Figure 5.10.

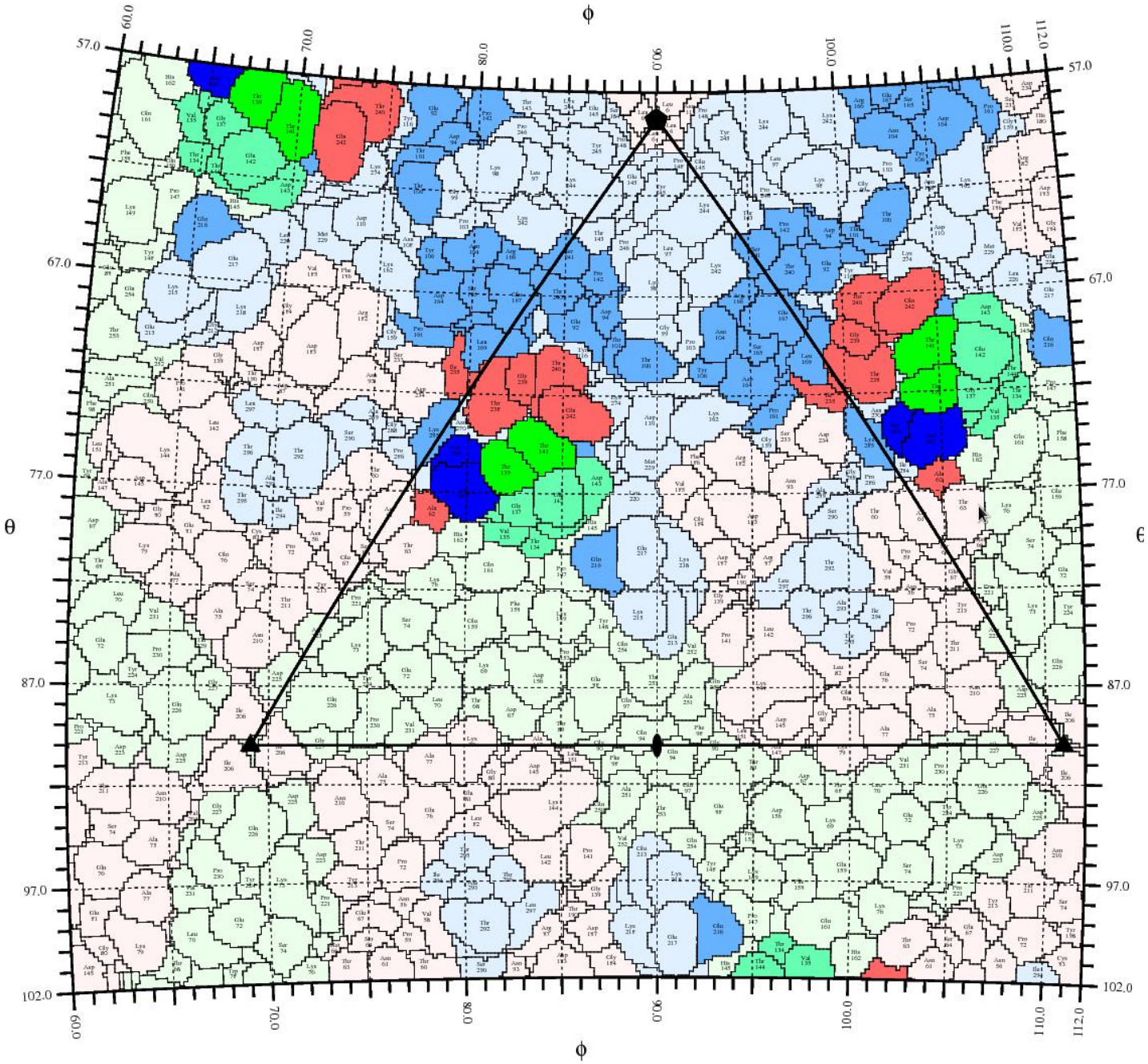

Figure 5.18 Roadmap of Fab 16-3-10B binding residues and escape mutant substitutions, colored as in Figure 5.10.

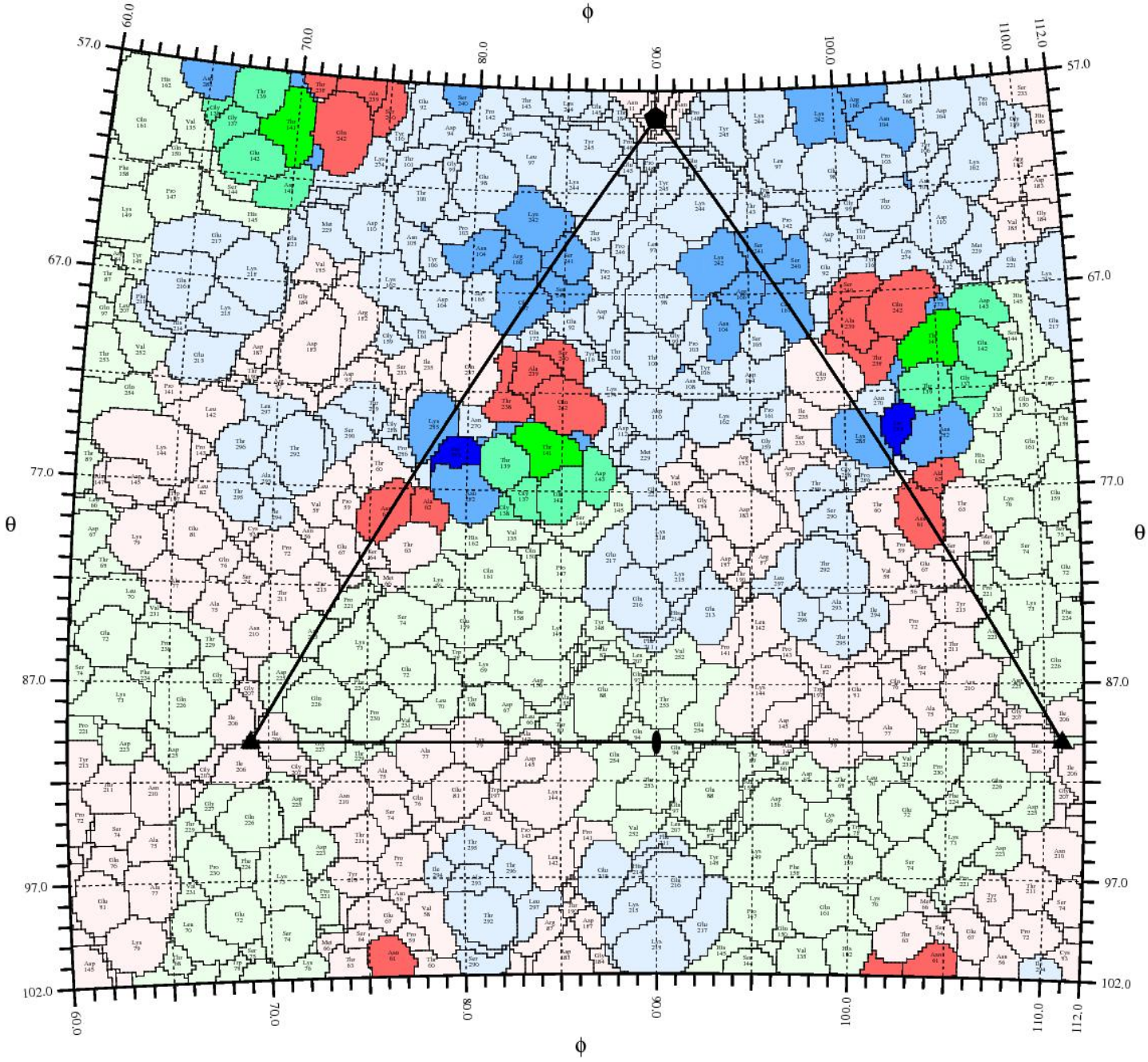

Figure 5.19 Roadmap of Fab 17-2-2B binding residues and escape mutant substitutions, colored as in Figure 5.10.

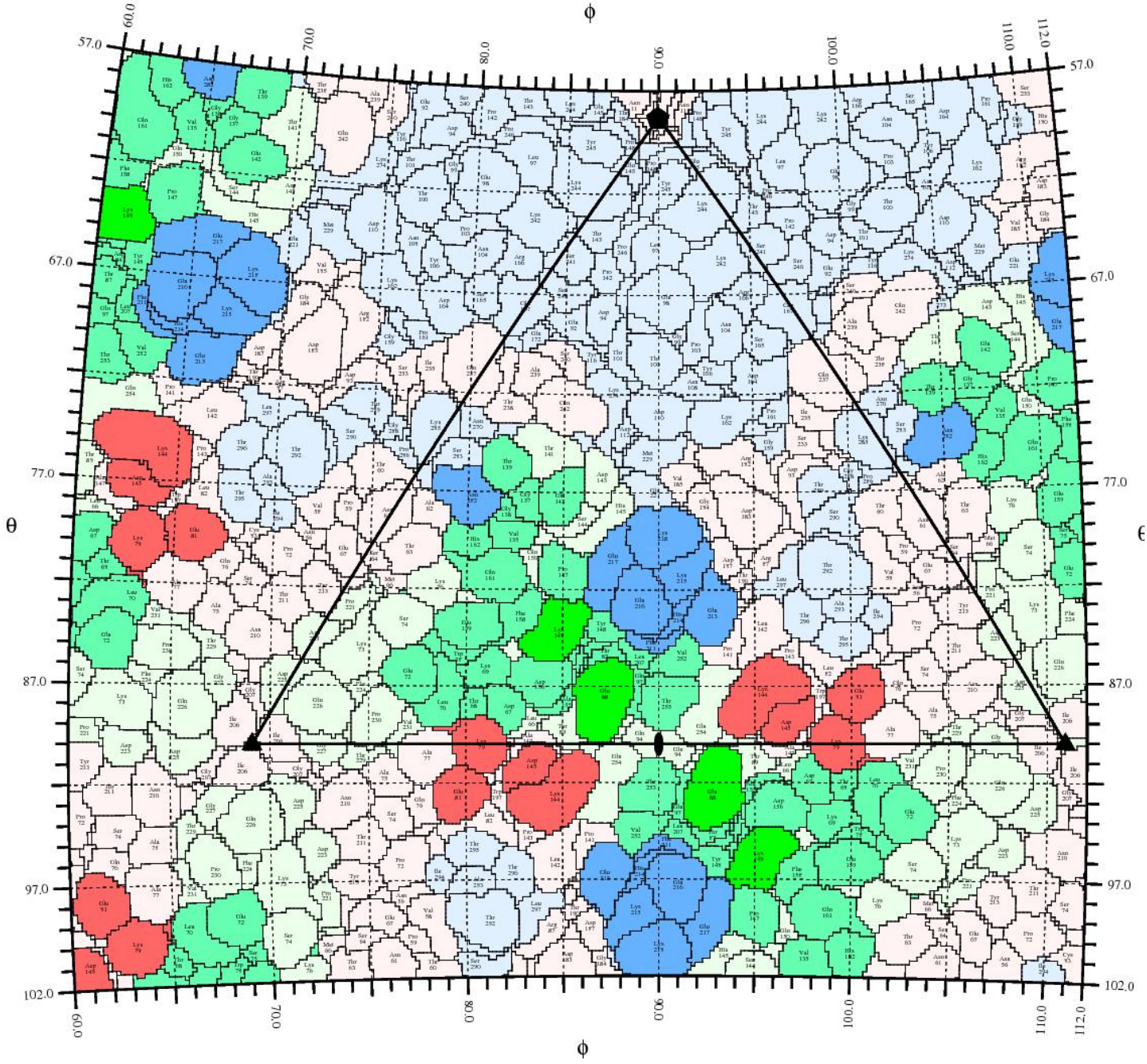

Figure 5.20 Roadmap of Fab 17-1-12A binding residues and escape mutant substitutions, colored as in Figure 5.10.

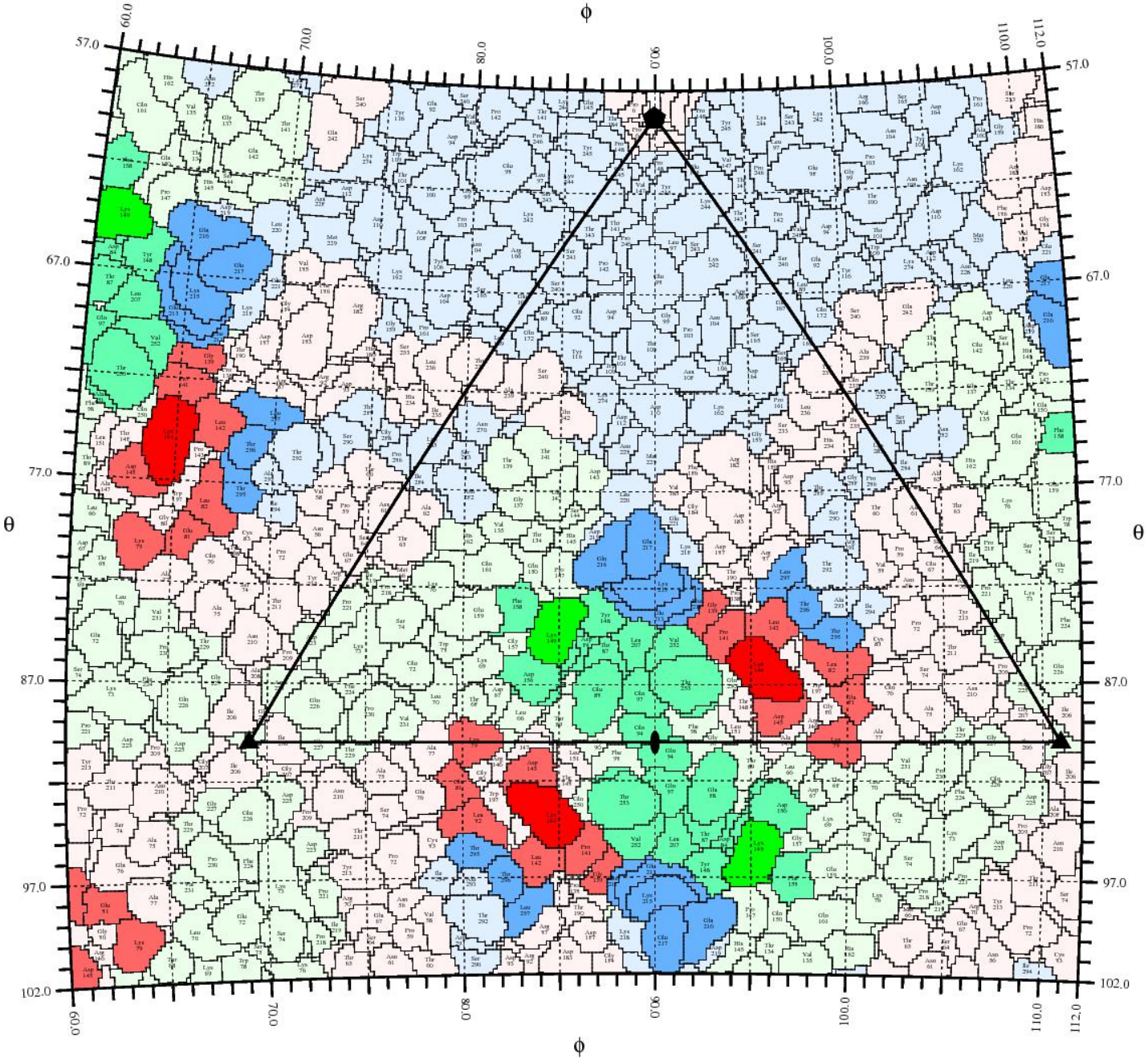

Figure 5.21 Roadmap of Fab 17-2-12A binding residues and escape mutant substitutions, colored as in Figure 5.10.

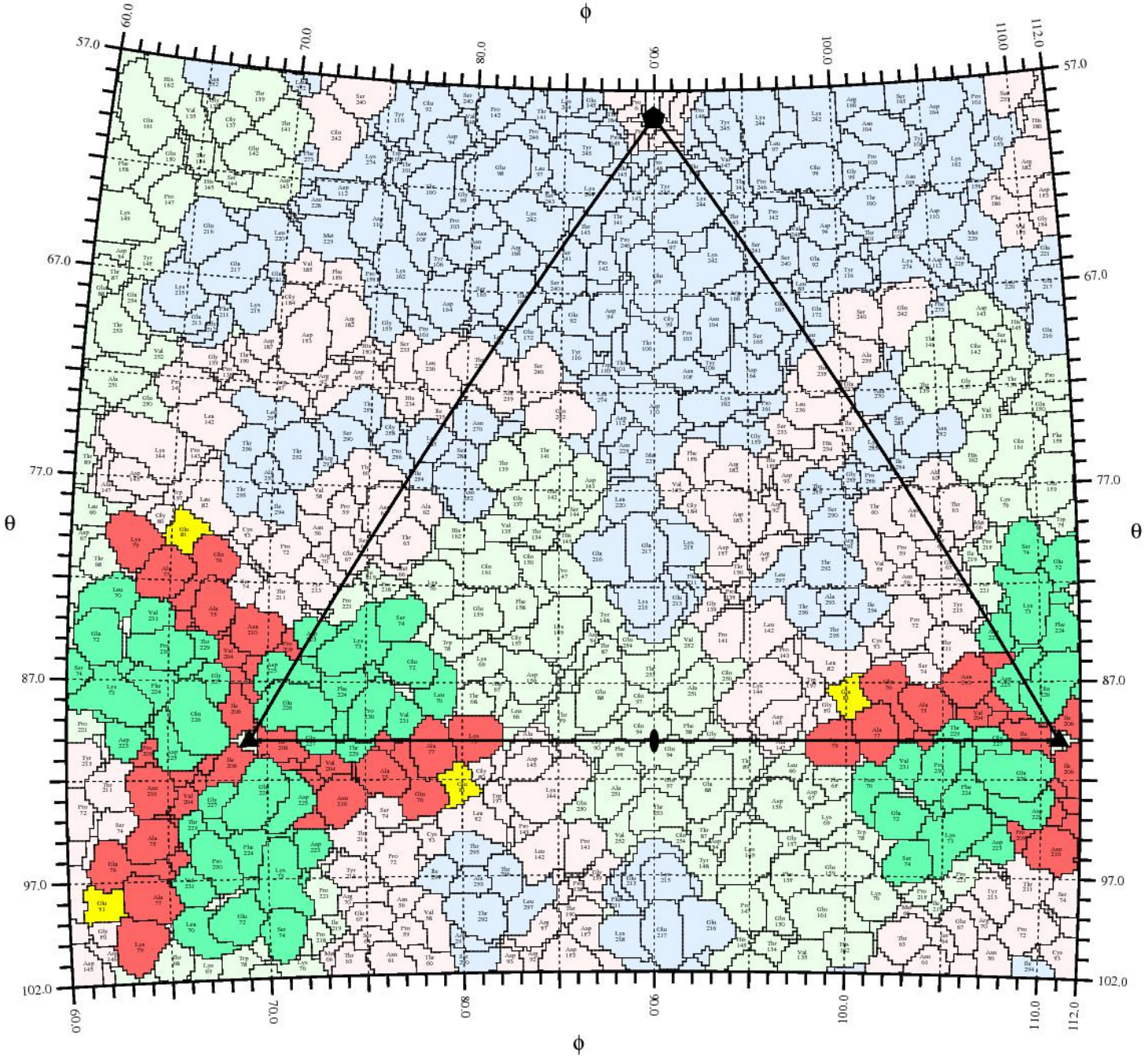

Figure 5.22 Roadmap of Fab 16-3-4D binding residues and escape mutant substitutions, colored as in Figure 5.10. Substitution VP3 E81G causes escape from this antibody, but is not directly involved in binding (colored in yellow).

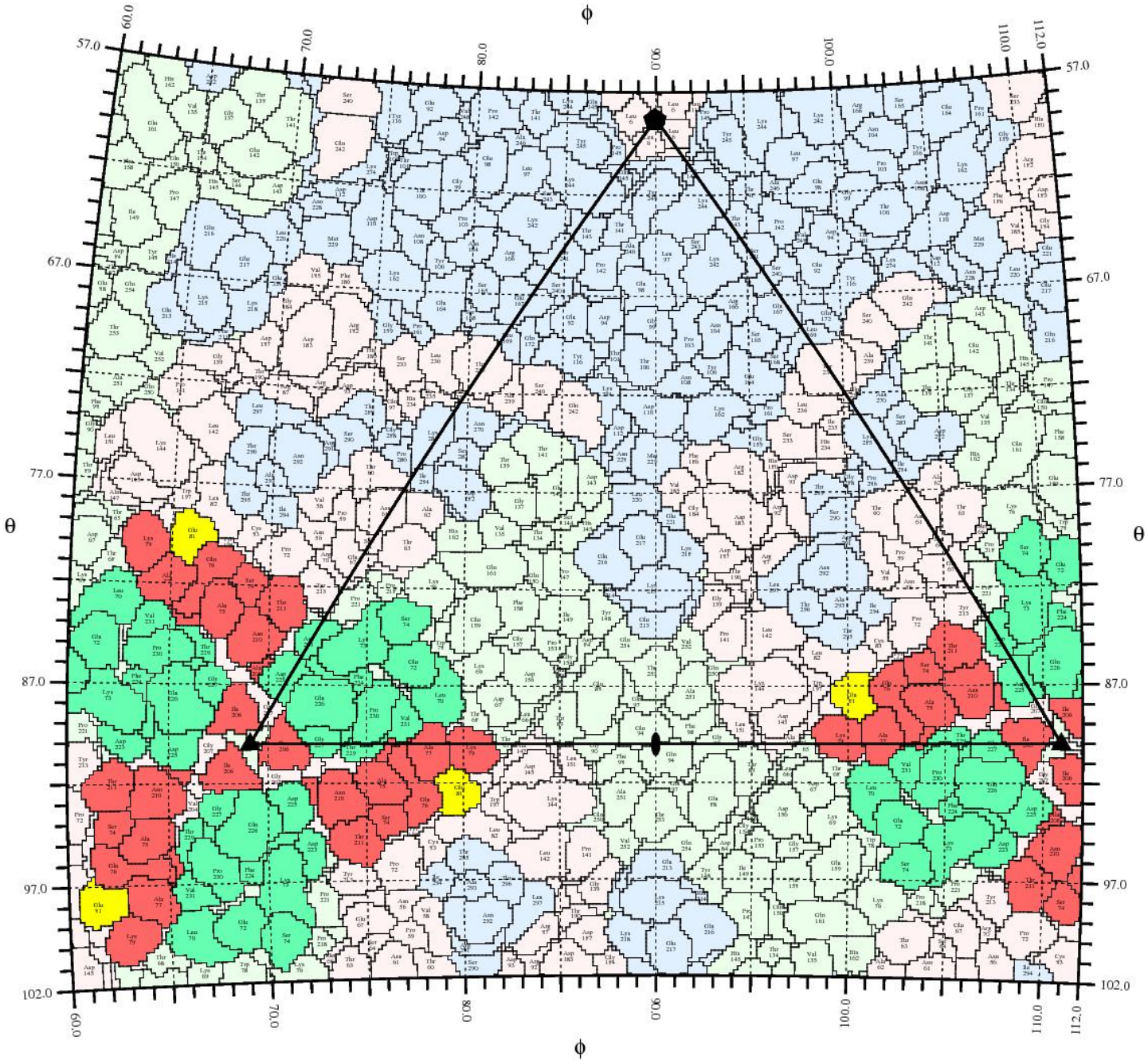

Figure 5.23 Roadmap of Fab 34-1-6D binding residues and escape mutant substitutions, colored as in Figure 5.10. Substitution VP3 E81G causes escape from this antibody, but is not directly involved in binding (colored in yellow).

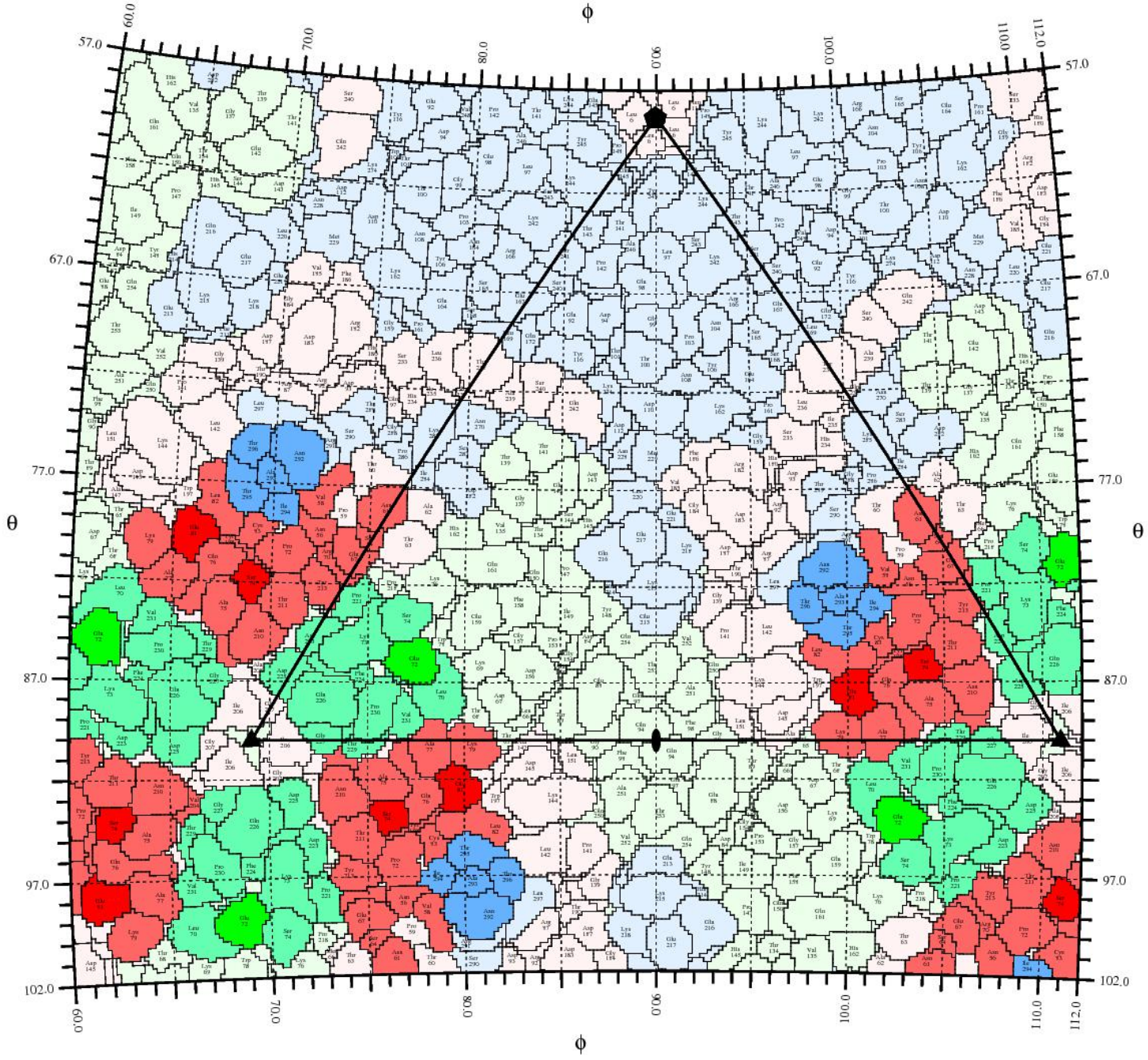

Figure 5.24 Roadmap of Fab 38-1-10A binding residues and escape mutant substitutions, colored as in Figure 5.10.

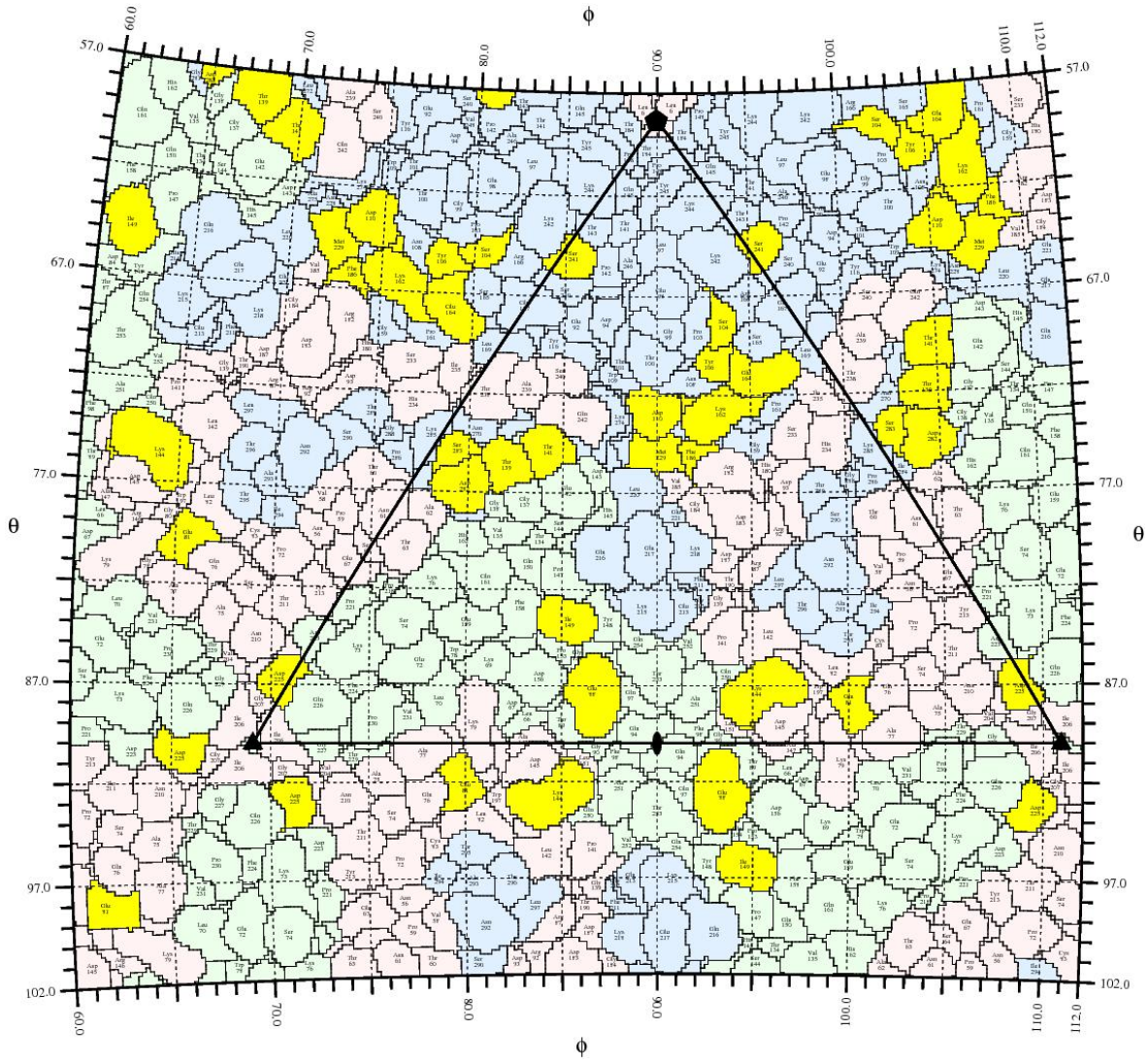

Figure 5.25 Roadmap showing sites of escape mutations (yellow) on the EV71 capsid. colored as in Figure 5.12.

5.6 MAbs' inability to neutralize some strains of EV71

Most of the 13 mAbs have broad potency against strains of EV71 genotypes B4, B5 and C4, however, mAb 16-3-3C cannot neutralize some strains of EV71 B4 (strain 01-1437 included) and mAbs 16-3-4D and 17-2-12A failed to neutralize some strains of EV71 genotype C4 (strain 11-96023 included) and one tested C5 strain 07-72043. Most antibodies cannot neutralize some EV71 C2 strains (98-2086 included) and one

tested EV71 C1 strain 98-4215[208]. We have aligned the available sequences of different strains (Figure 5.26), to seek structural explanations for these and the mutations are mapped to the capsid surface in Figure 5.27, note that only 10 out of 29 variations are located on the surface of EV71 capsid (these sites include VP1 145, VP1 164, VP1 240, VP1 289, VP1 297, VP2 144, VP2 224, VP3 93, VP3 239, VP3 240) and mutations at these 10 sites only induced different residues with similar side chains, indicating the surface of the EV71 capsid is not very changeable between genotypes, in part presumably due to conserved receptor interactions.

```
        VP1
        22                                        60  145                 164
EV71-C1 QALPAPTGQNTQVSSHRLDTGKVPALQAAEIGASSNASD...QVVPQLLQYMFVPPGAPKPD...
EV71-C5 QALPAPTGQNTQVSSHRLDTGKVPALQAAEIGASSNASD...EVVPQLLQYMFVPPGAPKPD...
EV71-C2 RALPAPTGQDTQVSSHRLDTGKVPALQAAEIGASSNASD...EVVPQLLQYMFVPPGAPKPD...
EV71-C4 HALPAPTGQNTQVSSHRLDTGKVPALQAAEIGASSNASD...QVVPQLLQYMFVPPGAPKPD...
EV71-B5 QALPAPTGQNTQVSSHRLDTGEVPALQAAEIGASSNTSD...EVVPQLLQYMFVPPGAPKPD...
EV71-B4 QALPAPTGQNTQVSSHRLDTGEVPALQAAEIGASSNTSD...EVVPQLLQYMFVPPGAPKPE...

        VP1
        184     240                   262 289     297
EV71-C1 TDPPA...TSKSKYPLVIRIYMRMKHVRAWV...ASRTAITTF
EV71-C5 SDPPA...TSKSKYPLVIRIYMRMKHVRAWV...ASRTAITTL
EV71-C2 SDPPA...TSKSKYPLVIRIYMRMKHVRAWI...ASRTAITTL
EV71-C4 SDPPA...TSKSKYPLVVRIYMRMKHVRAWI...ASRTAITTL
EV71-B5 TDPPA...SSKSKYPLVVRIYMRMKHVRAWI...TSRTAITTL
EV71-B4 TDPPA...SSKSKYPLVVRIYMRMKHVRAWI...TSRTAITTL

        VP2
        26                    47  124     142     175     197    218   224
EV71-C1 LEAANIIVGYGEWPSYCSDSDA...VAVLP...EDSHP...LTVCP...YINA...HISPLDF...
EV71-C5 QEAANIIVGYGEWPSYCSDSDA...VAVLP...EDSHP...LTVCP...YINA...PISPLDF...
EV71-C2 QEAANIIVGYGEWPSYCSDSDA...VAVLP...EDSHP...LTVCP...YINA...PINPLDY...
EV71-C4 QEAANIIVGYGEWPSYCSDSDA...VAVLP...EDTHP...LTVCP...YINA...PISPLDY...
EV71-B5 QEAANIIVGYGEWPSYCSDDDA...VAILP...EDSHP...LTICP...YMNT...PISPLDF...
EV71-B4 QEAANIIVGYGEWPSYCSDDDA...VAILP...EDSHP...LTVCP...YMNT...PISPLDF...

        VP3
        3     9   93     100 232       242
EV71-C1 PTELKPG...NGPWQSTL...ASDILQTGTIQ
EV71-C5 PTELKPG...SGPWQSTL...ASDILQTGTIQ
EV71-C2 PTELKPG...SGPWQSTL...ASDILQTGTIQ
EV71-C4 PTELKPG...NGPWQSTL...ASDILQTGTIQ
EV71-B5 PTEPKPG...DGPWQSTM...TSHILQTASIQ
EV71-B4 PTEPKPG...DGPWQSTM...TSHILQTASIQ
```

Figure 5.26 Sequence alignment of VP1 – VP3 showing variations (colored in red) between different EV71 strains. These strains are EV71 B4 (01-1437), EV71 B5 (12-

96015), EV71 C1 (98-4215), EV71 C2 (98-2086), EV71 C4 (11-96023) and EV71 C5 (07-72043). 12 out of 13 anti-EV71 antibodies (except antibody 38-1-10A) have been tested and showed different neutralizing abilities against these EV71 clinical strains (Table 1.3)[208].

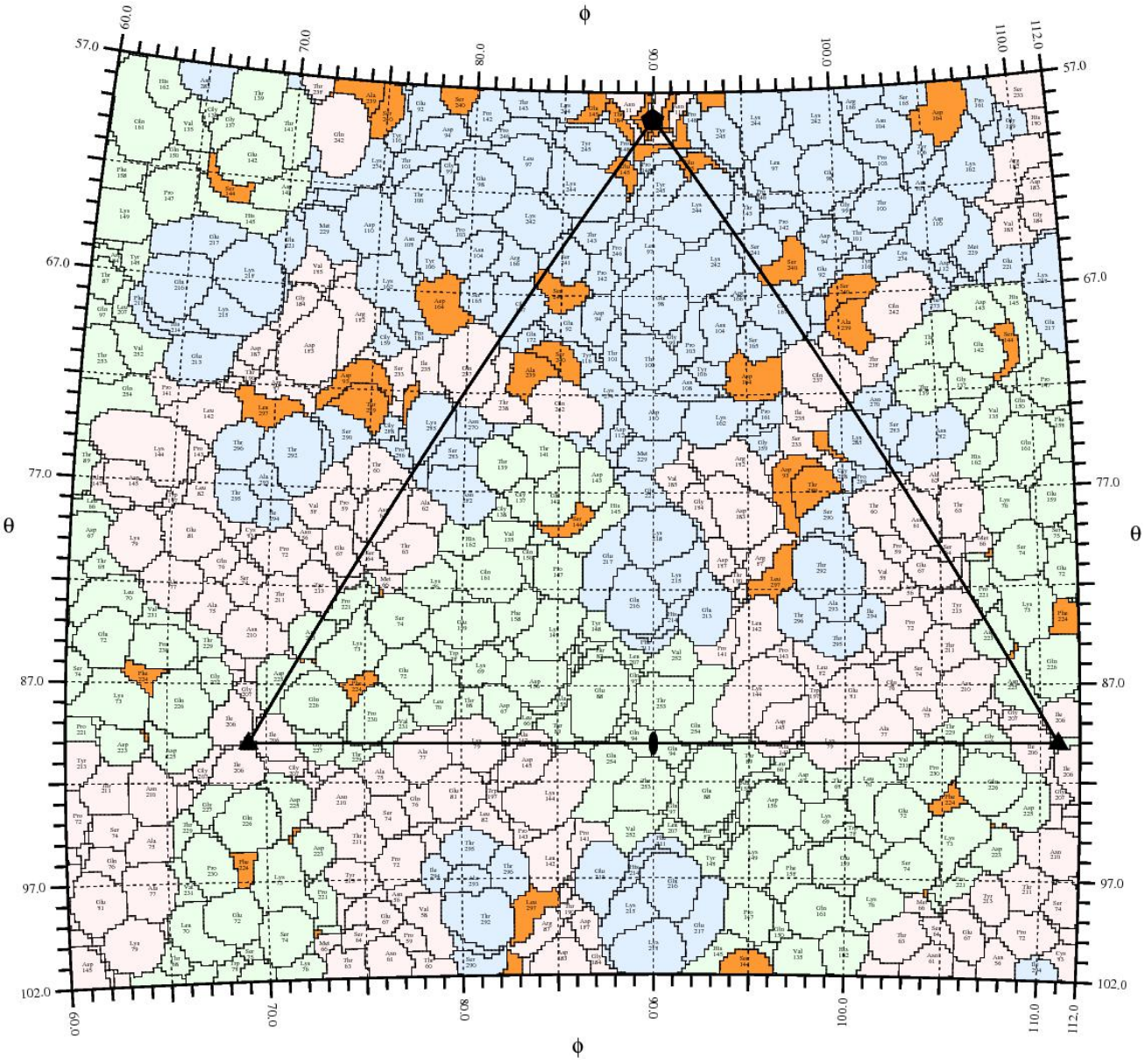

Figure 5.27 Roadmap showing variations between EV71 strains mentioned in Figure 5.26. The sites where variations occurred are colored in orange. VP1 – VP3 are colored as in Figure 5.12. Cryo-EM structure of EV71 genotype B5 (strain 12-96015) is used to draw the roadmap.

In the structure of EV71-B5 complexed with Fab 16-3-3C, VP1 164D interacts with Fab 16-3-3C. The substation VP1 D164E in EV71 B4 strains will lead to a longer side chain, impairing this interaction thus leading to B4 escaping from mAb 16-3-3C. In fact, it was also mentioned in Huang's paper that mutations at this residue (VP1 D164G/N/V) led to escape from mAb 16-3-3C[208]. Another substitution VP2 I177V between EV71 B4 and B5 does not contribute to the escape because VP2 177 is far from the binding site of mAb 16-3-3C and has no interaction with this antibody.

Nevertheless, with the current structural information it is hard to explain some of the neutralization data, for instance the limited cross-reactivities of MAb 16-3-4D and 17-2-12A. Furthermore, most antibodies cannot neutralize EV71 genotypes C1 and C2, which we cannot currently explain.

5.7 Comparison of binding areas of mAbs and SCARB2

Blocking the attachment of virus to receptor is one possible neutralization mechanism used by antibodies, so we compared the binding residues of the mAbs to that of SCARB2 on the EV71 capsid. All mAbs binding at the canyon and 2-fold axis show some overlap in binding residues with SCARB2, indicating these mAbs will compete with SCARB2 when binding to EV71 virions. 3-fold-axis binders (16-3-4D, 34-1-6D and 38-1-10A) share no common binding residues with SCARB2 so they are likely to have little or no ability to block SCARB2 binding (Figure 5.4, 5.28 - 40).

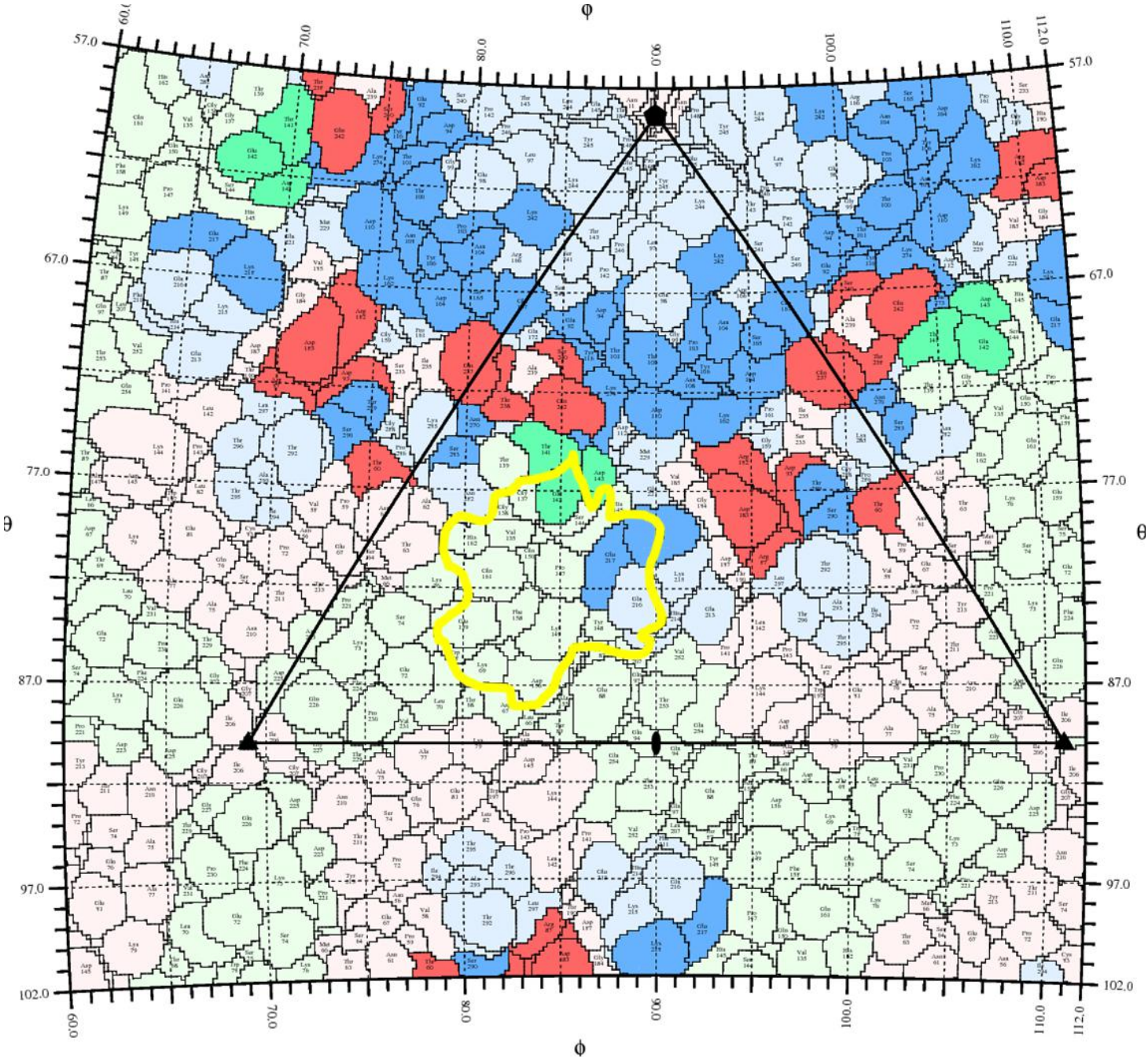

Figure 5.28 Roadmap of Fab 16-2-2D binding residues and SCARB2 binding area (whose outline is marked with a yellow line for this and all the subsequent roadmaps). Coloring is as for Figure 5.12.

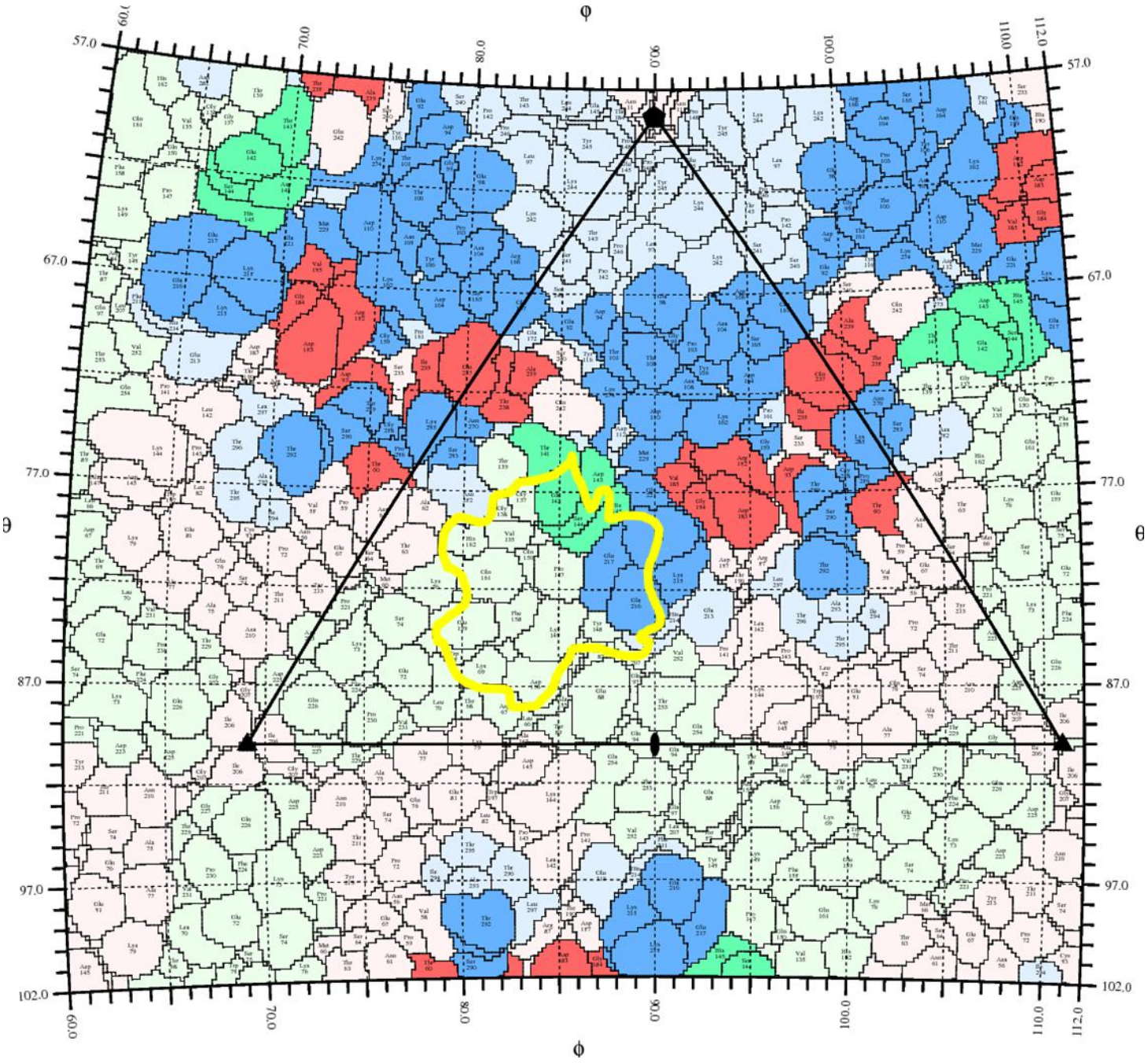

Figure 5.29 Roadmap of Fab 16-2-8C binding residues and SCARB2 binding area. Coloring is as for Figure 5.10.

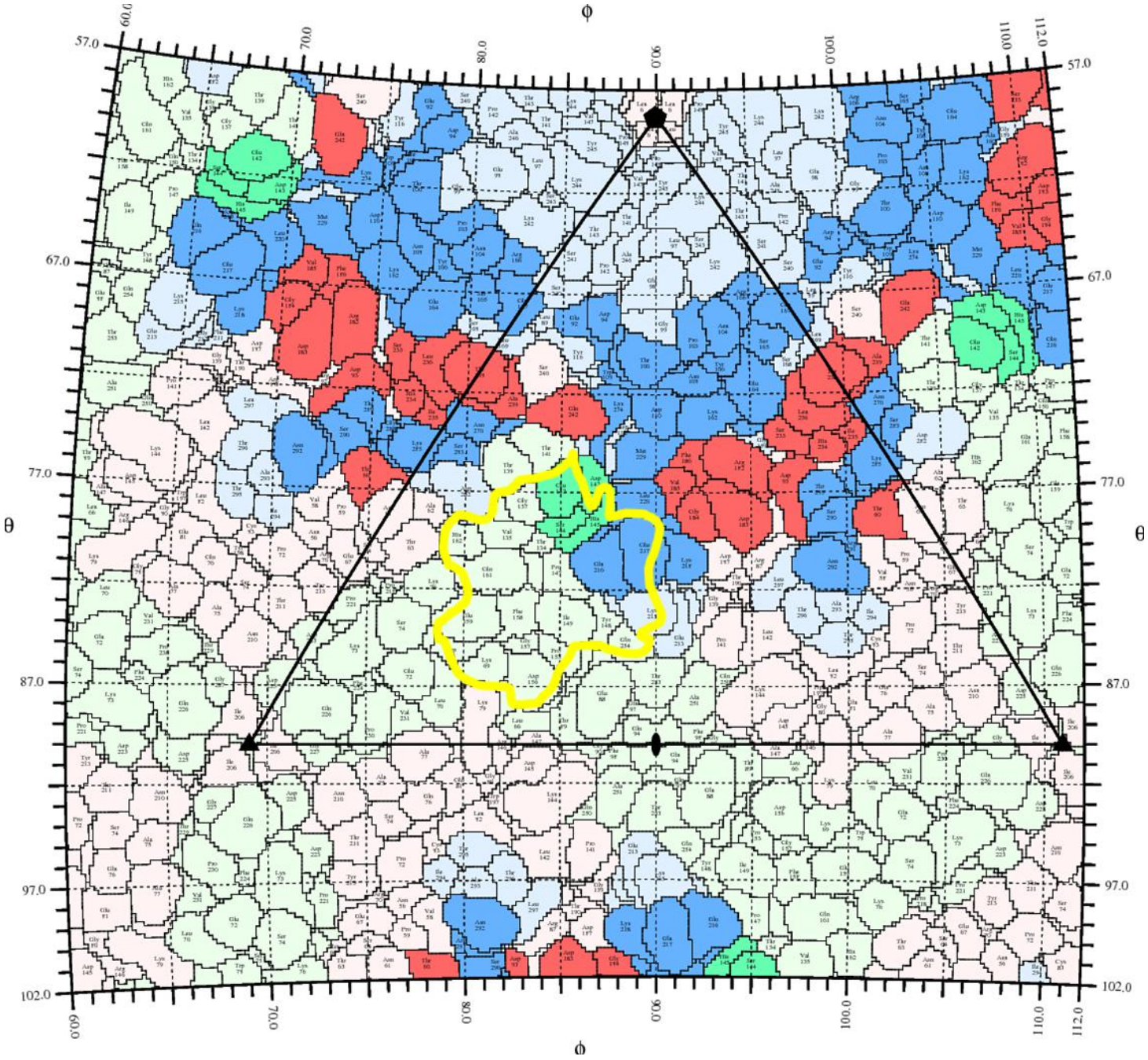

Figure 5.30 Roadmap of Fab 16-2-9D binding residues and SCARB2 binding area. Coloring is as for Figure 5.10.

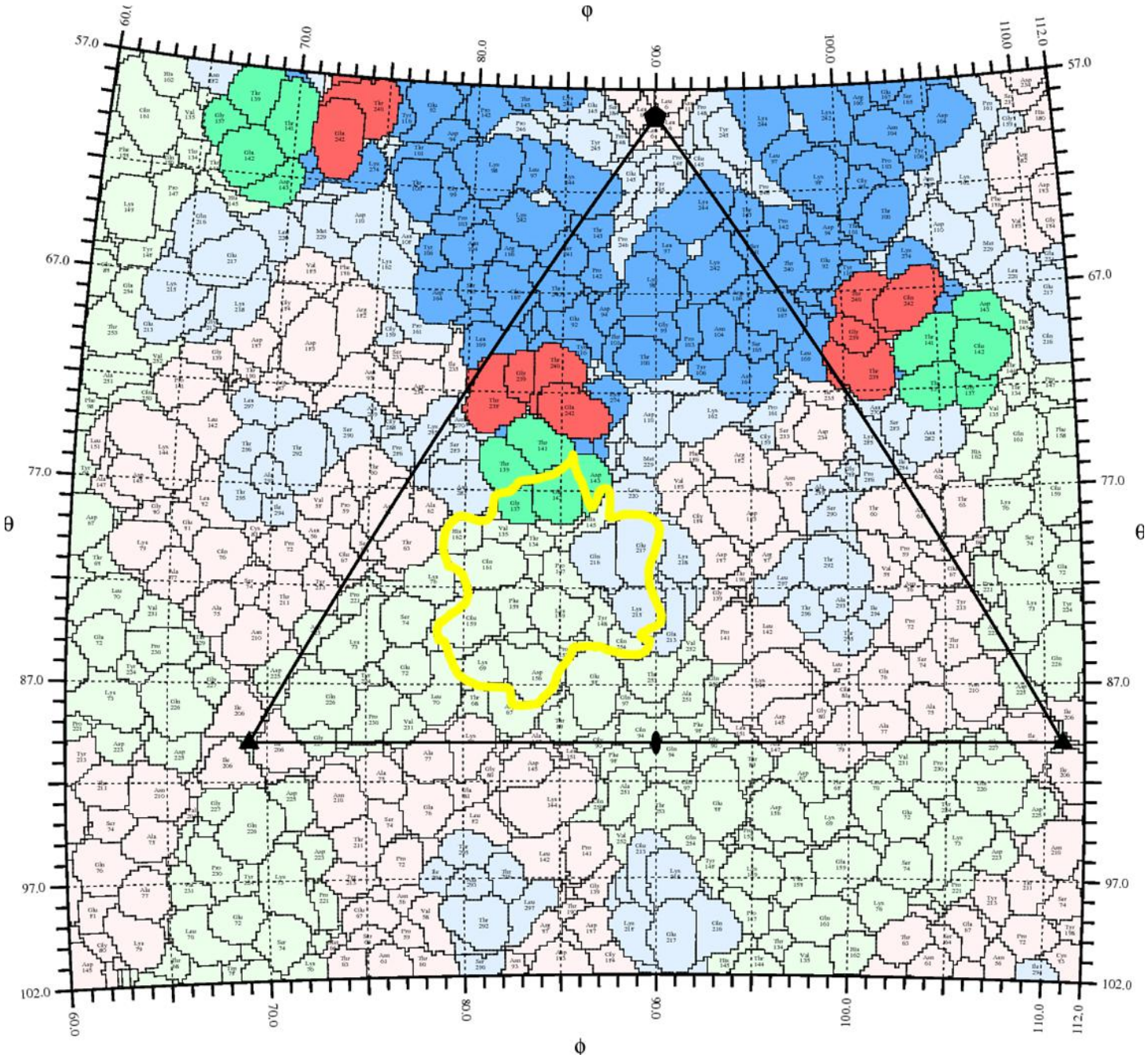

Figure 5.31 Roadmap of Fab 16-2-11B binding residues and SCARB2 binding area. Coloring is as for Figure 5.10.

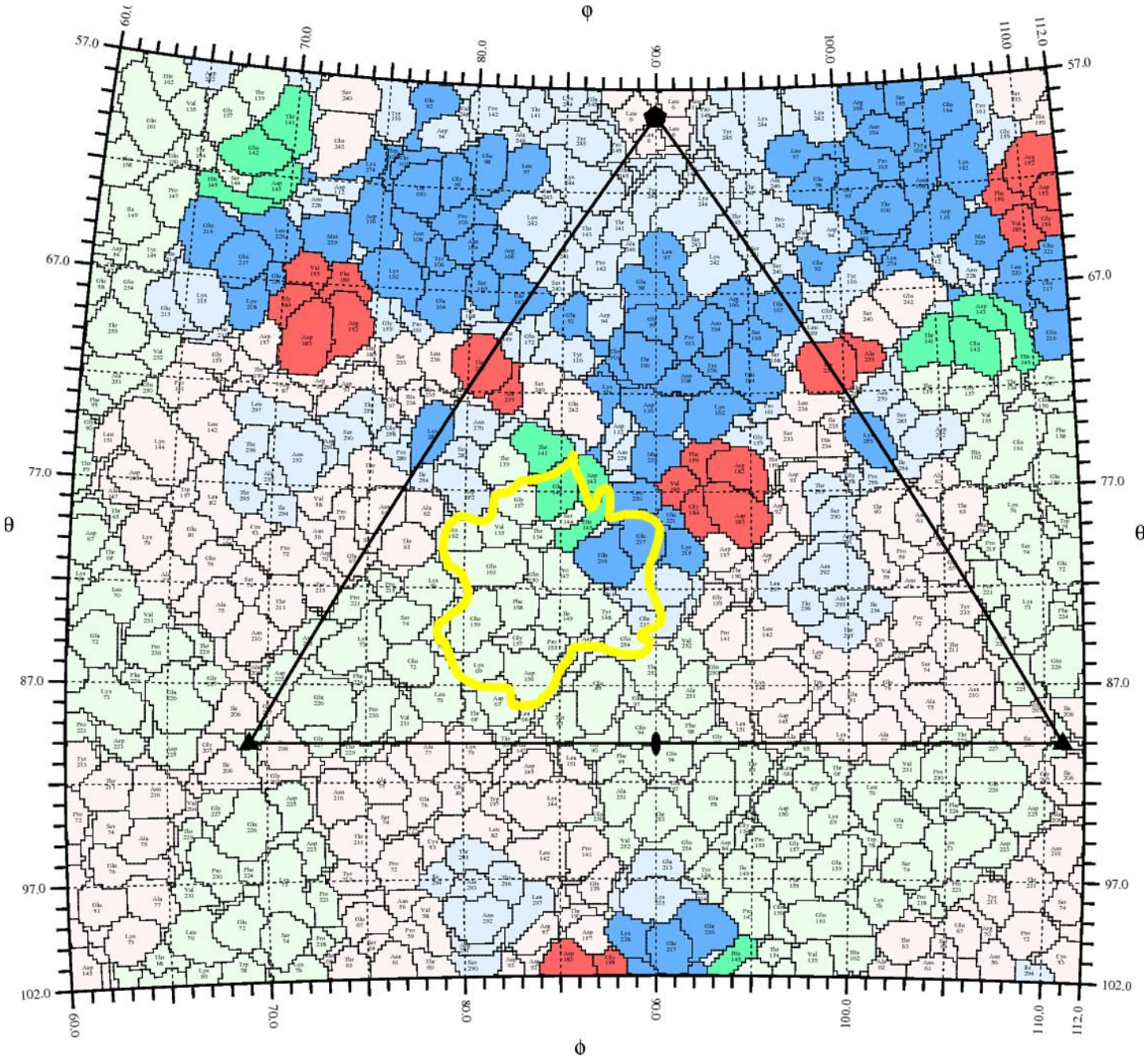

Figure 5.32 Roadmap of Fab 16-2-12D binding residues and SCARB2 binding area. Coloring is as for Figure 5.10.

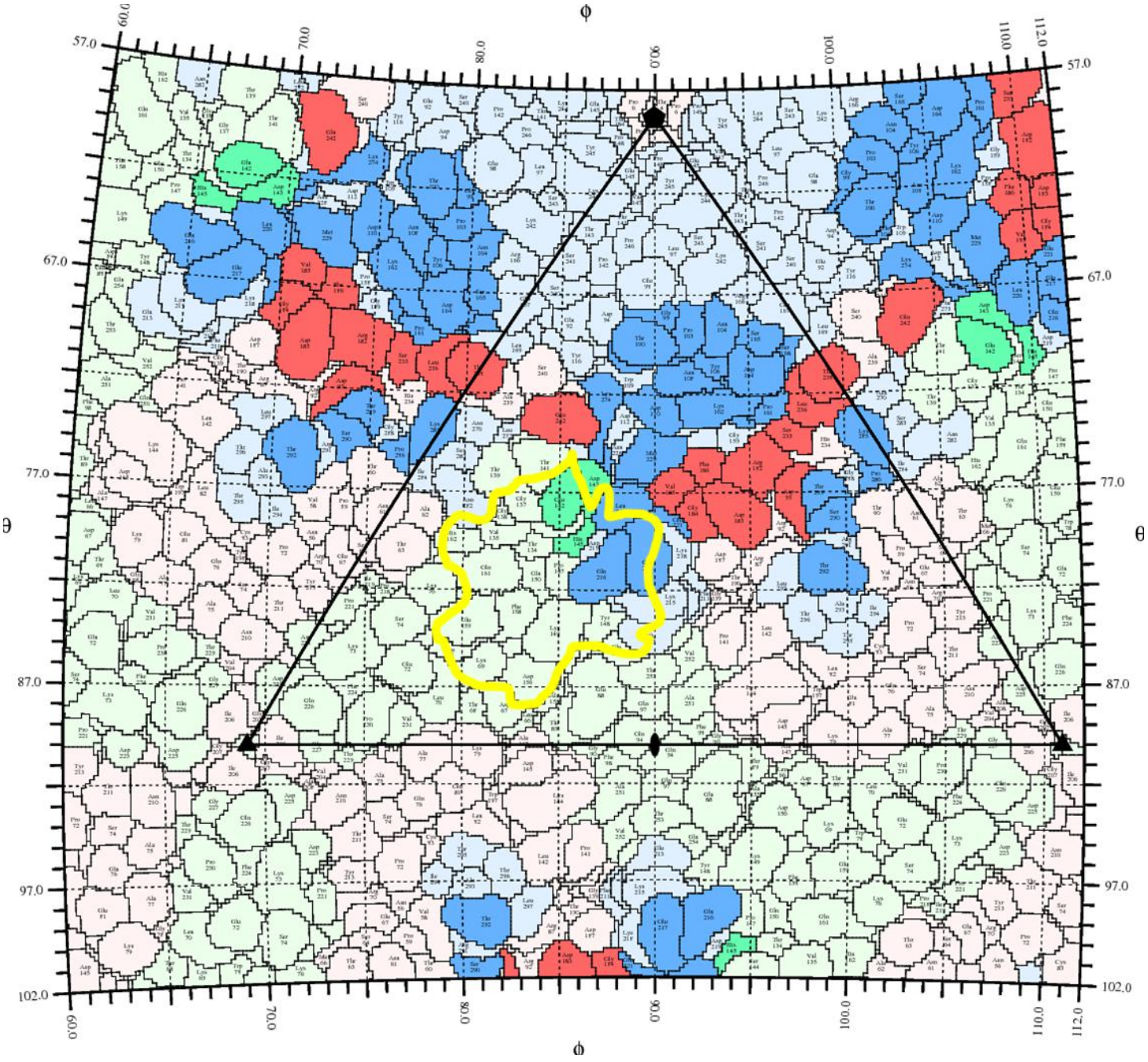

Figure 5.33 Roadmap of Fab 16-3-3C binding residues and SCARB2 binding area. Coloring is as for Figure 5.10.

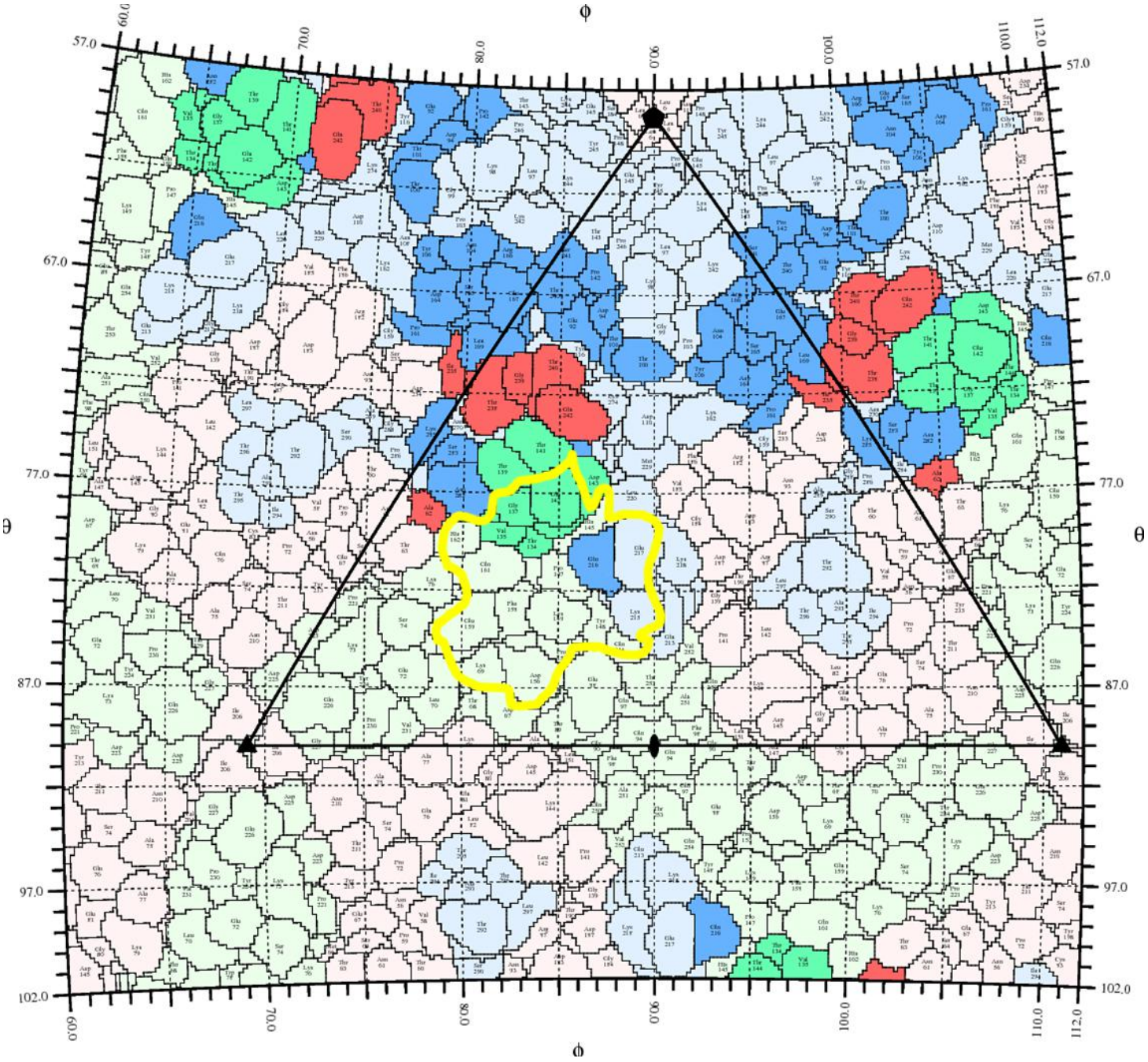

Figure 5.34 Roadmap of Fab 16-3-10B binding residues and SCARB2 binding area. Coloring is as for Figure 5.10.

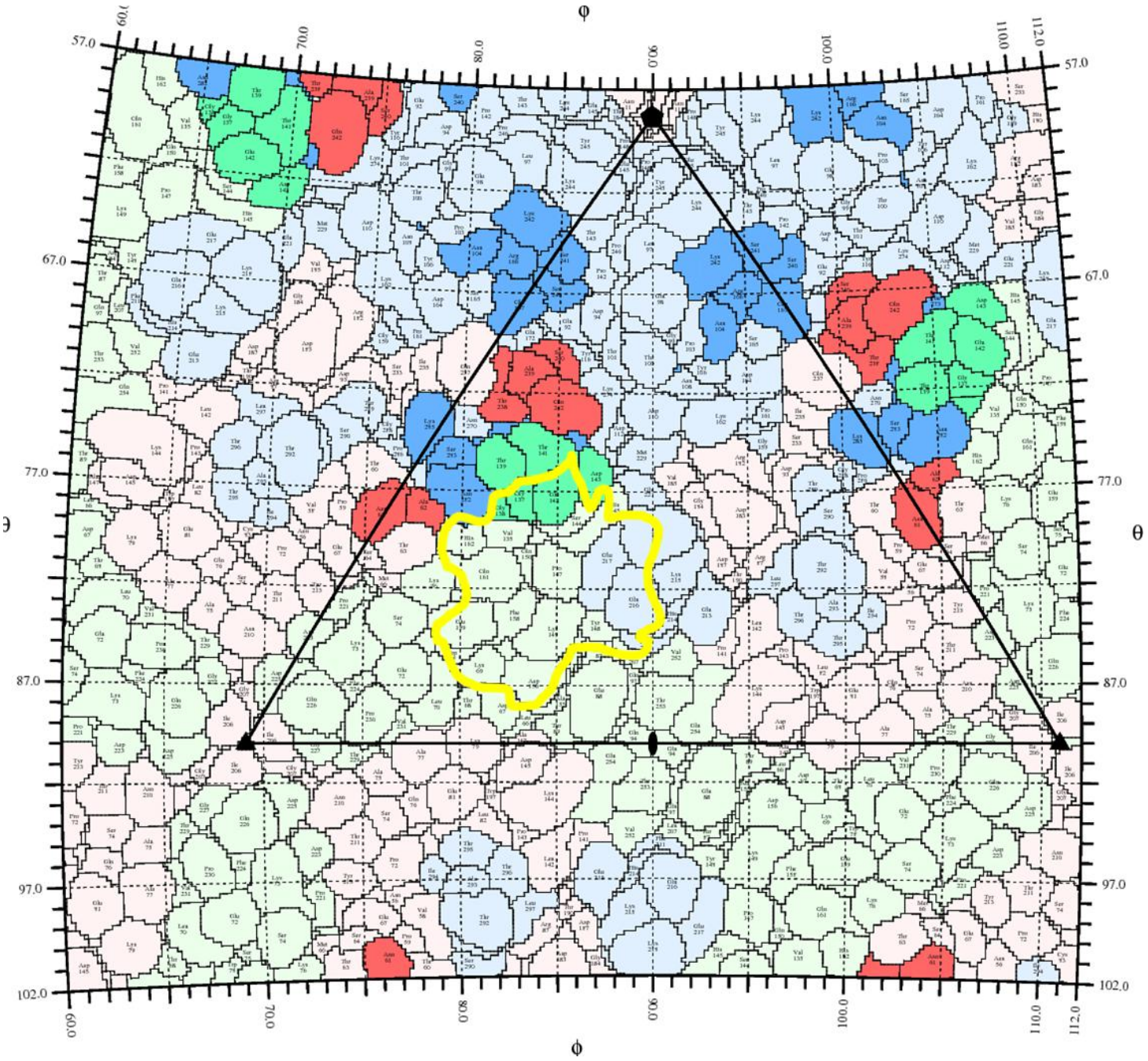

Figure 5.35 Roadmap of Fab 17-2-2B binding residues and SCARB2 binding area. Coloring is as for Figure 5.10.

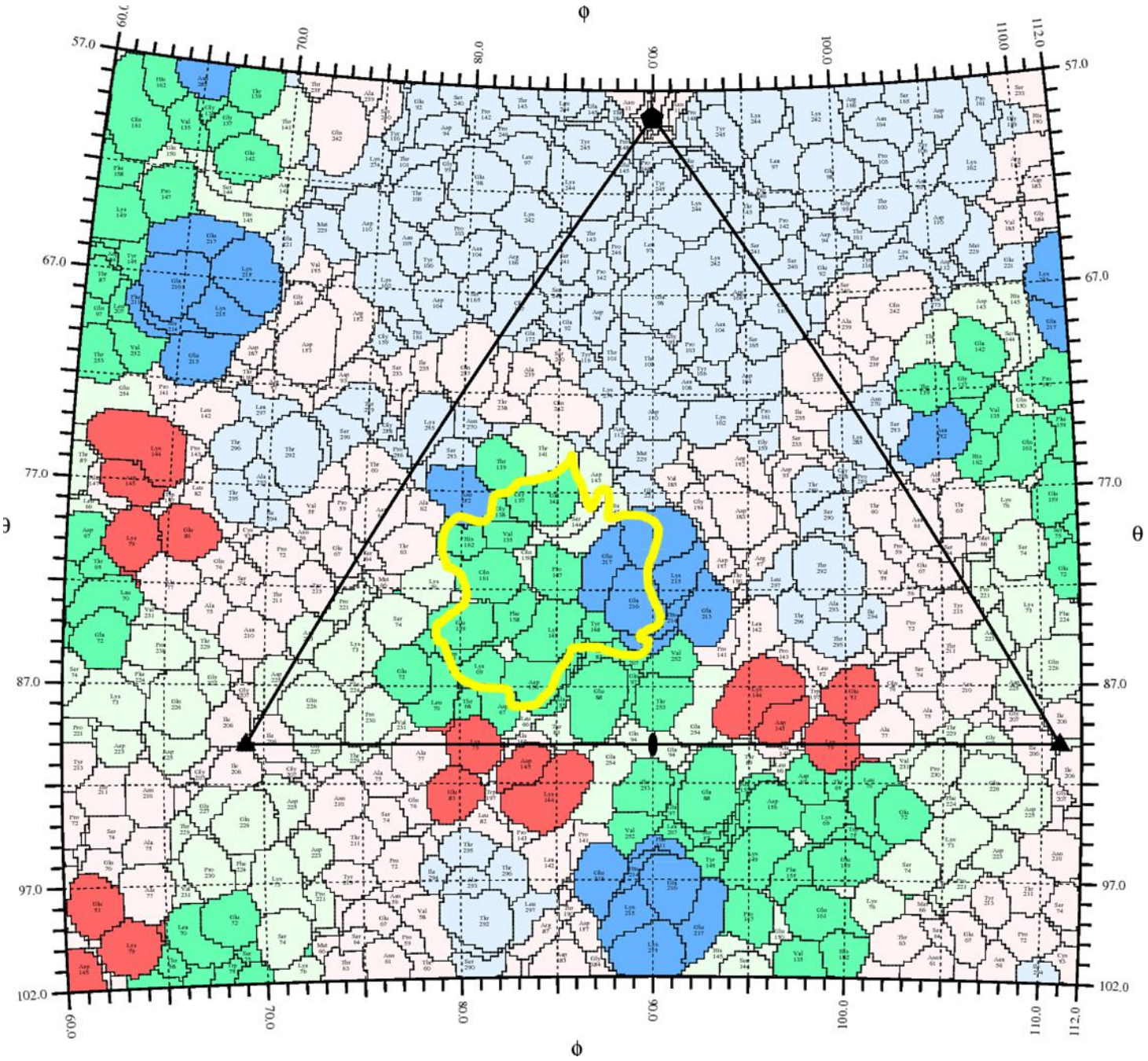

Figure 5.36 Roadmap of Fab 17-1-12A binding residues and SCARB2 binding area. Coloring is as for Figure 5.10.

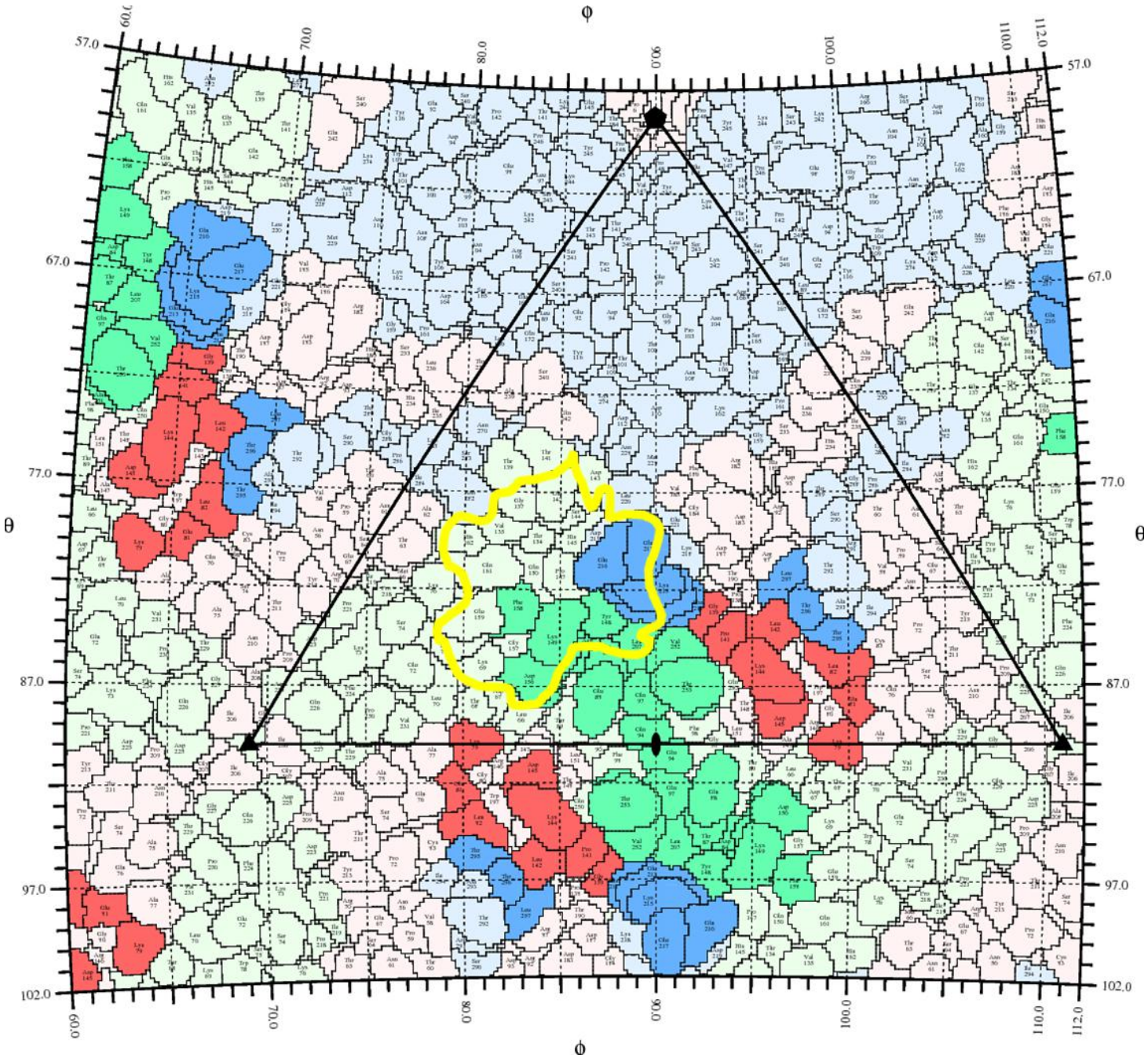

Figure 5.37 Roadmap of Fab 17-2-12A binding residues and SCARB2 binding area. Coloring is as for Figure 5.10.

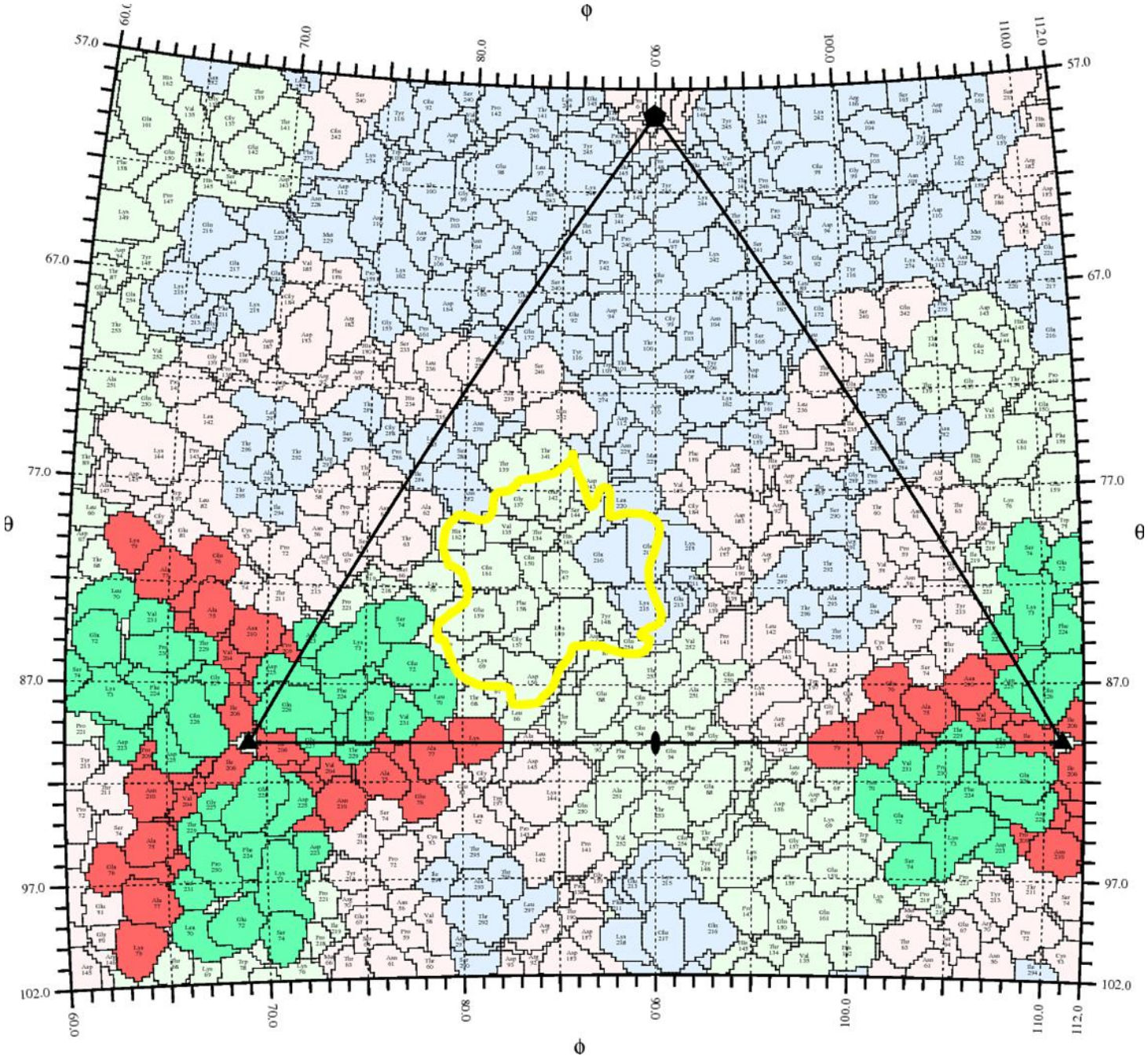

Figure 5.38 Roadmap of Fab 16-3-4D binding residues and SCARB2 binding area. Coloring is as for Figure 5.10.

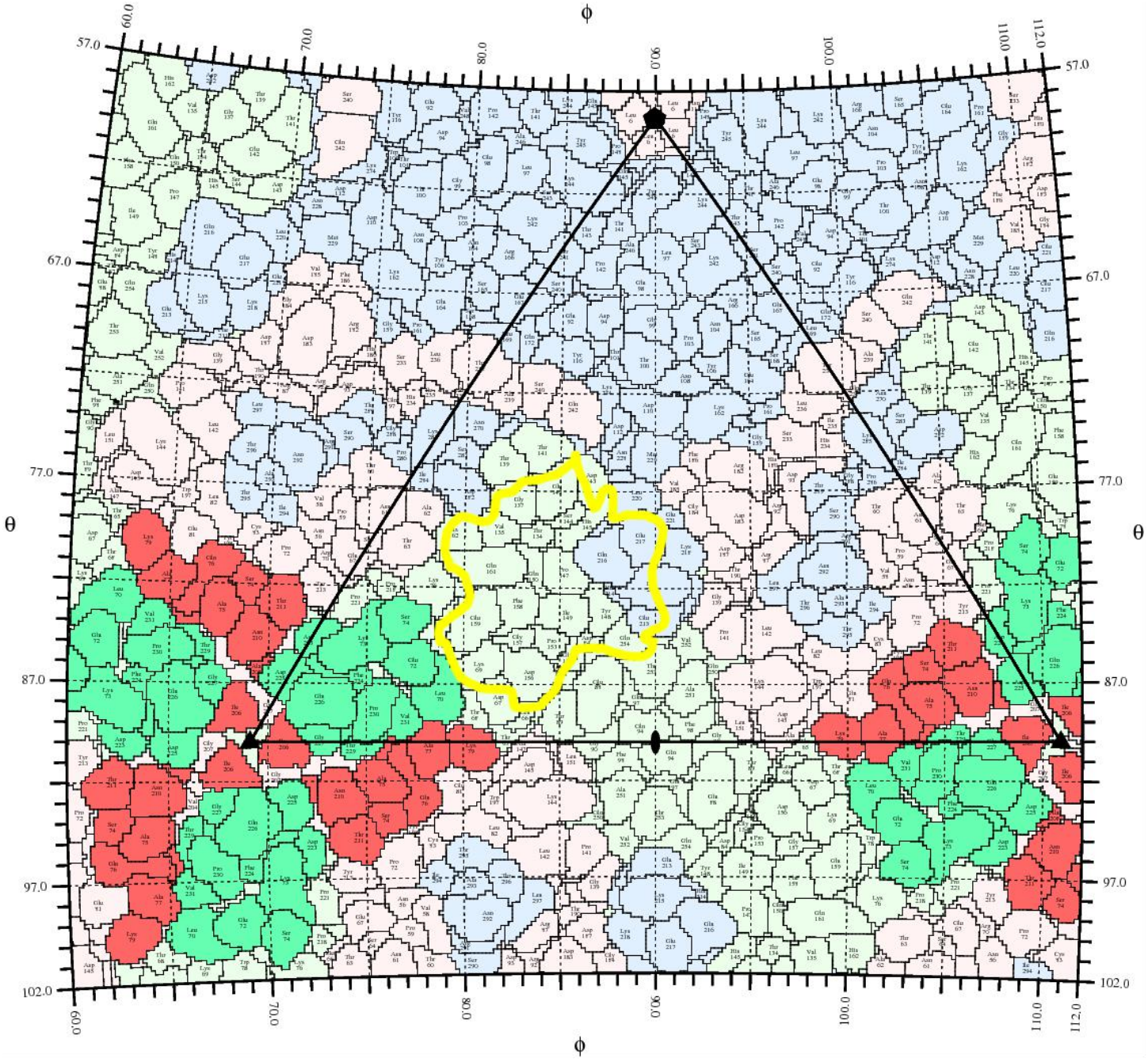

Figure 5.39 Roadmap of Fab 34-1-6D binding residues and SCARB2 binding area. Coloring is as for Figure 5.10.

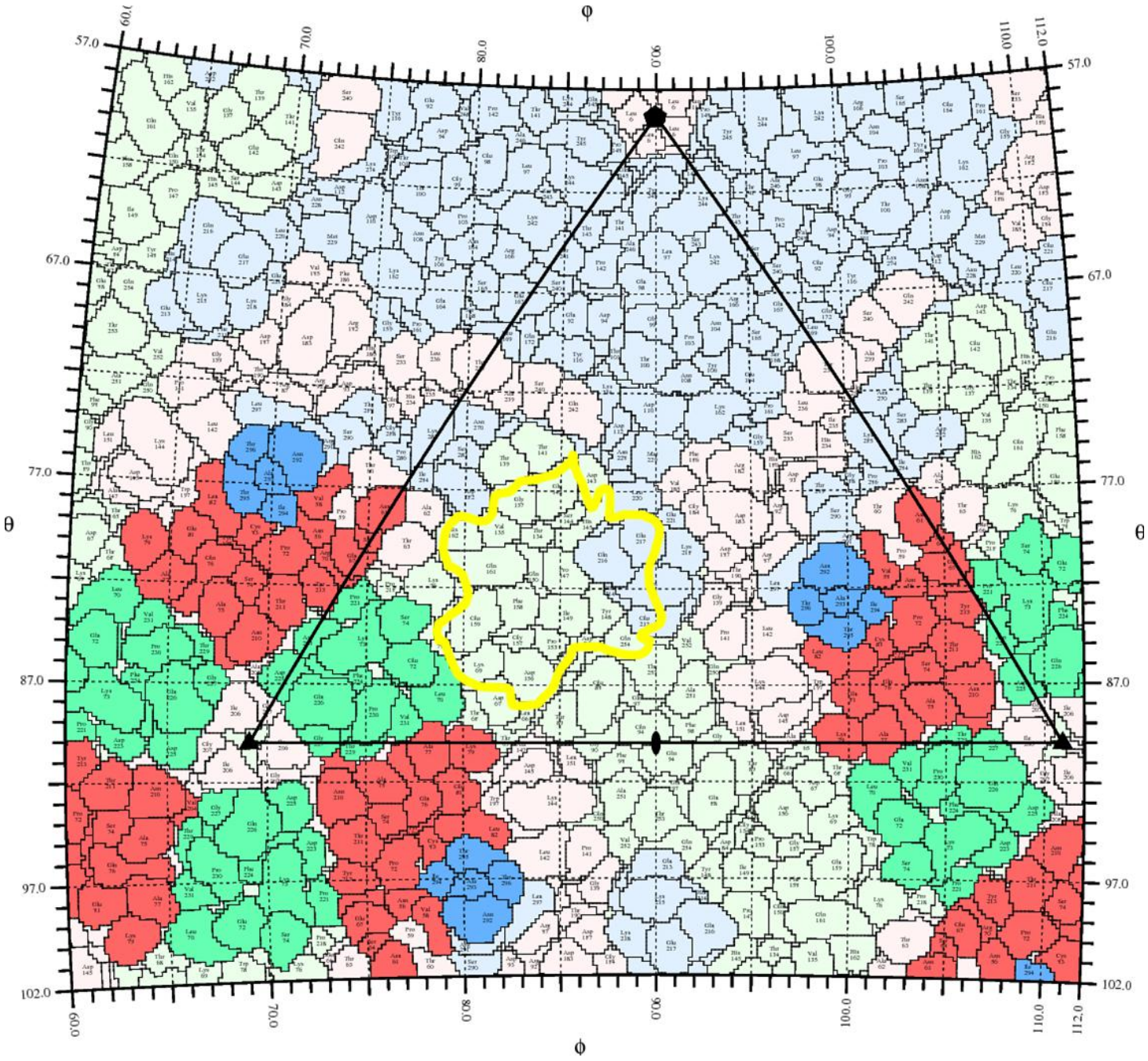

Figure 5.40 Roadmap of Fab 38-1-10A binding residues and SCARB2 binding area. Coloring is as for Figure 5.10.

5.8 Overlapped volume of Fabs and SCARB2 binding on EV71 capsid

To calculate the scale of the steric clash between SCARB2 and the antibody on binding, we calculated the overlap in volume of the mAb VHVL regions with SCARB2 as bound to the EV71 capsid using the software Mol_Volume (https://www.ks.uiuc.edu/Development/MDTools/molvolume/), and compared this with the neutralizing abilities of the mAbs (Table 5.5). These show a slight negative correlation (Pearson correlation coefficient -0.43). This is not altogether surprising since steric hindrance may be an all or nothing effect and different mAbs may have different binding affinities with EV71 capsid. All the binding Fabs (except 16-2-11B) share some overlapped volume with binding SCARB2, indicating they may have the ability to block SCARB2 binding (Figure 5.41). The VHVL part of Fab 16-2-11B has no overlapped volume with SCARB2, so it is unlikely to directly block receptor binding, and a different mechanism of neutralization may be at work.

mAb	pre-attachment EC_{50}(μg/ml)	post-attachmentEC_{50} (μg/ml)	neutralizing ability	overlapped volume Fab_VHVL with SCARB2 ($Å^3$)
16-3-10B	0.05	1.41	+++++	306 (+)
17-2-2B	0.05	1.39	+++++	631 (++)
38-1-10A	0.17	No data	++++	1267 (+++)
16-2-11B	0.28	7.55	++++	0 (-)
16-3-3C	0.28	7.61	++++	1207 (+++)
16-2-2D	0.27	38.53	+++	412 (+)
16-2-8C	0.27	109.78	+++	339 (+)
16-2-9D	1.41	99.96	+++	355 (+)

17-1-12A	1.42	58.83	++	6643 (+++++)
34-1-6D	1.43	267.15	++	1605 (++++)
16-2-12D	1.5	>400	++	421 (+)
16-3-4D	4.37	>400	++	2960 (++++)
17-2-12A	234.24	292.77	+	2907 (++++)

Table 5.5 Pre- and post-attachment neutralizing abilities of anti-EV71 mAbs compared to overlapped volume of mAbs' VHVL parts with SCARB2 (for ease of comparison the volumes are also mapped onto a simple – to +++++ scale.

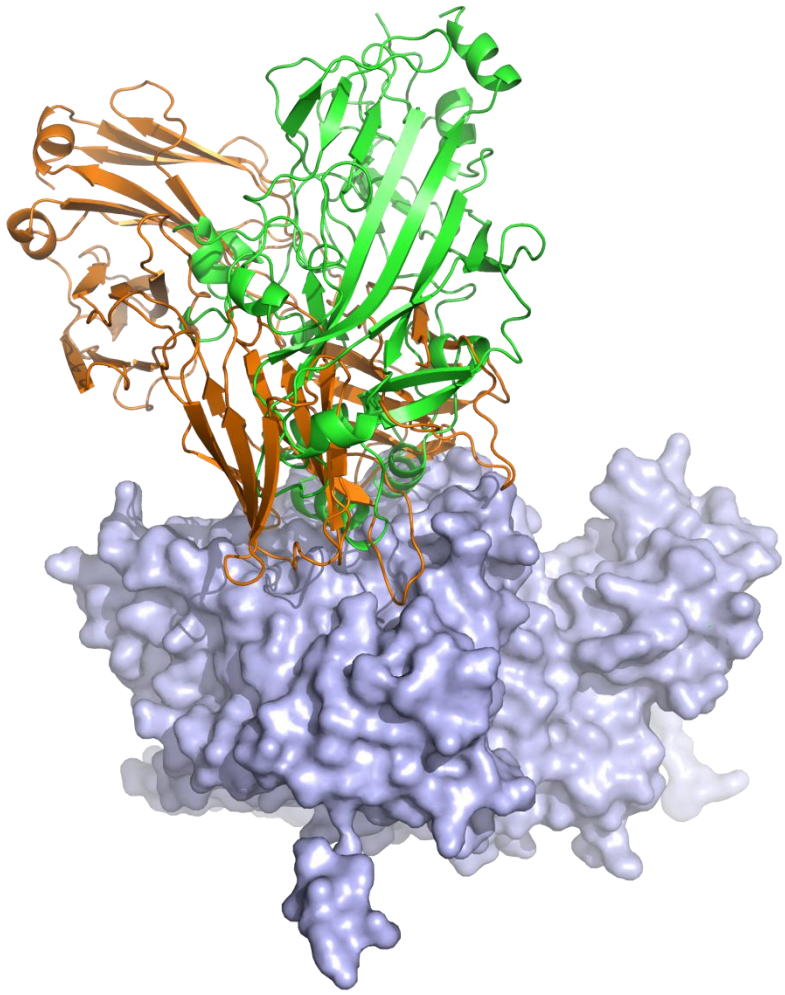

Figure 5.41. Overlap of Fab 17-1-12A (orange) with SCARB2 (green) as bound to the EV71 capsid (grey). Fab 17-1-12A takes up the binding area of SCARB2 thus can block SCARB2 binding.

5.9 Binding affinities of Fabs with full or empty particles of EV71

We performed binding kinetics assays on an Octet RED96 machine (Molecular Devices), as described in Chapter 2, and the results show that these Fabs have different binding K_Ds with full or empty particles of EV71 (Table 5.6, Figure 5.42). A scatter plot shows there is little correlation between binding K_Ds of Fabs for full and empty particles, although if a couple of major outliers are removed, there is some correlation (Figure 5.43). All these Fabs (except 16-3-4D) have lower K_Ds (tighter binding) for the EV71 virion, compared to the EV71 empty particle. This is reasonable because these antibodies were produced by patients presumably against live EV71 (although some researchers found immunization with virus-like particles of EV71 can induce potent immune responses and protect mice against lethal EV71 challenge[266,267]), and the fact that there is not a constant factor between full and empty is probably because the epitopes are affected differently by the transition from full to empty. In contrast to this, Fab 16-3-4D has a much lower K_D binding with empty EV71 particle, compared to full particle, this is interesting but the cause for this is still unclear, although since empty EV71 is found as a major component upon purification[31], it is possible that a significant number of empty particles were present in the patient.

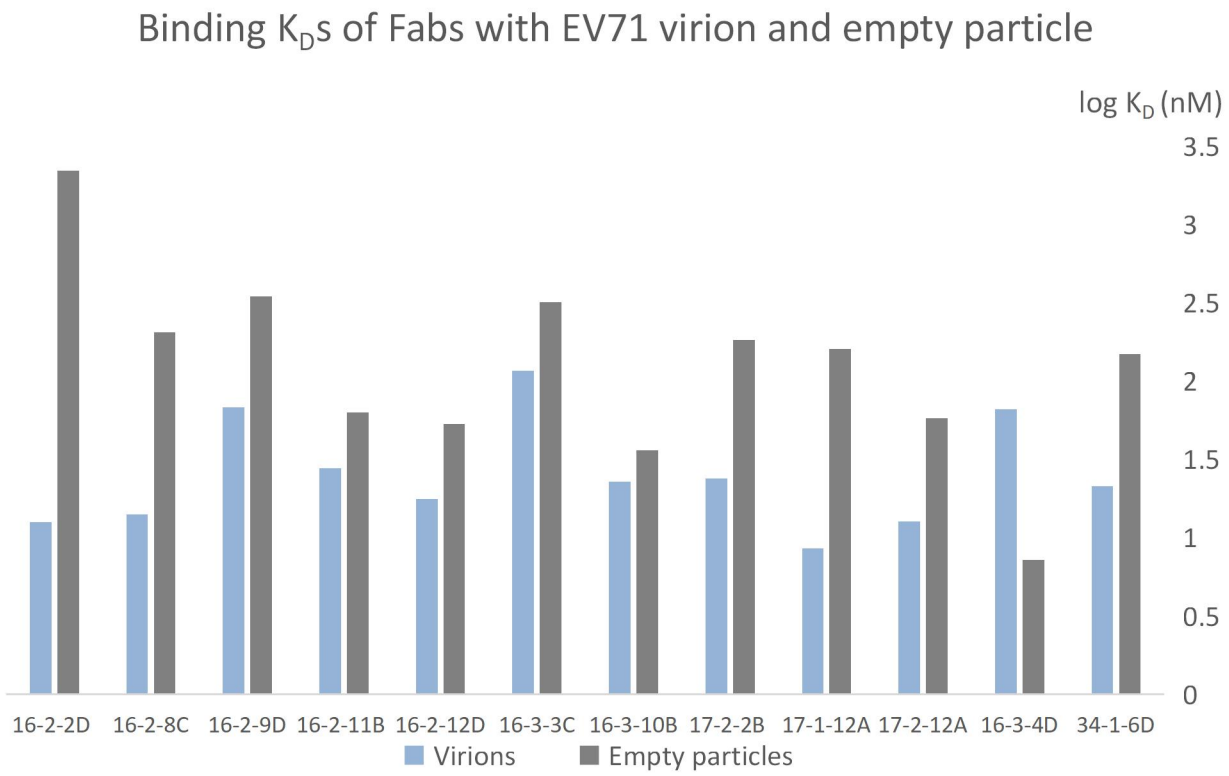

Figure 5.42 Binding K_Ds of 12 anti-EV71 Fabs with EV71 full and empty particles. The K_Ds (Y axis) are at a log scale.

Fab	Binding K_Ds with EV71 virion (nM)	Binding K_Ds with EV71 empty particle (nM)	EC_{50} (pre-attachment, μg/mL)
16-2-2D	12.6 ± 0.11	2207 ± 10.5	0.27
16-2-8C	14.1 ± 0.19	204.6 ± 1.55	0.27
16-2-9D	68.4 ± 0.92	349.6 ± 2.8	1.41
16-2-11B	27.8 ± 0.43	63.2 ± 0.53	0.28
16-2-12D	17.7 ± 0.15	53.5 ± 0.39	1.5
16-3-3C	117 ± 1.85	320 ± 3.39	0.28
16-3-10B	22.8 ± 0.19	36.3 ± 1.44	0.05
17-2-2B	24 ± 0.66	184.4 ± 1.35	0.05
17-1-12A	8.6 ± 0.09	161 ± 2.16	1.42
17-2-12A	12.7 ± 0.08	58 ± 0.81	234.24
16-3-4D	66.3 ± 0.92	7.2 ± 0.11	4.37
34-1-6D	21.4 ± 0.29	148.6 ± 0.99	1.43

Table 5.6 Binding K_Ds of 12 anti-EV71 Fabs with EV71 full and empty particles and EC_{50}s of corresponding IgGs in the pre-attachment stage.

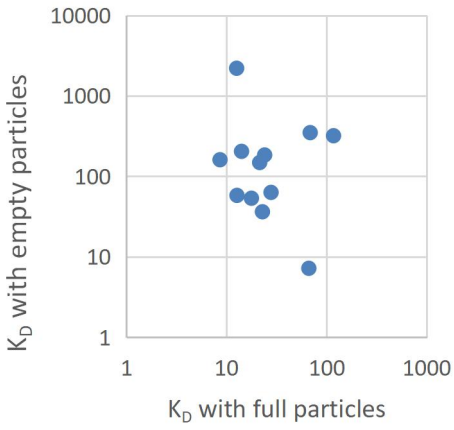

Figure 5.43 Scatter plot with log/log scale axes showing correlation between the binding K_Ds of Fabs with full and empty particles

We also compare the K_Ds of 12 anti-EV71 Fabs with the EC_{50}s of corresponding IgGs in the pre-attachment stage (Figure 5.44) and find there is very little evidence of correlation. At present we have no explanation for this.

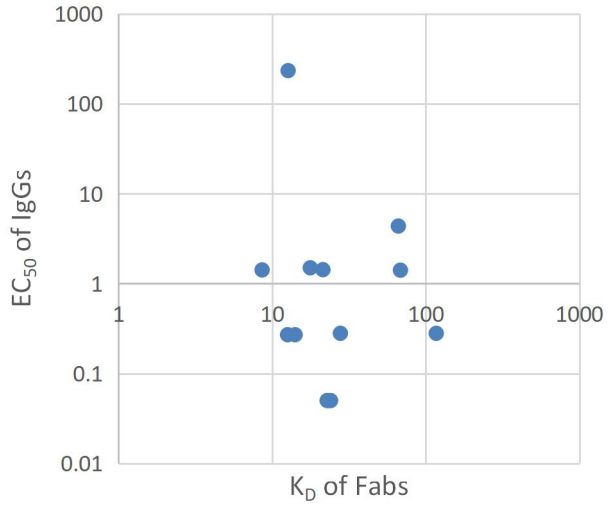

Figure 5.44 Scatter plot showing correlation between the binding K_Ds of Fabs and the EC_{50}s of corresponding IgGs, with log/log axes for the K_Ds and EC_{50}s separately.

5.10 Fabs' effect on the stability of EV71 virions

The results of thermal shift assays (Chapter 2) show that for most of these anti-EV71 Fabs, when the molar ratio of Fab: EV71 virion increases from 6 to 600, the Tm (melting temperature) of EV71 virions increases slightly by about 0.5 – 1 °C, indicating that Fab binding slightly increases the stability of EV71 virions. Fab 16-2-2D is a special case, it can decrease the Tm of EV71 virions by ~ 2.5 °C when Fab: EV71=600 (in mole). Thus Fab 16-2-2D has a significant ability to destabilize EV71 virions. This is consistent with the ability of Fab 16-2-2D to cause the formation of the empty particles of EV71 observed on micrographs using cryo-EM. (Chapter 5.2)

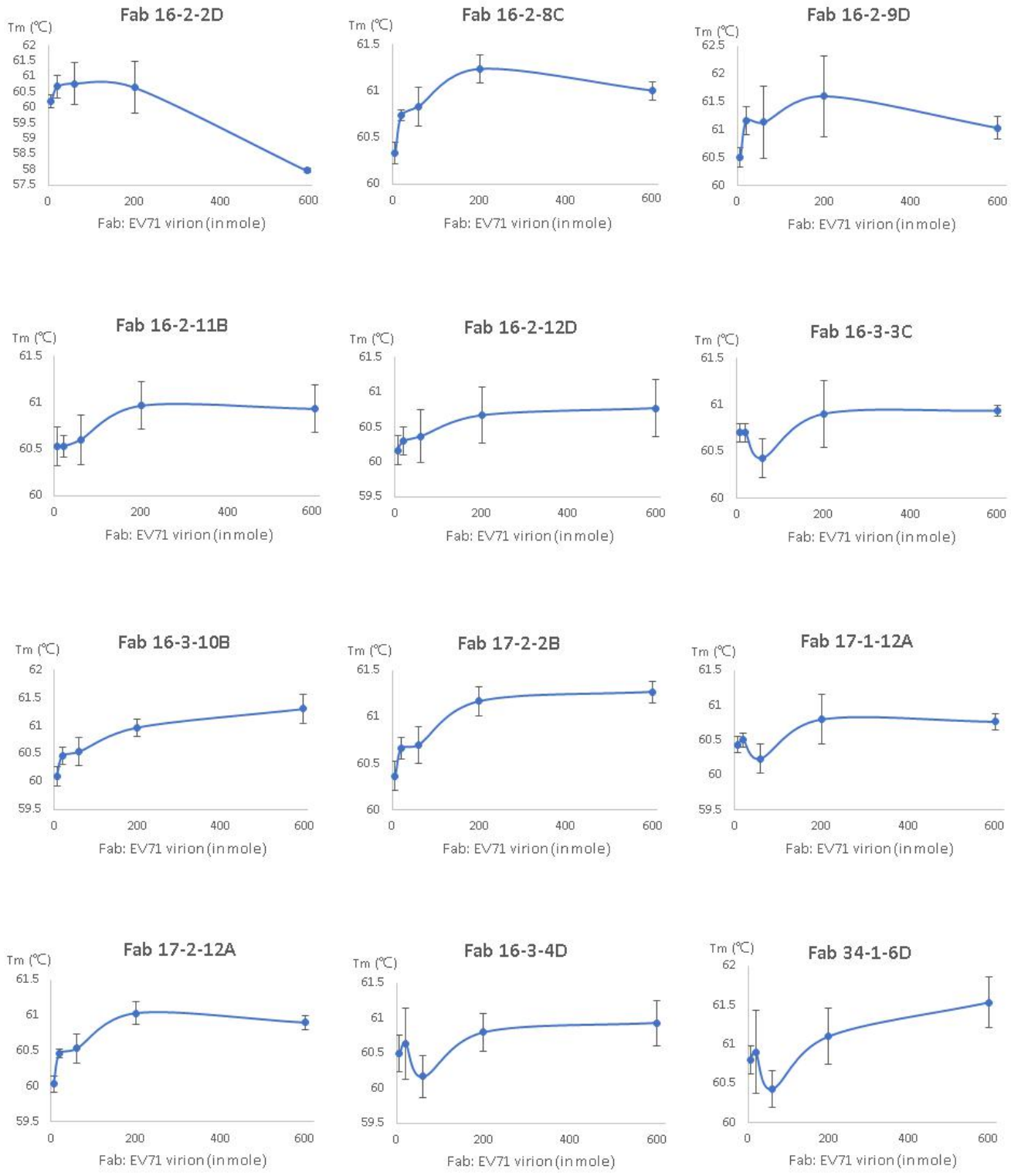

Figure 5.45 The effects of Fabs on the melting temperature of EV71 virions determined by thermal shift assay.

5.11 Summary

All the 13 antibodies generated by EV71-infected patients can neutralize EV71 virions and our cryo-EM structures of EV71-Fab complexes illuminate the interactions between these antibodies and EV71 capsid. The binding sites of these antibodies can be classified into three groups: canyon area (Fabs 16-2-2D, 16-2-8C 16-2-9D, 16-2-11B, 16-2-12D, 16-3-3C, 16-3-10B, 17-2-2B), 2-fold-axis area (Fabs 17-1-12A and 17-2-12A) and 3-fold-axis area (Fabs 16-3-4D, 34-1-6D and 38-1-10A). Antibodies belonging to the same group have partially overlapped footprints, which explains our collaborator's results that antibodies of the same group can cross-inhibit each other in the binding assay. Antibodies belonging to different groups share no or few common binding residues, so they can hardly compete with each other.

Antibodies 16-3-10B and 17-2-2B have totally different binding patterns from other canyon binders. These two antibodies have rather shorter HCDR3s. Instead of HCDR3, the light-chain CDR1 of mAb 16-3-10B stretches deep into the canyon and no part of mAb 17-2-2B goes deep into the canyon at all, while all the other canyon binders have longer HCDR3s, with which they can stretch deep into the canyon and interact with the residues at the bottom of the canyon.

Conformational changes can be observed in the binding interfaces between EV71 and Fabs for most of the 13 EV71-Fab complexes. These conformational changes mainly occur at some flexible regions of the structures, including HCDR3s of antibodies and VP1 B-C and G-H loops of EV71 capsid. These conformational changes are essential for the EV71-antibody interactions. Two mAbs 16-2-12D and 16-3-3C have the ability

to induce genome release of EV71 virions but the mechanism is not clear. They may induce this in a similar way as the uncoating receptors of EV71.

Some substitutions in viral proteins of EV71 can cause escape mutants from these anti-EV71 antibodies. Based on our structures, we can say that most of these substitutions occurred at residues directly involved in EV71-antibody interaction, while a few other substitutions are not directly involved in EV71-antibody interactions, but are likely to affect the presentation of residues that are directly involved in the binding, and in this way probably change the EV71-Fab interaction indirectly.

All the mAbs binding at canyon and 2-fold axis area share some common binding residues with SCARB2 and most of these mAbs (except 16-2-11B) have overlapped volume with SCARB2 when binding with EV71, so all the antibodies have the ability to block SCARB2 binding, thus neutralizing EV71 infection. Antibodies binding at the 2-fold-axis area can potentially block the genome release of EV71, since the channel right at 2-fold axis is where EV71 is thought to release its genome. Most of the antibodies slightly increase the stability of EV71 virions while Fab 16-2-2D notably destabilizes EV71 virions, these stabilizing or destabilizing effects may also contribute to the neutralization of EV71 by these antibodies.

Chapter 6

Final summary and future plan

6.1 Summary

SCARB2 is the major receptor for EV71 and there is good evidence that SCARB2 attachment mediates EV71 internalization and uncoating at low pH. We solved the cryo-EM structure of the EV71–SCARB2 complex and this structure reveals that SCARB2 binds EV71 on the southern rim of the canyon, rather than across the canyon. Helices 152-163 (α5) and 183-193 (α7) of SCARB2 and the VP1 GH and VP2 EF loops of EV71 dominate the interaction. Many residues within the binding footprint are not conserved across SCARB2-dependent enteroviruses. Only a proline and glycine residues are conserved. These two conserved residues may help in the design of anti-EV71 drugs.

Our collaborator has isolated 13 neutralizing anti-EV71 monoclonal antibodies. The high-resolution structures of 13 Fabs from these antibodies indicate these antibodies have variable lengths of CDRs, especially HCDR3s. Cryo-EM structures of EV71-Fab complexes illuminate the interactions between these antibodies and EV71 capsid. The binding sites of these antibodies can be classified into three groups: canyon area (mAbs 16-2-2D, 16-2-8C 16-2-9D, 16-2-11B, 16-2-12D, 16-3-3C, 16-3-10B, 17-2-2B), 2-fold-axis area (mAbs 17-1-12A and 17-2-12A) and 3-fold-axis area (mAbs 16-3-4D, 34-1-6D and 38-1-10A). Canyon binders tend to have longer HCDR3s, compared to 2- and 3-fold-axis binders. With these long HCDR3s, most canyon binders can go deep into the canyon and interact with residues on the canyon floor. Most somatic hypermutations of these antibodies are located in the framework regions, rather than CDRs. Mutations in the framework regions are basically not directly involved in interaction with EV71, but they have an effect on the neutralizing abilities of these Fabs.

All the mAbs can compete with SCARB2 when binding EV71, so they have the ability

to block SCARB2 binding. Antibodies binding at the 2-fold-axis area can potentially block the genome release of EV71 from the channel at 2-fold-axis. Fabs 16-2-2D, 16-2-12D and 16-3-3C can induce empty particles of EV71. Most of the antibodies slightly increase the stability of EV71 virions while Fab 16-2-2D notably destabilizes EV71 virions. All these effects Fabs have on EV71 virions are likely to contribute to their neutralization of the virus.

6.2 Future Plan

We have solved the cryo-EM structure of the EV71-SCARB2 complex to illuminate the virus-receptor interaction and determined the residues of EV71 and SCARB2 involved in the interaction. However, we still have little understanding about the whole entry process of EV71. Uncoating receptor and acidic environment are both necessary for the uncoating of EV71, but how the conformational changes of SCARB2 at acidic environment lead to conformational changes of EV71 capsid and subsequent release of pocket factor is still not clear, so understanding this process could be one of my future research projects.

Although the viral residues involved in the virus-SCARB2 interaction are not highly conserved across SCARB2-dependent viruses (EV71, CVA7, CVA14 and CVA16), they are conserved across all genotypes of EV71, while SCARB2 is a key receptor of EV71, so the binding area of SCARB2 on EV71 capsid can be used as a target to develop structure-based drugs. Since two flexible loops (VP1 GH and VP2 EF loops) comprise the binding area of SCARB2, small compounds may not be good choices for anti-EV71 drugs, but monoclonal antibodies targeting at this area seem promising. In Chapter 5, we

found some anti-EV71 human monoclonal antibodies that target at the SCARB2 binding area thus have the ability to block SCARB2 binding. Modifying or re-designing these antibodies for future clinical use might be another interest of mine, although antibody-based therapy is expensive at the current stage.

As mentioned in Chapter 1.4.6.1, SCARB2 is not the only receptor utilized by EV71 and CypA can also induce uncoating of EV71, so our structure of EV71-SCARB2 complex does not show the whole picture of how EV71 use human proteins as receptor in its entry process. To understand how EV71 interacts with these receptors by solving the cryo-EM structures of other EV71-receptor complexes is another project I am interested in.

Most somatic hypermutations of the anti-EV71 antibodies we studied occurred in the framework regions. We still do not know if these mutations are neutral or if not, how they contribute to the neutralization of EV71. Although most of these mutations are not directly involved in interaction with EV71, they may enhance potency of antibodies by increasing flexibility. Besides, we are not sure whether these mutations were randomly selected or hotspot directed. More experiments need to be done to explain this.

Appendix

Gene name	Vector	5' tag	3' tag	fwd primer (5’ to 3’)	reverse primer (5’ to 3’)
16-2-11B HC	pOPINhuVH	5’-TGGGTTGCGTAGCT-3’	5’-GCCTCCACCAAGGGC-3’	tgggttgcgtagctCAGGTTCAGCTGGTGCAG	gcccttggtggaggctGAGGAGACGGTGACCAGG
16-2-2D HC				tgggttgcgtagctGAGGTGCAGCTGGTGCAG’	gcccttggtggaggctGAGGAGACGGTGACCGTG
16-3-3C HC				tgggttgcgtagctGAGGTGCAGCTGGTGGAG	gcccttggtggaggctGAGGAGACGGTGACCGTG
17-1-12A HC				tgggttgcgtagctGAGGTGCAGCTGGTGGAG	gcccttggtggaggctGAGGAGACGGTGACCGTG
17-2-12A HC				tgggttgcgtagctCAGGTGCAGCTGGTGGAG	gcccttggtggaggctGAGGAGACGGTGACCGTG
16-2-8C HC				tgggttgcgtagctCAGCTGCAGCTGCAGGAG	gcccttggtggaggctGAGGAGACGGTGACCAGG
16-2-12D HC				tgggttgcgtagctCAGCTGCAGCTGCAGGAG	gcccttggtggaggctGAGGAGACGGTGACCAGG
16-3-4D HC				tgggttgcgtagctCAGCTGCAGCTGCAGGAG	gcccttggtggaggctGAGGAGACGGTGACCGTG
16-3-10B HC				tgggttgcgtagctGAGGTGCAGCTGGTGCAG	gcccttggtggaggctGAGGAGACGGTGACCAGG
34-1-6D HC				tgggttgcgtagctGAGGTGCAGCTGGTGGAG	gcccttggtggaggctGAGGAGACGGTGACCGTG
16-2-9D HC				No primer needed	
17-2-2B HC					
38-1-10A HC					
16-2-11B Lambda LC	pOPINhuVL_lambda		5’-CTAGGTCAGCCCAAG-3’	tgggttgcgtagctCAGTCTGTGCTGACTCAGC	cttgggctgacctagGAGGACGGCCAGCTTGG
16-2-2D Lambda LC				tgggttgcgtagctCAGTCTGTGCTGACTCAGC	cttgggctgacctagTAGGACGGTGACCTTGGTCC
16-3-3C Lambda LC				tgggttgcgtagctCAGTCTGCCCTGACTCAGC	cttgggctgacctagTAGGACGGTCAGCTTGGTCC
17-2-12A Lambda LC				tgggttgcgtagctCAGGCTGTGGTGACTCAGG	cttgggctgacctagTAGGACGGTGACCTTGGTCC
16-2-8C Lambda LC				tgggttgcgtagctCAGTCTGTGCTGACTCAG	cttgggctgacctagTAGGACGGTGACCTTGGTCC
16-2-12D Lambda LC				tgggttgcgtagctCAGTCTGCCCTGACTCAGC	cttgggctgacctagTAGGACGGTGACCTTGGTCC
16-3-4D Lambda LC				tgggttgcgtagctCAGTCTGTGCTGACTCAGC	cttgggctgacctagTAGGACGGTGACCTTGGTCC
16-3-10B Lambda LC				tgggttgcgtagctCAGTCTGCCCTGACTCAGC	cttgggctgacctagTAGGACGGTGACCTTGGTCC
16-2-9D Lambda LC				No primer needed	
17-2-2B Lambda LC					
34-1-6D Kappa LC	pOPINhuVH_kappa		5’-ACGGTGGCTGCACCA-3’	tgggttgcgtagctGACATCCAGATGACCCAGTC	tggtgcagccaccgTACGTTTGATTTCCACCTTGGTCCC
17-1-12A Kappa LC				tgggttgcgtagctGATATTGTGATGACTCAGTCTC	tggtgcagccaccgTACGTTTGATTTCCACCTTGGTCCC
38-1-10A Kappa LC				No primer needed	

Appendix table 1. Vectors, tags and primers used in the plasmid construction

	Fab 16-2-2D	**Fab 16-2-8C**	**Fab 16-2-9D**	**Fab 16-2-11B**
Data collection				
wavelength (Å)	0.9763	0.9282	0.9282	0.9282
Space group	*P* 1 2_1 1	*P* 1 2_1 1	*P* 1 2_1 1	*P* 1 2_1 1
Cell dimensions				
a, b, c (Å)	63.3, 104.0, 86.1	47.0, 80.4, 57.6	47.7, 80.3, 57.5	75.3, 83.9, 85.0
α, β, γ (°)	90, 104.0, 90	90, 93.8, 90	90, 94.9, 90	90, 103.5, 90
Resolution (Å)	1.92	1.14	1.18	2.57
No. reflections	82492 (4093)	153940 (7168)	141520 (7009)	32644 (1595)
CC 1/2	1.0 (0.7)	1.0 (0.5)	1.0 (0.7)	1.0 (0.6)
I/σI	20.4 (1.3)	11.5 (1.5)	10.6 (2.0)	14.4 (1.6)
R_{merge}	0.14 (-)	0.05 (-)	0.07 (-)	0.06 (-)
Completeness (%)	100 (100)	99.1 (92.6)	100 (99.6)	99.0 (97.7)
Redundancy	43.2 (8.4)	6.0 (4.2)	6.3 (4.9)	6.7 (5.9)
Refinement				
No. reflections	78359/4018	153906 (7535)	141486 (7068)	32629 (1592)
No. molecules in each asymmetric unit	2	1	1	2
R_{work} / R_{free}	0.165/0.188	0.170/0.194	0.152/0.177	0.198/0.252
No. atoms				
Protein	6749	3476	3439	6623
Ligand/ion	99	0	12	33
Water	482	576	618	84
B-factor				
Protein	52	20	18	82
Ligand/ion	77	-	37	42
Water	55	35	35	66
R.m.s. deviations				
Bond lengths (Å)	0.005	0.007	0.007	0.012
Bond angles (°)	0.85	1.16	1.12	1.58
Ramachandran plot				
Favored (%)	95.62	95.32	95.19	91.19
Allowed (%)	3.69	4.19	4.57	7.55
Outliers (%)	0.69	0.49	0.24	1.26

Appendix table 2. Data collection and refinement statistics of X-ray diffraction. (Outer shell in parenthesis)

	Fab 16-2-12D	**Fab 16-3-3C**	**Fab 16-3-4D**	**Fab 16-3-10B**
Data collection				
wavelength (Å)	0.9282	0.9763	0.9282	0.9282
Space group	*C* 2 2 2	*C* 2 2 2_1	*P* 6_5 2 2	*P* 1 2_1 1
Cell dimensions				
a, b, c (Å)	130.2, 265.3, 81.5	77.8, 156.6, 78.5	121.4, 121.4, 361.7	67.8, 50.1, 74.5
α, β, γ (°)	90, 90, 90	90, 90, 90	90, 90, 120	90, 116.5, 90
Resolution (Å)	3.06	1.32	2.78	2.12
No. reflections	27241 (1299)	112322 (5448)	40825 (1957)	25701 (1197)
CC 1/2	1.0 (0.9)	1.0 (0.6)	1.0 (0.5)	1.0 (0.5)
I/σI	8.1 (1.4)	18.9 (1.4)	15.5 (1.1)	9.0 (1.5)
Rmerge	0.5 (-)	0.1 (-)	0.1 (-)	0.1 (-)
Completeness (%)	99.9 (97.2)	99.9 (98.2)	100 (97.0)	99.7 (92.8)
Redundancy	26.0 (27.0)	69.4 (29.4)	18.9 (18.5)	6.3 (5.1)
Refinement				
No. reflections	22548 (1233)	112292 (5646)	37321 (1957)	23270 (1229)
No. molecules in each asymmetric unit	2	1	2	1
Rwork / Rfree	0.201/0.251	0.148/0.176	0.224/0.280	0.210/0.256
No. atoms				
Protein	6630	3394	6635	3259
Ligand/ion	80	51	90	2
Water	75	501	59	87
B-factor				
Protein	43	21	95	52
Ligand/ion	30	42	166	67
Water	23	35	68	48
R.m.s. deviations				
Bond lengths (Å)	0.004	0.007	0.004	0.003
Bond angles (°)	0.77	1.24	0.87	0.62
Ramachandran plot				
Favored (%)	92.91	94.55	90.33	93.76
Allowed (%)	6.17	4.95	8.08	5.31
Outliers (%)	0.91	0.50	1.59	0.92

Appendix table 3. Data collection and refinement statistics of X-ray diffraction. (Outer shell in parenthesis)

	Fab 17-1-12A	**Fab 17-2-2B**	**Fab 17-2-12A**	**Fab 34-1-6D**
Data collection				
wavelength (Å)	0.9282	0.9795	0.9686	0.9282
Space group	*P* 6 2 2	*P* 1 2_1 1	*P* 1	*P* 1
Cell dimensions				
a, b, c (Å)	152.8, 152.8, 120.5	72.5, 71.7, 93.1	40.8, 72.6, 87.8	54.2, 56.0, 75.4
α, β, γ (°)	90, 90, 120	90, 105.8, 90	104.4, 93.2, 96.6	86.7, 86.4, 67.1
Resolution (Å)	2.83	2.56	2.68	1.63
No. reflections	20091 (994)	29400 (1109)	27165 (1277)	98557 (4808)
CC 1/2	0.98 (0.56)	1.0 (0.5)	1.0 (0.5)	1.0 (0.7)
I/σI	7.6 (1.2)	9.7 (1.0)	4.2 (1.2)	11.2 (1.5)
Rmerge	0.3 (-)	0.2 (-)	0.3 (-)	0.04 (-)
Completeness (%)	98.7 (99.5)	98.6 (74.5)	99.5 (90.8)	97.1 (94.6)
Redundancy	9.8 (10.0)	11.9 (3.0)	5.1 (5.2)	3.4 (2.8)
Refinement				
No. reflections	20089 (1027)	29388 (1397)	25799 (1313)	98557 (4614)
No. molecules in each asymmetric unit	1	2	2	2
Rwork / Rfree	0.227/0.278	0.223/0.261	0.222/0.260	0.166/0.211
No. atoms				
Protein	3400	6505	6507	6642
Ligand/ion	14	33	0	23
Water	61	97	119	739
B-factor				
Protein	11	61	54	37
Ligand/ion	88	80	-	40
Water	47	74	38	46
R.m.s. deviations				
Bond lengths (Å)	0.004	0.01	0.005	0.008
Bond angles (°)	0.835	1.432	0.780	1.156
Ramachandran plot				
Favored (%)	93.44	95.71	94.02	96.13
Allowed (%)	4.98	3.82	5.28	2.78
Outliers (%)	1.58	0.46	0.70	1.09

Appendix table 4. Data collection and refinement statistics of X-ray diffraction. (Outer shell in parenthesis)

	Fab 38-1-10A
Data collection	
wavelength (Å)	0.9763
Space group	*P* 2_1 2_1 2
Cell dimensions	
a, b, c (Å)	292.4, 87.1, 177.0
α, β, γ (°)	90, 90, 90
Resolution (Å)	2.70
No. reflections	124934 (6090)
CC 1/2	1.0 (0.6)
I/σI	16.4 (1.1)
Rmerge	0.37 (-)
Completeness (%)	100 (99.4)
Redundancy	53.8 (8.1)
Refinement	
No. reflections	118703 (6151)
No. molecules in each asymmetric unit	9
Rwork / Rfree	0.190 (0.240)
No. atoms	
Protein	29206
Ligand/ion	0
Water	483
B-factor	
Protein	66.6
Water	48.8
R.m.s. deviations	
Bond lengths (Å)	0.006
Bond angles (°)	0.98
Ramachandran plot	
Favored (%)	93.84
Allowed (%)	5.08
Outliers (%)	1.08

Appendix table 5. Data collection and refinement statistics of X-ray diffraction. (Outer shell in parenthesis)

	16-2-2D	16-2-8C	16-2-9D	16-2-11B
Data collection and reconstruction				
Voltage (kV)	300	300	300	300
Frames/movie	25	30	40	24
Dose rate (e^-/ Å ^{2}/ s)	6	4	4	4
Total dose (e^-/ Å ^{2})	29	22	30	27
Pixel size (Å)	1.35	1.35	1.35	1.35
Defocus (μm)	0.5-2.5	0.5-2.5	0.5-2.5	0.5-2.5
Movies	903	424	2086	1129
Particles	1399	3665	3668	5881
Map resolution (Å)	3.4	3.8	3.7	3.3
Map sharpening B-factor (Å^2)	-103.1	-123.7	-145.4	-140.0
Model refinement				
Model-to-map fit, CC_mask	0.810	0.763	0.784	0.811
R.m.s.d., bonds (Å)	0.01	0.009	0.009	0.01
R.m.s.d., angles (°)	0.85	0.880	0.862	0.96
All-atom Clash score	4.86	4.73	4.70	7.79
Rotamer outliers (%)	0	0	0	0.33
Ramachandran plot				
Favored (%)	93.81	93.11	95.33	92.73
Allowed (%)	6.00	6.79	4.67	7.27
Outliers (%)	0.19	0.11	0.00	0.00

Appendix table 6. Cryo-EM data collection and refinement statistics of EV71-Fab complexes

	16-2-12D	16-3-3C	16-3-4D	16-3-10B
Data collection and reconstruction				
Voltage (kV)	300	300	300	300
Frames	40	40	40	24
Dose rate (e^-/ Å ^{2}/ s)	4	4	4	4
Total dose (e^-/ Å ^{2})	30	30	30	27
Pixel size (Å)	1.35	1.35	1.35	1.35
Defocus (μm)	0.5-2.5	0.5-2.5	0.5-2.5	0.5-2.5
Movies	468	1559	1177	1157
Particles	16774	2770	26427	2852
Map resolution (Å)	3.1	3.6	3.0	3.3
Map sharpening B-factor (Å^2)	-132.8	-124.6	-127.6	-110.5
Model refinement				
Model-to-map fit, CC_mask	0.839	0.792	0.841	0.817
R.m.s.d., bonds (Å)	0.013	0.01	0.007	0.01
R.m.s.d., angles (°)	1.067	0.953	0.863	1.07
All-atom Clash score	4.42	4.35	4.76	7.99
Rotamer outliers (%)	0.43	0.22	0.06	0.45
Ramachandran plot				
Favored (%)	93.74	93.56	95.03	93.57
Allowed (%)	6.07	6.16	4.86	6.34
Outliers (%)	0.19	0.28	0.11	0.09

Appendix table 7. Cryo-EM data collection and refinement statistics of EV71-Fab complexes

	17-1-12A	17-2-2B	17-2-12A	34-1-6D
Data collection and reconstruction				
Voltage (kV)	300	300	300	300
Frames	25	25	40	24
Dose rate (e^-/ Å ^{2}/ s)	6	5	4	4
Total dose (e^-/ Å ^{2})	29	25	30	27
Pixel size (Å)	1.35	1.35	1.35	1.35
Defocus (μm)	0.5-2.5	0.5-2.5	0.5-2.5	0.5-2.5
Movies	470	668	1170	1133
Particles	3919	10037	40169	9700
Map resolution (Å)	4.1	3.4	3.1	3.0
Map sharpening B-factor (Å^2)	-175.3	-156.5	-150.5	-113.0
Model refinement				
Model-to-map fit, CC_mask	0.704	0.779	0.831	0.823
R.m.s.d., bonds (Å)	0.01	0.006	0.007	0.01
R.m.s.d., angles (°)	0.85	0.809	0.865	0.99
All-atom Clash score	4.86	4.12	4.82	7.51
Rotamer outliers (%)	0.11	0.12	0	0.33
Ramachandran plot				
Favored (%)	90.68	93.97	94.82	93.83
Allowed (%)	9.23	5.81	5.09	6.08
Outliers (%)	0.09	0.21	0.09	0.09

Appendix table 8. Cryo-EM data collection and refinement statistics of EV71-Fab complexes

	EV71_38-1-10A	EV71_SCARB2
Data collection and reconstruction		
Voltage (kV)	300	300
Frames	40	32
Dose rate (e^-/ Å ^{2}/ s)	4	4
Total dose (e^-/ Å ^{2})	30	35
Pixel size (Å)	1.35	1.35
Defocus (μm)	0.5-2.5	0.5 - 2.5
Movies	324	757
Particles	10074	10443
Map resolution (Å)	3.1	3.4
Map sharpening B-factor (Å^2)	-131.2	-150.4
Model refinement		
Model-to-map fit, CC_mask	0.812	0.748
R.m.s.d., bonds (Å)	0.007	0.01
R.m.s.d., angles (°)	0.875	0.956
All-atom Clash score	5.26	4.89
Rotamer outliers (%)	0.09	0.38
Ramachandran plot		
Favored (%)	94.21	93.91
Allowed (%)	5.79	5.93
Outliers (%)	0	0.16

Appendix table 9. Cryo-EM data collection and refinement statistics of EV71-Fab 38-1-10A and EV71-SCARB2 complexes

Residue in EV71	Residue in SCARB2	Distance (Å)
Potential hydrogen bonds		
A214 HIS	E163 TYR	3.76
B78 TRP	E154 GLU	3.95
B148 TYR	E163 TYR	3.38
B161 GLN	E192 ARG	3.42
Hydrophobic interactions		
A216 GLN	E186 SER	3.99
A216 GLN	E187 LEU	3.30
B135 VAL	E190 VAL	3.45
B135 VAL	E193 PRO	3.84
B137 GLY		3.59
B138 GLY		3.69
B144 SER	E190 VAL	3.99
B147 PRO	E187 LEU	3.67
	E190 VAL	3.71
	E191 PHE	3.93
B148 TYR	E163 TYR	2.94
B149 ILE	E158 ALA	3.69
	E159 MET	2.80
	E162 ALA	3.72
	E163 TYR	3.84
B150 GLN	E191 PHE	3.66
B156 ASP	E161 LYS	3.88
B158 PHE	B191 PHE	3.42
B161 GLN	E155 ILE	3.51
	E191 PHE	3.77
	E192 ARG	3.93
Potential Charged interactions		
A217 GLU	E181 LYS	3.16
B156 ASP	E161 LYS	3.83

Appendix table 10. List of interactions between EV71 and SCARB2. The protein chain names for the viral proteins are as VP1, A; VP2, B; and the receptor, E.

Fab	Solvent accessible area (Å^2)								
	HC-VP1	HC-VP2	HC-VP3	HC-EV71	LC-VP1	LC-VP2	LC-VP3	LC-EV71	Fab-EV71
Canyon binders									
16-2-2D	785	144	165	1094	329	0	257	586	1680
16-2-8C	756	121	232	1109	473	0	144	617	1726
16-2-9D	731	133	230	1094	406	0	125	531	1625
16-2-11B	546	176	233	955	463	0	0	463	1418
16-2-12D	711	173	166	1050	279	0	24	303	1353
16-3-3C	610	16	293	919	310	75	8	393	1312
16-3-10B	174	318	14	505	530	83	287	900	1405
17-2-2B	234	151	106	491	222	160	102	483	974
2-fold-axis binders									
17-1-12A	231	720	218	1169	161	153	0	315	1484
17-2-12A	235	617	35	887	110	46	230	385	1272
3-fold-axis binders									
16-3-4D	0	642	297	939	0	27	20	47	986
34-1-6D	0	492	120	612	0	59	259	317	929
38-1-10A	0	465	173	638	195	136	427	758	1396

Appendix table 11. Solvent accessible areas between chains of Fabs (HC: heavy chain, LC: light chain) and viral proteins of EV71 in the EM structures of 13 EV71-Fab complexes

Appendix figure 1. Below are binding curves of Fabs with EV71 full particles measured by bio-layer interferometry on Octet RED96e. Different colors of the curves stand for different concentration (nm) of the Fabs used. The red curves indicate the global fitting models used. Some bad curves were not used for the model fitting.

16-2-2D

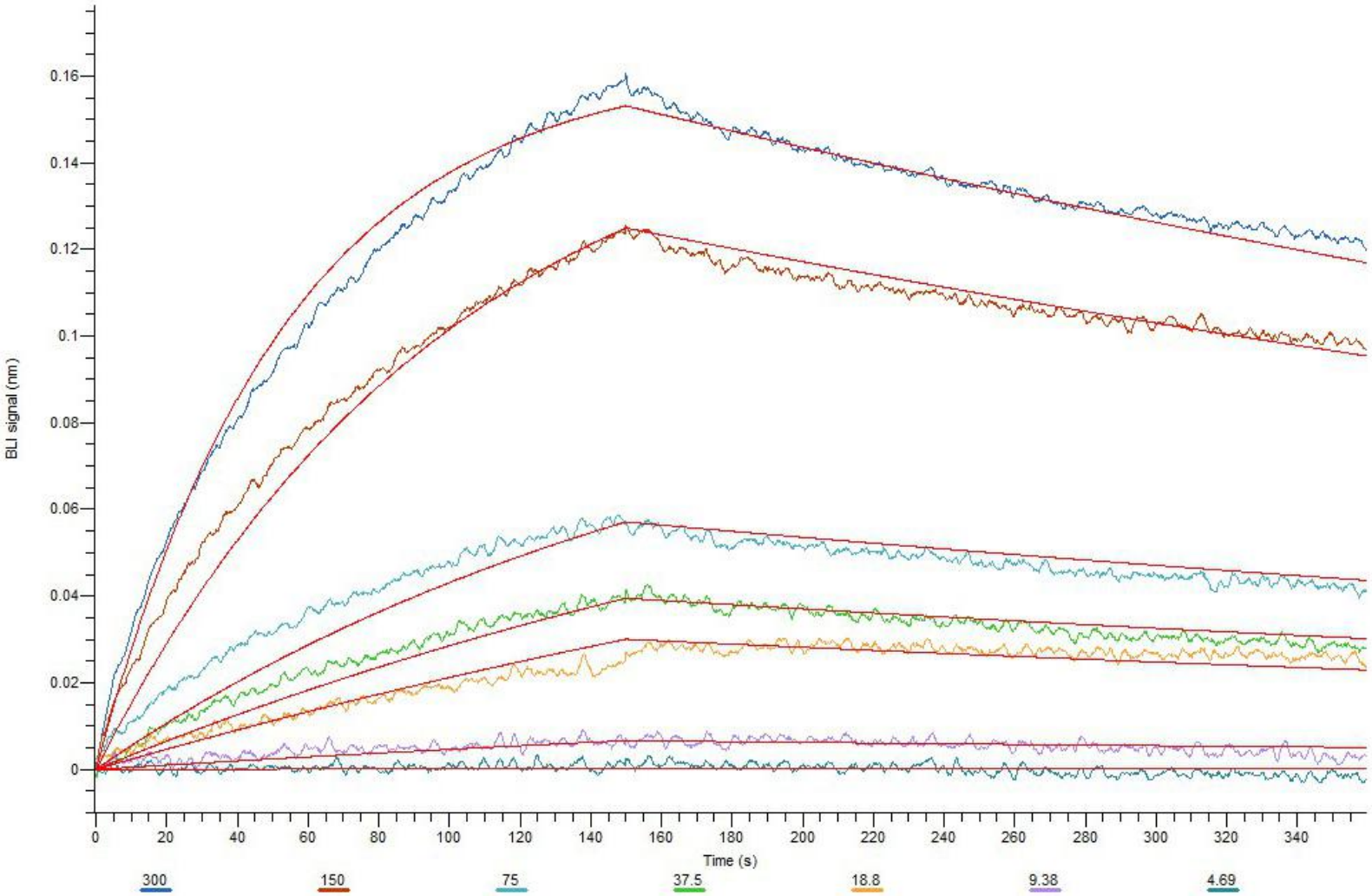
BLI signal (nm)
0.16
0.14
0.12
0.1
0.08
0.06
0.04
0.02
0
0
20
40
60
80
100
120
140
160
180
200
220
240
260
280
300
320
340
Time (s)
300
150
75
37.5
18.8
9.38
4.69

16-2-8C

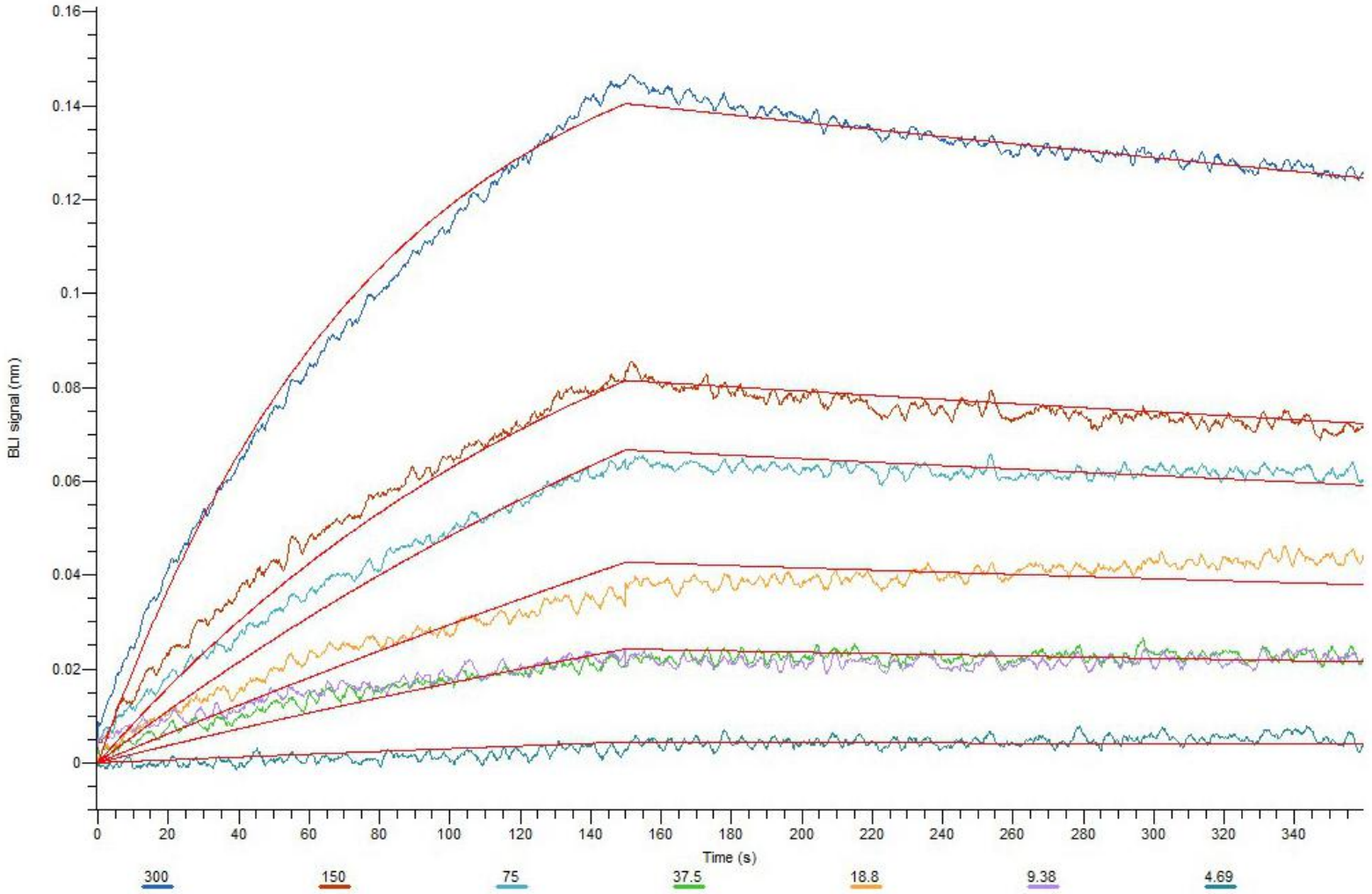
BLI signal (nm)
0.16
0.14
0.12
0.1
0.08
0.06
0.04
0.02
0
0 20 40 60 80 100 120 140 160 180 200 220 240 260 280 300 320 340
Time (s)
300
150
75
37.5
18.8
9.38
4.69

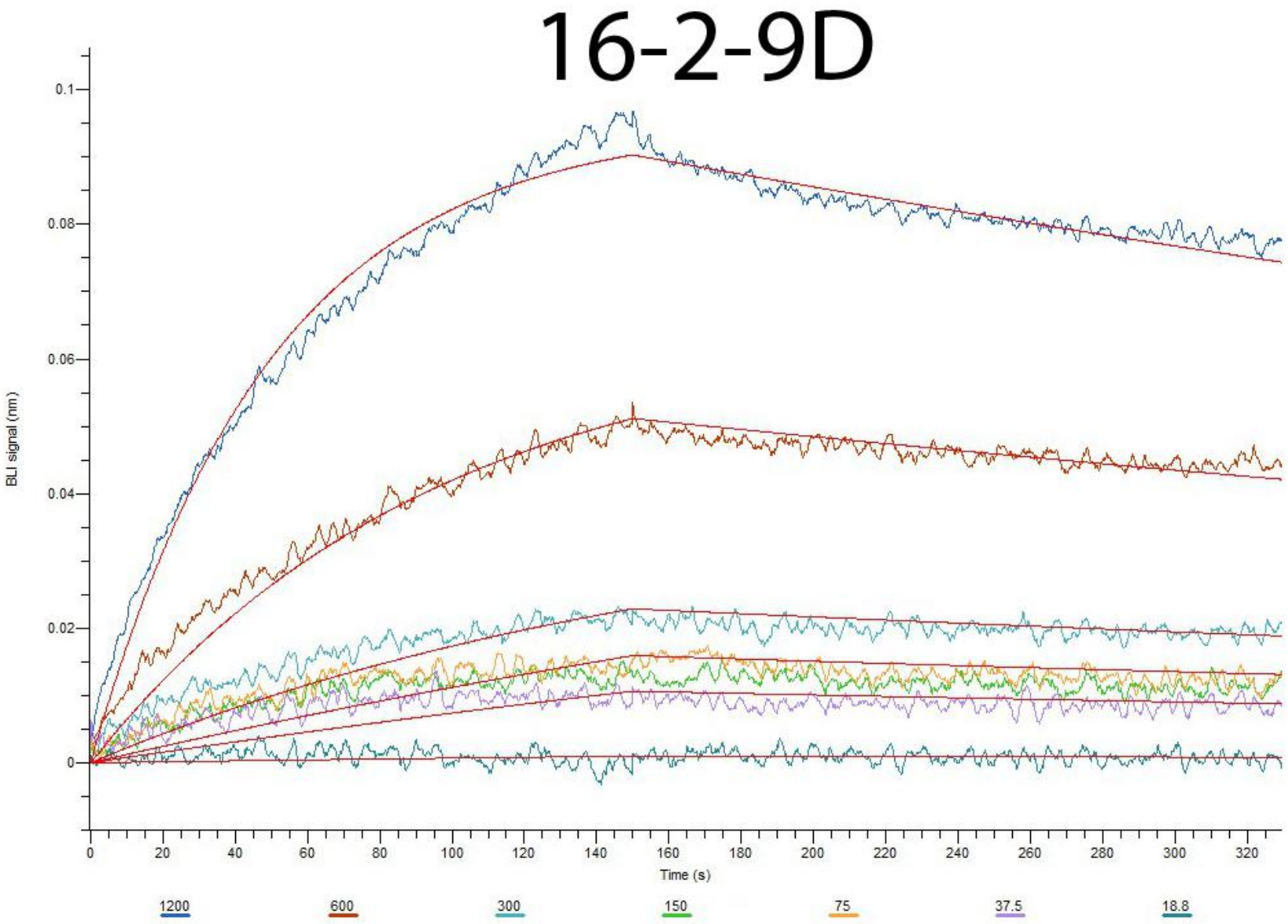
16-2-9D
BLI signal (nm)
0.1
0.08
0.06
0.04
0.02
0
0
20
40
60
80
100
120
140
160
180
200
220
240
260
280
300
320
Time (s)
1200
600
300
150
75
37.5
18.8

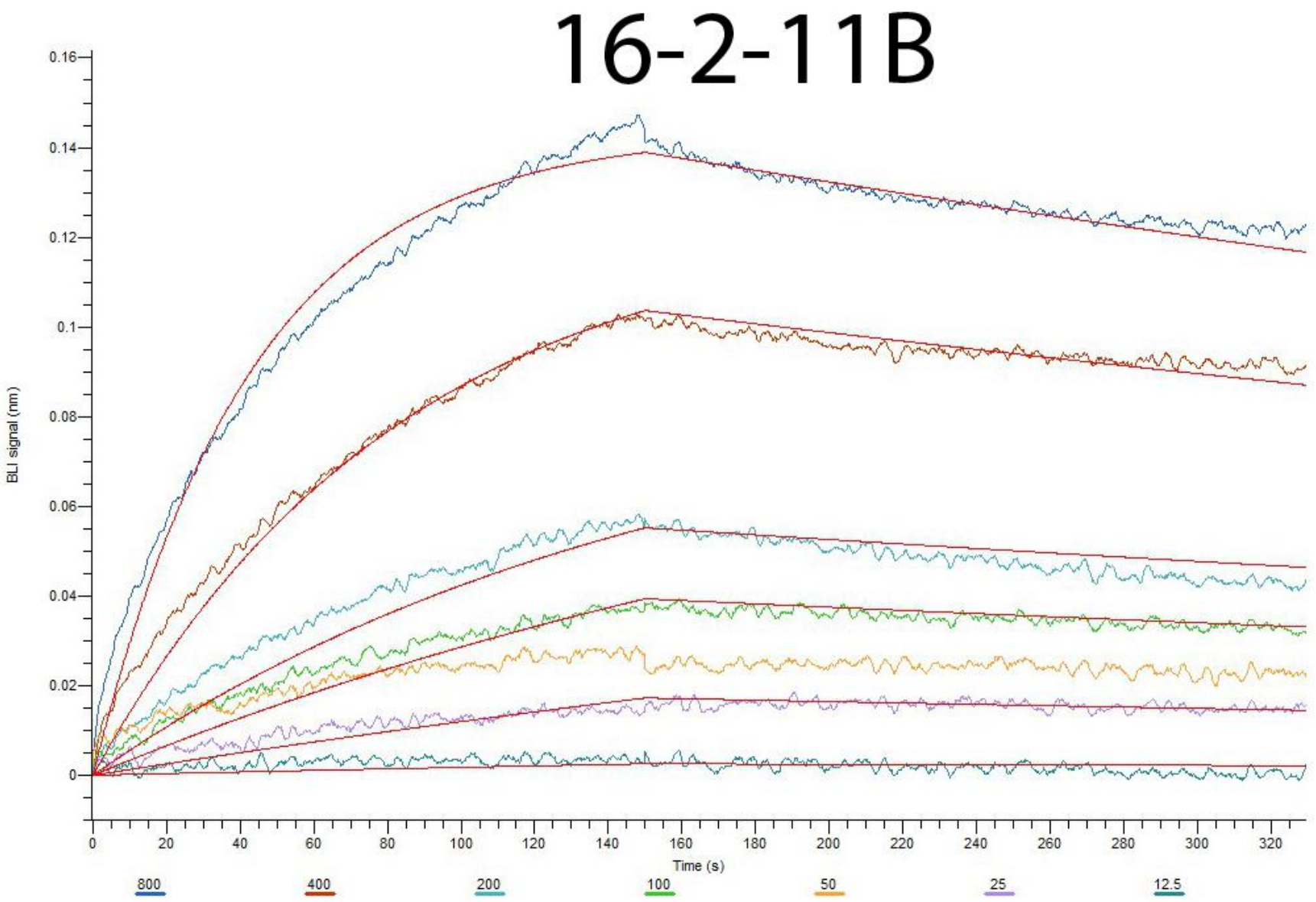
16-2-11B
BLI signal (nm)
0.16
0.14
0.12
0.1
0.08
0.06
0.04
0.02
0
0
20
40
60
80
100
120
140
160
180
200
220
240
260
280
300
320
Time (s)
800
400
200
100
50
25
12.5

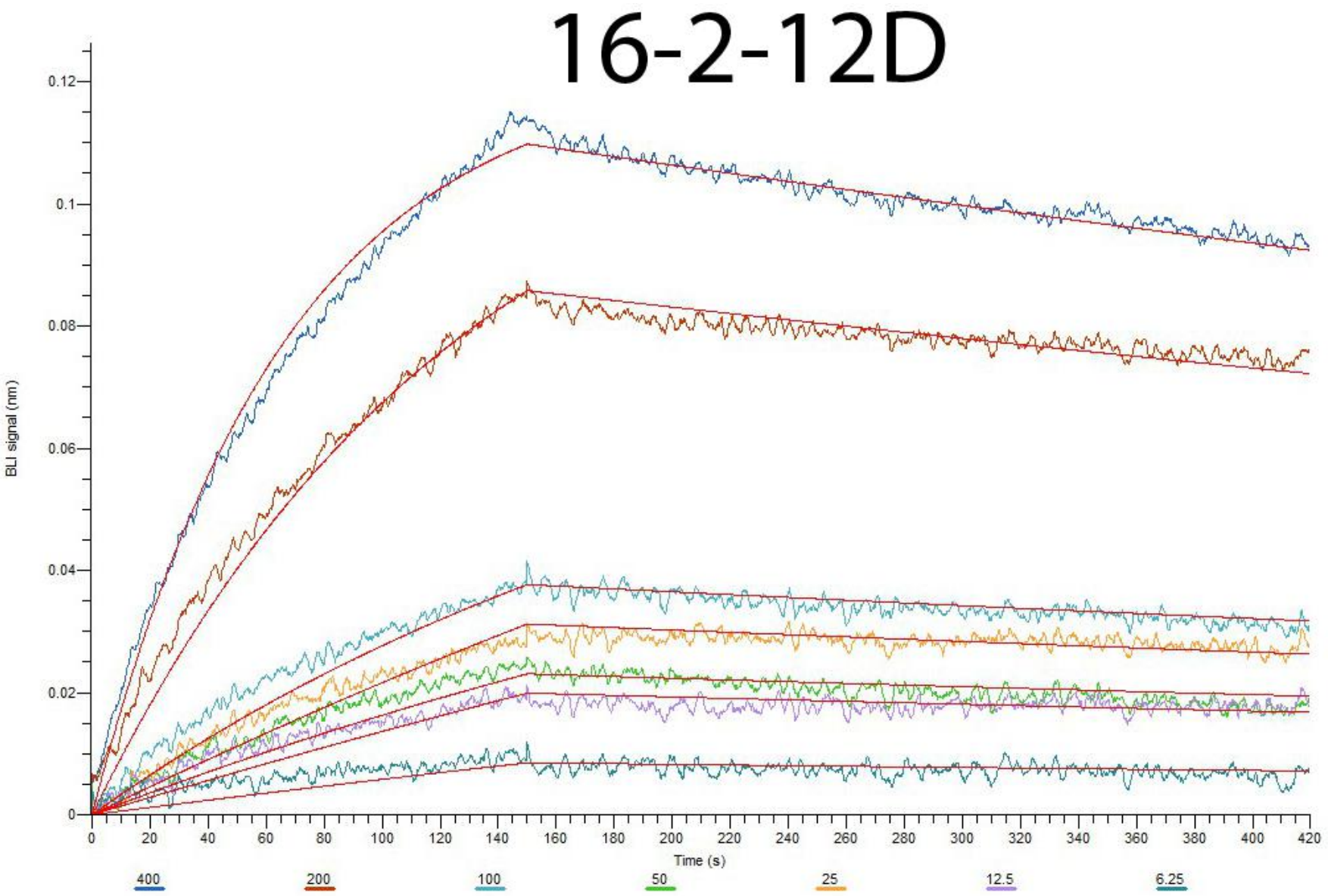
16-2-12D
BLI signal (nm)
0.12
0.1
0.08
0.06
0.04
0.02
0
0
20
40
60
80
100
120
140
160
180
200
220
240
260
280
300
320
340
360
380
400
420
Time (s)
400
200
100
50
25
12.5
6.25

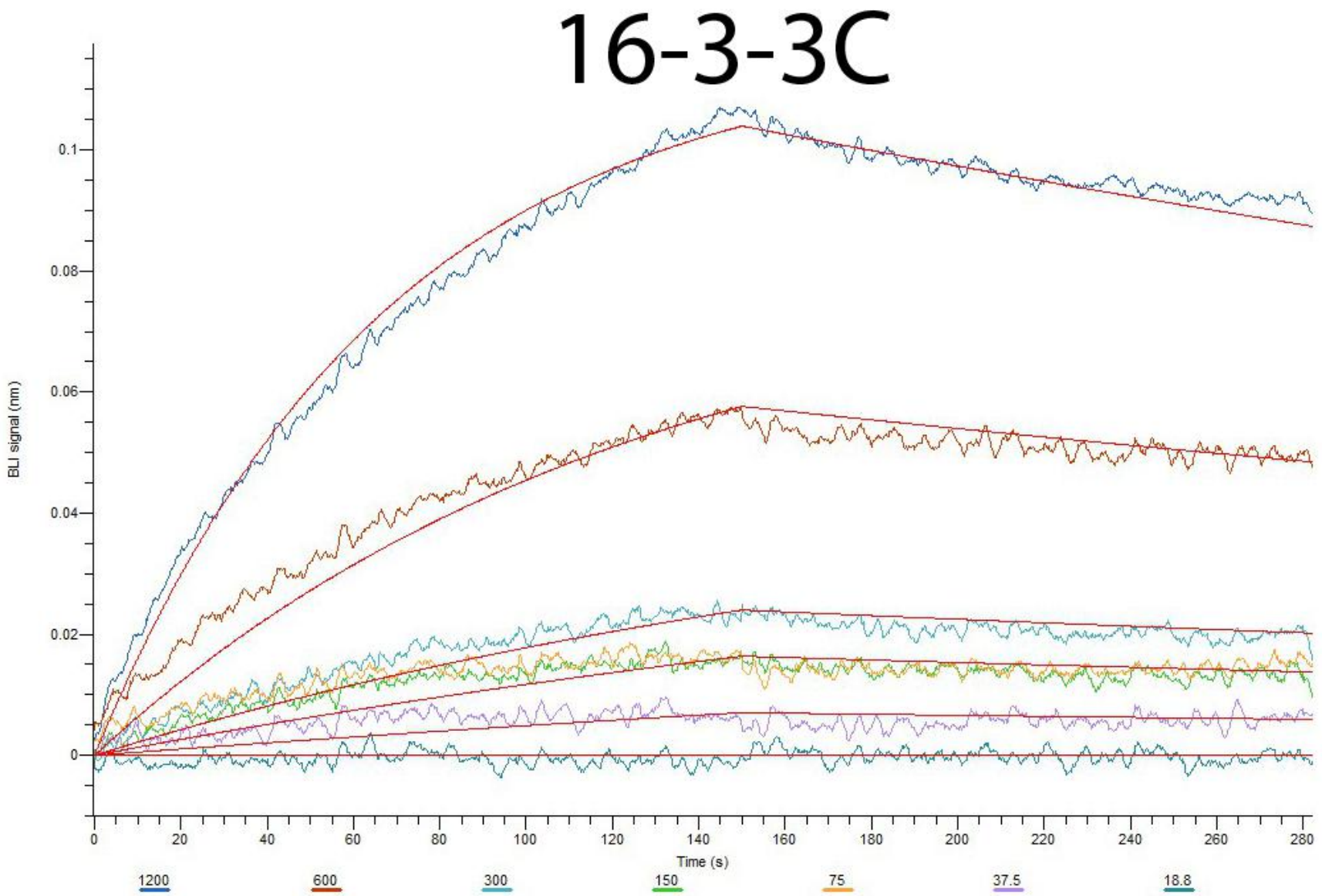
16-3-3C
BLI signal (nm)
0.1
0.08
0.06
0.04
0.02
0
0
20
40
60
80
100
120
140
160
180
200
220
240
260
280
Time (s)
1200
600
300
150
75
37.5
18.8

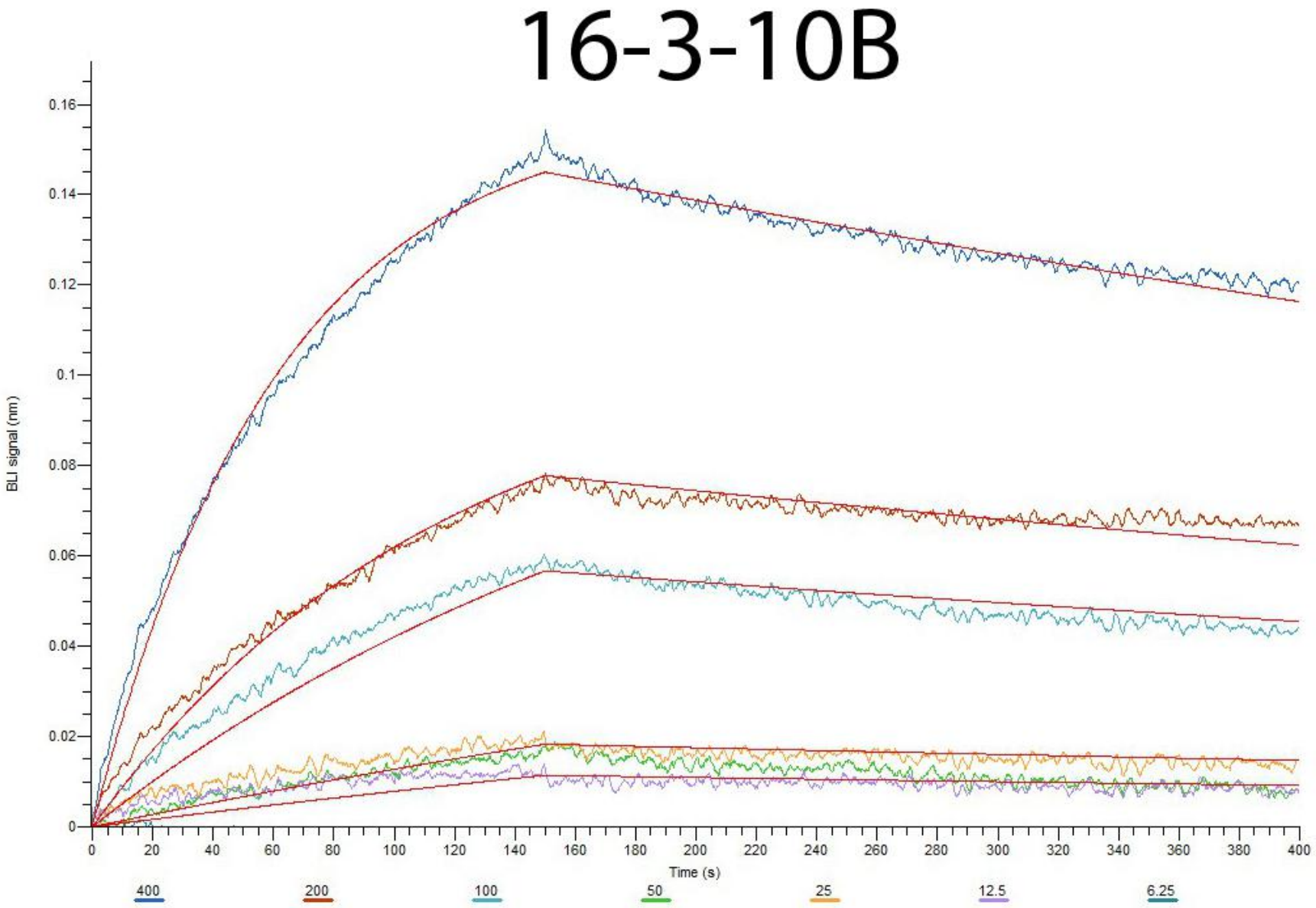
16-3-10B
BLI signal (nm)
0.16
0.14
0.12
0.1
0.08
0.06
0.04
0.02
0
0
20
40
60
80
100
120
140
160
180
200
220
240
260
280
300
320
340
360
380
400
Time (s)
400
200
100
50
25
12.5
6.25

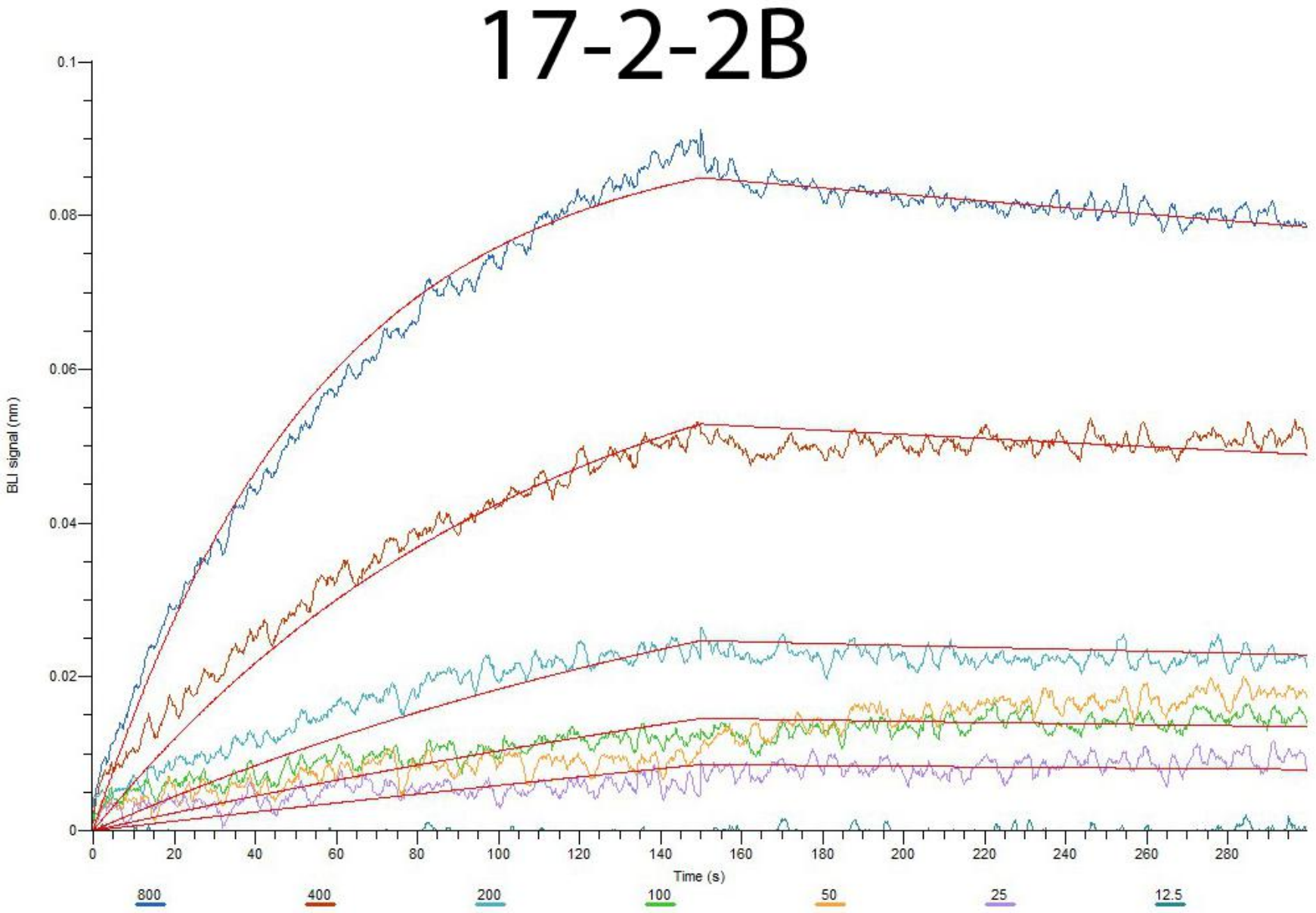
17-2-2B
BLI signal (nm)
0.1
0.08
0.06
0.04
0.02
0
0
20
40
60
80
100
120
140
160
180
200
220
240
260
280
Time (s)
800
400
200
100
50
25
12.5

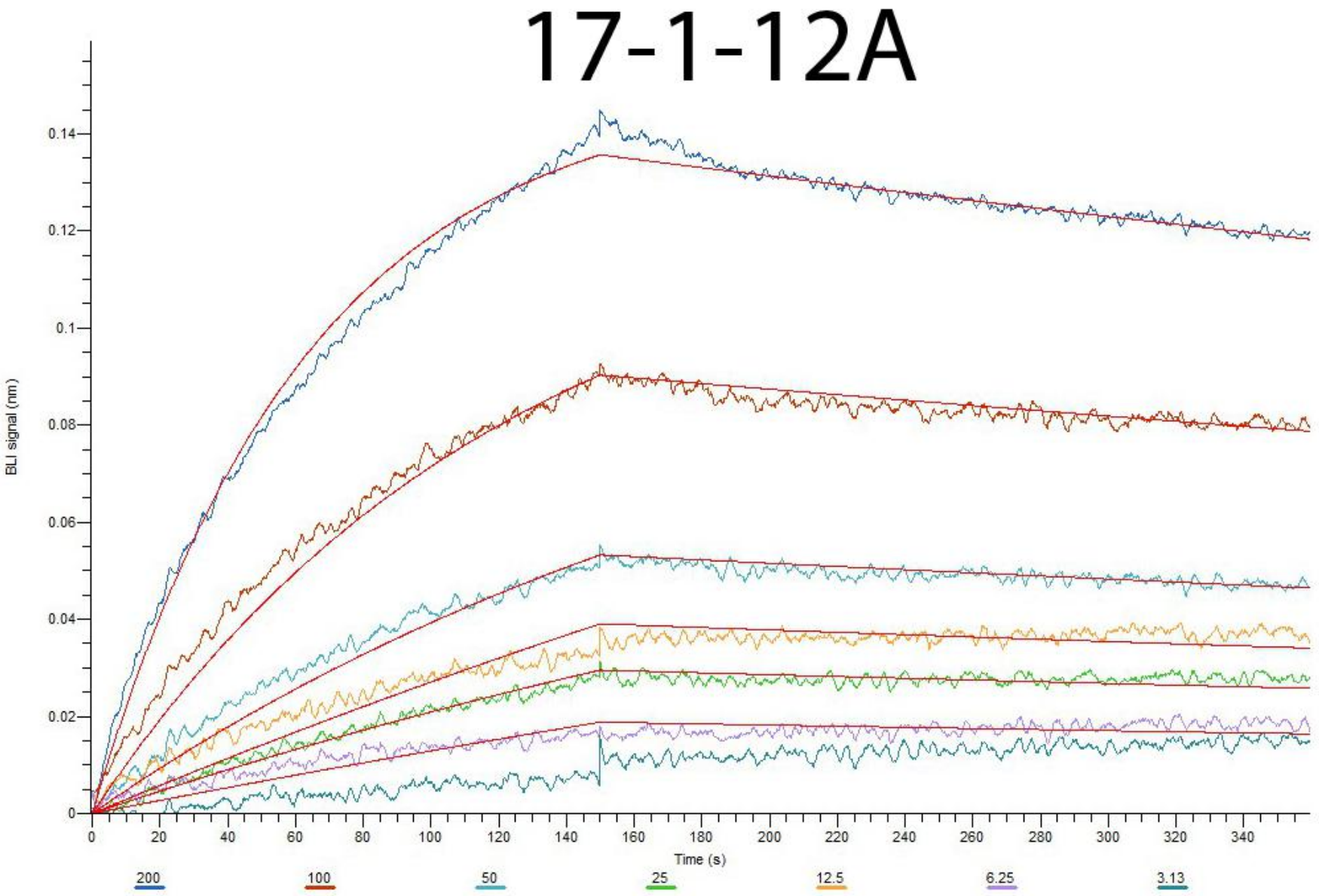
17-1-12A
BLI signal (nm)
0.14
0.12
0.1
0.08
0.06
0.04
0.02
0
0
20
40
60
80
100
120
140
160
180
200
220
240
260
280
300
320
340
Time (s)
200
100
50
25
12.5
6.25
3.13

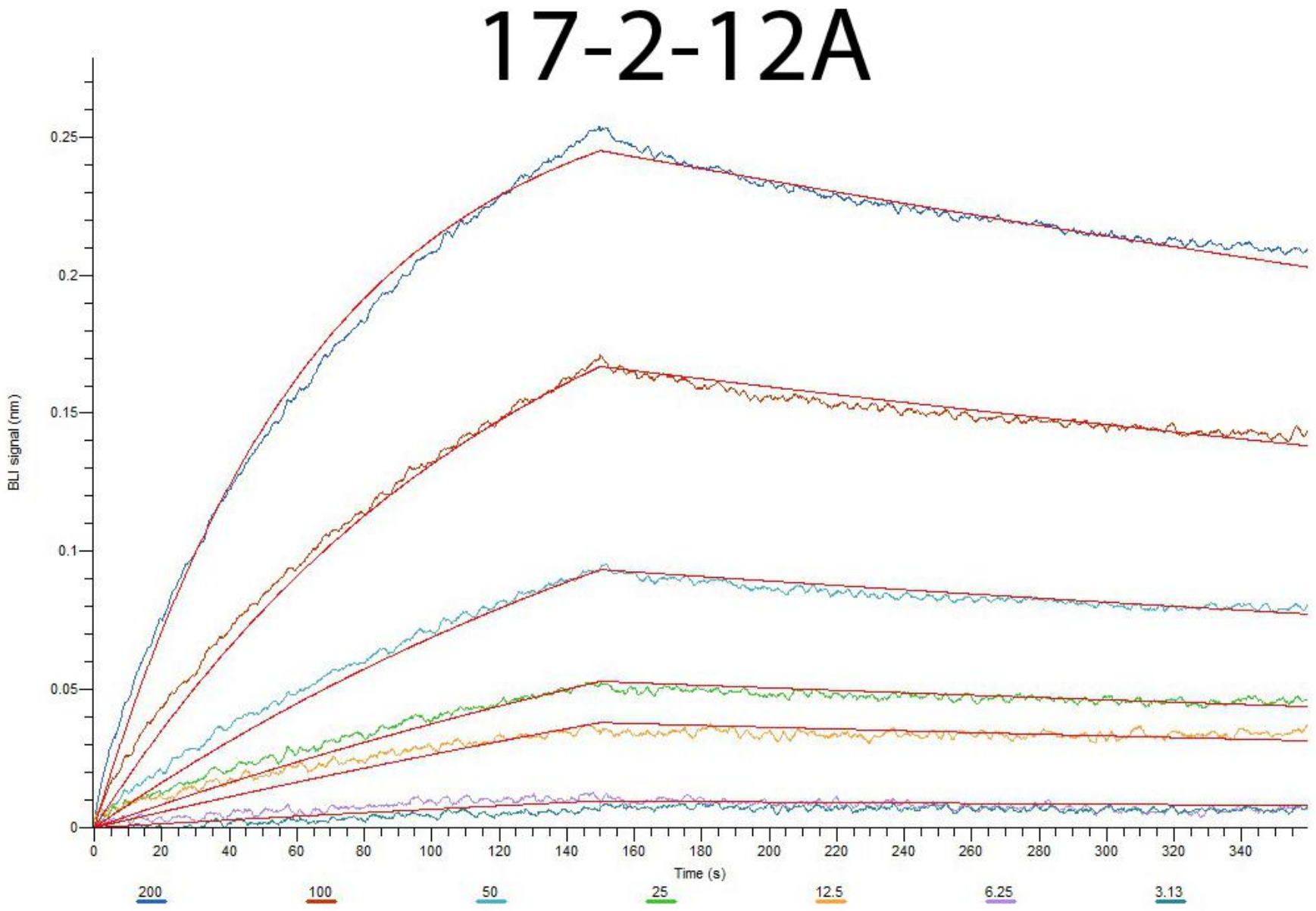
17-2-12A
BLI signal (nm)
0.25
0.2
0.15
0.1
0.05
0
0
20
40
60
80
100
120
140
160
180
200
220
240
260
280
300
320
340
Time (s)
200
100
50
25
12.5
6.25
3.13

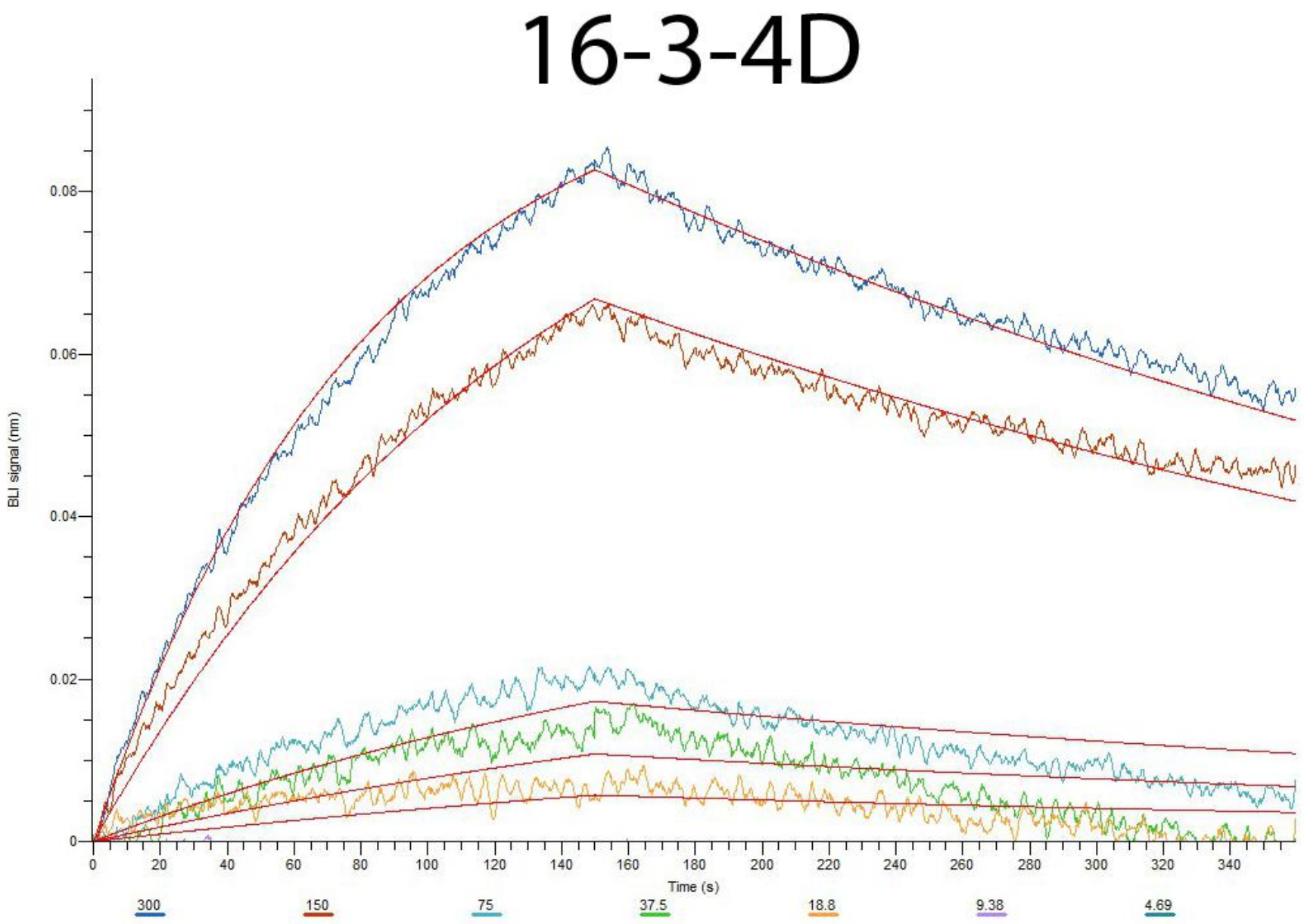
16-3-4D
BLI signal (nm)
0.08
0.06
0.04
0.02
0
0
20
40
60
80
100
120
140
160
180
200
220
240
260
280
300
320
340
Time (s)
300
150
75
37.5
18.8
9.38
4.69

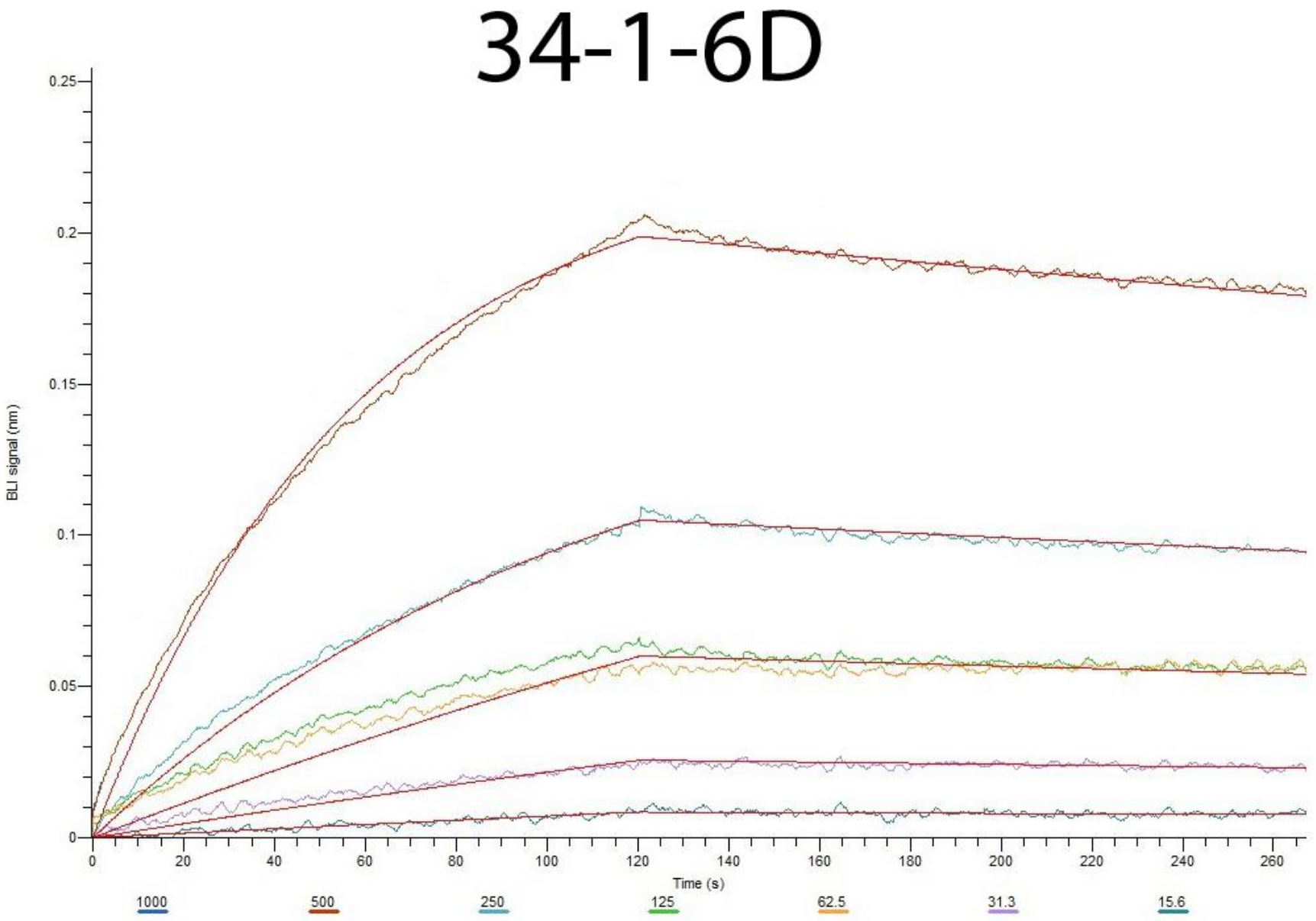
34-1-6D
BLI signal (nm)
0.25
0.2
0.15
0.1
0.05
0
0
20
40
60
80
100
120
140
160
180
200
220
240
260
Time (s)
1000
500
250
125
62.5
31.3
15.6

Appendix figure 2. Below are binding curves of Fabs with EV71 empty particles measured by bio-layer interferometry on Octet RED96e. Different colors of the curves stand for different concentration (nm) of the Fabs used. The red curves indicate the global fitting models used. Some bad curves were not used for the model fitting.

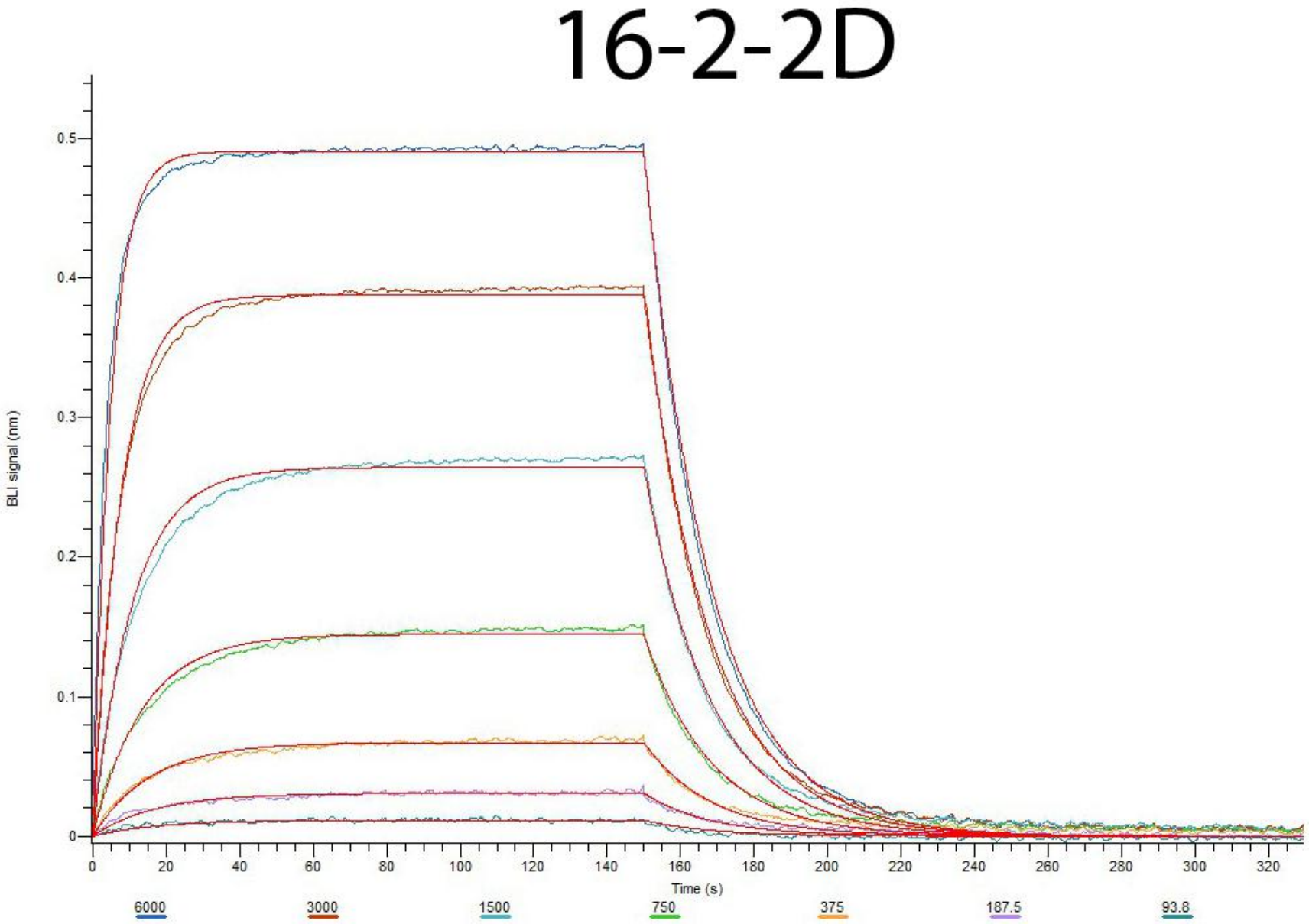
16-2-2D
BLI signal (nm)
0.5
0.4
0.3
0.2
0.1
0
0
20
40
60
80
100
120
140
160
180
200
220
240
260
280
300
320
Time (s)
6000
3000
1500
750
375
187.5
93.8

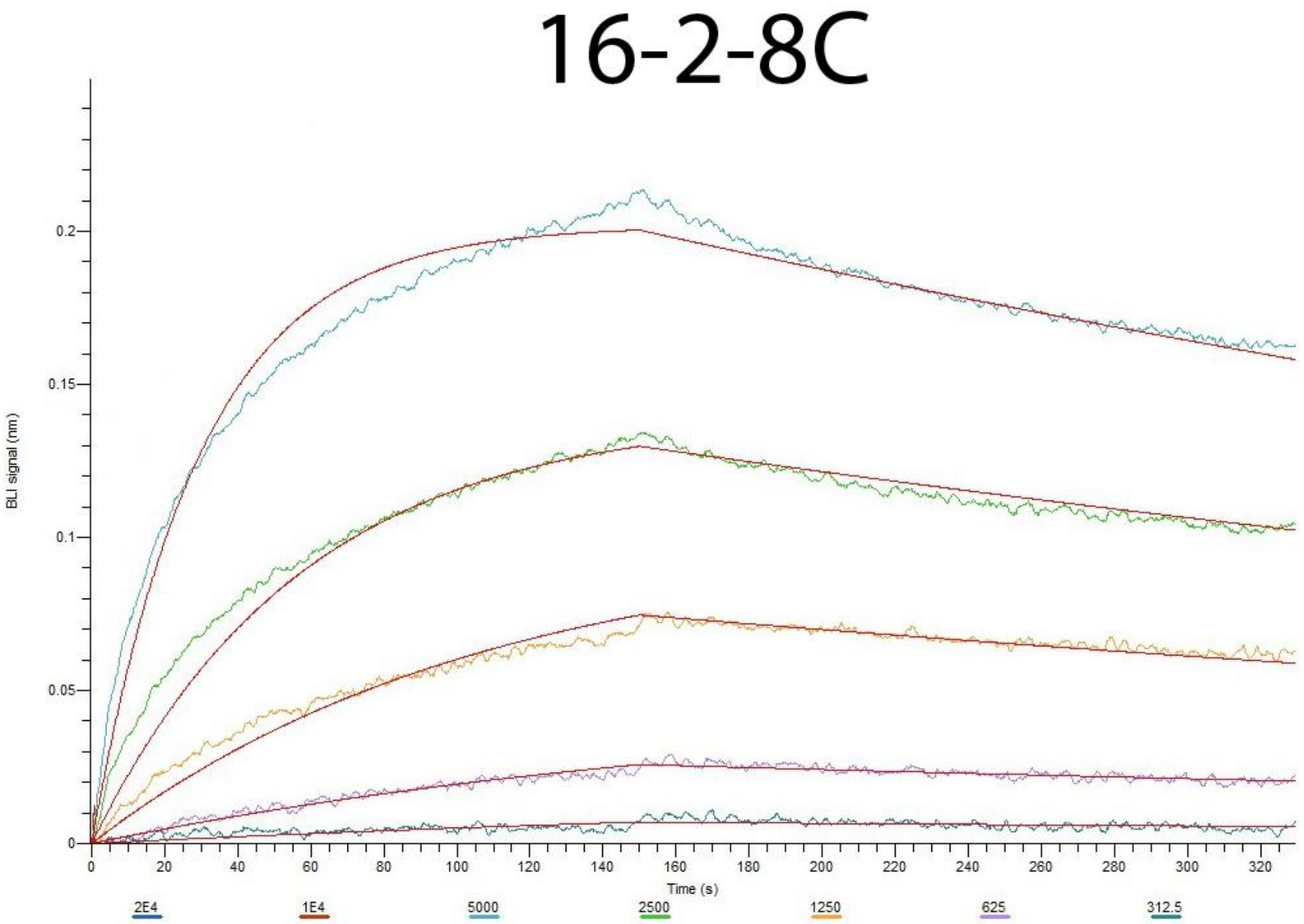
16-2-8C
BLI signal (nm)
0
0.05
0.1
0.15
0.2
0
20
40
60
80
100
120
140
160
180
200
220
240
260
280
300
320
Time (s)
2E4
1E4
5000
2500
1250
625
312.5

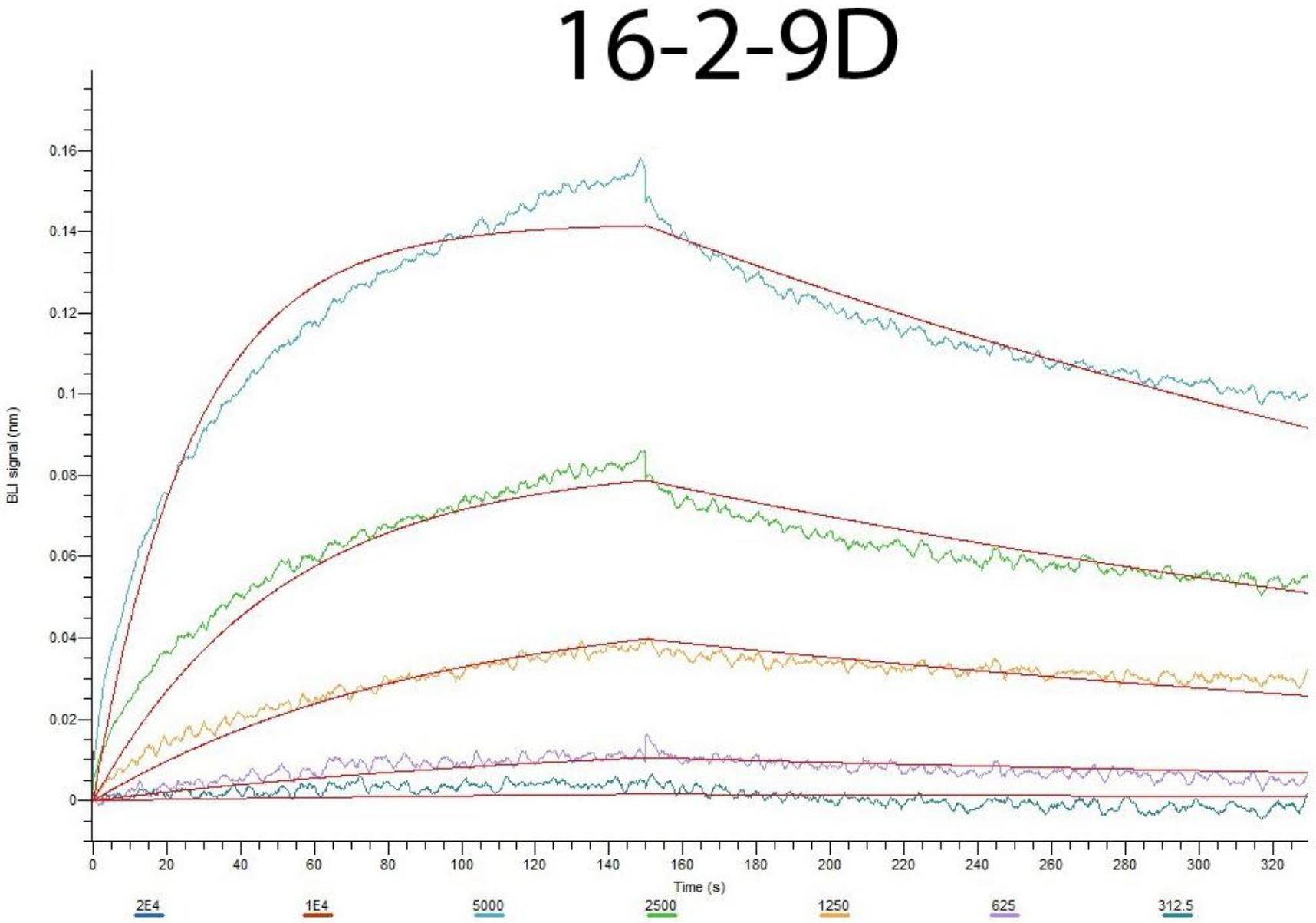
16-2-9D
BLI signal (nm)
0.16
0.14
0.12
0.1
0.08
0.06
0.04
0.02
0
0
20
40
60
80
100
120
140
160
180
200
220
240
260
280
300
320
Time (s)
2E4
1E4
5000
2500
1250
625
312.5

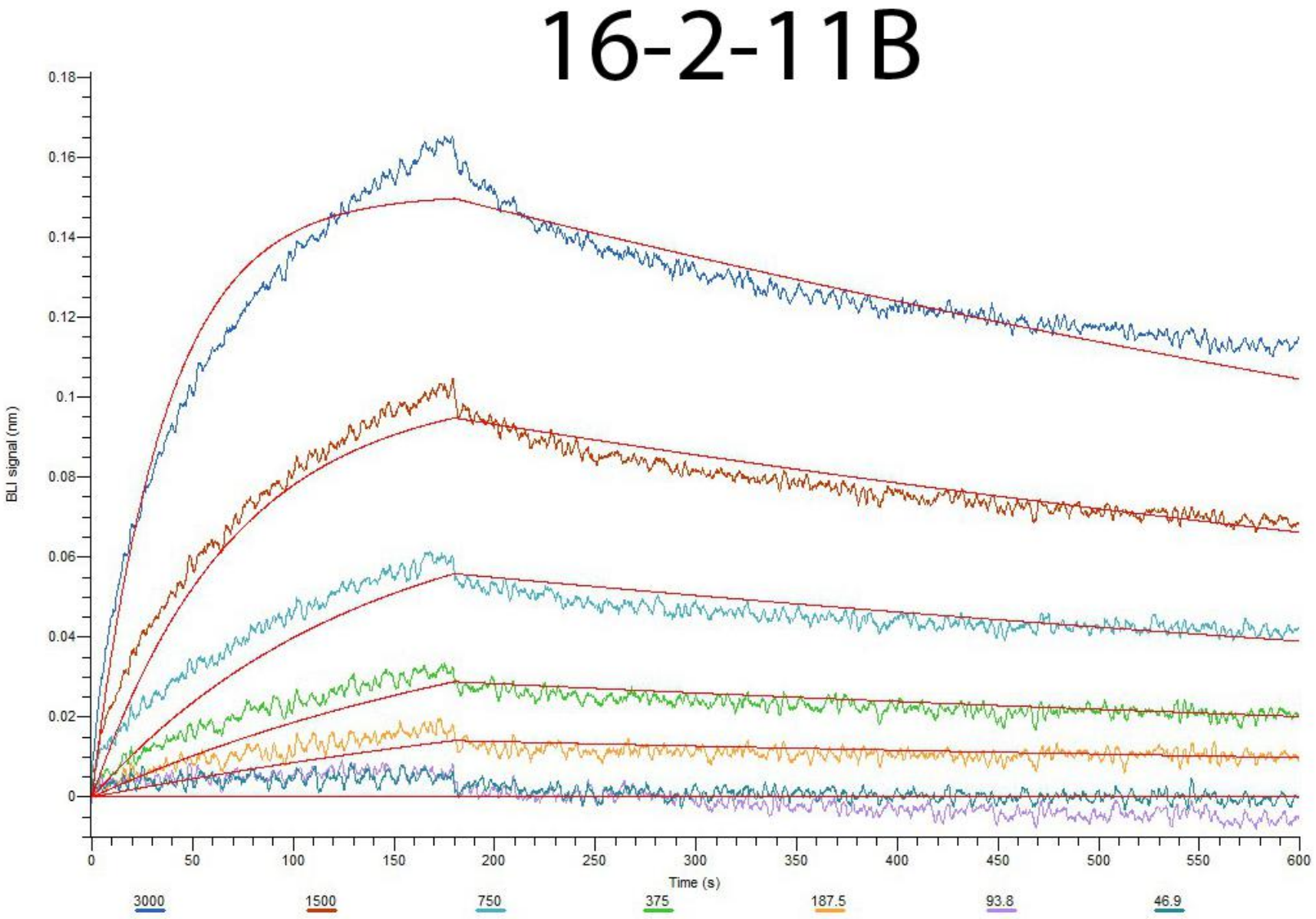
16-2-11B
BLI signal (nm)
0.18
0.16
0.14
0.12
0.1
0.08
0.06
0.04
0.02
0
0
50
100
150
200
250
300
350
400
450
500
550
600
Time (s)
3000
1500
750
375
187.5
93.8
46.9

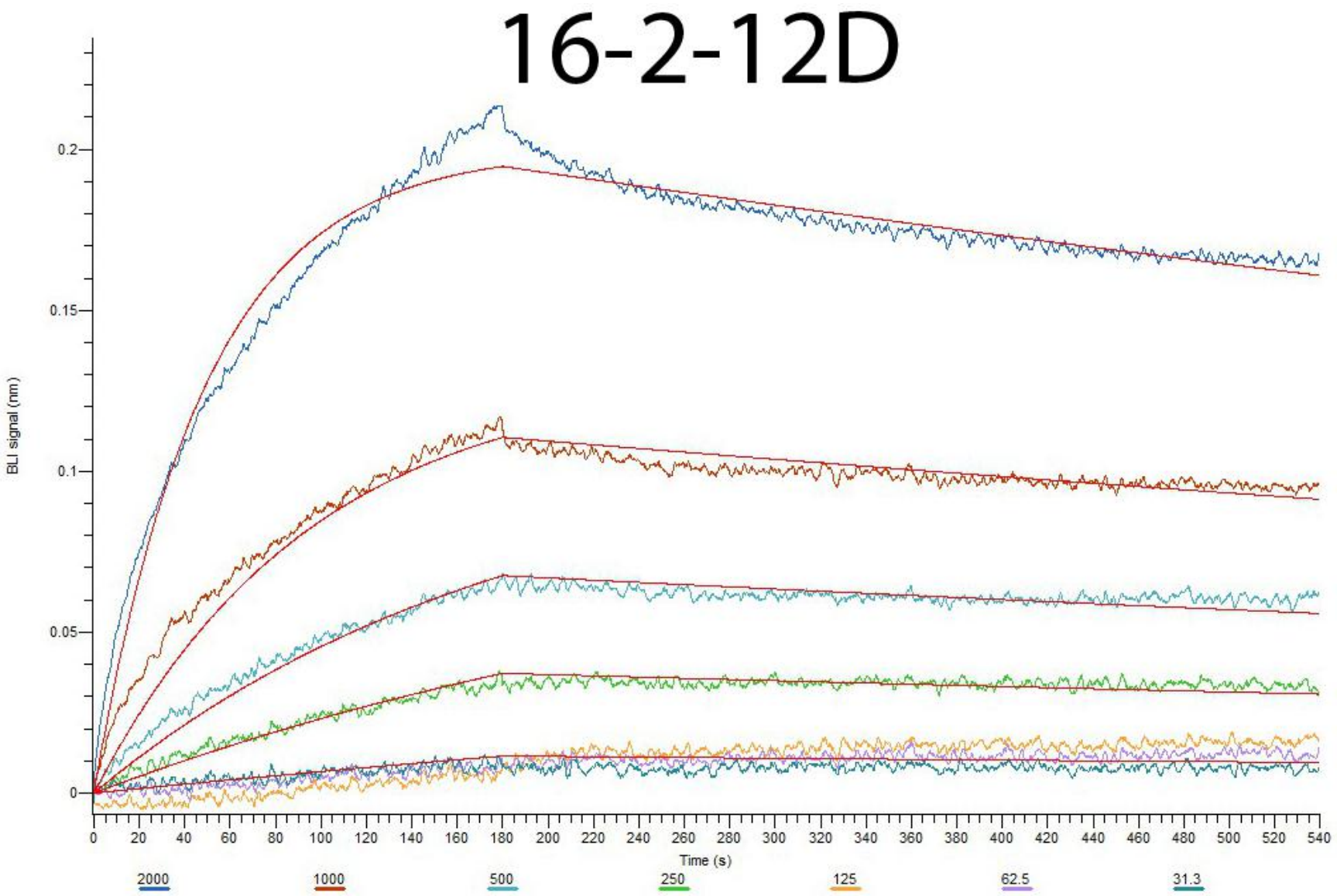
16-2-12D
BLI signal (nm)
0.2
0.15
0.1
0.05
0
0 20 40 60 80 100 120 140 160 180 200 220 240 260 280 300 320 340 360 380 400 420 440 460 480 500 520 540
Time (s)
2000
1000
500
250
125
62.5
31.3

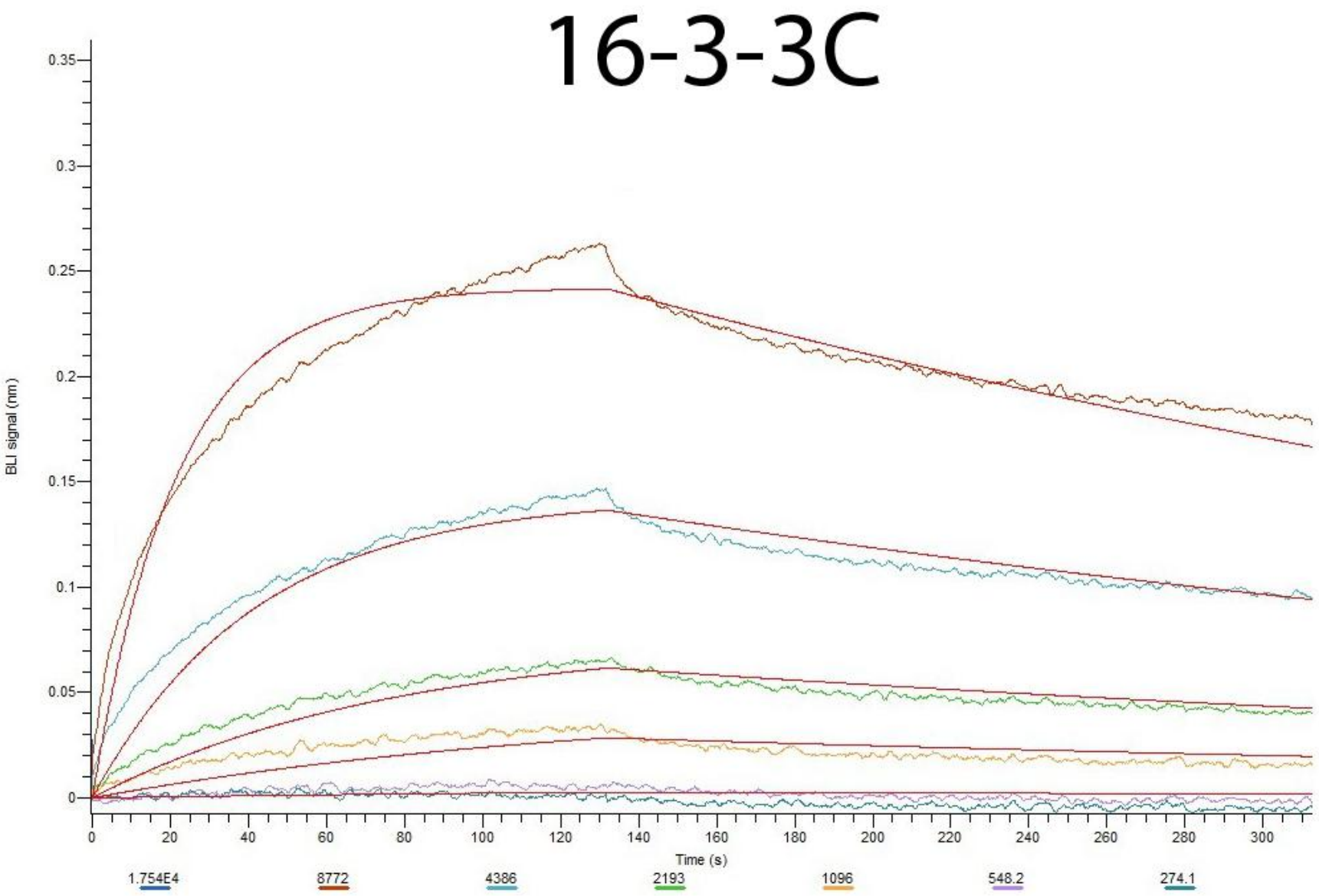
16-3-3C
BLI signal (nm)
0.35
0.3
0.25
0.2
0.15
0.1
0.05
0
0
20
40
60
80
100
120
140
160
180
200
220
240
260
280
300
Time (s)
1.754E4
8772
4386
2193
1096
548.2
274.1

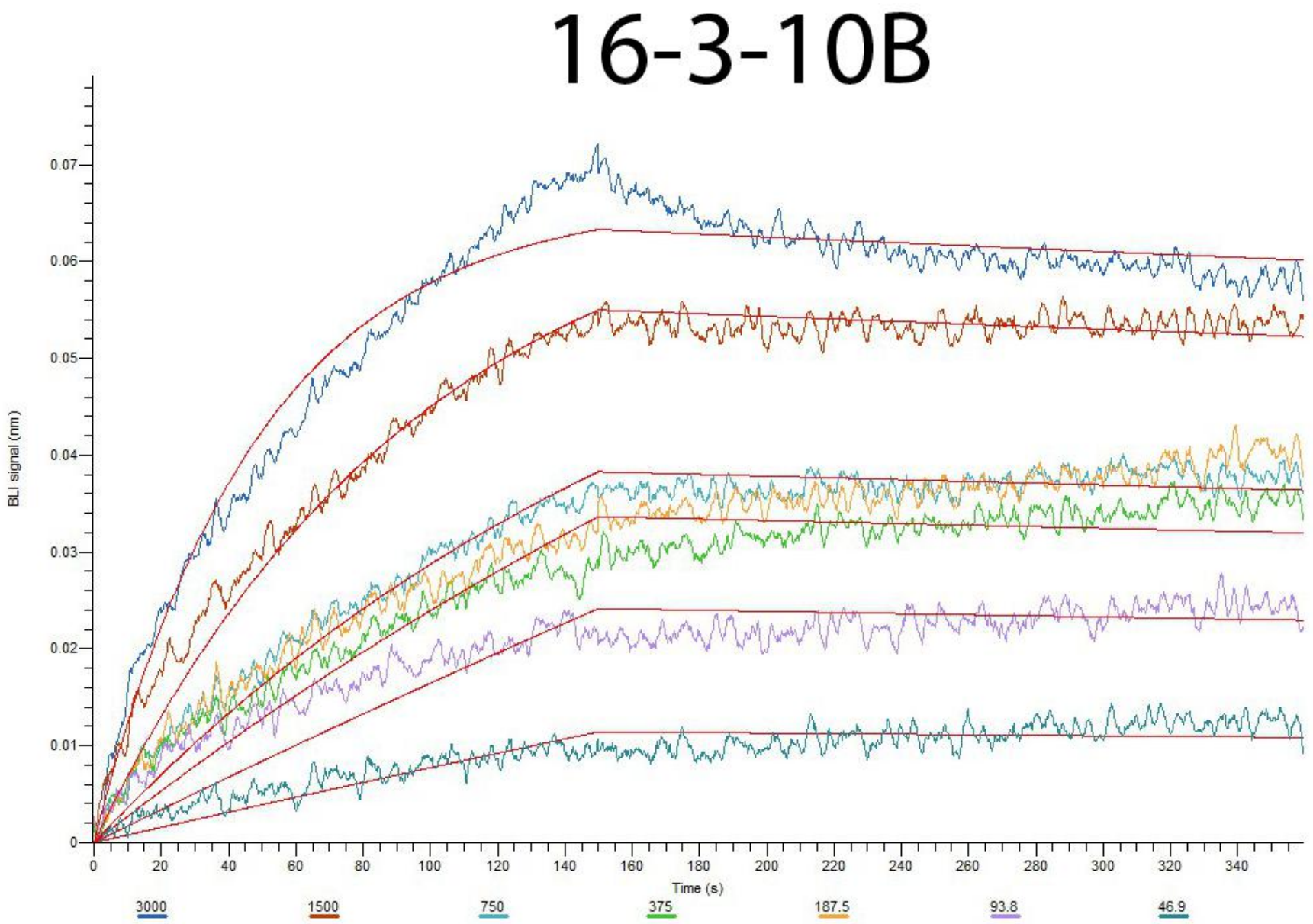
16-3-10B
BLI signal (nm)
0
0.01
0.02
0.03
0.04
0.05
0.06
0.07
0
20
40
60
80
100
120
140
160
180
200
220
240
260
280
300
320
340
Time (s)
3000
1500
750
375
187.5
93.8
46.9

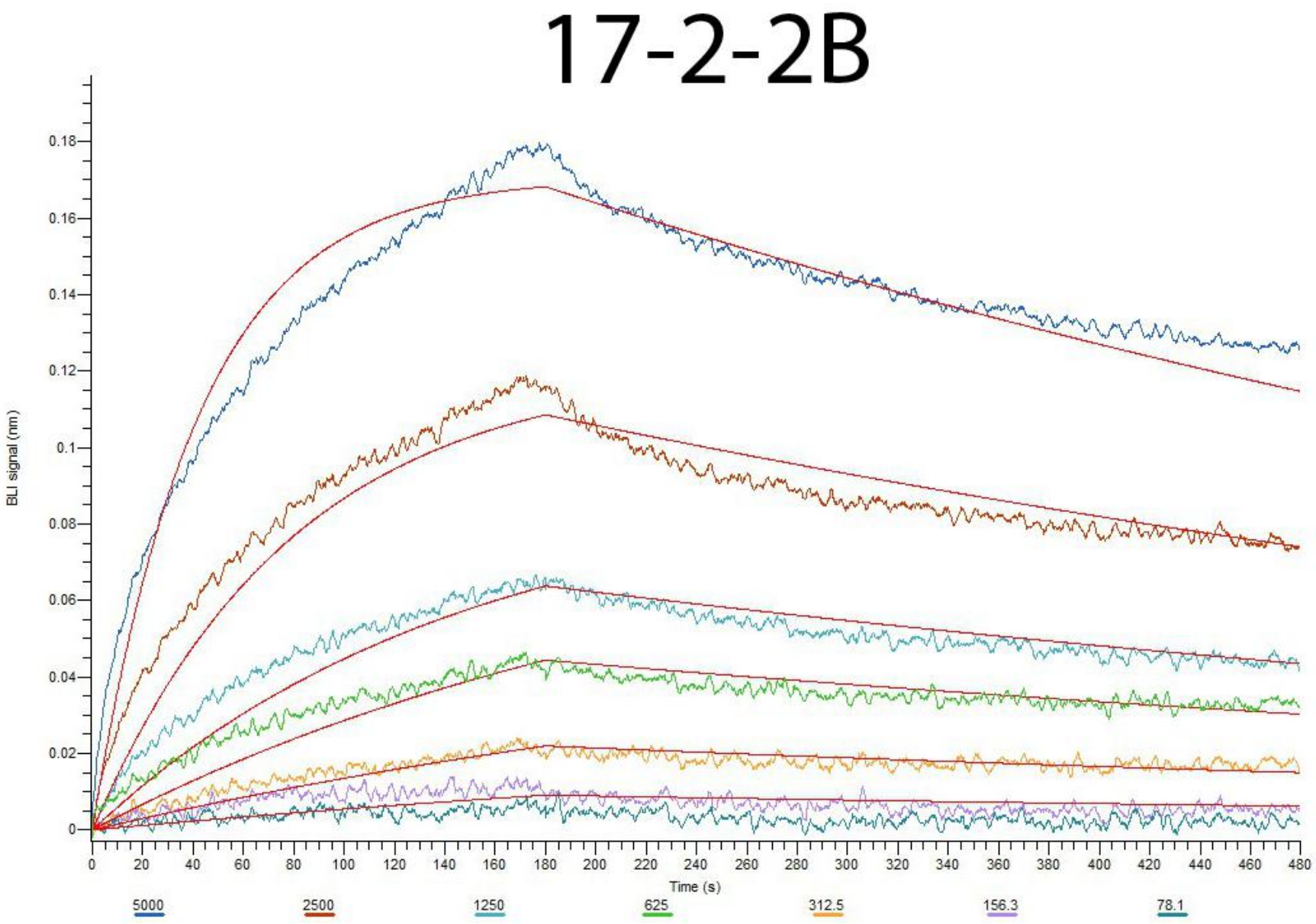
17-2-2B
BLI signal (nm)
0.18
0.16
0.14
0.12
0.1
0.08
0.06
0.04
0.02
0
0 20 40 60 80 100 120 140 160 180 200 220 240 260 280 300 320 340 360 380 400 420 440 460 480
Time (s)
5000
2500
1250
625
312.5
156.3
78.1

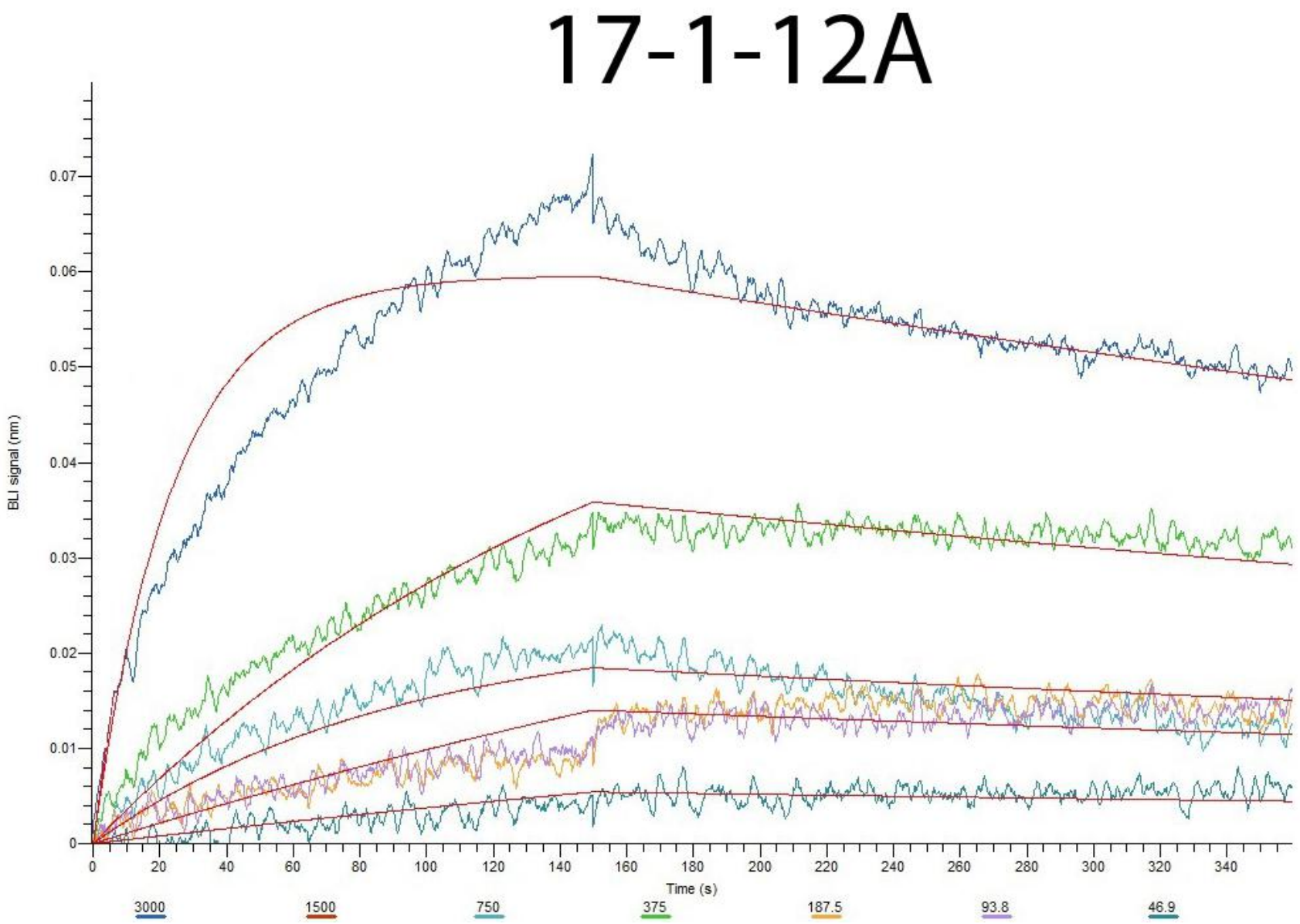
17-1-12A
BLI signal (nm)
0
0.01
0.02
0.03
0.04
0.05
0.06
0.07
0
20
40
60
80
100
120
140
160
180
200
220
240
260
280
300
320
340
Time (s)
3000
1500
750
375
187.5
93.8
46.9

17-2-12A

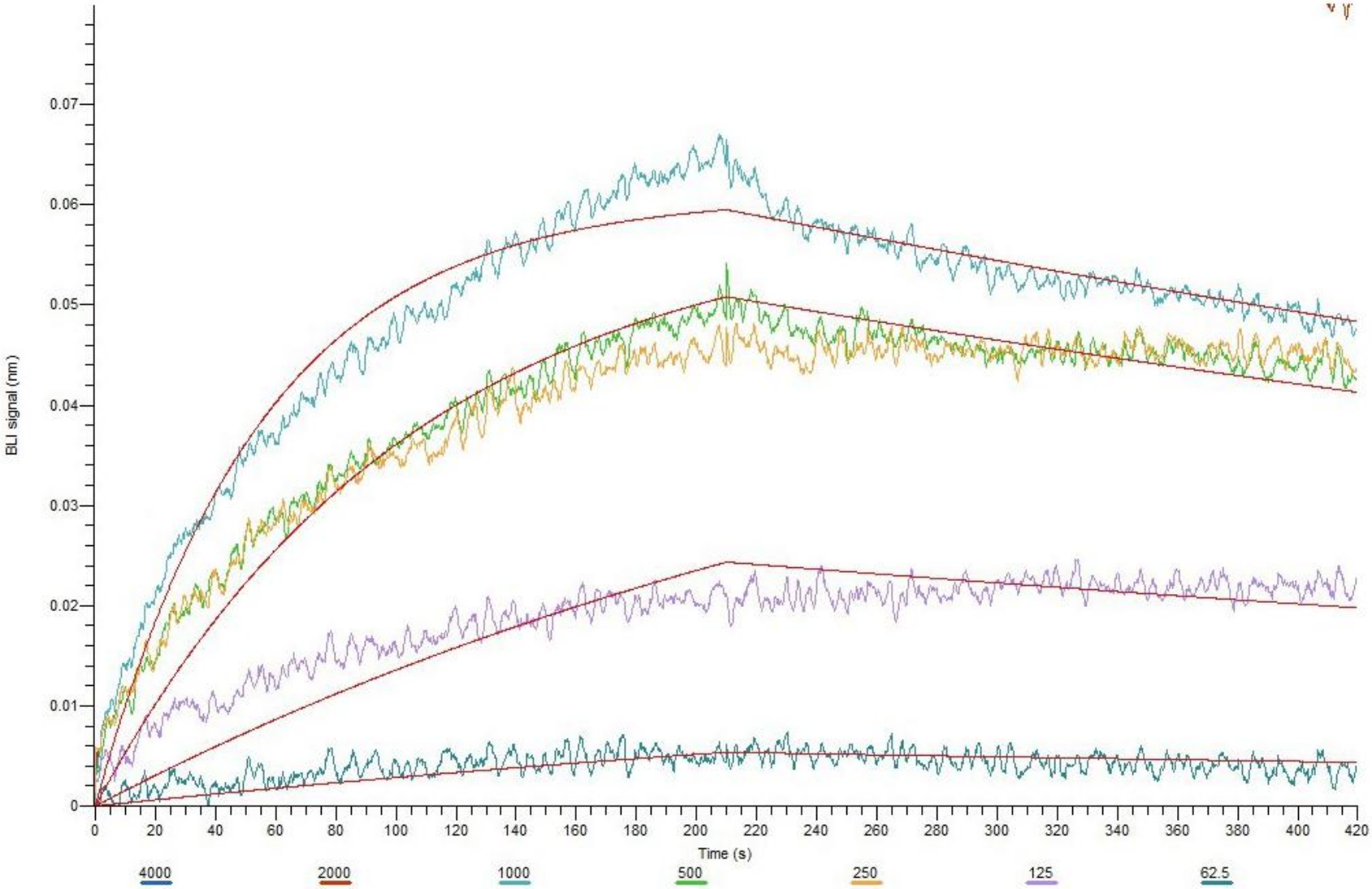
BLI signal (nm)
0
0.01
0.02
0.03
0.04
0.05
0.06
0.07
0
20
40
60
80
100
120
140
160
180
200
220
240
260
280
300
320
340
360
380
400
420
Time (s)
4000
2000
1000
500
250
125
62.5

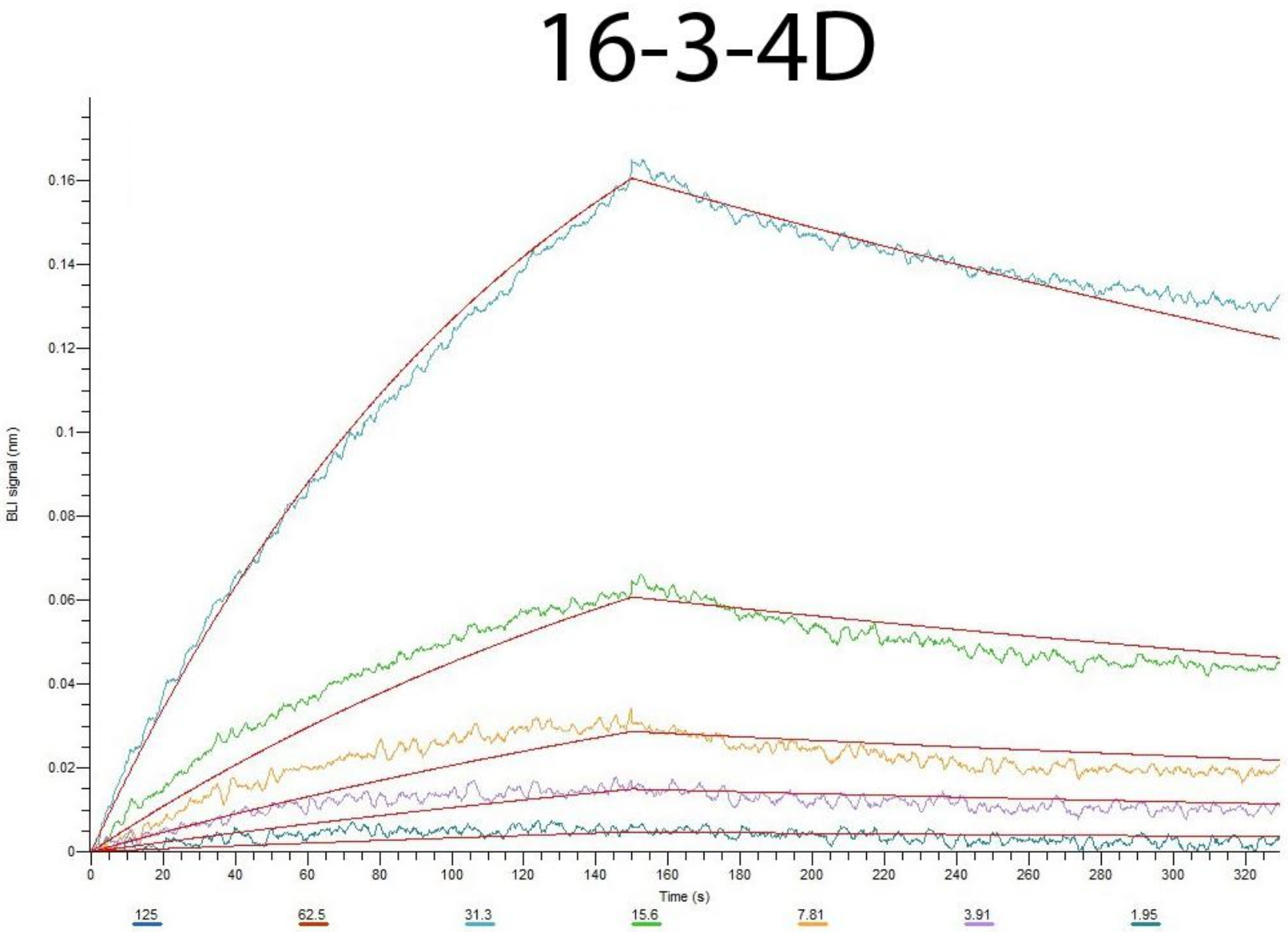
16-3-4D
BLI signal (nm)
0.16
0.14
0.12
0.1
0.08
0.06
0.04
0.02
0
0
20
40
60
80
100
120
140
160
180
200
220
240
260
280
300
320
Time (s)
125
62.5
31.3
15.6
7.81
3.91
1.95

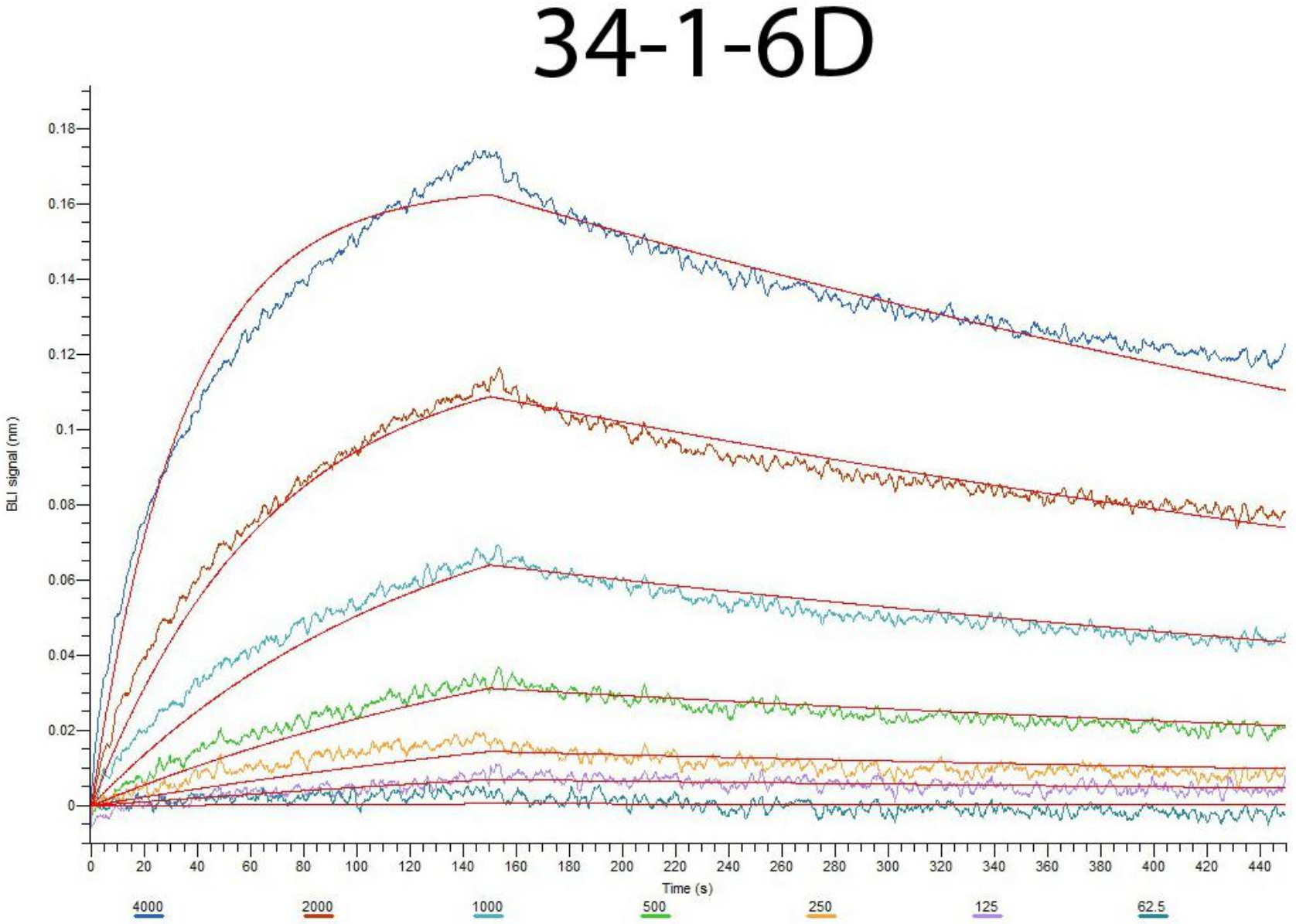
34-1-6D
BLI signal (nm)
0.18
0.16
0.14
0.12
0.1
0.08
0.06
0.04
0.02
0
0 20 40 60 80 100 120 140 160 180 200 220 240 260 280 300 320 340 360 380 400 420 440
Time (s)
4000
2000
1000
500
250
125
62.5

Reference

1 Robinson, C., Doane, F. W. & Rhodes, A. Report of an outbreak of febrile illness with pharyngeal lesions and exanthem: Toronto, summer 1957—isolation of group A coxsackie virus. *Canadian Medical Association Journal* 79, 615 (1958).

2 Huang, J. *et al.* Epidemiology of recurrent hand, foot and mouth disease, China, 2008–2015. *Emerging infectious diseases* 24, 432 (2018).

3 Li, L., Yin, H., An, Z. & Feng, Z. Considerations for developing an immunization strategy with enterovirus 71 vaccine. *Vaccine* 33, 1107-1112 (2015).

4 Starr, M. & Frydenberg, A. Hand, foot and mouth disease. *Australian family physician* 32, 594 (2003).

5 Ooi, M. H., Wong, S. C., Lewthwaite, P., Cardosa, M. J. & Solomon, T. Clinical features, diagnosis, and management of enterovirus 71. *The Lancet Neurology* 9, 1097-1105 (2010).

6 Kaminska, K., Martinetti, G., Lucchini, R., Kaya, G. & Mainetti, C. Coxsackievirus A6 and Hand, Foot and Mouth Disease: Three Case Reports of familialchild-to-immunocompetent adult transmission and a literature review. *Case reports in dermatology* 5, 203-209 (2013).

7 Xing, W. *et al.* Hand, foot, and mouth disease in China, 2008–12: an epidemiological study. *The Lancet infectious diseases* 14, 308-318 (2014).

8 Huang, C.-C. *et al.* Neurologic complications in children with enterovirus 71 infection. *New England Journal of Medicine* 341, 936-942 (1999).

9 Sun, L. *et al.* Evaluating the transmission routes of hand, foot, and mouth disease in Guangdong, China. *American journal of infection control* 44, e13-e14 (2016).

10 Onozuka, D. & Hashizume, M. The influence of temperature and humidity on the incidence of hand, foot, and mouth disease in Japan. *Science of the Total Environment* 410, 119-125 (2011).

11 Wu, J.-S. *et al.* Patterns of polymorphism and divergence in the VP1 gene of enterovirus 71 circulating in the Asia-Pacific region between 1994 and 2013. *Journal of virological methods* 193, 713-728 (2013).

12 Chan, L. *et al.* Deaths of children during an outbreak of hand, foot, and mouth disease in Sarawak, Malaysia: clinical and pathological characteristics of the disease. *Clinical infectious diseases* 31, 678-683 (2000).

13 Van, P. T. *et al.* Epidemiologic and virologic investigation of hand, foot, and mouth disease, southern Vietnam, 2005. *Emerging infectious diseases* 13, 1733-1741 (2007).

14 Ho, M. *et al.* An epidemic of enterovirus 71 infection in Taiwan. *New England Journal of Medicine* 341, 929-935 (1999).

15 Shah, V., Chong, C., Chan, K., Ng, W. & Ling, A. Clinical characteristics of an outbreak of hand, foot and mouth disease in Singapore. *Annals of the Academy of Medicine, Singapore* 32, 381-387 (2003).

16 Tan, X. *et al.* The persistent circulation of enterovirus 71 in People's Republic of China: causing emerging nationwide epidemics since 2008. *PloS one* 6, e25662 (2011).

17 WHO. *Hand, Foot and Mouth Disease Situation Update*, <https://www.who.int/westernpacific/emergencies/surveillance/archives/hand-foot-and-mouth-disease>

18 Lei, X., Cui, S., Zhao, Z. & Wang, J. Etiology, pathogenesis, antivirals and vaccines of hand, foot, and mouth disease. *National Science Review* 2, 268-284 (2015).

19 Repass, G. L., Palmer, W. C. & Stancampiano, F. F. Hand, foot, and mouth disease: identifying and managing an acute viral syndrome. *Cleve Clin J Med* 81, 537-543 (2014).

20 Liu, S. L. *et al.* Comparative epidemiology and virology of fatal and nonfatal cases of hand, foot and mouth disease in mainland China from 2008 to 2014. *Reviews in medical virology* 25, 115-128 (2015).

21 Li, Y. *et al.* Emerging enteroviruses causing hand, foot and mouth disease, China, 2010–2016. *Emerging infectious diseases* 24, 1902 (2018).

22 Xu, M. *et al.* Genotypes of the enterovirus causing hand foot and mouth disease in Shanghai, China, 2012-2013. *PloS one* 10, e0138514 (2015).

23 Sarma, N. Hand, foot, and mouth disease: current scenario and Indian perspective. *Indian Journal of Dermatology, Venereology, and Leprology* 79, 165 (2013).

24 Gopalkrishna, V., Patil, P. R., Patil, G. P. & Chitambar, S. D. Circulation of multiple enterovirus serotypes causing hand, foot and mouth disease in India. *Journal of medical microbiology* 61, 420-425 (2012).

25 Klein, M. & Chong, P. Is a multivalent hand, foot, and mouth disease vaccine feasible? *Human vaccines & immunotherapeutics* 11, 2688-2704 (2015).

26 Zhang, T. *et al.* Epidemics and frequent recombination within species in outbreaks of human enterovirus B-associated hand, foot and mouth disease in Shandong China in 2010 and 2011. *PloS one* 8, e67157 (2013).

27 Tapparel, C., Siegrist, F., Petty, T. J. & Kaiser, L. Picornavirus and enterovirus diversity with associated human diseases. *Infection, Genetics and Evolution* 14, 282-293 (2013).

28 Puenpa, J. *et al.* Prevalence and characterization of enterovirus infections among pediatric patients with hand foot mouth disease, herpangina and influenza like illness in Thailand, 2012. *PloS one* 9, e98888 (2014).

29 Zell, R. *et al.* ICTV Virus Taxonomy Profile: Picornaviridae. *The Journal of general virology* 98, 2421-2422, doi:10.1099/jgv.0.000911 (2017).

30 Yin-Murphy, M. & Almond, J. W. Picornaviruses. *Medical Microbiology. 4th edition* (University of Texas Medical Branch at Galveston, 1996).

31 Wang, X. *et al.* A sensor-adaptor mechanism for enterovirus uncoating from structures of EV71. *Nature structural & molecular biology* 19, 424 (2012).

32 Plevka, P., Perera, R., Cardosa, J., Kuhn, R. J. & Rossmann, M. G. Crystal structure of human enterovirus 71. *Science* 336, 1274-1274 (2012).

33 Hogle, J., Chow, M. & Filman, D. Three-dimensional structure of poliovirus at 2.9 A resolution. *Science* 229, 1358-1365 (1985).

34 Rossmann, M. G. *et al.* Structure of a human common cold virus and functional relationship to other picornaviruses. *Nature* 317, 145 (1985).

35 Acharya, R. *et al.* The three-dimensional structure of foot-and-mouth disease virus at 2.9 Å resolution. *Nature* 337, 709 (1989).

36 Hendry, E. *et al.* The crystal structure of coxsackievirus A9: new insights into the uncoating mechanisms of enteroviruses. *Structure* 7, 1527-1538 (1999).

37 Muckelbauer, J. K. *et al.* The structure of coxsackievirus B3 at 3.5 Å resolution. *Structure* 3, 653-667 (1995).

38 Oliveira, M. A. *et al.* The structure of human rhinovirus 16. *Structure* 1, 51-68 (1993).

39 Smyth, M. *et al.* Implications for viral uncoating from the structure of bovine enterovirus. *Nature Structural Biology* 2, 224-231, doi:10.1038/nsb0395-224 (1995).

40 Christian, P. D. & Scotti, P. D. in *The insect viruses* 301-336 (Springer, 1998).

41 Cholleti, H., Hayer, J., Fafetine, J., Berg, M. & Blomström, A.-L. Genetic characterization of a novel picorna-like virus in Culex spp. mosquitoes from Mozambique. *Virology journal* 15, 71 (2018).

42 Fujiyuki, T. *et al.* Novel insect picorna-like virus identified in the brains of aggressive worker honeybees. *Journal of virology* 78, 1093-1100 (2004).

43 Zhu, L. *et al.* Structures of Coxsackievirus A10 unveil the molecular mechanisms of receptor binding and viral uncoating. *Nature Communications* 9, 4985, doi:10.1038/s41467-018-07531-0 (2018).

44 Ren, J. *et al.* Structures of Coxsackievirus A16 Capsids with Native Antigenicity: Implications for Particle Expansion, Receptor Binding, and Immunogenicity. *Journal of Virology* 89, 10500-10511, doi:10.1128/jvi.01102-15 (2015).

45 Liu, Y. *et al.* Atomic structure of a rhinovirus C, a virus species linked to severe childhood asthma. *Proceedings of the National Academy of Sciences* 113, 8997, doi:10.1073/pnas.1606595113 (2016).

46 Liu, Y. *et al.* Structure and inhibition of EV-D68, a virus that causes respiratory illness in children. *Science* 347, 71-74, doi:10.1126/science.1261962 (2015).

47 Curry, S., Chow, M. & Hogle, J. M. The poliovirus 135S particle is infectious. *Journal of Virology* 70, 7125-7131 (1996).

48 Salo, R. & Cliver, D. Effect of acid pH, salts, and temperature on the infectivity and physical integrity of enteroviruses. *Archives of virology* 52, 269-282 (1976).

49 Hughes, J. H., Thomas, D. C. & Hamparian, V. V. Acid lability of rhinovirus type 14: effect of pH,

time, and temperature. *Proceedings of the Society for Experimental Biology and Medicine* 144, 555-560 (1973).
50 Domingo, E., Martin, V., Perales, C. & Escarmis, C. Coxsackieviruses and quasispecies theory: evolution of enteroviruses. *Group B Coxsackieviruses,* 3-32 (Springer, 2008).
51 Santti, J., Hyypiä, T., Kinnunen, L. & Salminen, M. Evidence of recombination among enteroviruses. *Journal of virology* 73, 8741-8749 (1999).
52 Melnick, J. L. Enteroviruses. *Viral infections of humans.* 187-251 (Springer, 1984).
53 Pallansch, M. A. Enteroviruses: polioviruses, coxsackieviruses, echoviruses, and newer enteroviruses. *Fields virology* (2001).
54 Sawyer, M. H. Enterovirus infections: diagnosis and treatment. *Seminars in pediatric infectious diseases.* 40-47 (Elsevier, 2002).
55 Palacios, G. & Oberste, M. Enteroviruses as agents of emerging infectious diseases. *Journal of neurovirology* 11, 424-433 (2005).
56 Khan, F. *et al.* Progress toward polio eradication—worldwide, January 2016–March 2018. *Morbidity and Mortality Weekly Report* 67, 524 (2018).
57 Schmidt, N. J., Lennette, E. H. & Ho, H. H. An apparently new enterovirus isolated from patients with disease of the central nervous system. *Journal of Infectious Diseases* 129, 304-309 (1974).
58 Hagiwara, A., Tagaya, I. & Yoneyama, T. Epidemic of hand, foot and mouth disease associated with enterovirus 71 infection. *Intervirology* 9, 60-63 (1978).
59 Gilbert, G. L. *et al.* Outbreak of enterovirus 71 infection in Victoria, Australia, with a high incidence of neurologic involvement. *The Pediatric infectious disease journal* 7, 484-488 (1988).
60 Chumakov, M. *et al.* Enterovirus 71 isolated from cases of epidemic poliomyelitis-like disease in Bulgaria. *Archives of virology* 60, 329-340 (1979).
61 Alexander Jr, J. P., Baden, L., Pallansch, M. A. & Anderson, L. J. Enterovirus 71 infections and neurologic disease—United States, 1977–1991. *Journal of Infectious Diseases* 169, 905-908 (1994).
62 Solomon, T. *et al.* Virology, epidemiology, pathogenesis, and control of enterovirus 71. *The Lancet infectious diseases* 10, 778-790 (2010).
63 Melnick, J. L. Enterovirus type 71 infections: a varied clinical pattern sometimes mimicking paralytic poliomyelitis. *Reviews of infectious diseases* 6, S387-S390 (1984).
64 Wong, K. T. *et al.* The distribution of inflammation and virus in human enterovirus 71 encephalomyelitis suggests possible viral spread by neural pathways. *Journal of Neuropathology & Experimental Neurology* 67, 162-169 (2008).
65 Bird, S. W., Maynard, N. D., Covert, M. W. & Kirkegaard, K. Nonlytic viral spread enhanced by autophagy components. *Proceedings of the National Academy of Sciences* 111, 13081-13086 (2014).
66 Krogvold, L. *et al.* Detection of a low-grade enteroviral infection in the islets of langerhans of living patients newly diagnosed with type 1 diabetes. *Diabetes* 64, 1682-1687 (2015).
67 Cavalcante, P. *et al.* Detection of poliovirus-infected macrophages in thymus of patients with myasthenia gravis. *Neurology* 74, 1118-1126 (2010).
68 Baj, A. *et al.* Post-poliomyelitis syndrome as a possible viral disease. *International Journal of Infectious Diseases* 35, 107-116 (2015).
69 Rossmann, M. G. & Johnson, J. E. Icosahedral RNA virus structure. *Annual review of biochemistry* 58, 533-569 (1989).
70 Yi, E.-J., Shin, Y.-J., Kim, J.-H., Kim, T.-G. & Chang, S.-Y. Enterovirus 71 infection and vaccines. *Clinical and experimental vaccine research* 6, 4-14 (2017).
71 Chow, M. *et al.* Myristylation of picornavirus capsid protein VP4 and its structural significance. *Nature* 327, 482 (1987).
72 Zhao, M. *et al.* Immunization of N terminus of enterovirus 71 VP4 elicits cross-protective antibody responses. *BMC microbiology* 13, 287 (2013).
73 Rossmann, M. The canyon hypothesis. Hiding the host cell receptor attachment site on a viral surface from immune surveillance. *Journal of Biological Chemistry* 264, 14587-14590 (1989).
74 Strauss, M. *et al.* Nectin-like interactions between poliovirus and its receptor trigger conformational changes associated with cell entry. *Journal of virology* 89, 4143-4157, doi:10.1128/JVI.03101-14 (2015).

75 Baggen, J. *et al.* Role of enhanced receptor engagement in the evolution of a pandemic acute hemorrhagic conjunctivitis virus. *Proceedings of the National Academy of Sciences* 115, 397-402, doi:10.1073/pnas.1713284115 (2018).

76 Zhao, X. *et al.* Human Neonatal Fc Receptor is the Cellular Uncoating Receptor for Enterovirus B. *Cell* 177, 1553-1565. e1516 (2019).

77 He, Y. *et al.* Interaction of coxsackievirus B3 with the full length coxsackievirus-adenovirus receptor. *Nature Structural & Molecular Biology* 8, 874 (2001).

78 Levy, H. C., Bostina, M., Filman, D. J. & Hogle, J. M. Catching a virus in the act of RNA release: a novel poliovirus uncoating intermediate characterized by cryo-electron microscopy. *Journal of virology* 84, 4426-4441 (2010).

79 McMinn, P. C. An overview of the evolution of enterovirus 71 and its clinical and public health significance. *FEMS microbiology reviews* 26, 91-107 (2002).

80 van Ooij, M. J. *et al.* Structural and functional characterization of the coxsackievirus B3 CRE (2C): role of CRE (2C) in negative-and positive-strand RNA synthesis. *Journal of General Virology* 87, 103-113 (2006).

81 Lin, J.-Y., Li, M.-L. & Shih, S.-R. Far upstream element binding protein 2 interacts with enterovirus 71 internal ribosomal entry site and negatively regulates viral translation. *Nucleic acids research* 37, 47-59 (2008).

82 Lin, J. Y., Li, M. L., Huang, P. N., Chien, K. Y., Horng, J. T., & Shih, S. R.Heterogeneous nuclear ribonuclear protein K interacts with the enterovirus 71 5′ untranslated region and participates in virus replication. *Journal of General Virology* 89, 2540-2549 (2008)

83 Thompson, S. R. & Sarnow, P. Enterovirus 71 contains a type I IRES element that functions when eukaryotic initiation factor eIF4G is cleaved. *Virology* 315, 259-266 (2003).

84 Kok, C. C., Phuektes, P., Bek, E. & McMinn, P. C. Modification of the untranslated regions of human enterovirus 71 impairs growth in a cell-specific manner. *Journal of virology* 86, 542-552 (2012).

85 Merkle, I. *et al.* Biological significance of a human enterovirus B-specific RNA element in the 3′ nontranslated region. *Journal of virology* 76, 9900-9909 (2002).

86 Dobrikova, E., Florez, P., Bradrick, S. & Gromeier, M. Activity of a type 1 picornavirus internal ribosomal entry site is determined by sequences within the 3′ nontranslated region. *Proceedings of the National Academy of Sciences* 100, 15125-15130 (2003).

87 Dobrikova, E. Y., Grisham, R. N., Kaiser, C., Lin, J. & Gromeier, M. Competitive translation efficiency at the picornavirus type 1 internal ribosome entry site facilitated by viral cis and trans factors. *Journal of virology* 80, 3310-3321 (2006).

88 Yuan, J. *et al.* Enterovirus A71 proteins: structure and function. *Frontiers in microbiology* 9, 286 (2018).

89 Liu, H. *et al.* siRNA targeting the 2Apro genomic region prevents enterovirus 71 replication in vitro. *PloS one* 11, e0149470 (2016).

90 Li, X., Lu, H.-H., Mueller, S. & Wimmer, E. The C-terminal residues of poliovirus proteinase 2Apro are critical for viral RNA replication but not for cis-or trans-proteolytic cleavage. *Journal of General Virology* 82, 397-408 (2001).

91 Shih, S.-R. *et al.* Mutations at KFRDI and VGK domains of enterovirus 71 3C protease affect its RNA binding and proteolytic activities. *Journal of biomedical science* 11, 239-248 (2004).

92 Sun, D., Chen, S., Cheng, A. & Wang, M. Roles of the picornaviral 3C proteinase in the viral life cycle and host cells. *Viruses* 8, 82 (2016).

93 Watters, K. & Palmenberg, A. C. Differential processing of nuclear pore complex proteins by rhinovirus 2A proteases from different species and serotypes. *Journal of virology* 85, 10874-10883 (2011).

94 Flather, D. & Semler, B. L. Picornaviruses and nuclear functions: targeting a cellular compartment distinct from the replication site of a positive-strand RNA virus. *Frontiers in microbiology* 6, 594 (2015).

95 Lei, X. *et al.* Cleavage of the adaptor protein TRIF by enterovirus 71 3C inhibits antiviral responses mediated by Toll-like receptor 3. *Journal of virology* 85, 8811-8818 (2011).

96 Lei, X. *et al.* Cleavage of interferon regulatory factor 7 by enterovirus 71 3C suppresses cellular

responses. *Journal of virology* 87, 1690-1698 (2013).
97 Wang, B. *et al.* Enterovirus 71 protease 2Apro targets MAVS to inhibit anti-viral type I interferon responses. *PLoS pathogens* 9, e1003231 (2013).
98 Lu, J. *et al.* Enterovirus 71 disrupts interferon signaling by reducing the level of interferon receptor 1. *Journal of virology* 86, 3767-3776 (2012).
99 Kuo, R.-L., Kung, S.-H., Hsu, Y.-Y. & Liu, W.-T. Infection with enterovirus 71 or expression of its 2A protease induces apoptotic cell death. *Journal of General Virology* 83, 1367-1376 (2002).
100 Li, M.-L. *et al.* The 3C protease activity of enterovirus 71 induces human neural cell apoptosis. *Virology* 293, 386-395 (2002).
101 Li, J. *et al.* Enterovirus 71 3C promotes apoptosis through cleavage of PinX1, a telomere binding protein. *Journal of virology* 91, e02016-02016 (2017).
102 Wang, Y.-F. *et al.* A mouse-adapted enterovirus 71 strain causes neurological disease in mice after oral infection. *Journal of virology* 78, 7916-7924 (2004).
103 Marcotte, L. L. *et al.* Crystal structure of poliovirus 3CD protein: virally encoded protease and precursor to the RNA-dependent RNA polymerase. *Journal of virology* 81, 3583-3596 (2007).
104 Xiang, W., Harris, K. S., Alexander, L. & Wimmer, E. Interaction between the 5'-terminal cloverleaf and 3AB/3CDpro of poliovirus is essential for RNA replication. *Journal of virology* 69, 3658-3667 (1995).
105 Xie, S. *et al.* DIDS blocks a chloride-dependent current that is mediated by the 2B protein of enterovirus 71. *Cell research* 21, 1271 (2011).
106 Cong, H. *et al.* Enterovirus 71 2B induces cell apoptosis by directly inducing the conformational activation of the proapoptotic protein bax. *Journal of virology* 90, 9862-9877 (2016).
107 Xia, H. *et al.* Human enterovirus nonstructural protein 2CATPase functions as both an RNA helicase and ATP-independent RNA chaperone. *PLoS pathogens* 11, e1005067 (2015).
108 Du, H. *et al.* Enterovirus 71 2C protein inhibits NF-κB activation by binding to RelA (p65). *Scientific reports* 5, 14302 (2015).
109 Xiao, X. *et al.* Enterovirus 3A facilitates viral replication by promoting phosphatidylinositol 4-kinase IIIβ–ACBD3 interaction. *Journal of virology* 91, e00791-00717 (2017).
110 Lei, X. *et al.* The Golgi protein ACBD3 facilitates Enterovirus 71 replication by interacting with 3A. *Scientific reports* 7, 44592 (2017).
111 Sun, Y. *et al.* Enterovirus 71 VPg uridylation uses a two-molecular mechanism of 3D polymerase. *Journal of virology* 86, 13662-13671 (2012).
112 Wang, W. *et al.* EV71 3D protein binds with NLRP3 and enhances the assembly of inflammasome complex. *PLoS pathogens* 13, e1006123 (2017).
113 Deshpande, J., Nadkarni, S. & Francis, P. Enterovirus 71 isolated from a case of acute flaccid paralysis in India represents a new genotype. *Current Science*, 1350-1353 (2003).
114 Bessaud, M. *et al.* Molecular characterization of human enteroviruses in the Central African Republic: uncovering wide diversity and identification of a new human enterovirus A71 genogroup. *Journal of clinical microbiology* 50, 1650-1658 (2012).
115 Sadeuh-Mba, S. A. *et al.* High frequency and diversity of species C enteroviruses in Cameroon and neighboring countries. *Journal of clinical microbiology* 51, 759-770 (2013).
116 Yu, H. *et al.* Genetic analysis of the VP1 region of enterovirus 71 reveals the emergence of genotype A in central China in 2008. *Virus genes* 41, 1-4 (2010).
117 Bessaud, M. *et al.* Molecular comparison and evolutionary analyses of VP1 nucleotide sequences of new African human enterovirus 71 isolates reveal a wide genetic diversity. *PloS one* 9, e90624 (2014).
118 Wang, J.-R. *et al.* Change of major genotype of enterovirus 71 in outbreaks of hand-foot-and-mouth disease in Taiwan between 1998 and 2000. *Journal of clinical microbiology* 40, 10-15 (2002).
119 Sanjuán, R., Nebot, M. R., Chirico, N., Mansky, L. M. & Belshaw, R. Viral mutation rates. *Journal of virology* 84, 9733-9748 (2010).
120 Drake, J. W. Rates of spontaneous mutation among RNA viruses. *Proceedings of the National Academy of Sciences* 90, 4171-4175 (1993).
121 Kirkegaard, K. & Baltimore, D. The mechanism of RNA recombination in poliovirus. *Cell* 47, 433-443 (1986).

122 Chan, Y.-F. & AbuBaker, S. Recombinant human enterovirus 71 in hand, foot and mouth disease patients. *Emerging infectious diseases* 10, 1468-1470 (2004).

123 Zhao, K. *et al.* Circulating coxsackievirus A16 identified as recombinant type A human enterovirus, China. *Emerging infectious diseases* 17, 1537 (2011).

124 Zhang, Y. *et al.* An emerging recombinant human enterovirus 71 responsible for the 2008 outbreak of hand foot and mouth disease in Fuyang city of China. *Virology journal* 7, 94 (2010).

125 Yip, C. C. *et al.* Emergence of enterovirus 71 "double-recombinant" strains belonging to a novel genotype D originating from southern China: first evidence for combination of intratypic and intertypic recombination events in EV71. *Archives of virology* 155, 1413-1424 (2010).

126 Huang, S.-C. *et al.* Appearance of intratypic recombination of enterovirus 71 in Taiwan from 2002 to 2005. *Virus research* 131, 250-259 (2008).

127 Bible, J. M., Pantelidis, P., Chan, P. K. & Tong, C. W. Genetic evolution of enterovirus 71: epidemiological and pathological implications. *Reviews in medical virology* 17, 371-379 (2007).

128 Yi, L., Lu, J., Kung, H.-f. & He, M.-L. The virology and developments toward control of human enterovirus 71. *Critical reviews in microbiology* 37, 313-327 (2011).

129 Yamayoshi, S. *et al.* Scavenger receptor B2 is a cellular receptor for enterovirus 71. *Nature medicine* 15, 798 (2009).

130 Nishimura, Y. *et al.* Human P-selectin glycoprotein ligand-1 is a functional receptor for enterovirus 71. *Nature medicine* 15, 794 (2009).

131 Qing, J. *et al.* Cyclophilin A associates with enterovirus-71 virus capsid and plays an essential role in viral infection as an uncoating regulator. *PLoS pathogens* 10, e1004422 (2014).

132 Yang, B., Chuang, H. & Yang, K. D. Sialylated glycans as receptor and inhibitor of enterovirus 71 infection to DLD-1 intestinal cells. *Virology journal* 6, 141 (2009).

133 Du, N. *et al.* Cell surface vimentin is an attachment receptor for enterovirus 71. *Journal of virology* 88, 5816-5833 (2014).

134 Su, P.-Y. *et al.* Cell surface nucleolin facilitates enterovirus 71 binding and infection. *Journal of virology* 89, 4527-4538 (2015).

135 Yang, S.-L., Chou, Y.-T., Wu, C.-N. & Ho, M.-S. Annexin II binds to capsid protein VP1 of enterovirus 71 and enhances viral infectivity. *Journal of virology* 85, 11809-11820 (2011).

136 Tan, C. W., Poh, C. L., Sam, I.-C. & Chan, Y. F. Enterovirus 71 uses cell surface heparan sulfate glycosaminoglycan as an attachment receptor. *Journal of virology* 87, 611-620 (2013).

137 Lin, Y.-W., Wang, S.-W., Tung, Y.-Y. & Chen, S.-H. Enterovirus 71 infection of human dendritic cells. *Experimental biology and medicine* 234, 1166-1173 (2009).

138 Su, P.-Y. *et al.* Cell surface sialylation affects binding of enterovirus 71 to rhabdomyosarcoma and neuroblastoma cells. *BMC microbiology* 12, 162 (2012).

139 Eskelinen, E.-L., Tanaka, Y. & Saftig, P. At the acidic edge: emerging functions for lysosomal membrane proteins. *Trends in cell biology* 13, 137-145 (2003).

140 Jiao, X.-Y., Guo, L., Huang, D.-Y., Chang, X.-L. & Qiu, Q.-C. Distribution of EV71 receptors SCARB2 and PSGL-1 in human tissues. *Virus research* 190, 40-52 (2014).

141 Zhou, D., Mei, Q., Li, J. & He, H. Cyclophilin A and viral infections. *Biochemical and biophysical research communications* 424, 647-650 (2012).

142 Fuchs, E. & Weber, K. Intermediate filaments: structure, dynamics, function and disease. *Annual review of biochemistry* 63, 345-382 (1994).

143 Losfeld, M.-E. *et al.* The cell surface expressed nucleolin is a glycoprotein that triggers calcium entry into mammalian cells. *Experimental cell research* 315, 357-369 (2009).

144 Waisman, D. M. Annexin II tetramer" structure and function. *Signal Transduction Mechanisms,* 301-322 (Springer, 1995).

145 Medeiros, G. F. *et al.* Distribution of sulfated glycosaminoglycans in the animal kingdom: widespread occurrence of heparin-like compounds in invertebrates. *Biochimica et Biophysica Acta (BBA)-General Subjects* 1475, 287-294 (2000).

146 Laszik, Z. *et al.* P-selectin glycoprotein ligand-1 is broadly expressed in cells of myeloid, lymphoid, and dendritic lineage and in some nonhematopoietic cells. *Blood* 88, 3010-3021 (1996).

147 Geijtenbeek, T. B. *et al.* Identification of DC-SIGN, a novel dendritic cell–specific ICAM-3 receptor

that supports primary immune responses. *Cell* 100, 575-585 (2000).
148 Dang, M. *et al.* Molecular mechanism of SCARB2-mediated attachment and uncoating of EV71. *Protein & cell* 5, 692-703 (2014).
149 Fujii, K. *et al.* Transgenic mouse model for the study of enterovirus 71 neuropathogenesis. *Proceedings of the National Academy of Sciences* 110, 14753-14758 (2013).
150 Wang, Y.-F. & Yu, C.-K. Animal models of enterovirus 71 infection: applications and limitations. *Journal of biomedical science* 21, 31 (2014).
151 Liu, J. *et al.* Transgenic expression of human P-selectin glycoprotein ligand-1 is not sufficient for enterovirus 71 infection in mice. *Archives of virology* 157, 539-543 (2012).
152 Rossmann, M. G., He, Y. & Kuhn, R. J. Picornavirus–receptor interactions. *Trends in microbiology* 10, 324-331 (2002).
153 Yamayoshi, S. *et al.* Human SCARB2-dependent infection by coxsackievirus A7, A14, and A16 and enterovirus 71. *Journal of virology* 86, 5686-5696 (2012).
154 Calvo, D., Dopazo, J. & Vega, M. A. The CD36, CLA-1 (CD36L1), and LIMPII (CD36L2) gene family: cellular distribution, chromosomal location, and genetic evolution. *Genomics* 25, 100-106 (1995).
155 Fukuda, M. Lysosomal membrane glycoproteins. Structure, biosynthesis, and intracellular trafficking. *Journal of Biological Chemistry* 266, 21327-21330 (1991).
156 Yamayoshi, S. & Koike, S. Identification of a human SCARB2 region that is important for enterovirus 71 binding and infection. *Journal of virology* 85, 4937-4946 (2011).
157 Chen, P. *et al.* Molecular determinants of enterovirus 71 viral entry cleft around Gln-172 on VP1 protein interacts with variable region on scavenge receptor B 2. *Journal of Biological Chemistry* 287, 6406-6420 (2012).
158 Ku, Z. *et al.* Single neutralizing monoclonal antibodies targeting the VP1 GH loop of enterovirus 71 inhibit both virus attachment and internalization during viral entry. *Journal of virology* 89, 12084-12095 (2015).
159 Schwake, M., Schröder, B. & Saftig, P. Lysosomal membrane proteins and their central role in physiology. *Traffic* 14, 739-748 (2013).
160 Kaksonen, M. & Roux, A. Mechanisms of clathrin-mediated endocytosis. *Nature Reviews Molecular Cell Biology* 19, 313 (2018).
161 Leong, K. L. J., Ng, M. M.-L. & Chu, J. J. H. The essential role of clathrin-mediated endocytosis in the infectious entry of human enterovirus 71. *Journal of Biological Chemistry* 286, 309-321 (2011).
162 Lin, H.-Y. *et al.* Caveolar endocytosis is required for human PSGL-1-mediated enterovirus 71 infection. *Journal of virology* 87, 9064-9076 (2013).
163 Kovtun, O., Tillu, V. A., Ariotti, N., Parton, R. G. & Collins, B. M. Cavin family proteins and the assembly of caveolae. *J Cell Sci* 128, 1269-1278 (2015).
164 Pelkmans, L. & Helenius, A. Insider information: what viruses tell us about endocytosis. *Current opinion in cell biology* 15, 414-422 (2003).
165 Hayer, A. *et al.* Caveolin-1 is ubiquitinated and targeted to intralumenal vesicles in endolysosomes for degradation. *The Journal of cell biology* 191, 615-629 (2010).
166 Rossmann, M. G. *et al.* Cell recognition and entry by rhino-and enteroviruses. *Virology* 269, 239-247 (2000).
167 Plevka, P. *et al.* Structure of human enterovirus 71 in complex with a capsid-binding inhibitor. *Proceedings of the National Academy of Sciences* 110, 5463-5467 (2013).
168 De Colibus, L. *et al.* More-powerful virus inhibitors from structure-based analysis of HEV71 capsid-binding molecules. *Nature structural & molecular biology* 21, 282 (2014).
169 Koike, S. A pH-dependent molecular switch for virion uncoating. *Protein & cell* 5, 653-654 (2014).
170 Buchta, D. *et al.* Enterovirus particles expel capsid pentamers to enable genome release. *Nature communications* 10, 1138 (2019).
171 Gamarnik, A. V. & Andino, R. Switch from translation to RNA replication in a positive-stranded RNA virus. *Genes & development* 12, 2293-2304 (1998).
172 Paul, A. V., Rieder, E., Kim, D. W., van Boom, J. H. & Wimmer, E. Identification of an RNA hairpin in poliovirus RNA that serves as the primary template in the in vitro uridylylation of VPg. *Journal of*

virology 74, 10359-10370 (2000).
173 Jiang, P., Liu, Y., Ma, H.-C., Paul, A. V. & Wimmer, E. Picornavirus morphogenesis. *Microbiol. Mol. Biol. Rev.* 78, 418-437 (2014).
174 Shingler, K. L. *et al.* The enterovirus 71 A-particle forms a gateway to allow genome release: a cryoEM study of picornavirus uncoating. *PLoS pathogens* 9, e1003240 (2013).
175 Huang, S. C., Chang, C. L., Wang, P. S., Tsai, Y. & Liu, H. S. Enterovirus 71 - induced autophagy detected in vitro and in vivo promotes viral replication. *Journal of medical virology* 81, 1241-1252 (2009).
176 Zhang, X.-Y., Xi, X.-Y. & Zhao, Z.-D. Autophagy inhibitor 3-MA decreases the production and release of infectious enterovirus 71 particles. *Zhonghua shi yan he lin chuang bing du xue za zhi= Zhonghua shiyan he linchuang bingduxue zazhi= Chinese journal of experimental and clinical virology* 25, 176-178 (2011).
177 Wang, C., Zhou, R., Zhang, Z., Jin, Y., Cardona, C.J. and Xing, Z. Intrinsic apoptosis and proinflammatory cytokines regulated in human astrocytes infected with enterovirus 71. *Journal of General Virology* 96(10), 3010-3022 (2015).
178 Chang, S.-C., Lin, J.-Y., Lo, L. Y.-C., Li, M.-L. & Shih, S.-R. Diverse apoptotic pathways in enterovirus 71-infected cells. *Journal of neurovirology* 10, 338-349 (2004).
179 Liang, C. C. *et al.* Human endothelial cell activation and apoptosis induced by enterovirus 71 infection. *Journal of medical virology* 74, 597-603 (2004).
180 Chen, L. C. *et al.* Enterovirus 71 infection induces Fas ligand expression and apoptosis of Jurkat cells. *Journal of medical virology* 78, 780-786 (2006).
181 Shih, S.-R., Weng, K.-F., Stollar, V. & Li, M.-L. Viral protein synthesis is required for Enterovirus 71 to induce apoptosis in human glioblastoma cells. *Journal of neurovirology* 14, 53-61 (2008).
182 Chen, S.-C. *et al.* Sumoylation-promoted enterovirus 71 3C degradation correlates with a reduction in viral replication and cell apoptosis. *Journal of Biological Chemistry* 286, 31373-31384 (2011).
183 Zhang, G. *et al.* In vitro and in vivo evaluation of ribavirin and pleconaril antiviral activity against enterovirus 71 infection. *Archives of virology* 157, 669-679 (2012).
184 Shih, S.-R. *et al.* Mutation in enterovirus 71 capsid protein VP1 confers resistance to the inhibitory effects of pyridyl imidazolidinone. *Antimicrobial agents and chemotherapy* 48, 3523-3529 (2004).
185 Weng, T.-Y. *et al.* Lactoferrin inhibits enterovirus 71 infection by binding to VP1 protein and host cells. *Antiviral research* 67, 31-37 (2005).
186 Thibaut, H. J. *et al.* Towards the design of combination therapy for the treatment of enterovirus infections. *Antiviral research* 90, 213-217 (2011).
187 Wang, J. *et al.* Crystal structures of enterovirus 71 3C protease complexed with rupintrivir reveal the roles of catalytically important residues. *Journal of virology* 85, 10021-10030 (2011).
188 Patick, A. K. *et al.* In vitro antiviral activity and single-dose pharmacokinetics in humans of a novel, orally bioavailable inhibitor of human rhinovirus 3C protease. *Antimicrobial agents and chemotherapy* 49, 2267-2275 (2005).
189 Wang, Y. *et al.* Peptidyl aldehyde NK-1.8 k suppresses enterovirus 71 and enterovirus 68 infection by targeting protease 3C. *Antimicrobial agents and chemotherapy* 59, 2636-2646 (2015).
190 Wang, Y. *et al.* Structure of the Enterovirus 71 3C Protease in Complex with NK-1.8 k and Indications for the Development of Antienterovirus Protease Inhibitor. *Antimicrobial agents and chemotherapy* 61, e00298-00217 (2017).
191 Arita, M., Takebe, Y., Wakita, T. & Shimizu, H. A bifunctional anti-enterovirus compound that inhibits replication and the early stage of enterovirus 71 infection. *Journal of General Virology* 91, 2734-2744 (2010).
192 Hung, H.-C. *et al.* Inhibition of enterovirus 71 replication and the viral 3D polymerase by aurintricarboxylic acid. *Journal of antimicrobial chemotherapy* 65, 676-683 (2010).
193 Meng, T. & Kwang, J. Attenuation of human enterovirus 71 high-replication-fidelity variants in AG129 mice. *Journal of virology* 88, 5803-5815 (2014).
194 Chen, T.-C. *et al.* Novel antiviral agent DTriP-22 targets RNA-dependent RNA polymerase of enterovirus 71. *Antimicrobial agents and chemotherapy* 53, 2740-2747 (2009).
195 Tsai, F.-J. *et al.* Kaempferol inhibits enterovirus 71 replication and internal ribosome entry site (IRES)

activity through FUBP and HNRP proteins. *Food chemistry* 128, 312-322 (2011).
196 Arita, M., Wakita, T. & Shimizu, H. Characterization of pharmacologically active compounds that inhibit poliovirus and enterovirus 71 infectivity. *Journal of General Virology* 89, 2518-2530 (2008).
197 Sim, A. C. N., Luhur, A., Tan, T. M. C., Chow, V. T. K. & Poh, C. L. RNA interference against enterovirus 71 infection. *Virology* 341, 72-79 (2005).
198 Lu, W.-W., Hsu, Y.-Y., Yang, J.-Y. & Kung, S.-H. Selective inhibition of enterovirus 71 replication by short hairpin RNAs. *Biochemical and biophysical research communications* 325, 494-499 (2004).
199 Liu, M.-L. *et al.* Type I interferons protect mice against enterovirus 71 infection. *Journal of General Virology* 86, 3263-3269 (2005).
200 Steinhauer, D. A. & Holland, J. Rapid evolution of RNA viruses. *Annual Reviews in Microbiology* 41, 409-431 (1987).
201 Reed, Z. & Cardosa, M. J. Status of research and development of vaccines for enterovirus 71. *Vaccine* 34, 2967-2970 (2016).
202 Mao, Q.-y., Wang, Y., Bian, L., Xu, M. & Liang, Z. EV71 vaccine, a new tool to control outbreaks of hand, foot and mouth disease (HFMD). *Expert Review of Vaccines* 15, 599-606 (2016).
203 Wu, W.-H. *et al.* Molecular epidemiology of enterovirus 71 infection in the central region of Taiwan from 2002 to 2012. *PloS one* 8, e83711 (2013).
204 Li, L. *et al.* Genetic characteristics of human enterovirus 71 and coxsackievirus A16 circulating from 1999 to 2004 in Shenzhen, People's Republic of China. *Journal of clinical microbiology* 43, 3835-3839 (2005).
205 Zhang, Y. *et al.* An outbreak of hand, foot, and mouth disease associated with subgenotype C4 of human enterovirus 71 in Shandong, China. *Journal of Clinical Virology* 44, 262-267 (2009).
206 Takahashi, S. *et al.* Hand, foot, and mouth disease in China: modeling epidemic dynamics of enterovirus serotypes and implications for vaccination. *PLoS medicine* 13, e1001958 (2016).
207 Zhu, F. *et al.* Efficacy, safety, and immunogenicity of an enterovirus 71 vaccine in China. *New England Journal of Medicine* 370, 818-828 (2014).
208 Huang, K.-Y. A. *et al.* Epitope-associated and specificity-focused features of EV71-neutralizing antibody repertoires from plasmablasts of infected children. *Nature communications* 8, 762 (2017).
209 Zhao, Y., Ren, J., Padilla-Parra, S., Fry, E. E. & Stuart, D. I. Lysosome sorting of β-glucocerebrosidase by LIMP-2 is targeted by the mannose 6-phosphate receptor. *Nature communications* 5, 4321 (2014).
210 Berrow, N. S., Alderton, D. & Owens, R. J. in *High Throughput Protein Expression and Purification* 75-90 (Springer, 2009).
211 Nettleship, J. E. *et al.* A pipeline for the production of antibody fragments for structural studies using transient expression in HEK 293T cells. *Protein expression and purification* 62, 83-89 (2008).
212 Brown, J. *et al.* A procedure for setting up high-throughput nanolitre crystallization experiments. II. Crystallization results. *Journal of applied crystallography* 36, 315-318 (2003).
213 Walter, T. S. *et al.* A procedure for setting up high-throughput nanolitre crystallization experiments. Crystallization workflow for initial screening, automated storage, imaging and optimization. *Acta Crystallographica Section D: Biological Crystallography* 61, 651-657 (2005).
214 Walter, T. S. *et al.* Semi-automated microseeding of nanolitre crystallization experiments. *Acta Crystallographica Section F: Structural Biology and Crystallization Communications* 64, 14-18 (2008).
215 Allan, D. *et al.* Status of the crystallography beamlines at Diamond Light Source. *The European Physical Journal Plus* 130, 56 (2015).
216 Winter, G. xia2: an expert system for macromolecular crystallography data reduction. *Journal of applied crystallography* 43, 186-190 (2010).
217 Winter, G. *et al.* DIALS: implementation and evaluation of a new integration package. *Acta Crystallographica Section D* 74, 85-97 (2018).
218 Tickle, I. *et al.* Staraniso. *Global Phasing Ltd., Cambridge, United Kingdom* (2018).
219 Vagin, A. & Teplyakov, A. Molecular replacement with MOLREP. *Acta Crystallographica Section D: Biological Crystallography* 66, 22-25 (2010).
220 McCoy, A. J. *et al.* Phaser crystallographic software. *Journal of applied crystallography* 40, 658-674

(2007).
221 Langer, G., Cohen, S. X., Lamzin, V. S. & Perrakis, A. Automated macromolecular model building for X-ray crystallography using ARP/wARP version 7. *Nature protocols* 3, 1171 (2008).
222 Murshudov, G. N., Vagin, A. A. & Dodson, E. J. Refinement of macromolecular structures by the maximum-likelihood method. *Acta Crystallographica Section D: Biological Crystallography* 53, 240-255 (1997).
223 Adams, P. D. *et al.* PHENIX: a comprehensive Python-based system for macromolecular structure solution. *Acta Crystallographica Section D: Biological Crystallography* 66, 213-221 (2010).
224 Emsley, P., Lohkamp, B., Scott, W. G. & Cowtan, K. Features and development of Coot. *Acta Crystallographica Section D: Biological Crystallography* 66, 486-501 (2010).
225 DeLano, W. L. & Lam, J. W. PyMOL molecular viewer: Updates and refinements. *Abstracts of Papers of the American Chemical Society.* U1371-U1372 (AMER CHEMICAL SOC 1155 16TH ST, NW, WASHINGTON, DC 20036 USA).
226 Colowick, S. & Kaplan, N. Spectrophotometric and turbidimetric methods for measuring proteins. *Methods in Enzymology," Vol. Ill*, 450 (1957).
227 Mastronarde, D. N. SerialEM: a program for automated tilt series acquisition on Tecnai microscopes using prediction of specimen position. *Microscopy and Microanalysis* 9, 1182-1183 (2003).
228 Zheng, S. Q. *et al.* MotionCor2: anisotropic correction of beam-induced motion for improved cryo-electron microscopy. *Nature methods* 14, 331 (2017).
229 Mindell, J. A. & Grigorieff, N. Accurate determination of local defocus and specimen tilt in electron microscopy. *Journal of structural biology* 142, 334-347 (2003).
230 Kivioja, T., Ravantti, J., Verkhovsky, A., Ukkonen, E. & Bamford, D. Local average intensity-based method for identifying spherical particles in electron micrographs. *Journal of structural biology* 131, 126-134 (2000).
231 Tang, G. *et al.* EMAN2: an extensible image processing suite for electron microscopy. *Journal of structural biology* 157, 38-46 (2007).
232 Scheres, S. H. RELION: implementation of a Bayesian approach to cryo-EM structure determination. *Journal of structural biology* 180, 519-530 (2012).
233 Kimanius, D., Forsberg, B. O., Scheres, S. H. & Lindahl, E. Accelerated cryo-EM structure determination with parallelisation using GPUs in RELION-2. *Elife* 5, e18722 (2016).
234 Scheres, S. H. & Chen, S. Prevention of overfitting in cryo-EM structure determination. *Nature methods* 9, 853 (2012).
235 Pettersen, E. F. *et al.* UCSF Chimera—a visualization system for exploratory research and analysis. *Journal of computational chemistry* 25, 1605-1612 (2004).
236 Afonine, P., Headd, J., Terwilliger, T. & Adams, P. New tool: phenix. real_space_refine. *Computational Crystallography Newsletter* 4, 43-44 (2013).
237 Krissinel, E. & Henrick, K. Protein interfaces, surfaces and assemblies service PISA at European Bioinformatics Institute. *J Mol Biol* 372, 774-797 (2007).
238 Xiao, C. & Rossmann, M. G. Interpretation of electron density with stereographic roadmap projections. *Journal of structural biology* 158, 182-187 (2007).
239 Walter, T. S. *et al.* A plate-based high-throughput assay for virus stability and vaccine formulation. *Journal of virological methods* 185, 166-170 (2012).
240 Staring, J. *et al.* KREMEN1 is a host entry receptor for a major group of enteroviruses. *Cell host & microbe* 23, 636-643. e635 (2018).
241 Baggen, J., Thibaut, H. J., Strating, J. R. & van Kuppeveld, F. J. The life cycle of non-polio enteroviruses and how to target it. *Nature Reviews Microbiology* 16, 368 (2018).
242 Ren, R., Costantini, F., Gorgacz, E. J., Lee, J. J. & Racaniello, V. R. Transgenic mice expressing a human poliovirus receptor: a new model for poliomyelitis. *Cell* 63, 353-362 (1990).
243 Evans, D. J. & Almond, J. W. Cell receptors for picornaviruses as determinants of cell tropism and pathogenesis. *Trends in microbiology* 6, 198-202 (1998).
244 Muehlenbachs, A., Bhatnagar, J. & Zaki, S. R. Tissue tropism, pathology and pathogenesis of enterovirus infection. *The Journal of pathology* 235, 217-228 (2015).
245 Lin, J.-Y. & Shih, S.-R. Cell and tissue tropism of enterovirus 71 and other enteroviruses infections.

Journal of biomedical science 21, 18 (2014).
246 Stuart, D. I., Levine, M., Muirhead, H. & Stammers, D. K. Crystal structure of cat muscle pyruvate kinase at a resolution of 2.6 Å. *Journal of molecular biology* 134, 109-142 (1979).
247 Yamayoshi, S., Ohka, S., Fujii, K. & Koike, S. Functional comparison of SCARB2 and PSGL1 as receptors for enterovirus 71. *Journal of virology* 87, 3335-3347 (2013).
248 Neculai, D. *et al.* Structure of LIMP-2 provides functional insights with implications for SR-BI and CD36. *Nature* 504, 172 (2013).
249 Zhang, X. *et al.* The binding of a monoclonal antibody to the apical region of SCARB2 blocks EV71 infection. *Protein & cell* 8, 590-600 (2017).
250 Zhou, D. *et al.* Unexpected mode of engagement between enterovirus 71 and its receptor SCARB2. *Nature microbiology* 4, 414 (2019).
251 Plevka, P. *et al.* Interaction of decay-accelerating factor with echovirus 7. *Journal of virology* 84, 12665-12674 (2010).
252 Kotecha, A. *et al.* Rules of engagement between αvβ6 integrin and foot-and-mouth disease virus. *Nature communications* 8, 15408 (2017).
253 Ren, J. *et al.* Picornavirus uncoating intermediate captured in atomic detail. *Nature communications* 4, 1929 (2013).
254 Yuan, S. *et al.* Identification of positively charged residues in enterovirus 71 capsid protein VP1 essential for production of infectious particles. *Journal of virology* 90, 741-752 (2016).
255 Victorio, C. B. L. *et al.* Cooperative effect of the VP1 amino acids 98E, 145A and 169F in the productive infection of mouse cell lines by enterovirus 71 (BS strain). *Emerging microbes & infections* 5, 1-14 (2016).
256 Fujii, K. *et al.* VP1 amino acid residue 145 of enterovirus 71 is a key residue for its receptor attachment and resistance to neutralizing antibody during cynomolgus monkey infection. *Journal of virology* 92, e00682-00618 (2018).
257 Xu, L. *et al.* A broadly cross-protective vaccine presenting the neighboring epitopes within the VP1 GH loop and VP2 EF loop of enterovirus 71. *Scientific reports* 5, 12973 (2015).
258 Abhinandan, K. & Martin, A. C. Analysis and improvements to Kabat and structurally correct numbering of antibody variable domains. *Molecular immunology* 45, 3832-3839 (2008).
259 Shi, B. *et al.* Comparative analysis of human and mouse immunoglobulin variable heavy regions from IMGT/LIGM-DB with IMGT/HighV-QUEST. *Theoretical Biology and Medical Modelling* 11, 30 (2014).
260 Fanning, L. J., Connor, A. M. & Wu, G. E. Development of the immunoglobulin repertoire. *Clinical immunology and immunopathology* 79, 1-14 (1996).
261 Weitkamp, J.-H., LaFleur, B. J., Greenberg, H. B. & Crowe Jr, J. E. Natural evolution of a human virus-specific antibody gene repertoire by somatic hypermutation requires both hotspot-directed and randomly-directed processes. *Human immunology* 66, 666-676 (2005).
262 Ye, J., Ma, N., Madden, T. L. & Ostell, J. M. IgBLAST: an immunoglobulin variable domain sequence analysis tool. *Nucleic acids research* 41, W34-W40 (2013).
263 Klein, F. *et al.* Somatic mutations of the immunoglobulin framework are generally required for broad and potent HIV-1 neutralization. *Cell* 153, 126-138, doi:10.1016/j.cell.2013.03.018 (2013).
264 Koshland, D. E. Application of a theory of enzyme specificity to protein synthesis. *Proceedings of the National Academy of Sciences* 44, 98-104 (1958).
265 Plevka, P. *et al.* Neutralizing antibodies can initiate genome release from human enterovirus 71. *Proceedings of the National Academy of Sciences* 111, 2134-2139 (2014).
266 Li, H.-Y., Han, J.-F., Qin, C.-F. & Chen, R. Virus-like particles for enterovirus 71 produced from Saccharomyces cerevisiae potently elicits protective immune responses in mice. *Vaccine* 31, 3281-3287 (2013).
267 Chung, Y.-C. *et al.* Immunization with virus-like particles of enterovirus 71 elicits potent immune responses and protects mice against lethal challenge. *Vaccine* 26, 1855-1862 (2008).